AN INVESTIGATION OF FACTORS AFFECTING SURFACE GENERATION IN ULTRA-PRECISION MACHINING WITH FAST TOOL SERVO

KWOK TSZ CHUN

M.Phil

The Hong Kong Polytechnic University

2011

THE HONG KONG POLYTECHNIC UNIVERSITY

Department of Industrial and Systems Engineering

An Investigation of Factors Affecting Surface Generation in Ultra-precision Machining with Fast Tool Servo

by

KWOK Tsz Chun

A thesis submitted in partial fulfilment of the requirements for the degree of Master of Philosophy

August 2008

CERTIFICATION OF ORIGINALITY

I hereby declare that this thesis is my own work and that, to the best of my knowledge and belief, it reproduces no material previously published or written, nor material that has been accepted for the award of any other degree of diploma, expect where due acknowledgement has been made in the text.

____________________________________ (Signed)

KWOK Tsz Chun (Name of student)

Abstract

Abstract of thesis entitled "An Investigation of Factors Affecting Surface Generation in Ultra-precision Machining with Fast Tool Servo" submitted by Mr. Kwok, Tsz Chun for the degree of Master of Philosophy at the Hong Kong Polytechnic University in May, 2010.

Ultra-precision machining with fast tool servo (FTS) is one of the emerging technologies for the fabrication of high-quality optical surfaces. A diamond tool is fixed on the FTS is activated back and forth by a stacked type of piezoelectric actuator. Complex optical surfaces with sub-micrometer form accuracy and nanometric surface finish can be fabricated without the need for any subsequent post processing.

Although there has been extensive research work on the design and control of tool actuators for FTS machining, relatively little research work has been reported in the study of nano-surface generation in FTS machining. As a result, this study aims at investigating the factors affecting surface generation in ultra-precision machining with FTS. The factors under investigation include process factors, wear of diamond tool and error motion of FTS actuation.

Regarding process factors, a series of experiments were conducted under various cutting conditions such as spindle speed, feed rate, depth of cut, etc. The results indicate that the surface quality of the machined surface can be improved by appropriate selection of cutting conditions. Moreover, a tool compensation method has been developed which is found to be effective in improving the surface quality of machined surfaces. To study the form errors in FTS machining of optical components with complex profiles such as micro-lens arrays, pattern analysis has been employed to determine the surface quality of the machined surface. The experimental results indicate that the influence due to process factors can be minimized with appropriate selection of cutting conditions.

Since a diamond tool with a small radius is usually used in FTS machining, the surface quality of the workpiece is highly susceptible to the tool wear. As a result, the study continues by investigating the effect of the tool wear in FTS machining. A series of cutting experiments were conducted by FTS machining of a tilted flat surface by a predetermined distance. The traditional method for determination of tool wear based on the maximum height and the width of flank wear has been used to characterize the tool wear. In order to investigate the diamond tool wear quantitatively, a digital image processing method has been proposed to quantitatively characterize the tool wear. It is not only found to be effective in exploring the wear phenomena but also quantifying the material loss in various wear stages of the diamond tool. To investigate the effect of tool wear on surface generation in FTS machining, an experimental study has been done by machining tilted flat surface and micro-lense array. It is interesting to note that the form error of the FTS machined surface is adversely affected by tool wear.

As FTS machining technology is built based on the single-point diamond turning technology, the error motion of the ultra-precision machine and the stroke error of the FTS play important roles in the surface generation. Based on the experimental results and cutting mechanisms in FTS machining, a theoretical analysis is attempted to address two major error motions, which are due to the systematic characteristics of the ultra-precision machine and the stroke error due to the FTS actuation. Afterwards, a surface generation model was established to predict the surface quality in terms of the form error in FTS machining. The model has been verified through a series of cutting experiments. The result shows that the trend of the theoretical prediction by the simulation system is found to agree reasonably well with the experimental results.

On the whole, this study not only contributes significantly to a better understanding of the factors affecting surface generation in FTS machining but also provides an important means for the improvement of the surface quality in ultra-precision machining with Fast Tool Servo. This is vital for the technological achievement of ultra-precision machining technology.

Acknowledgments

I would like to express my sincere appreciation and thanks to my chief supervisor, Dr. Benny C.F. Cheung, Associate Professor and Associate Director of the Advanced Optics Manufacturing Centre (AOMC), Department of Industrial and Systems Engineering of The Hong Kong Polytechnic University, for his patient guidance, cheerful encouragement, academic support, numerous enthusiastic discussions and helpful editorial comments during my study.

Moreover, I would like to thank my co-supervisors, Professor W.B. Lee, Chair Professor and Director of the AOMC, Department of Industrial and Systems Engineering of The Hong Kong Polytechnic University, and Dr Sandy S. To, Assistant Professor and Associate Director of the AOMC, Department of Industrial and Systems Engineering of The Hong Kong Polytechnic University, for their constant patient guidance and helpful support during my study.

Many thanks are also due to the Research Grants Council of the Hong Kong Special Administrative Region of the People's Republic of China for the financial support of the research work under project no. PolyU 5140/05E. I would like to thank all staff in the AOMC of The Hong Kong Polytechnic University. Especially, Mr. L.B. Kong, Mr. T.W. Chung, Mr. K.C. Cheung, and Mr. M.C. Chan who shared their invaluable experience and provided full technical support for the research work.

Finally, I would like to express my sincerely thank to my family, co-workers and friends within and outside The Hong Kong Polytechnic University for their kind encouragement and support during the period of my study.

TABLE OF CONTENTS

LIST OF FIGURES

LIST OF TABLES

LIST OF PUBLICATIONS

Refereed Journal Papers

(1) Kwok, T.C., To, S., Cheung, C.F., Wang, S.J. and Lee, W.B. "An Investigation of Form Compensation in Fabricating Microlens Array by Fast Tool Servo Technology", Material Science Forum, Vols. 532-533, p.689-692 (2006).

(2) Kwok, T.C., Cheung, C.F., To, S. and Lee, W.B. "A Framework of a Surface Generation Model in Fast Tool Servo (FTS) Machining of Optical Microstructures", Key Engineering Materials, Vols. 364-366, p.1274-1279 (2008).

(3) Kwok, T.C., Cheung, C.F., Kong, L.B., To, S. and Lee, W.B. "Analysis of Surface Generation in Fast Tool Servo Machining of Optical Microstructures", Proceedings of The Institute of Mechanical Engineers, Part B, Journal of Engineering Manufacture, 224(9), 1351-1367 (2010).

Conference Paper

(1) Kwok, T.C., Cheung, C.F., To, S., Lee, W.B. "Characterization of Errors Affecting Surface Generation in Fast Tool Servo (FTS) Machining", Proceedings of ASPE's 22nd Annual Meeting, October 14-19, Dallas, Texas, USA, Vol. 42, p.371-374 (2007).

CHAPTER 1 INTRODUCTION

1.1 Background of Study

In the photonic and telecommunication industries, high quality optical components greatly enhance the performance and dramatically increase the design flexibility of high-end products. Ultra-precision machining is one of the supreme production technologies commonly applied in the fabrication of super mirror finished surfaces with nanometric surface roughness and submicrometre form accuracy. The fabrication of high-quality optical components by ultra-precision diamond turning requires tool actuation at a bandwidth significantly higher than the rotational frequency of the surfaces. This requirement cannot be met by standard slide drives due to their large mass and consequent low natural frequency. Ultra-precision machining with a Fast Tool Servo (FTS) has been developed based on single-point diamond turning (SPDT) technology. The FTS is an independently operated positioning device which is mounted on the ultra-precision machine for increasing the tool positioning accuracy and actuating the diamond tool back and forth. The rapid actuation of the diamond tool by the FTS facilitates the fabrication of complex optical profiles such as non-symmetric surfaces and micro-optical structures such as micro-lens arrays.

Although there is extensive research work on the design and control of tool actuators for FTS machining, relatively little research work has been undertaken in the investigation of nano-surface generation in FTS machining. Moreover, the factors affecting surface generation in FTS machining are more than for SPDT. A better understanding of surface generation and the factors affecting surface quality of the machined profile in FTS machining allows better determination and control of surface quality of the fabricated profile as well as contributing to a better understanding of the research field of FTS machining, and hence facilitates the further development of ultra-precision machining technology and the better design of machines to meet the needs of the future.

In the present study, the first effort was focused on exploring the effect of the process factors in FTS machining, which has received little attention and is the fundamental part of this research. The process factors affecting surface generation in FTS machining have been investigated by a series of cutting experiments. For achieving better surface quality, appropriate ranges of cutting conditions and tool compensation are recommended. Some other factors such as the characteristics of the material being machined are recommended for further study. After the study of the FTS machining of a single lens, pattern analysis was proposed to characterize the surface generation of microlens arrays.

In FTS machining, the radius of the diamond tool is usually smaller than the radius of curvature of the machined profile, which is why a diamond tool with a small radius is always employed to enable the fabrication of complex optical surfaces. The sharp tool with a very small tool nose radius is easily susceptible to wear. Since the machined profile is formed by the repetition of the tool profile in the plane of the normal cutting direction, cutting by a worn diamond tool directly affects the surface generation in ultra-precision machining using a fast tool servo. Tool wear not only degrades the surface quality of the machined profile but it also raises the machining cost. Although a lot of previous studies were carried out for a better understanding of the tool wear phenomena in ultra-precision machining, most focus on wear phenomena in ultra-precision machining rather than FTS machining. This tool wear study helps to provide a better understanding of the performance of diamond tools in FTS machining and contributes to better control of the surface quality of the machined profile. Moreover, an image digital processing method has successfully been employed to quantitatively determine the material loss on the used diamond tool.

Fabrication of high quality optical surfaces still highly relies on the technical experience of machine operators, and the optimum cutting conditions are determined based on an expensive trial and error approach when machining new surface designs. There is a need for the establishment of a surface generation model for the prediction of the form error in ultra-precision machining with FTS. According to the literature, the material removal process and surface generation in FTS machining is governed not only by the geometry of fabricated profile, tool geometry, tool wear, material properties, and cutting parameters such as feed rate, spindle speed and depth of cut but is also affected by the errors that occur during the motion of actuation of FTS. The FTS actuation motion is associated with the bandwidth and the stroke of the FTS, and the synchronized motion between the cutting tool and the workpiece. These movements play an important role in the material removal process and surface generation in FTS machining but they have received relatively little research attention. After importing the process factors results determined previously and the determined error motions, a surface generation model can be employed to analyze form errors of the machined profile. Moreover, the results of the analytical study are consistent with the results of the experimental cutting tests. In future studies, it is suggested to further investigate the effect of cutting mechanics on surface generation in FTS machining, in which a prediction of the detailed surface topography could be conducted.

1.2 Project Objectives

The objectives of the present study are:

(i) To investigate into the process factors affecting surface generation in ultra-precision machining with a fast tool servo;

(ii) To study the diamond tool wear phenomena which significantly affects surface generation in FTS machining;

(iii) To establish a surface generation model for predicting form error in ultra-precision machining with FTS

1.3 Organization of Thesis

The thesis consists of six chapters. The first chapter is an introduction which describes key issues to be addressed and the objectives of the project. Chapter 2 contains an overview of ultra-precision machining and its applications. It is in the form of a literature review for discussing the development of ultra-precision machining with FTS technology, as well as the factors affecting surface generation such as cutting parameters and tool wear. The surface metrology involved in the present study is also discussed.

In Chapter 3, the theoretical background of the study is presented which includes the cutting mechanism and surface generation mechanisms and the factors affecting surface generation in FTS machining. The commonly used experimental set-up employed is also mentioned, together with the design of experiments and ultra-precision measurement facilities for assessing the surface quality of machined profiles.

As a preliminary study for the theoretical study, a series of cutting experiments were conducted, as reported in Chapter 4, for investigating the effect of process factors affecting the surface generation in FTS machining. In Chapter 5, the effect of tool wear in surface generation was studied. The relationship between tool wear and surface quality is elaborated. Two quantitative methods for the characterization of tool wear are also discussed.

Chapter 6 describes a theoretical study of the effect of error motion of the FTS on surface generation. An empirical analysis was developed based on the systematic errors of the feeding slide of an ultra-precision machine and the stroke errors or error motion of the FTS. Stroke error is the exclusive error of FTS machining and involves the synchronized motion of the rotational spindle and the diamond tool actuated by the FTS. The conclusion of the study and some suggestions for further work are discussed in Chapter 7 and Chapter 8, respectively.

CHAPTER 2 LITERATURE REVIEW

2.1 Overview of the Optics Industry

Over the last few decades, the optics industry has grown from a skill and manually based industry to one where advanced optics design and advanced manufacturing are used. In the USA alone, there are more than 5000 small companies with an estimated total turnover of more than US$ 50 billion. The mass production of cheap spherical glass lenses and plastic aspheric lenses has moved to low cost manufacturing centers such as the Far East and Mainland China.

With the increasing demand for precision optical products, aspheric surfaces have been widely used in optical systems. Due to the problems in machining such kinds of surfaces and the problems with the processes in dealing with conventional optical glass, the development and application of aspheric optical components has been hindered. With the development of ultra-precision machining technology, aspheric optical components have become more popular and are now widely found in the optics industry. With the widespread use of personal computers, the market demand for optical pick-up lenses for CD-ROMs is huge. This has expanded to cover other photonics products such as digital cameras, mobile phones, CD/DVD drives, etc. The expansion of the market for commercial and for military applications has stimulated the development of ultra-precision NC manufacturing technology.

However, the more high-value-added part of the product spectrum has shifted to the design and fabrication of novel surfaces involving detailed microstructural features such as V-groove, pyramid structures and arrays, and freeform surfaces, which are crucial to the development of complex and micro-optical-electro-mechanical devices used in many photonics and telecommunication products and systems. Typical products include laser printers, hand held scanners, tube TV compensators, phase modulation mirrors, LCD backlights and broadband optical fiber connectors. The market demand for such products is huge and is rapidly increasing. Moreover, the market for a variety of optical products is expanding because of the demand for the latest electronic consumer products (See Figure 2.1).

Figure 2.1 Consumer products with backlighting system

According to the market research firm Ovum RHK, the global demand for optical components (WAN, datacom, and access) will reach almost USD6 billion by 2012. Sales demand is led by WAN optical components, growing to USD3.5 billion in 2012, followed by datacom at USD1.5 billion, and access at USD0.97 billion. Total demand for 40-Gbit/sec modules is expected to reach nearly USD900 million by 2012. Demand for 10-Gbit/sec modules will reach USD1.6 billion. The sector for signs and displays will come to dominate the overall HB-LED market by 2012, depending on whether most of the major players working on LED the LCD backlighting for TVs and PC monitors make a major transition to LED technology. Figure 2.1 shows some consumer products with backlighting technology. As the complexity of optical networks increase, integrating more optical components into network equipment enhances network performance. The worldwide markets have optical components, now at USD2.9 billion, are expected to reach USD7.6 billion by 2012 (http://www.electronics.ca/reports/optical/optical-components.html).

2.2 Review of Optical Surface Generation

In the optics industry, high-added-value optical surfaces, which are composed of freeform optical elements and microstructured optical surfaces, are heavily used in the design and production of high-value-added products for the photonics and telecommunication industry. Examples can be found in the fabrication of head and tail automotive lighting systems, the optical pick up of holographic elements used in optical memory disks, F-theta lenses used in laser beam printers and scanners, microgroove components used in the fabrication of micro-grating and micro-grating lenses, head mounted displays used in virtual reality applications, progressive lens inserts and fiber optic connectors, etc.

Freeform surfaces are large scale surface topologies with shapes that are either anamorphic or cylindrical, and generally possessing non-rotational symmetry. Whereas optical microstructures are small scale topologies generally classified as grooves, lenticulations and echells. However, freeform surfaces and optical microstructures cannot be manufactured to the high degree of precision required for photonics products using conventional machining technology or magnetorheological finishing. Ultra-precision multi-axis freeform non-conformal machining based on fast tool servo machining, multi-axis raster milling, micro-grooving and grinding is an enabling technology which provides a solution for machining non-rotational symmetry freeform optical surfaces and optical microstructures with sub-micrometer form accuracy and nanometric surface finish, without the need for any subsequent polishing.

2.2.1 Applications of freeform surfaces

Freeform surfaces are described as curved surfaces with complex geometrical features. According to ISO 17450-1 (2005), complex geometrical features have no invariance degree. The invariance degree of a geometrical feature is the displacement of the ideal feature for which the feature is kept identical. It corresponds to the degree of freedom used in kinematics.

Freeform shaped components are of great interest in many applications, either for functional or aesthetical reasons. A lot of previous work (Brinksmeier et al., 1996 and 2004; Katahira et al., 2003; Klocke, 2003; Pfeifer, 2001; Rodgers and Thompson, 2004; Savio and Chiffre, 2001) has been devoted to the research of the complex functional surfaces and their application in the design and manufacturing of advanced products .These components are important for various industries, such as automotive, aerospace, household appliances, etc. Functional surfaces may have a great influence on the performances of a product. For example, freeform geometry for both static and rotating components is of paramount importance in the design of a turbo machine.

As compared with conventional flat and spherical surfaces, freeform optics can significantly improve the performance, in terms of both the miniaturization of the system and improved optical functionality (i.e. lower wavefront error). Examples can be found in many important applications including computational imaging, compact projection displays, document security, curing of polymer dental filling material, controlled diffusers for lithography, microscopy, etc (Clayton, 2004). When conventional optics are used, the optical system usually dictates the mechanical design. For the specific mechanical design of an optical system, the number of components can be significantly reduced with the use of freeform optics. The components can be placed in mechanically favored positions while the optical quality of the system can even be increased. They are widely used in many industries ranging from mass production of consumer products to the manufacturing of single special components for large space projects.

One of the mass production examples is the use of optics for laser printers. Until recently, their optical scanning systems utilized several optical elements to form a system. By replacing these elements with a single freeform mirror, the number of components is reduced, with corresponding benefits in lower cost and miniaturization. Further benefits include the elimination of chromatic aberration and the ability to select any laser wavelengths. Since the shorter wavelength laser results in spot size reduction, the precision of the printing output is improved. Conversely, a long wavelength laser can be used in a less expensive mass production printer with the same freeform optical scanning system (Davis, 2003).

The freeform mirror was introduced to help to reduce the size of the system by a significant order of magnitude (Garrard, 2005). Significant reduction in the size of the system can dramatically reduce the use of exotic materials (such as beryllium) and this ensures mass reduction is possible for enhancing the performance of lightweight space systems. Freeform surfaces can also be used to control astigmatism at multiple locations in the field of view and this reduces wave front aberration.

Where freeform surfaces are applied in optics, they have revolutionized the industry beyond all expectations in terms of optical quality, whilst minimizing size, weight and number of components. The humble flat bed scanner is an example, where the application of freeform optics, such as an F-Theta lens, has enabled a totally novel technology to be widely and economically available. Another example is the freeform lens in the ubiquitous phone camera in mobile phones.

The rapidly increasing use of ultra-precision freeform surfaces is not limited to the optics field, bio-implants such as knee prostheses make use of freeform surfaces as the bearing components (Blunt and Charlton, 2006). One of the primary advances in this field is freeform hard bearing couples requiring micron scale form control with nanometric surface roughness. Other examples include ground and space based telescopes, defense and satellite based imaging systems and large laser facilities, where the smooth surfaces with complex optical shapes are required to have a precision up to a 1 part in 10^8 (Shore and Burman, 2004).

2.2.2 Fabrication of Optical Freeform Surfaces

Unlike conventional surfaces, optical freeform surfaces have a non-rotational symmetric axis. For fulfilling their stringent functional requirements in the end technological applications, they are required to be fabricated with sub-micrometer form accuracy and surface roughness in nanometer range. The geometry of freeform surfaces cannot be described by a single universal equation, as is the case for aspheric surfaces. However, they can be expressed by a myriad of equations including: toroidal, biconic, microstructures (such as V-groove, lenticulation and echells, pyramid), Non-Uniform Rational B-Spline (NURBS), etc. Micro-lens arrays also belong to freeform surfaces since they have the same aspects in fabrication, alignment and measurement (ASPE, 2004; Optonet Workshop, 2004). Ultra-precision multi-axis machining, single point diamond turning, CNC milling, CNC grinding, and CNC polishing are enabling technologies that allow the designed freeform surface to be fabricated. In the present study, the research effort is focused on the surface generation in fabricating another optical surface – the microstructure surface. The applications and conventional fabrication method of optical microstructure surfaces are reviewed and discussed in the following sections.

2.2.3 Application of microstructure surfaces

Micro-structured plastic optics are a family of components which incorporate features such as facets, lenticles, prisms, surface relief structures, or micro-lenses, to achieve some design intent, and to discover new applications in display optics, lighting and telecommunications. A micro-lens array is one of the popular microstructures applied in the optical industry, which encompasses many micro-lens applications. Each lens can be considered as a tiny refractive index distribution lens and acts as a convex lens.

The SEM photos show some of the many MicroLens™ patterns that can be customized to meet visual applications, as shown in Figure 2.2. These micro-lenses result in a reflective matrix that diffuses and directs light across the surface of the display in a very efficient and consistent manner. Another key application of micro-lens arrays is when they are used in an LED backlit module (see Figure 2.3), where the applications include mobile phones, hand-held palm pilots, TVs, etc.

The radii of the micro-lens within the rows can be varied to suit the design. Before the introduction of the micro-lens, many LEDs were needed to achieve a uniform distribution of light. With the use of micro-lens arrays to extract the light to illuminate the LCD panel, fewer light sources (one or several LEDs) are sufficient to achieve a uniform light distribution. This directly saves energy and optimizes the display functions. It is also used as a lens array for high-speed optical communications between computers.

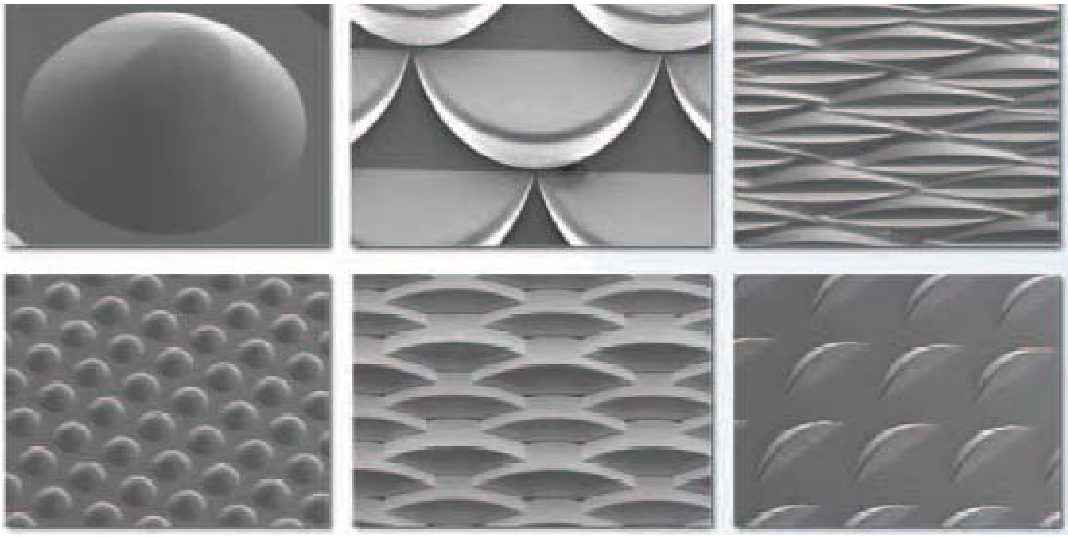

Figure 2.2 Family of optical microstructures (Source: Global Lighting Technologies Inc)

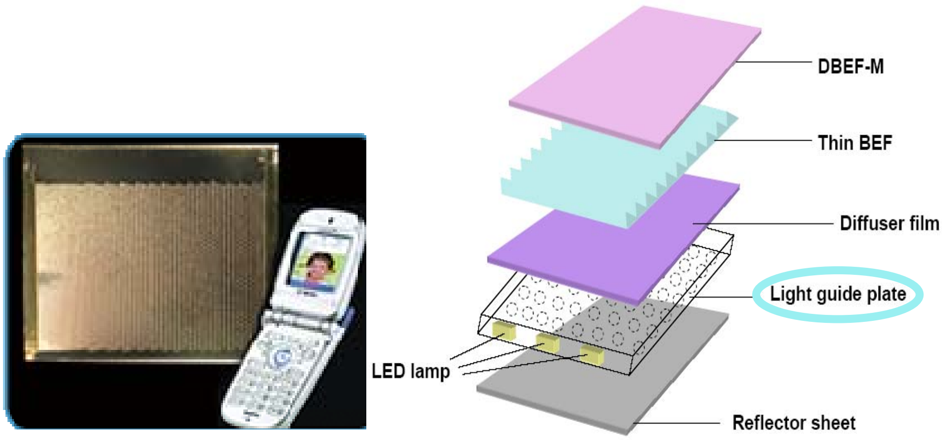

Figure 2.3 Micro-lens Arrays for Flat-Panel Devices (LCD Backlights) (Source: 3M)

Micro-structural surfaces (e.g. micro-lens arrays) are widely used in critical components in many photonics and telecommunication products such as flat panel displays, TV projection systems, commercial CCD and CMOS cameras, photocopiers, etc (Quan C. et al., 2003). The increasing demand for high-tech products provides huge scope for the development of micro-fabrication technology. Growing research interest in fabricating high precision micro-optical and light efficiency optical microstructures at a low cost will be a future trend. Other application areas of the micro-lens array are given as follows:

- Displays
- Illumination systems
- Solid-state lighting
- Semiconductor processing
- Medical systems
- Beam shaping
- Beam homogenizers
- Detector arrays
- Wave-front Sensors
- Optical interconnections
- Optical computing
- Imaging systems
- Con-focal microscopy
- Others

In addition to conventional applications, micro-optics have been applied in a number of areas. One of the widest applications is in imaging. These include photocopier imaging systems, oscilloscope cameras and other “close-up” imaging systems (Anderson, 1979). A technique known as micro-lens lithography has been proposed (Volkel et. al., 1996) which make use of a 1:1 imaging system composed of micro-lens arrays to copy a pattern to photo-resist. Advantages of this method include an increased depth of focus and a larger working distance (1 mm) than customary proximity printing. One of the advantages is that no wear occurs in the mask, as found in contact lithography. Micro-optics could also be applied in integral photography, which was invented by Gabriel Lippmann in 1908. It involves the use of micro-lens arrays as the imaging system on a camera. Hence, it records an array of images of a distant object on the photographic film. The image is an object as seen from the position of each of the lenses. The developed film is then projected using the same type of micro-lens array to form a three dimensional image of the object. A detailed discussion of this technique has been given by Stevens and Davies (1991).

Furthermore, optical microstructures have been used as components in atmospheric wave-front sensors, known as Shack-Hartmann arrays (Lindlein et. al., 1991). They are used to improve the images obtained from ground based telescopes. They provide a measurement of the wave-front distortion caused by the earth's atmosphere. This information is then used to deform either the main mirror or a smaller secondary mirror to remove the distortion. This method can be used to produce diffraction limited images of stars despite atmospheric distortion. An example of optimising refractive micro-lens arrays for this purpose has been discussed by Artzner (1992). The micro-lens arrays are also used in the area of optical interconnects. They have been used in many types of interconnects, which include spatially variant connections using multiple arrays (Hutley et. al., 1992), board-to-board and chip-to-chip connections in the electronics sector (Craft and Feldblum, 1992).

2.2.4 Conventional technologies for the fabrication of microstructure surfaces

In the last few decades, a lot of methods have been developed for ultra-precision machining, such as single-point diamond turning, ultra-precision raster milling, contour boring, micro grinding and ultrasonic assisted diamond cutting as well as ultrasonic lapping. These methods are particularly relevant for the fabrication of high precision microstructure surfaces (Chiffre et al. 2003). For the ultra-precision manufacturing of complex surfaces and microstructures, diamond turning and fly-cutting are commonly employed. However, these processes have geometric and kinematic limitations for certain tasks. Being suitable machining methods for the fabrication of microstructures, diamond contour boring and ball-end milling extend the types of surfaces which can be generated to almost arbitrarily shaped mirror arrays and profiles with high aspect ratio, (Lucca, et al. 1998 and Brinksmeier et al., 1998, 2000, 2001 & 2002).

In the recent past, the study of microstructure fabrication has been evolving and a number of methods have been used to produce high quality microstructures for high-performance electronic devices or optical elements. Many methods have been examined for the production of microstructures, including chemical process methods such as reactive ion etching, ion diffusion, deep proton irradiation, optical methods such as optical interference methods, and physical methods such as hot embossing, and micro-machining. However, the limitations of different micro-fabrication technologies always constrain the flexibility of production.

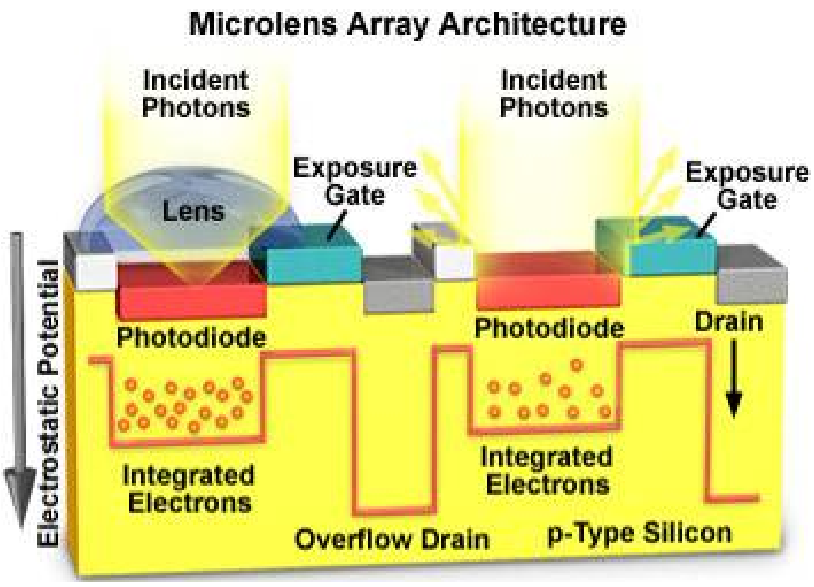

Figure 2.4 Ion etching of microstructure (Source:

http://micro.magnet.fsu.edu/primer/digitalimaging/concepts/microlensarray.html)

In the case of ion etched lenses, the quality is highly dependent on the working temperature and air pressure (Pekka Savander, 1994). This is graphically shown in Figure 2.4. The method is normally used to convert photo-resistant micro-lens arrays into the silica substrate. It involves the exposure of the lens array and substrate to a combination of O_2 and CHF_3 plasmas in a vacuum chamber. The plasma etches away the photo-resistant lens array and the photo-resistant pattern is converted into the substrate. Accurate control of the gas mixture and RF power supply must be achieved to assure high fidelity transfer of the lens array to the substrate. It is time-consuming to determine the specific optimal parameters for different patterns and working materials.

The microstructures produced by the photoresist reflow method can deviate widely from the spherical case. This method involves melting photoresist structures to form small lenses shaped by the surface tension of the liquid resistance. The profiles formed by this method can be much more complex than the simple spherical surfaces one might expect from simple surface energy minimization (Schilling, 2000). The fabricated lenses can have very large aberrations for certain fabrication parameters.

A recent fabrication method can be used to produce patterns in substrates by the hot embossing process, as carried out by Shen et al (2002). With the use of appropriate molds, lens arrays can be produced. The required mold is placed on top of the substrate and both are then placed on a heating plate. The substrate is then heated to above its glass transition temperature, and the soft substrate takes the form of the mold with which it is in contact. Although extremely low degrees of surface roughness of only a few nanometers can be achieved, the surface finish of the mold deteriorates after each embossing (Ong, 2002).

To meet the requirement of mass production, the designed microstructures profile is conventionally etched onto the metal substrates and fabricated by laser lithography (Dresel, 1996). As a result, the desired pattern can be etched. During the lithography, poor alignment of the patterns and positioning errors of the machine always limit the production efficiency (Lee Yung-Chun, 2005). Other drawbacks are that the surface roughness of the micro-lens array is always unfavorable and the laser is hard to handle because of its potential hazards.

Last but not least is the fact that most of the methods have a consistent limitation of a low freedom of fabrication. For example, ink-jet-deposited UV-cured lens have been employed to produce micro-lens arrays. The technique involves the controlled application of liquid drops of the UV curable material onto a substrate. The droplets are drawn into a spherical profile by the action of surface tension. The droplets are then exposed to UV radiation which cures the droplets. The controlled application of the resin has been achieved using computer controlled syringes by Keyworth et al. (1998), and an Ink-Jet fabrication process by Ishii et al. (2000). However, the ink-jet-deposited UV-curved microstructures are normally found to be spherical rather than aspheric (Neill et. al., 2005).

2.3 Ultra-precision machining with a Fast Tool Servo (FTS)

Ultra-precision machining with a fast tool servo (FTS) is one emerging method in the fabrication of non-rotationally symmetric surface (Dow 1991) and optical microstructures. Over the past few years, many methods for fabrication of optical microstructures, as discussed in Section 2.2, have been developed and applied in practice. Most can satisfy the uniformity requirements but the limitations of different micro-fabrication technologies always affect the efficiency and the precision of the final optical microstructures.

Fast tool servo (FTS) machining was developed based on single-point diamond turning (SPDT) technology by mounting a FTS motor on an ultra-precision machine. This facilitates the mechanically actuated motion of the diamond tool and enables the fabrication of high-quality optical microstructures. It makes use of auxiliary piezo-electric driven servos to rapidly actuate the diamond tool, with a fine resolution and sufficiently high bandwidth to machine optical microstructures with sub-micrometer form accuracy and nano-scale surface finish without the need for any subsequent post processing (Lee and Cheung, 2003).

2.3.1 Single-point diamond turning

Single-point diamond turning (SPDT) is a machining process making use of a monocystal diamond cutting tool, possessing a nanometric edge radius, form reproducibility and wear resistance. This process is capable of producing surfaces with complex shapes such as aspherics, with sub-micrometre accuracy, surface finish of the order of a few nanometres (Ra < 10nm), low surface and subsurface damage, with high removal rates (Franse, 1990). The superior surface finish and form accuracy of ultra-precision diamond turning allows the technology to be widely adopted for the manufacturing of a variety of precision opto-electronic components. Applications are now seen in the manufacturing of inserts for injection-moulded plastic camera lenses, scanner mirrors, photoconductor drums in photo-copiers and substrates for memory disks, etc. Some applications are the manufacture of optical parts with complex forms like aspheric surfaces (Cheung et al., 1997, and Cheung and To, 1998).

Figure 2.5: Ultra-precision diamond turning of nickel copper on the Nanoform 200 machine of Precitech Inc. (Source: AOMC)

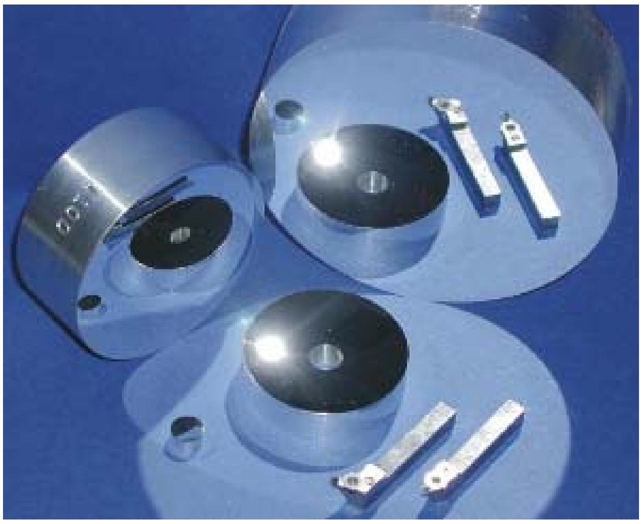

Figure 2.6: Examples of diamond turned workpieces (Source: Contour Fine Tooling)

Figures 2.5 and 2.6 show ultra-precision turning of nickel copper on a Nanoform 200 machine from Precitech Inc., USA and samples of diamond turned workpieces, respectively. Since ferrous materials cannot be machined by diamonds due to the diffusion of carbon from the diamond tool to the workpiece, leading to rapid tool wear, this technology is mainly applied for obtaining supermirror surfaces on non-ferrous materials by direct machining, without the need for subsequent post-polishing.

The achievable surface finish and form accuracy depend upon the stability of the machining environment. Any minute changes in the machining environment may cause a considerable variation in the machining accuracy. Variations in the temperature and delivery of the coolant can lead to form errors. The surface quality may be degraded through any motion that affects the relative position of the tool and workpiece. The sources of such disturbances can be acoustic vibrations, electrical noise, spindle runout, slideway vibration or inhomogeneity of the workpiece material that produces high frequency variations in the cutting forces and tool vibration. The stiffness of the machine tool also influences the characteristics of the machine surface.

The slides employed in this study are of a constrained and oil hydrostatic design. The machine consists of a natural granite base, where two horizontal “dovetail” slide-ways arranged in a "T" configuration as shown in Figure 2.7. The X and Z slides are rigidly mounted on the machine base. The work-holding spindle is mounted on the X-axis slide and traverses perpendicularly to the work-holding spindle's axis of rotation. The Z-axis slide holds the tool and traverses perpendicularly to the X-axis slide and parallel to the work-holding spindle. The X-axis and Z-axis slides are square to each other within 1.0 arc seconds.

An air bearing spindle with a single rear-mounted thrust plate is shown in Figure 2.8. The rear mounting thrust plate creates a higher radial stiffness at spindle nose. The spindle has an integral brushless DC motor with encoder feedback for controlled high torque, variable speed operation.

High quality cutting tools that can produce very fine chips are essential for machining components to a high dimensional accuracy and surface quality. Natural single-point diamond tools (see Figure 2.9) are exclusively used in micro-cutting due to their nanometric edge sharpness, form reproducibility, and wear resistance. They are well recognized to be ideal ultra-precision cutting tools. The design, manufacturing and proper use of diamond tools are among the key elements of single-point diamond turning (SPDT) technology.

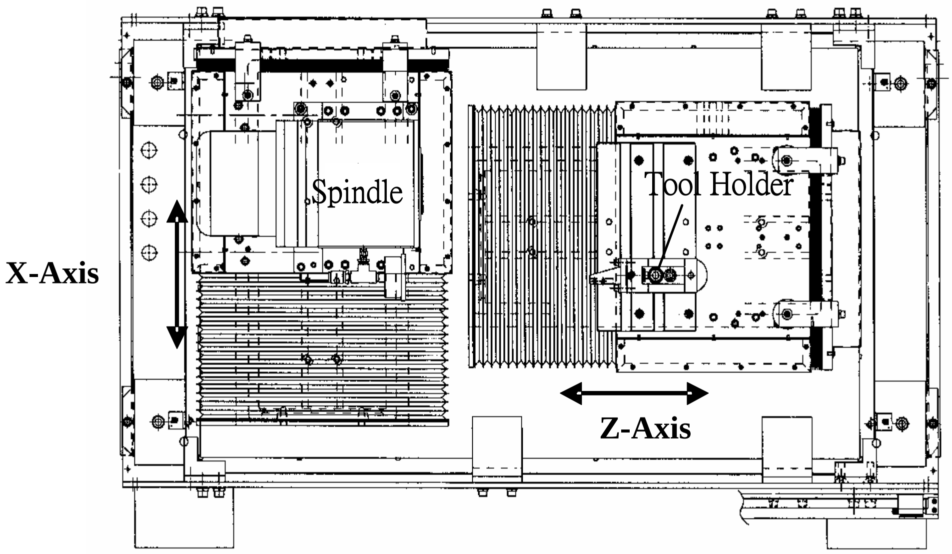

Figure 2.7 T-configuration of Nanoform 200 ultra-precision machine (Source: Precitech)

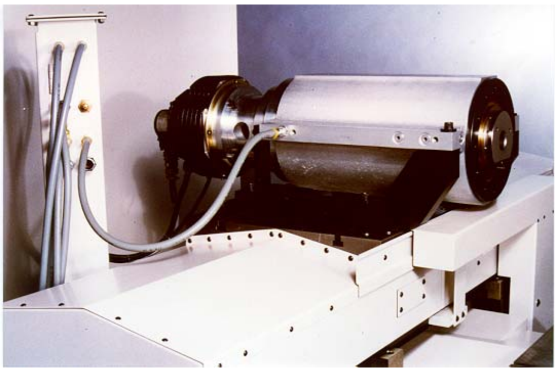

Figure 2.8 Air bearing spindle with air chuck mounted on Nanoform 200 with FTS (Source: Precitech)

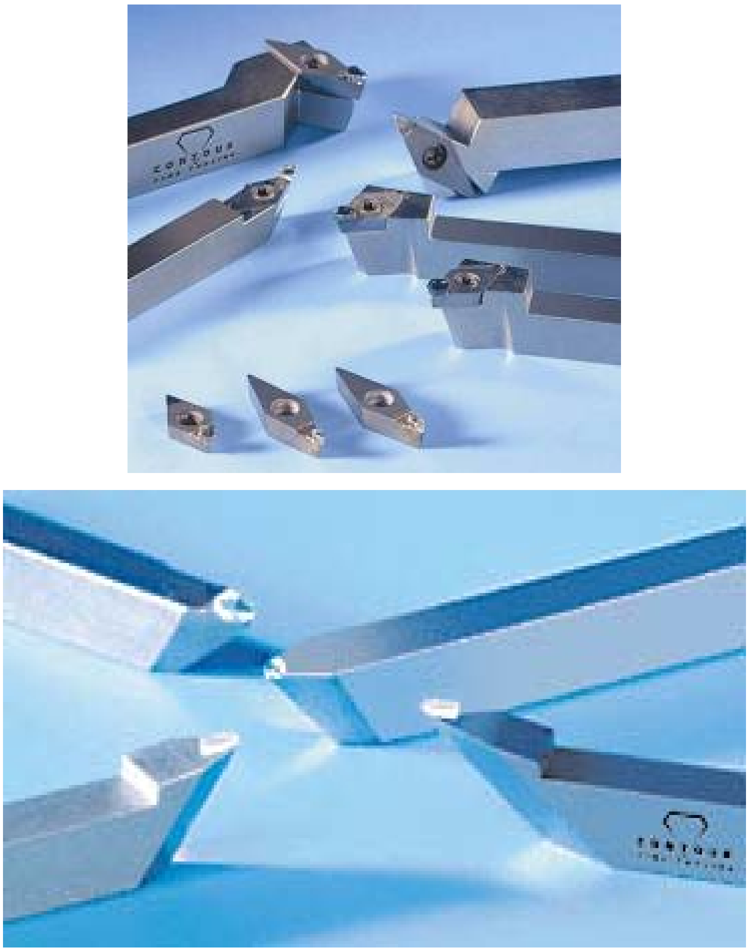

Figure 2.9: Natural single point diamonds (Source: Contour Fine Tooling)

The machining quality and manufacturing efficiency are significantly affected by the cutting tools. The sharpness of a cutting edge is a primary factor which determines the minimum depth of cut. A single-crystal diamond is considered to be the ideal tool material in ultra-precision and nano metric cutting because of its extreme hardness, better chemical stability at normal temperature and resistance to wear, and a very sharp edge, etc (Yuan, 2003). In the early 1990s, Ikawa et al. at the Lawrence Livermore National Laboratory carried out significant micromachining trials in order to determine the minimum cutting thickness. According to their reports, the minimum chip thickness can reach 1 nm, and hence a diamond tool with a cutting edge radius of 3nm to 5nm should be provided (Ikawa, 1992).

The profile of a machined surface is basically composed of a repetition of the tool profile transferred in the plane normal to the cutting direction. As a result, the geometrical accuracy of the cutting edge and its stability has great influence on the surface roughness of the workpiece being cut. The repetition of the tool profiles on the workpiece is affected, due to the complicated and unidentified interfacial phenomena between the cutting edges and workpiece materials, such as interfacial affinity. A less sharp tool leads to higher cutting forces, and hence more power dissipation in the cutting process and more heat development (Komanduri and Shaw 1975 and 1976; Evans, 1991; Casstevens, 1983). Cutting with a blunt tool adversely affects the machining accuracy. Ultra-precision diamond tools, which are used to produce high precision optical components, should not only be sharp but also be highly accurate in terms of the cutting edge geometry. The accuracy of the cutting edge profile has a great influence on the surface quality. Ultra-precision machining technology has been widely used in the fabrication of emerging products. Examples of applications are computer chips, data storage, MEMS, biomedical systems, Micro-optical systems, X-ray optics and implants. Ultra-precision surfaces which highly affect the properties and functional behavior play a vital role in these important applications.

The impact of computer technology has become possible because of the progressive downscaling of integrated circuits and storage devices. The smallest features of the most modern integrated circuits are already significantly smaller than 1 μm, and the scale reductions in storage media are equally impressive. The magnetic properties of a computer hard disk are influenced by a surface of roughness of several nanometers thick. In order to minimize head stiction to the disk surface, surface polishing is followed by a texturing process producing circumferential grooves or laser texturing, the overall roughness of the structured surface being Rq = 3-5 nm (Lonardo, 2002). Another important area is that of implants for medical use, where the current R&D on surface modifications point toward complex and multifunctional surfaces aimed at optimizing the topography (pore distribution, roughness, etc.).

Ultra-precision surfaces with nanometric surface roughness play a major role in reflective x-ray optics. X-rays incident at very shallow angles can be effectively reflected off smooth metallic or metal coated surfaces such as gold. Such mirrors, with designs of varying degrees of complexity, are widely used in x-ray telescopes and other x-ray imaging applications. In typical applications, an x-ray telescope mirror is made from glass ceramic material that is highly polished and coated with metal, or it can be made from nickel electrodeposited on a mandrel. In practice, such a telescope receives x-rays from sources in space and they first strike an annular parabolic surface and are then reflected on an annular hyperbolic surface (an optical configuration developed by Wolter). Such surfaces are frequently nested to improve the collecting efficiency of the telescope. In telescopes with the best angular resolution, the geometry of the individual mirrors is as close to perfection as possible but this implies a rigid surface that has a thickness of a few millimeters. For applications where less angular resolution is needed, foils can be used. In both cases, the surface texture of the surface significantly affects the performance of the mirror because it gives rise to x-ray scatter, hence low surface roughness is a vital aspect for the manufacture of the components. A number of researchers have demonstrated manufacturing textures with 0.4 nm surface roughness to be possible in the 1980s (Engdahl, 1981) and form accuracies of 0.2 nm have recently been achieved with polishing.

2.3.2 Ultra-precision machining with FTS

Ultra-precision machining with fast tool servo (FTS) has been developed based on the single point diamond turning (SPDT) technology. The FTS motor is an independently operated positioning device which is mounted on the X-Y stage of an ultra-precision machine. The FTS enables the diamond tool to be actuated back and forth. The rapid actuation of the diamond tool by the FTS facilitates the fabrication with a sufficiently high bandwidth, which enables complex optical profiles such as non-symmetric surfaces and micro-optical structures like the micro-lens array to be machined (Dow et. al, 1991).

By employing the FTS system in diamond turning technology, many shortcomings in ultra-precision machining can be minimized. In the past, machines have taken a passive role in the quality of surface finish; they were made of massive size in order to reduce their sensitivity to vibration. Cutting speed and feed had to be altered to prevent resonant frequencies affecting the desired surface quality. However, beyond that, the machine tool also had a limitation on its performance due to system vibration, thermal changes, and environmental disturbances. In order to achieve a higher precision, one possible solution is to improve the quality of the hardware which, as Rasmussen et al. (1994) noted, affects the cost exponentially. With increasing computer capabilities, it has become possible to actively improve the performance of existing machines by implementing devices such as FTS. Since machine tools are traditionally massive, the inertia involved makes high-speed actuation of the slide ways impractical. However, if a secondary actuation is implemented in the direction of interest, the slide way motors can be used in the traditional role of traversal/feed and the secondary actuation can limit itself to high speed control of a less massive cutting component over a smaller range (Marc and Kurfess, 2003).

Apart from the error due to vibration, another problem in the standard drive system of lead-screw driving mechanism is the effect of friction and backlash at the machine stage. In contour machining, it is virtually impossible to obtain nano-metric positioning accuracy with lead-screw mechanisms due to the presence of backlash and friction in the drive system from the actuation point at the servo motor rotor to the tool position (Cetinkunt et. al, 1992; Larsen et. al, 1995; Keauskopf et. al, 1984). The FTS has been proposed in order to increase the tool positioning accuracy as a nano-position device with a small range of motion but high accuracy of positioning, as compared to the lead-screw drive mechanism. By combining the nano-positioner with the conventional positioning mechanism such as the X-Y stage, a large motion with a very high accurate positioning capability can be obtained (Cetinkunt et. al, 1998).

It is well known that diamond turning technology facilitates the fabrication of a super mirror finished surface with nanometric surface roughness and a sub-micrometric level of form accuracy. With the use of the FTS technique (Kouno, 1984; Patterson and Magreb, 1985; Dow et. al, 1991; Miller et. al, 1994; Fawcett and Engelhaupt, 1995; Ludwick et. al, 1999; Gao et. al, 2000), surfaces of complex geometries, high form accuracy and excellent surface finish can be more easily fabricated.

In contrast to the electronic fabrication method and the optical fabrication method, diamond turning has difficulty in fabricating micro-structured surfaces with spatial wavelengths shorter than several micrometers. However, in the wavelength range of tens of micrometers to hundreds of micrometers, diamond turning is superior to the electronic method and the optical method. This is particularly true for the fabrication of high precision and complicated micro-structured surfaces (Sweeney and Sommargren, 1995). As a result, ultra-precision machining with FTS is one of the superior methods for the fabrication of micro-structured surface.

In addition to micro-structured surfaces, optical freeform surfaces with submicrometer form accuracy and nanometric surface finish have high demand in compact optical systems of multiple functions. Examples of such products include moulds for contact lenses, reference surfaces for planar encoders, as well as micro-optical devices such as multifocal lenses and micro-lens arrays. As a result, non-rotationally symmetric surfaces can be produced with optical quality finish. Possible applications include wavefront corrector plates for large optical systems, (Sechenz, 1988) scanning mirrors, optical encoders, extreme off-axis reflector, and special lenses and molds with intentional asymmetry such as coma and astigmatism.

2.3.3 Development of FTS technology

Having reviewed FTS machining technology, the development of FTS technology is reviewed. The development of piezoelectric actuator-based FTS for precision machining has been studied extensively by many researchers. For diamond turning applications, Patterson and Magrab (1985), Hara et al. (1990), Fawcett (1990), and Okazaki (1990) have presented piezo actuator-based designs for improved tool positioning accuracy as well as reduced tool vibration during precision machining. A FTS design for an ultra-precision lathe has been suggested by Donaldson and Thompson (1986), and Shamoto and Moriwaki (1997 and 1999) described a piezo actuator-based ultra-precision feed drive mechanism and an actuator design for elliptical vibration cutting, respectively.

To achieve precision positioning, the control strategy must adequately minimize cutting forces and piezo-ceramic nonlinearity. Zhu et al. (2001) presented a sliding mode control scheme for precision positioning during shaft machining, which demonstrated accurate disturbance rejection and compensation of piezo stack nonlinearity. Repetitive control techniques have been successfully implemented by Ludwick et al. (1999), Hanson and Tsao (1994) and Rasmussen et al. (1994) to achieve the minimum tracking errors in time varying positioning. Other authors, such as Kim and Kim (1998) and Kim and Nam (1997), have investigated piezo voltage feedback for position control. They have developed a micro cutting device with a piezo-electric actuator to control depth of cut precisely and compensate for the waviness on the surface of the workpiece.

With the advent of improved machines and processes, interest has been growing in a FTS mechanism to increase the capability and the capacity of existing machines. The purpose of the FTS is to move the tool a small distance into and out of the workpiece several times per revolution of the workpiece. This helps to generate non-axisymmetric surfaces or correcting errors. Many of the earlier FTS systems were used to correct various machine-related errors, such as spindle error motions or parasitic vibrations (Douglas and Green, 1979, Patterson and Magreb, 1985). New adaptations of fast travel mechanisms with very high resolution and stiffness have addressed these needs and created challenging new areas of application (Falter and Dow, 1988; Fawcett, 1990; Moorefield G. M. et al, 1994).

Different kinds of actuators have been applied in FTS systems to achieve dynamic tool feeding. They are: linear motor (Huixing et. al, 1994, Alter and Tsao, 1993), magnetostrictive (Toshiro and Yamaguchi, 1996), hydraulic (Tsao and Masayoshi, 1994), piezoelectric, and voice-coil (Reddy et. al, 2001) actuators, or their combinations (Kazuhiko et. al, 1992, Pahk et. al, 2001, Kim, 2001). There are many advantages to piezo-electric actuation systems. It is possible to make extremely fine motion in the nanometer range by altering the applied voltage which changes the stroke of the piezo-electric actuator. Since the piezo-electric actuator has neither gear nor rotating shafts, nonlinear behavior such as backlash, dead band, and friction do not exist. The piezo effect directly converts electrical energy into linear motion. The element only absorbs energy during the expansion process, i.e. charging current flows. As a result, no further energy is needed to maintain the expansion. Moreover, the speed of a positioning movement is decisive for many applications. Piezo-electric actuators are the fastest responding positioning elements and their expansion speed is only limited by the speed of sound in the ceramic material. It is possible to achieve acceleration a few thousand times that of gravity. The advantages of the piezo-electric actuator are summarized as follows:

(i) there is no backlash or friction in the actuator;

(ii) the actuator can produce large forces;

(iii) it is small and easy to control (King, 1990).

However, this actuator also has some disadvantages such as: hysteretic behavior, time drift, temperature dependence, and finite stiffness (King, 1990). On the basis of the advantages, stack type piezo-electric actuators are often used in micro-positioning systems and have been used in a micro-positioning grinding table (Zhong and Nakagawa, 1992), a probe for scanning tunneling microscopy (Jung and Kim, 1994;

Jung et. al., 1993), and a dynamic absorber (Tzou H.S., 1991). In the present study, the piezoelectric actuator is one of the best choices, and is therefore used.

2.4 Surface Generation in FTS Machining

There are still a lot of uncertainties in different research areas of ultra-precision machining since there are many independent factors which affect the surface generation in such ultra-precision machining. In this section, the factors affecting surface generation in SPDT are reviewed, which is the foundation of ultra-precision machining with FTS. Then the factors that affect the surface generation in FTS machining are discussed.

Ultra-precision machining with FTS is developed based on SPDT. SPDT is an ultra-precision machining technique which is used to produce optical surfaces (e.g. spherical and aspherical) of submicrometre form accuracy, and surface finish in the nanometre range, and is applied in a variety of applications for aerospace, industrial, consumer, and medical uses (Ikawa N., 1991; Moriwaki T., 1995).The factors affecting surface generation in SPDT include the cutting parameters (i.e. cutting speed, feed rate, and depth of cut), material properties (i.e. material swelling and plastic anisotropic property) (Kong, 2006; Cheung, 2001), vibration between workpiece and machine tool (Lee, 1999), single point diamond tool (i.e. tool wear and set-up accuracy) (Zhou, 2003) and machine tool and control (i.e. backlash and friction in the feed system, rotational axial error of spindle) (Shinno H, 1987) etc.

Even if FTS machining is carried out with the ultra-precision machine tools mentioned in the previous section in the study, there will still be distortion on the Z-axis, where the air bearing spindle is mounted, and on the X-axis where the slide feeds. The out-of-straightness of the machined workpiece is influenced by Z-axis feed and the out-of-flatness of the workpiece is influenced by the X-slide feed and by the axial error motion of the spindle. The axial error motion in ultra-precision machining has been reviewed by Bryan, 1967; Shinno, 1987; Evans, 1996; Gao, 1997.

In ultra-precision machining with FTS, the diamond tool is actuated back and forth in order to fabricate a freeform profile within the whole cutting process. One of the exclusive errors in FTS machining is the error involved in the synchronization motion between the rotational spindle and the FTS actuation, since the motion of the X and Z slides cannot easily be perfectly synchronized. This refers to tracking errors which are errors in the position of the tool compared to the reference signal of the control system; there are many sources of these errors.

First of all, the loop control system of the piezoelectric FTS employed in the present study is an open loop design, which is widely used in the commercial precision industry. Compared with the closed loop control system, it is hard for an open loop FTS system to compensate for the tracking error according to the feedback signal in real time. In addition, the hysteresis, static stiffness, drift, and the frequency response are the critical characteristics affecting the performance of FTS. One of the drawbacks is that the expansion of a piezo actuator is not exactly proportional to the electric field strength. This nonlinear behavior is a typical characteristic of piezoelectric materials and is shown in Figure 2.10.

It is deemed that the hysteresis width largely depends on the magnitude of the input voltage. For a small input magnitude, the hysteresis width is small, and it increases with an increasing of the input magnitude. The maximum width of the hysteresis curve can be as much as 10 to 20% of the path covered, which is recommended for the FTS used in the Nanoform 200 from Precitech USA.

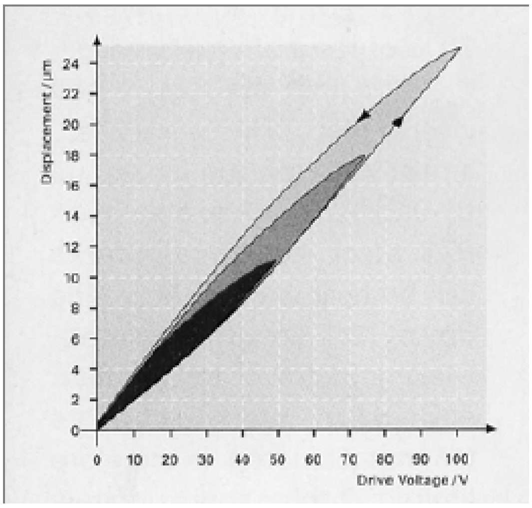

(a)Typical hysteresis loop of piezoelectric materials

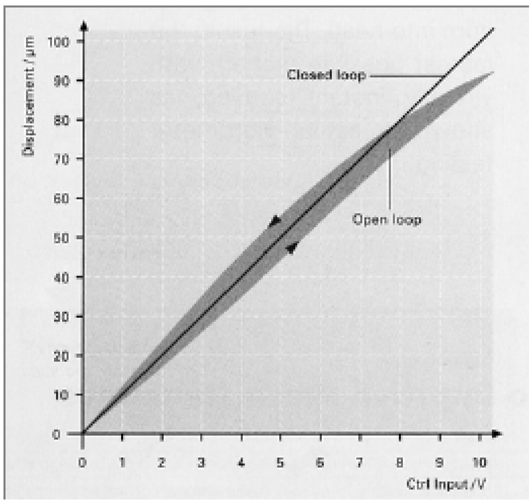

(b) Performance comparison between open loop and closed loop

Figure 2.10 Nonlinear behavior of piezoelectric materials (Sourced: Precitech, Inc.)

There are many independent factors affecting surface generation in ultra-precision machining. These factors include cutting parameters such as spindle speed, feed rate, depth of cut and surface speed, machine tool and tool geometry. Extensive research has been conducted on their effects. Cheung and Lee (2000, 2001) experimentally and theoretically investigated the effect of cutting conditions on surface generation in SPDT and developed a model-based simulation system for the prediction of the surface roughness of a machined profile by different combinations of cutting conditions. Under ideal conditions, the surface roughness profile is formed by the repetition of the tool profile at intervals of feed per workpiece revolution. Whitehouse (1994) also defined that the arithmetic roughness R_a of the ideal profile approximately by equation (2.1).

$$R_a \sim \frac{0.032 f^2}{RV^2} \tag{2.1}$$

Where R is the radius of diamond tool

f is the feed rate

V is the spindle speed

In ultra-precision machining with FTS, cutting parameters have a significant influence on the surface quality of the machined components. However, relatively little research has been focused on exploring the effect of these factors on surface generation in FTS machining. There is a vital need to investigate the factors affecting surface generation in FTS, and the results would contribute to the further study of the cutting mechanisms of FTS machining, facilitating the development of a prediction system in FTS machining.

A single crystal diamond tool is usually used in FTS machining and the wear of such a diamond tool would also plays an important role in surface generation. Tool wear is commonly divided into two types, which are progressive wear and chemical-abrasive wear, respectively. Cutting edge chipping of progressive wear takes place when the stress level in a tool edge exceeds the strength of the diamond at a specific location. Progressive wear occurs on both flank and rake faces in a submicrometer scale over a cutting distance of normally up to several hundred kilometers. The diffusion wear problem occurs in diamond turning of ferrous materials, which is due to the chemical affinity of the diamond with the carbon in the steel.

As diamonds have little affinity with a variety of materials, a diamond cutting edge is considered to have a high transfer fidelity, which is the ability to transfer the profile of a cutting edge to the work surface. Even when machining soft materials such as nonferrous metal, the wear on the cutting edge grows substantially as the cutting length increases (Taminiau and Dautzenberg 1991, Keen 1971). Moreover, the profile of a machined surface is basically composed of the repetition of the tool profile transferred to the plane normal to the cutting direction. As a result, the geometrical accuracy of the cutting edges and their stability have great influence on the surface roughness of the machined profile. Tool wear not only degrades product quality but also raises the machining cost.

For the single crystal diamond tool employed in FTS machining, the tool should be sharp with an extremely small tool radius, which is more easily degraded and susceptible to the influence of tool wear. To minimize diamond tool wear, many studies have been carried out to explore the characteristics (Yan 2003, Sharif Uddin, 2004 and 2006 and Durazo-Cardenas 2007). In addition, a better understanding of the performance of diamond tools employed in ultra-precision machining with FTS is resulted in significant enhancement of the fabrication process and easier control of the quality of the machined surface.

2.5 Measurement and Surface Characterization

The success of the FTS machining relies heavily on the associated surface metrology which helps to characterize the quality of the machined surface. As shown in Figure 2.11, the present situation concerning surface metrology can be illustrated with respect to the traceability of the surface measurement (Chiffre et al. 2003). There is a range of different measuring instruments in terms of amplitude and wavelength measurement. Figure 2.12 shows the calibration standards for various measuring instruments (Chiffre et al. 2003).

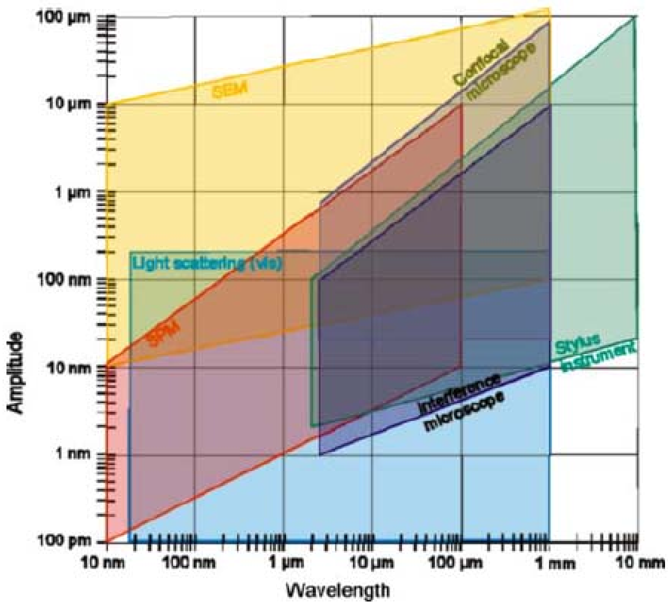

Figure 2.11 Diagram of wavelength vs. amplitude for different surface roughness instruments (courtesy of the PTB). (Source: Chiffre et al. 2003)

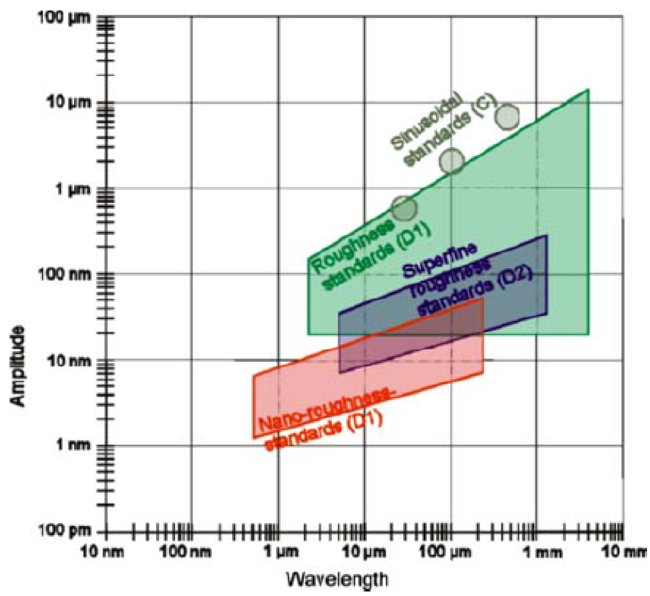

Figure 2.12 Diagram of wavelength vs. amplitude for different surface roughness calibration standards (courtesy of the PTB). (Source: Chiffre et al. 2003)

Actually, there are a lot of challenges in the field of surface metrology. Even with advanced design tools and ultra-precision manufacturing technologies, the required accuracy of optical surfaces can often not be achieved in a deterministic manufacturing process. Besides the statistical variation of the machining process, the least changes in the boundary conditions lead to noticeable form deviations. As a result, the manufacturing is performed iteratively. Hence the accurate measurement of the absolute shape of the surface is the missing key factor in the value chain of freeform optics manufacturing (NANOMEFOS Project, 2006). Even though a lot of effort has been made to establish machine integrated ultra-precision form testing and to enable an adaptive manufacturing process (Nishiguchi et.al, 1991; Schmitt and Doerner, 2006). The fundamental metrology specific challenges for optical surfaces still remain. Functional surfaces with their macroscopic dimensions demand a very high accuracy which is counted in the nanometer range. The dynamic range of the test equipment is the crucial point in measuring optical freeform shapes. Another important demand is that the delicate optical surfaces must not be damaged by any inspection.

Most of the surface topography measuring instruments operate under three major principles, which are touch probing, optical scanning and Scanning Probe Microscropy (SPM). All these instruments are well known in industry and are applied to give quantitative information of measured surface profiles. In the present study, the measurement instruments with touch probing and optical scanning techniques have both been employed.

Stylus profilometry instruments based on the touch probing technique has wide acceptance for surface measurement. This is not only due to its traceability but also its ability to measure large areas. While measuring surface profiles, a stylus is drawn over the surface and a transducer measures the vertical displacement with resolutions that can be nanometric over a range of 10 millimeters or even more (De Chiffre et al., 2000). However, this principle always limited their applications because the mechanical contact force may scratch the measured surface. In addition, tip geometry and size becomes another problem when measuring tiny objects.

Another measurement principle employed in the surface data collection process is the optical scanning technique which typically consists of optical profilometers, confocal microscopes and interferometers. The instruments using optical methods can measure without physical contact, even on soft surfaces. The Wyko NT8000 non-contact profiler system is employed in this research and operates under the principle of white light interferometer. It provides fast and high vertical resolution measurement without damage to the surface profile. The limitation encountered is lateral resolution and maximum detectable slope. This is because the data collection relies on the reflection of light from the measured surface. If the measured surfaces are too much inclined, the reflection light scatter and thus the instrument would fail to output the entire surface profile. Nevertheless, white light interferometer instruments are usually employed to measure the roughness of flat surfaces, film thickness, and low aspect ratio Micro-Electro-Mechanical Systems (MEMS) and optical surfaces.

After measuring the surface topography with a precision instrument, the next challenge is form characterization, which can be described as the reconstruction of a continuous surface from discrete data (Rice, 1983). For assessing the surface quality in an ultra-precision machined profile, one of the critical parameters is form accuracy or form error. Form accuracy cannot easily be directly outputed from the measured raw data. To obtain the form error, further analysis is always needed for separating the form and the irregularity. Algorithms for form characterization of discrete data from the measurement of spherical form have also been developed (Cross, 1996 and McBride 1996). The algorithms can be used for the analysis of surface form and for the separation of form and irregularity. The irregularity is a term used instead of waviness and/or roughness (Dagnall H, 1998), where the irregularity can be a combination of symmetrical and nonsymmetrical deviations from the nominal surface geometry. Conventionally, the separation of surface components is accomplished by using a polynomial fitting based on the least squares principle (ISO 4287-1997, 1997).

This principle, which is mathematically well defined and widely used in industry, is also employed in the present study. The criterion requires that the sum of the squared errors be minimized. Hence, all the measurement points contribute to the best fit result. The fitted feature is very stable and much less sensitive to the effect of asperities. Although the form error computed from the extreme points can be slightly higher than that obtained from the minimum zone method, the least-squares algorithm is very reliable and flexible, which makes it suitable for many practical applications (Yuai, 1996)

Another problem that must be solved for a best-fit surface is that the parameters must be derived through an error function or residual error. The residual error is usually defined as the shortest distance between the measured surface and the best-fit surface. In most cases, the aim is to find the parameters for which the residual error is the minimum. The parameters are then the best-fit parameters, with respect to the applied minimization norm (Rice, 1983).

In order to study the effect of process factors in surface generation in FTS machining, the surface quality of the workpiece is assessed based on a standardized reference. In the present study, the surface quality of the fabricated surface profile is assessed by the surface roughness and form accuracy in terms of standard parameters. The machined surface inherits characteristic irregularities on the surface caused by the cutting tool. The direction of the predominate surface pattern (known as the lay) in turning lies in the feed direction of the cutting tool. As shown in Figure 2.13, the commonly used standard parameters for surface quality are given as follows:

(i) Peak- to-valley height R_t which is the difference between the highest peak and the lowest valley over the sampling length.

(ii) Arithmetic roughness R_a which is obtained by measuring the mean deviation of the peaks from the center line of a profile trace.

(iii) R_q is the root-mean-square value which gives the root mean square deviation defined relative to a mean line. (RMS = 0.9 R_a for a sine wave).

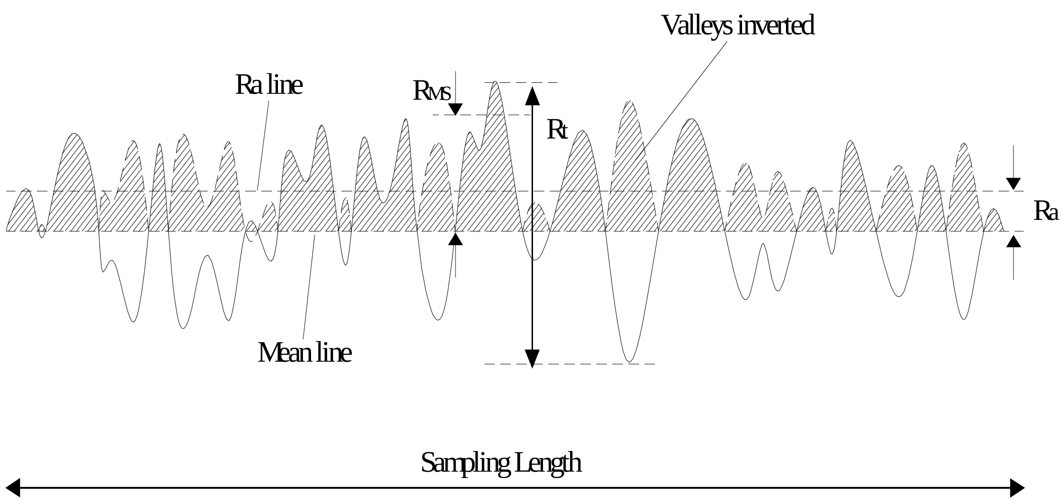

Figure 2.13 Description of surface parameter (Whitehouse, 1994)

2.6 Summary

In the last few decades, a lot of ultra-precision machining technologies have been developed and applied for the fabrication of complex surfaces. These methods have been widely used in the fabrication of emerging products. Examples of applications include computer chips, data storage, MEMS, biomedical system, Micro-optical systems, X-ray optics and implants.

Ultra-precision machining based on fast tool servo (FTS) machining provides a solution for machining complex surface profiles such as optical microstructures with sub-micrometer form accuracy and nanometric surface finish without the need for any subsequent post processing. Although there has been extensive research on the design and control of tool actuators for FTS machining (Ludwick et. al., 1999; Hanson and Tsao, 1994; Rasmussen et. al., 1994; Kim and Kim, 1998), relatively little work has been reported in studies of the nano-surface generation in the FTS machining. Moreover, there is a need to study the performance of FTS machining for minimizing the sources of error. As a result, a theoretical and experimental investigation was undertaken to study the process factors and systematic factors involved in FTS machining.

CHAPTER 3 RESEARCH METHODOLOGY AND THEORETICAL BACKGROUND

3.1 Research Methodology

In the present study, the research focuses on the investigation of factors affecting surface generation and hence on the development of a theoretical model for the analysis of the error motion in FTS machining. As shown in Figure 3.1, the entire project can be basically divided into three phases, i.e. Phase 1, Phase 2 and Phase 3, respectively.

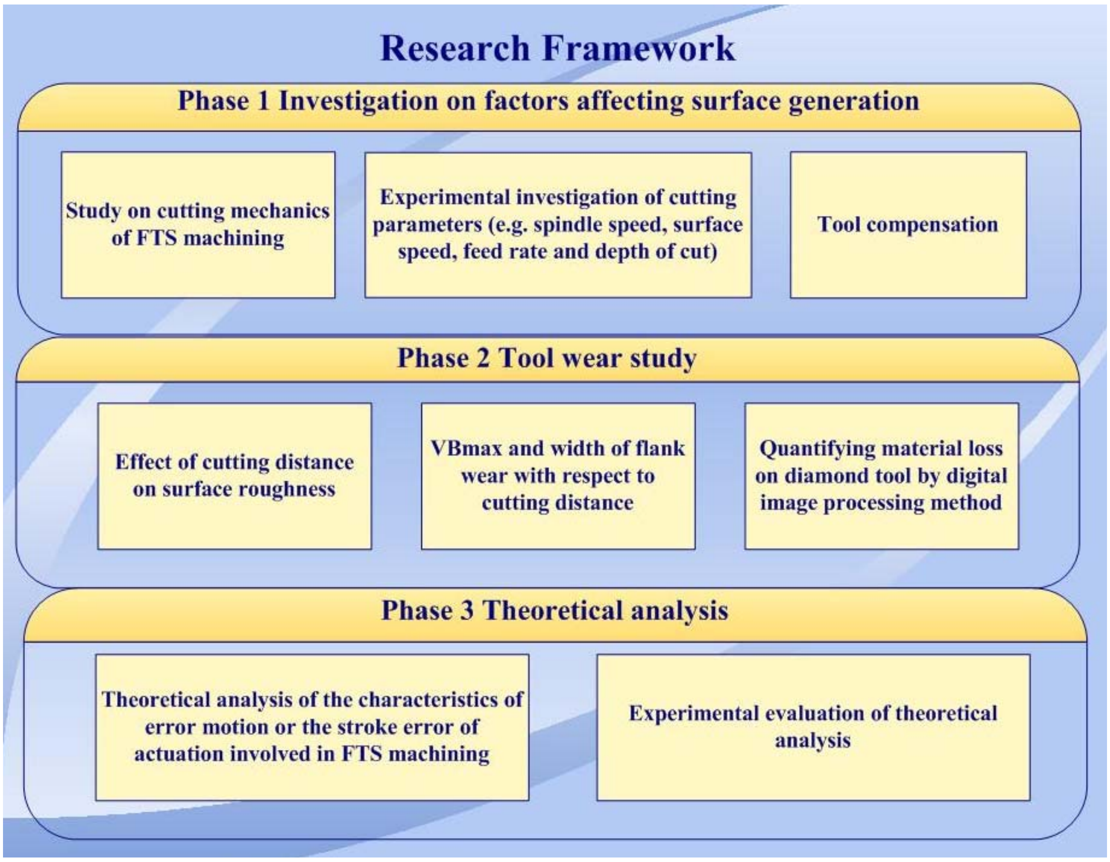

Figure 3.1 Research Framework

In Phase 1, the cutting mechanics and the surface generation mechanisms for the FTS machining are investigated first. A series of cutting experiments are conducted to study the factors affecting the surface generation in FTS machining. The experiments are undertaken on a Nanoform 200 ultra-precision machine which incorporates an FTS system. The factors studied include the cutting parameters such as spindle speed, surface speed, feed rate and depth of cut. The surface data of the machined surfaces are measured by a non-contact interferometric surface profiler. To further analyze factors affecting surface generation in FTS machining, defect analysis, tool compensation and pattern analysis were also conducted.

Single crystal diamond tools with small radii are usually employed in FTS machining to fabricate complex optical profiles. However, these sharp tools are easily susceptible from tool wear which adversely affects the surface quality of the machined surface. As a result, Phase 2 focuses on the characterization of the tool wear and investigating its effect on FTS cutting. A series of cutting experiments are conducted to determine the wear characteristics of the diamond tools and the surface quality. The material loss of tool wear is successfully quantified by a digital image processing method purposely built for the present study.

In order to investigate the exclusive factor encountered by FTS machining – error motion of FTS actuation – a specially designed experiment and theoretical analysis are undertaken. Although the hysteretic effect and the limitation of bandwidth constrains the quality of the machined profile, they are drawbacks in the use of piezo-electric actuators. In the present study, the major focus is to explore the characteristics of error motion or the stroke error of the motion of the actuation involved in FTS machining.

In this chapter, the design of the equipment employed in the cutting experiment, the measurement facilities employed for assessing the surface quality of the workpiece, the surface characterization algorithm and tool wear analysis method is described. This provides foundation information for the later parts of the investigation.

3.2 Cutting Mechanics of FTS Machining

Ultra-precision machining with FTS is developed based on single point diamond turning (SPDT) technology. The fundamental cutting mechanics of both SPDT and FTS machining are similar, which are distinctly different from conventional turning (Zhang, 1991) with respect to the depth of cut in the range of a few micrometers to hundred micrometers, which is comparable to the grain size, as shown in Figure 3.2.

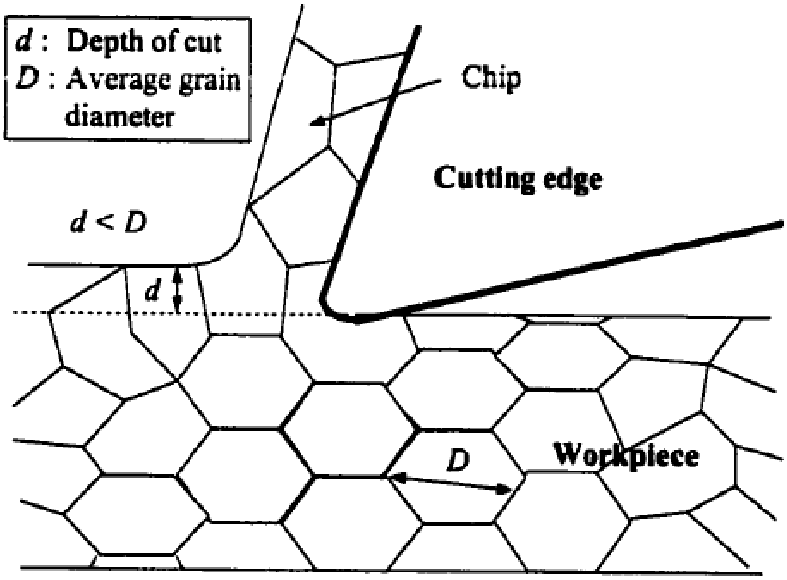

Figure 3.2 Orthogonal cutting of polycrystalline materials in Single Point Diamond Turning (Cheung and Lee, 2000)

In the conventional turning process, most of deformation occurs in the metal layer which is cut into chips, while the deformation below the machined surface is less. However, the deformation below the machined surface is very important in SPDT. This is because the undeformed chip thickness is very small while the deformation caused by the compression and friction between the tool and the machined surface plays a significant role in the cutting process (Zhang, 1991). With a small depth of cut and a fine feed, cutting naturally performs with single crystal nature.

As mentioned in literature review, the diamond tool should be positioned under the nanometric level and varied according the desired profile under a higher frequency than that of a rotational spindle in order to enable diamond turning of complex profiles, such as optical microstructures and non-rotationally symmetric surfaces. This is virtually impossible using the conventional turning process since there is backlash and friction in the lead-screw drive system from the actuation point at the servo motor rotor to the tool position. In FTS machining, the FTS is an independently operated positioning device mounted on the XY stage of the ultra-precision machine for increasing the tool positioning accuracy. The diamond tool fixed on the FTS can be activated back and forth by a stacked type piezoelectric actuator at a bandwidth significantly higher than the rotational frequency of the fabricated surfaces. By combining FTS with the ultra-precision machine, complex motion with high accurate positioning capability can be obtained. Consequently, a high quality optical surface with surface roughness in the nanometer range and form accuracy in sub-micrometer range can be fabricated without the need for any post processing.

In the present study, the cutting experiments were performed on a two-axis ultra-precision machining system named Nanoform 200 from Precitech Inc (USA). As shown in Figure 3.3, the Nanoform 200 is an ultra-precision computer controlled contouring machine for diamond turning of non-ferrous metals, crystals and polymers and grinding of various optical surfaces equipped with a compact, hydrostatic oil bearing sliding, two-axis linear motor and an air bearing spindle. In SPDT, a rotating spindle holds the workpiece and the cutting tool is fed into the work. Unlike a conventional lathe, the Nanoform 200 has the work holding spindle mounted on the

"X" axis which is perpendicular to the cutting tool in the "Z" axis.

(a) (b)

Figure 3.3 (a) Ultra-precision diamond turning machine (Nanoform 200) (Source: Precitech Inc, USA) equipped with (b) Fast Tool Servo

In FTS machining, a feed motion in the X-axis is provided, the same as SPDT, while the actuation of the diamond tool in the Z-axis is according to the preset cutting path under the uninterrupted rotation of the spindle. Figure 3.4 shows the configuration for FTS machining. Under ideal cutting conditions, the machined surface should be formed by the repetition of the tool tip profile at intervals of tool feed rate in the X-axis and the actuation of the diamond tool by FTS in the Z-axis, which is according to the cutting path of the desired profile. The cutting mechanism and machined profile of FTS machining are schematically shown in Figure 3.5.

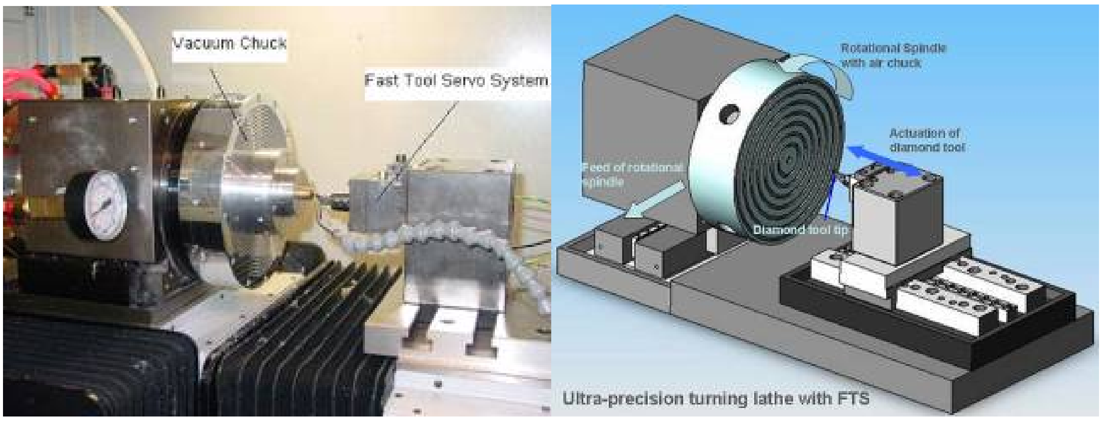

（a） (b)

Figure 3.4 (a) Equipment and (b) Configuration in FTS machining

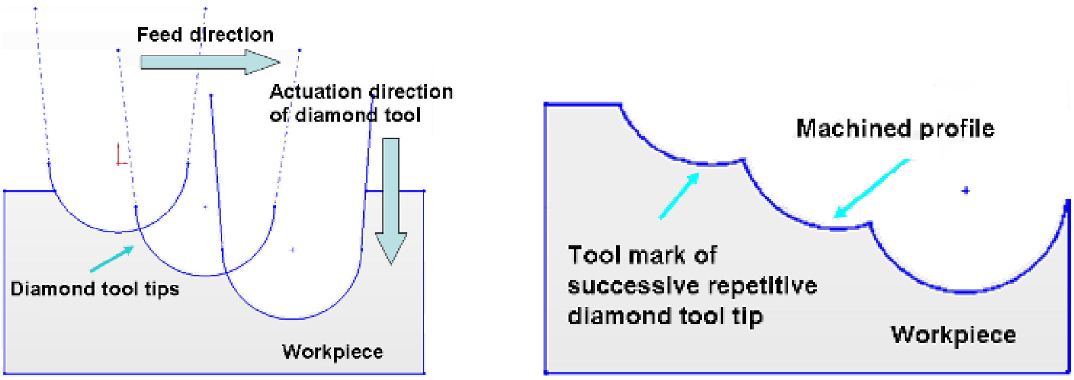

Figure 3.5 Schematic diagram of cutting mechanism in FTS machining

The FTS employed in the present study is a piezoelectric type of actuator and the full operating range is 35 μm, with a fast dynamic response of 1000 Hz cut frequency bandwidth. C-program or grayscale bitmap are used for communication with the Standard Operating Procedure (SOP) which is a control system for the FTS machining. In the SOP program, two specific parameters are defined for the location of the position of diamond tool in a polar coordinate system. They are radius (r) and phi (ϕ) which indicate the distance between the cutting tool and the center axis of the spindle and the angular location of the rotational spindle, respectively (See Figure 3.6).

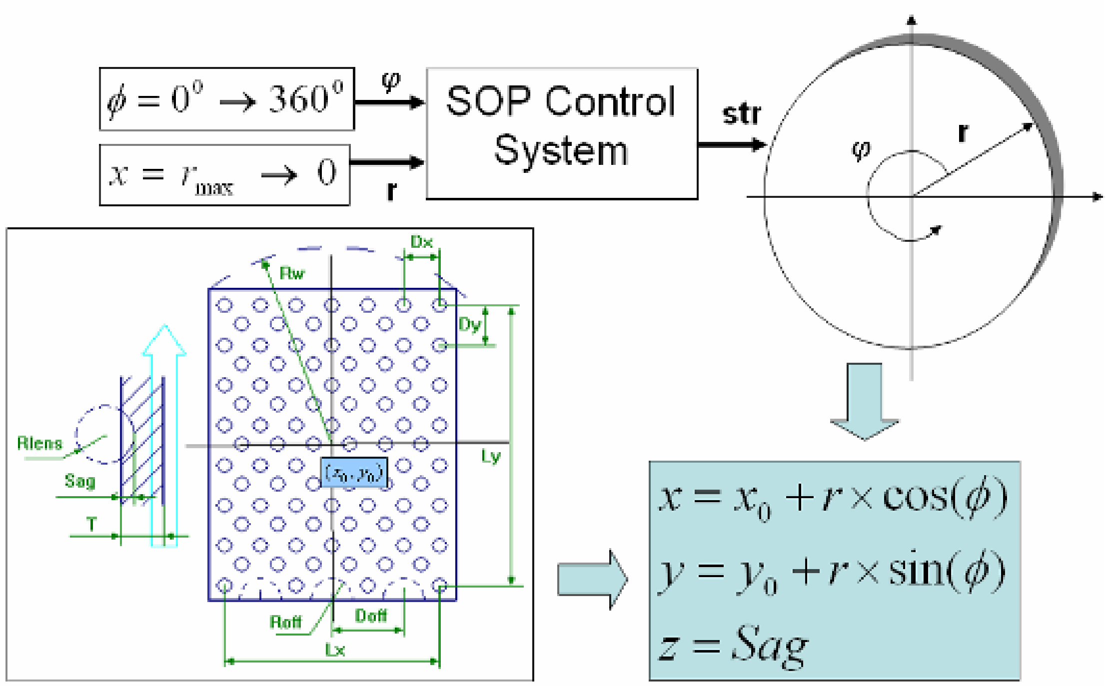

Figure 3.6 Mathematical communication with SOP control system

These two parameters can be employed to describe mathematically the position to be cut based on the reference point – the center of the workpiece. Based on the radius (r) and phi (ϕ), both conventional and non-rotationally symmetric optical elements could be mathematically determined quantitatively for the FTS machining system. Figure 3.7 shows the detailed mathematics and the profile of optical elements.

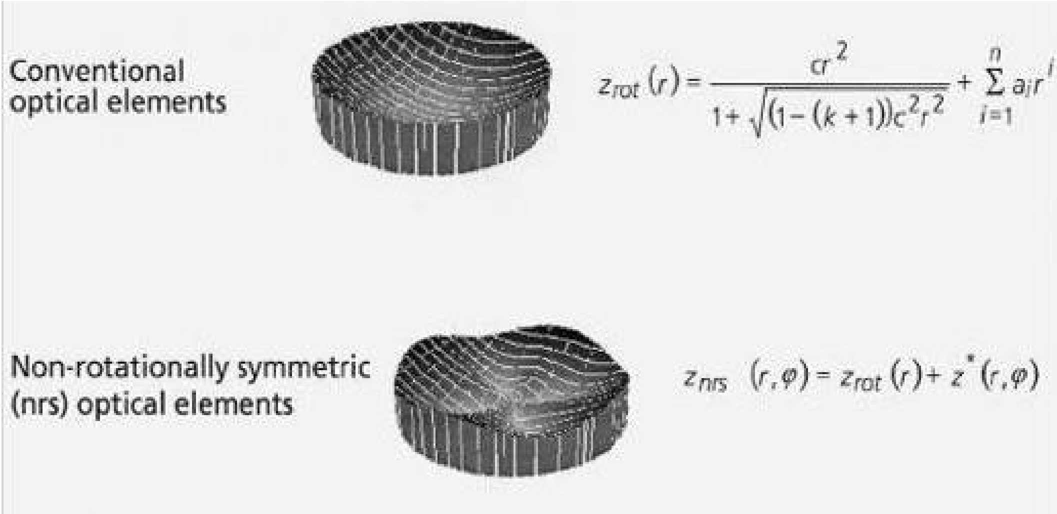

Figure 3.7 Mathematical description of FTS profiles (Source: Precitech, Inc.)

After the program input, simulation can be carried out by SOP before the actual cutting. Figure 3.8 shows the synchronization of the tool path for the FTS machining microlens array pattern. During the machining of an optical profile, the cutting path of the diamond tool nose is calculated in real time based on the feedback signal from the sensors mounted on the ultra-precision machine. In addition, the Z location of the diamond tool is also reported in real time for controlling the movement of the strokes.

During the cutting process, the cutting position of the diamond tool needs to be calculated in real time. Thus, angular and linear sensors are mounted on the rotational spindle and driving slide separately so as to transfer the feedback signal to the FTS control system. The linear sensor – Precitech 18000 – installed on the x-axis and the z-axis is capable to output 18000 imports per millimeter. An incremental angle encoder (ROD-260, made by Heidenhain Compact) is mounted on the spindle, and is used for measuring the rotation steps of the spindle to a resolution of 0.005°, with 5v and output 26000 of imports for one rotation. The machine interface, including the sensors feedback system, is shown in Figure 3.9. In combination with the SOP control system, which has a user friendly software interface, the FTS machining allows for the efficient fabrication of complex optical profiles.

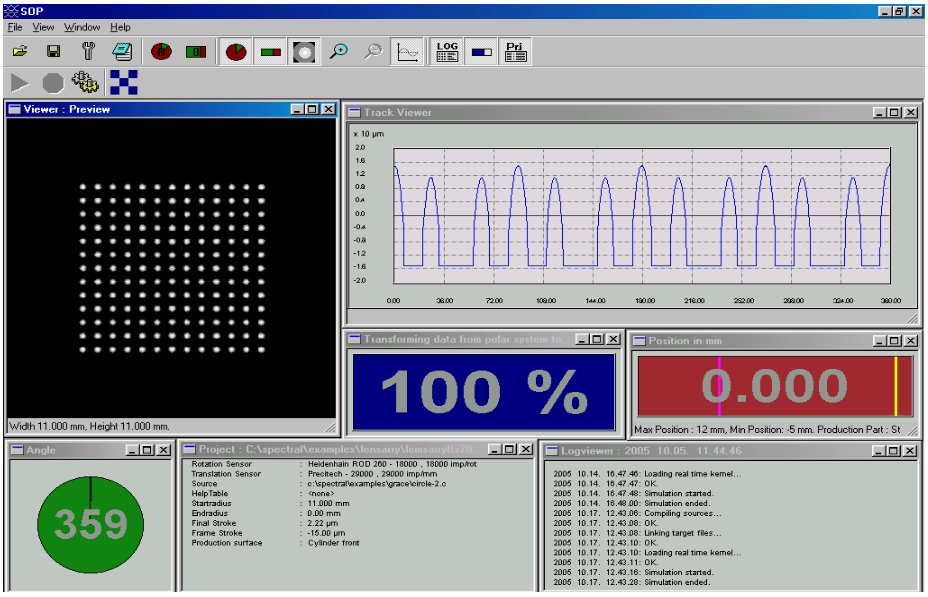

Figure 3.8 Tool path synchronization of microlens array pattern by the FTS controller

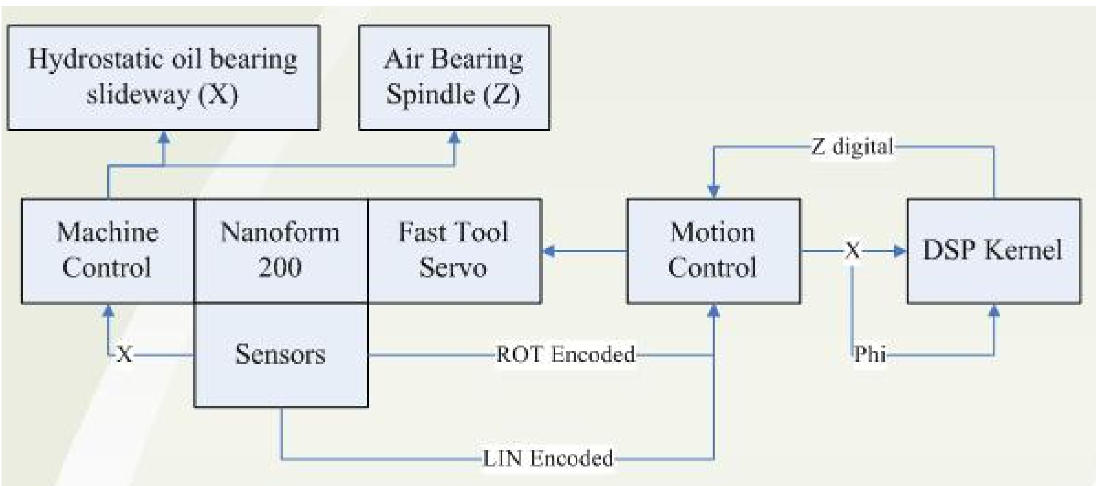

Figure 3.9 Signal processing in the fabrication of a microlens array

3.3 Measurement Instruments

In FTS machining, the machined surfaces possess submicrometer form accuracy and surface finish at the nanometer level. For measuring such kinds of surfaces, extreme high precision measuring instruments are used to inspect the surface quality of the fabricated profiles. A wide range of instruments have been employed for the measurement of machined surfaces. These instruments can be classified by their working principles into two main types, which are the stylus type and the optical interferometric type of instrument. Both types of measurement instrument have been employed in the present study.

Figure 3.10 shows a typical stylus type instrument named Form Talysurf, from Taylor-Hobson in the UK. The stylus type instrument makes use of touch probing (i.e. the stylus) technique to capture the surface data from the workpiece. The working principle is shown in Figure 3.11. Based on a very high resolution Linear Variable Differential Transformer (LVDT) or Laser Interferometric sensor, such as those used in Talysurf and Talystep and a diamond probe with a tip radius of typical 1 μm, the instrument can measure a surface profile with a height resolution of 1 nm. However, the stylus type of measuring instruments suffers from the potential risk of making scratch marks on the measured surface and the limitations imposed by the physical dimension of the stylus head. Talysurf is mainly employed to measure 2D machined surfaces.

Figure 3.10 Talyor-Hobson Form Talysurf

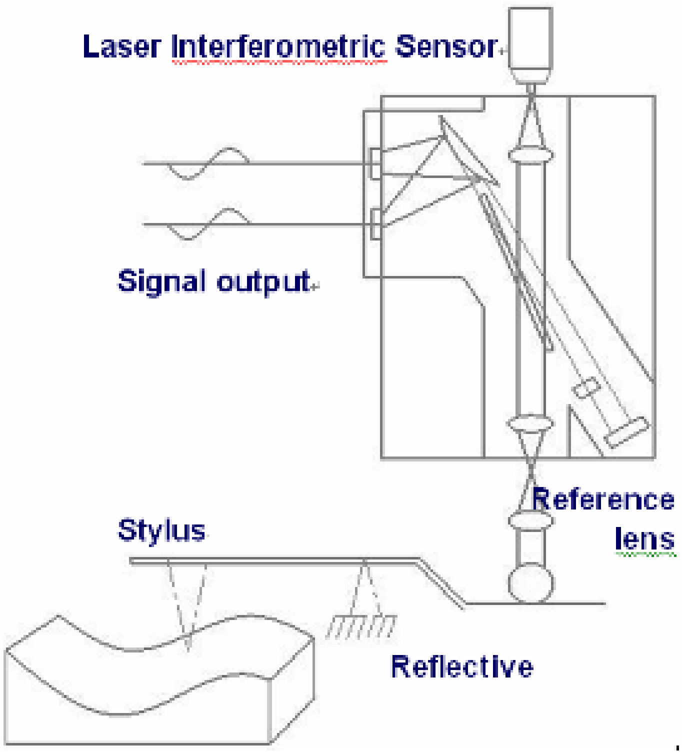

Figure 3.11 Schematic diagram of the working principle of the stylus type instrument

The optical interferometric type of surface metrology instrument employed in the present study is a Wyko NT 8000 (see Figure 3.12). This non-contact optical profiling system uses White Light Interferometry. Phase-measurement interferometry has been well known for many years, and various interferometeric techniques have been used to measure microsurface roughness.

Figure 3.13 presents the working principle of the interferometric type of surface metrology instrument. The optical data used to construct the surface topography of the measured surface are created from a phase interferometer. Both the light path reflecting off the workpiece surface and the light path reflecting off the reference surface are combined inside the magnification head to produce fringes, which are digitized and processed to give a 3D surface topography. It can measure the entire surface in a single measurement with a sub-nanometer resolution in a movement of the Z-axis. Surface roughness down to 0.01 nm can be measured with no contact or damage to the surface being measured. Other features include advanced 2D and 3D data analysis and visualization with stitching capability. The fast automation function makes the measurement of multiple devices rapid and easy. Interferometric techniques are limited by the amount of light which is reflected, or scattered off the measured surface and returned through the microscope objective. As a result, the performance is affected by the reflectivity of workpiece material. Although there are some available technologies for the evaluation of surface quality of the workpiece, they have their pros and cons. The use of a particular technology depends on the industrial need.

Figure 3.12 Wyko NT 8000

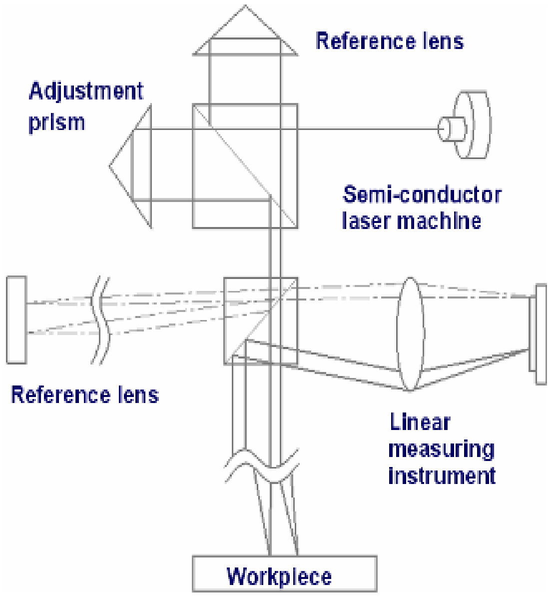

Figure 3.13 Schematic diagram of working principal of interferometric type instrument

To characterize tool wear phenomena, scanning electron microscopy (SEM) is used to capture the image of the the diamond tool tip. SEM is a microscopy method which is based on scanning an electron beam on the specimen. The interaction between the beam and the specimen surface leads to several emissions, which can be detected and used to characterize physical and chemical properties of the sample under investigation. The microscopy technique of SEM enables measurement with magnification levels of 100x to 100.000x, resolution down to 2 nm (for highest magnification), large depth of field, long working distance (allowing multiple positioning measurement strategies), elemental analysis capability and minimum diffraction effects (Rai-Choudhury, 1997). Compared with optical microscopy, SEM is limited by high vacuum requirement, relatively low throughput, potential for sample charging, electron beam/sample interaction etc. (Rai-Choudhury, 1997). Nevertheless, SEM is still a very good instrument with excellent performance on visualizing surface topography. The working principle of SEM is illustrated in Figure 3.14. The facility employed in the present research is in the Material Research Laboratory of The Hong Kong Polytechnic University, as shown in Figure 3.15.

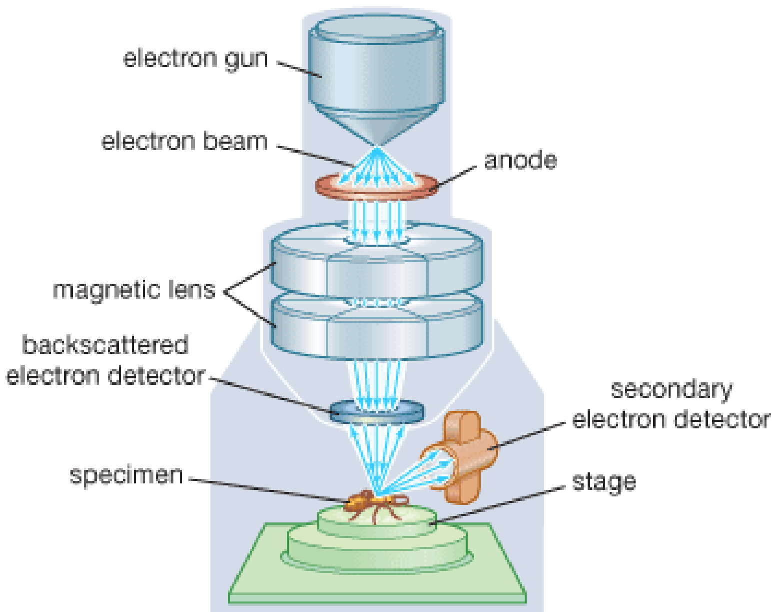

http://www.britannica.com/EBchecked/topic-art/380582/110970/Scanning-electron-microscope

Figure 3.14 Working principle of SEM (Source: Britannica, Inc)

Figure 3.15 Scanning Electron Microscope (Leica Stereoscan 440) in Material Research Laboratory of The Hong Kong Polytechnic University

3.4 Characterization of Surface Generation in FTS machining

As mentioned in the previous section, one of the precision instruments employed in the study is non-contact profiler system. With the aid of VISION software, the measured data can be analyzed and exported for the assessment of the surface quality of the workpiece. This specific software is a leading industrial data analysis software which provides true 3D mapping, with over 200 analysis tools, powerful filtering and a comprehensive parameter set.

3.4.1 Characterization of individual surfaces

To access surface quality, the measured machined surface such as individual optical microstructure is analyzed to obtain form error or accuracy. A form characterization algorithm built in the VISION software is needed for separating the form and irregularity by further aspherical subtraction between the theoretical profile and the measured data. This provides an important means for the characterization of surface quality in FTS machining of optical microstructures. In the measurement process, limited window size or field of view of optical instruments constrains data collection. The built-in stitching function is employed which allows for the making of a composite image from several “pieces” of a larger sampling area in a single process (See figure 3.16), and the area of the measurement is enlarged while preserving the resolution required to view small features.

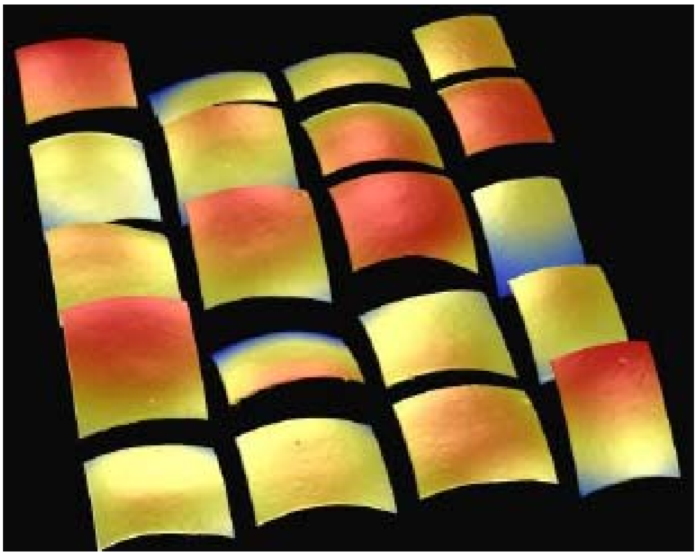

Figure 3.16 Stitching function of Vision – surface data analysis software (Source: Veeco Inc.)

In the present study, the methodology for analyzing the form accuracy is to generate a reference surface based on the original design parameters and then subtract the measured data. After subtraction, the output is a planar surface, which is the form error of the measured surface. The process flow is illustrated schematically in Figure 3.17. As a result, the first critical aspect is to correctly align the measured surface with the design surface. The alignment algorithm employed in Vision is the least root mean squares best fit. With the assistance of the Vision software, the subtracted reference algorithm can be used in aspheric subtraction after alignment of the measured and design spheres. The form accuracy of the machined surface is determined by further analysis of the measured data by Wyko NT8000 non-contact optical profiling system.

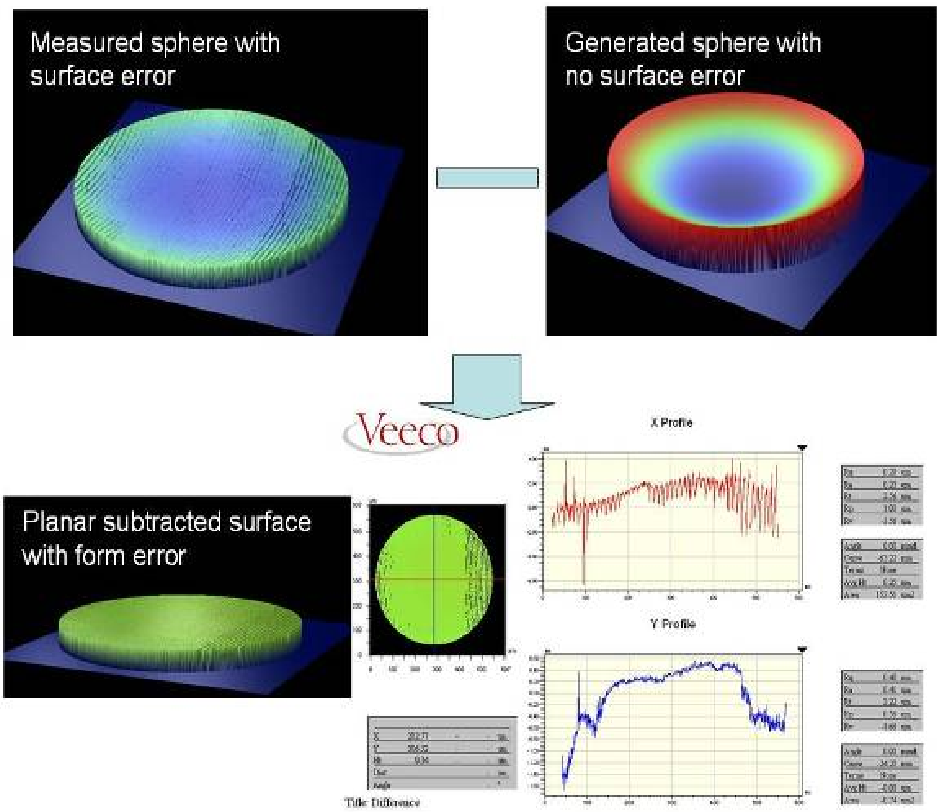

Figure 3.17 Assessing form error by subtraction of generated sphere from measured sphere

3.4.2 Characterization of the pattern of surfaces

FTS machining is usually used for the fabrication of complex optical profiles such as micro lens arrays. The technological challenges encountered in the analysis of the patterns of surfaces are characterization of the array patterns and matching of the generated patterns with the measured array patterns. With the contribution of the research team in the Advanced Optical Manufacturing Centre (AOMC) in Department of Industrial and Systems Engineering of The Hong Kong Polytechnic University, a surface characterization system based on pattern analysis technology was purposely built for the characterization of the microlens array pattern in the present study. A prototype of the system has been built using the Matlab software package. The system has been used in the study of surface generation of microlens array patterns in FTS machining.

The first step of the pattern characterization is to import the measured data into the system for analysis. In the measurement process, especially the optical profiling system employed here, it is impossible to collect all the data points on the machined profile, and any missing data may disrupt the data reconstruction and further analysis. To tackle this problem, the 4-neighboured points averaging method based on Equation (3.1) is used as a means for processing the missing points. Figure 3.18 shows the flow chart of the 4-neighboured points averaging method employed for filling up the missing points.

$$P_{m,n} = \left(P_{m-1,n} + P_{m+1,n} + P_{m,n-1} + P_{m,n+1}\right)/4 \tag{3.1}$$

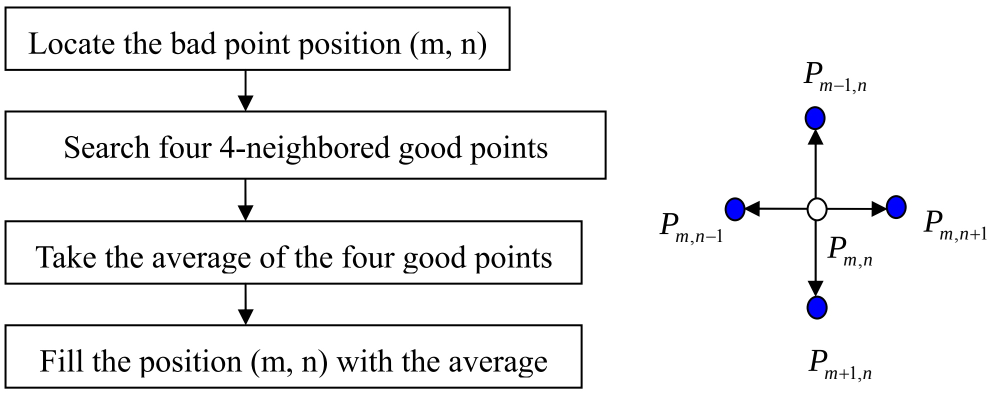

(a) (b)

Figure 3.18 4-neighboured points averaging for filling the bad (missing) points

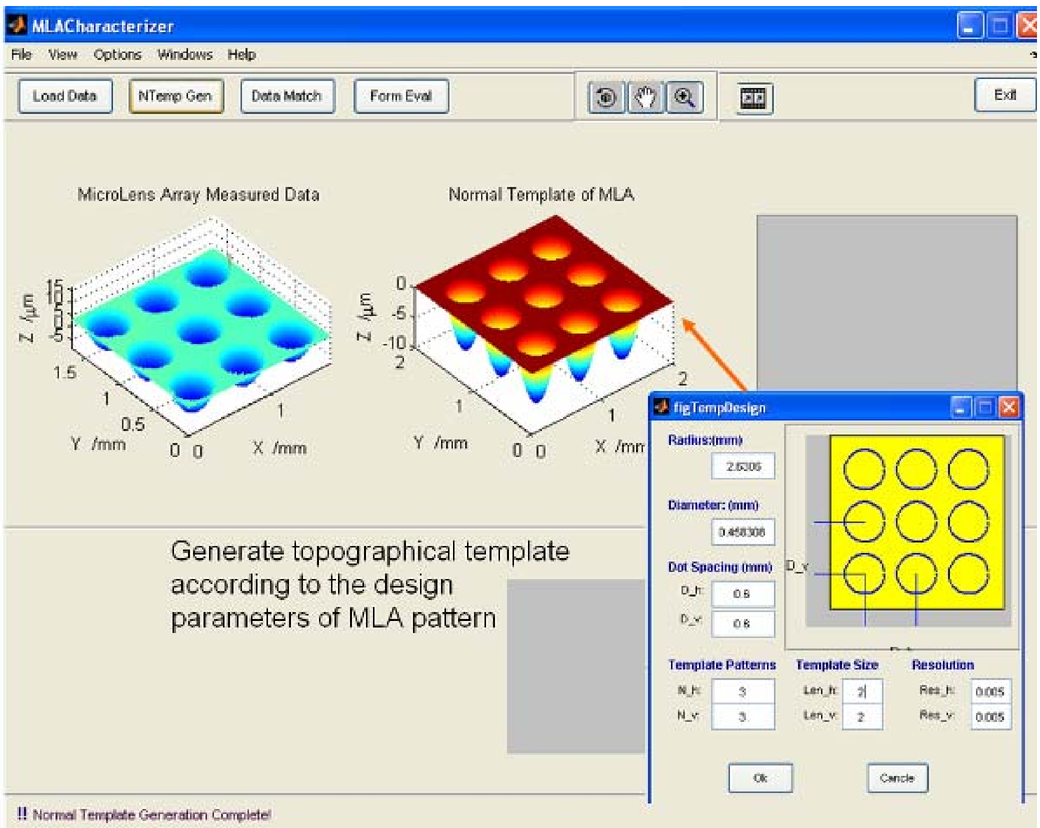

Figure 3.19 Interface of template generation in MLA pattern Analysis

Having imported the measured data, an ideal surface topography needs to be generated according to the design parameter of the microlens array (MLA) pattern, which would be used as the reference surface for assessing the form error of the machined profile (see Figure 3.19). The generated template of the MLA pattern consists of the micro-structural surface (SS) and the planar surface (PS). Figure 3.20 shows a graphical illustration of the generated microlens array pattern as well as the algorithm employed for template generation.

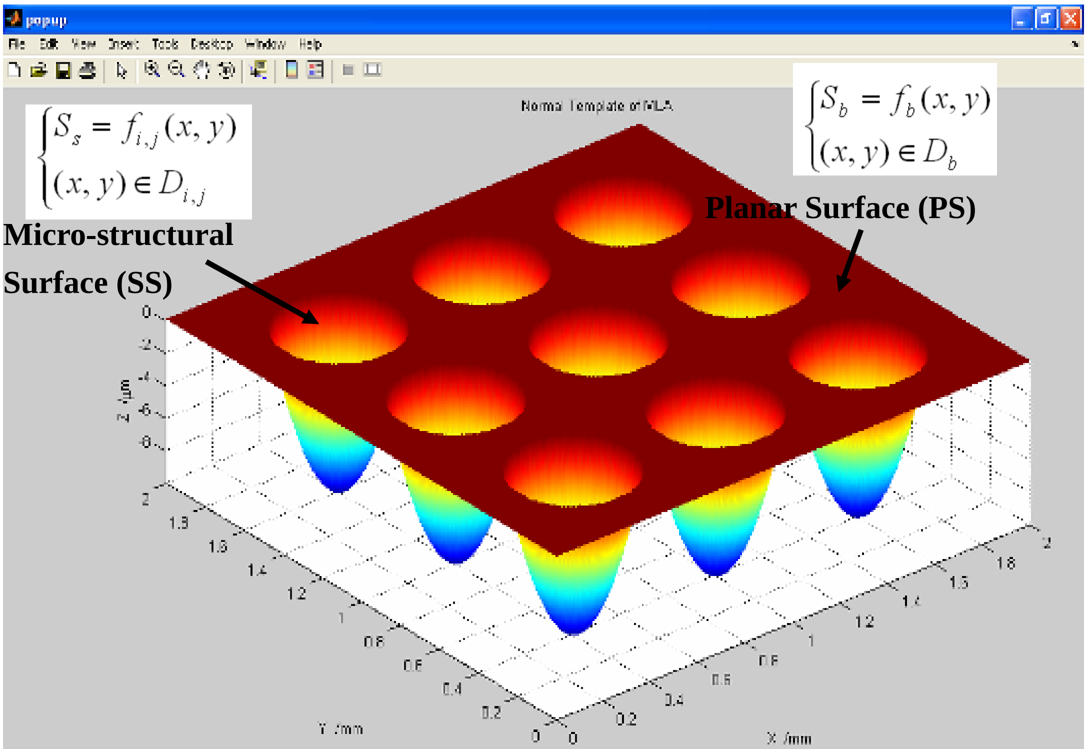

Figure 3.20 Graphical illustration of microlens array pattern

After generation of the ideal surface topography, the most critical technological problem to be solved is the matching of the measured microlens array (MLA) data with the simulated ideal profile for subsequent assessment of form accuracy. The surface characterization algorithm consists of two major procedures which are rough matching and precise matching, respectively. In the stage of rough matching, the planar surface of the microstructural surface and measured profile are employed for fitting in the Z-axis of the coordinate system. Afterwards, specific features of the microstructural surface such as valley points of the microlens are used for the reorganization of the relative location of the micro-lens in the coordinate system. The data are reconstructed into a format of $[(m_k, n_k), r]$. This process is repeated region by region until completion of the identification of the data of the structural surface as well as the X-axis and the Y-axis fitting in the rough scale. Figure 3.21 shows the flow chart for the regional identification process of the microstructural surface.

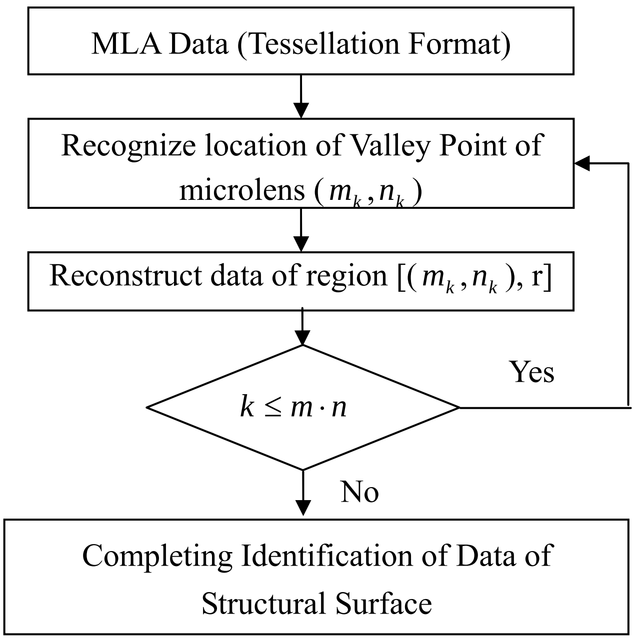

Figure 3.21 Flow chart for regional identification process of structural surface

Having finished the rough matching by feature recognition, precise matching is conducted. In this stage, the system searches for the best fit position between the measured and the generated profile. Afterwards, the method of linear squares is employed to calculate the residual error between the measured value and the generated ideal profile. Finally, the form error parameters such as root-mean-square value of 3D surface error (S_q) are used for quantifying the 3D profile. They are the output to assess the surface quality of the entire micro-structural array pattern. Figure 3.22 shows the schematic illustration employed for data matching.

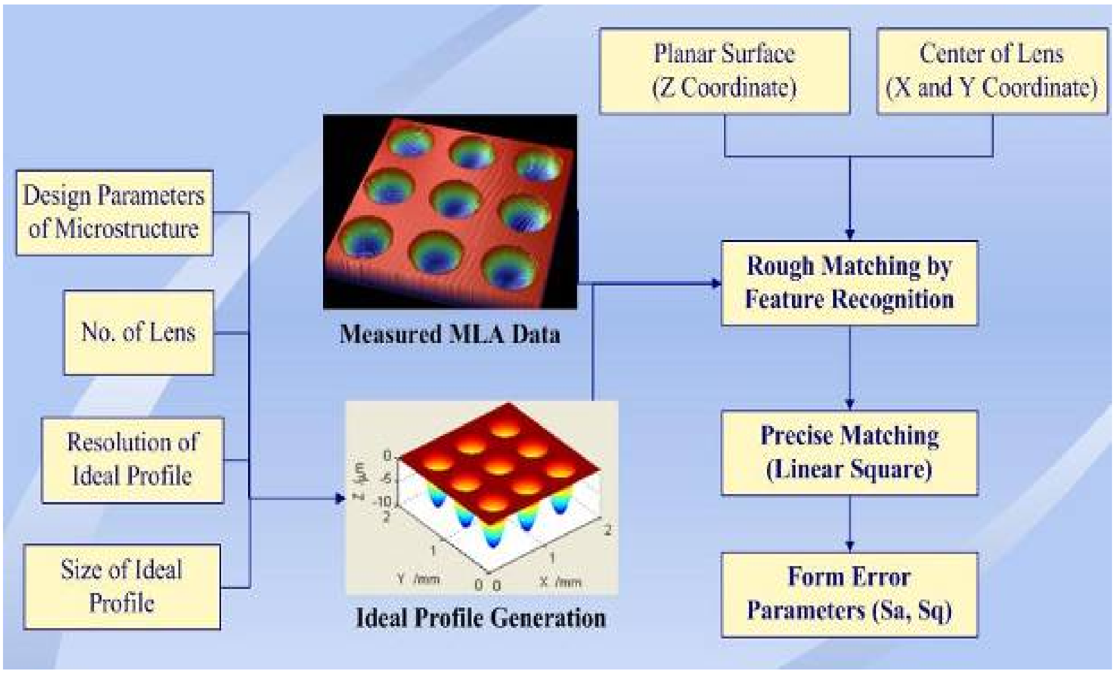

Figure 3.22 Schematic illustration of methodology employed for data matching

In the process of precise matching, the measured data and the design data are fitted as accurately as possible. The measured data are exported as a points cloud and they are matched with the data from the design surface. This is accomplished by the projection of points of the measured surface to the ideal surface. By using the method of Bi-Cubic B-spline data interpolation, the distance between corresponding points can be calculated. In the surface characterization method, Bi-Cubic B-spline surface interpolation is employed for the searching of the corresponding points, as shown schematically in Figure 3.23. The Bi-Cubic B-spline surface is expressed in Equation (3.2). Afterwards, the interpolation distances are aggregated and carried out by a rigid body (RB) transformation of measured data.

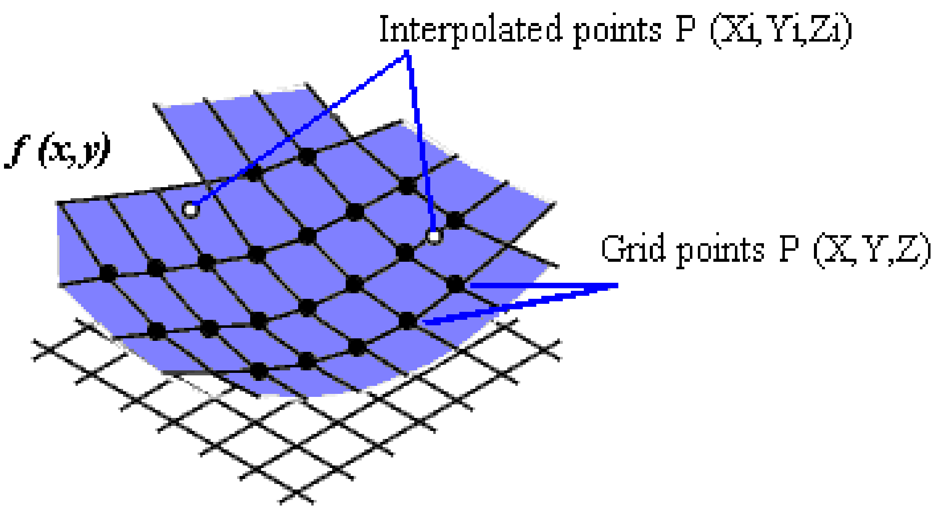

Figure 3.23 Bi-Cubic B-Spline Surface interpolations

$$f(x,y) = \sum_{i=0}^{n}\sum_{j=0}^{m} d_{i,j} N_{i,3}(u) N_{j,3}(v) \tag{3.2}$$

Where, $d_{i,j}$ is the control knot, $N_{i,3}(u)$ and $N_{j,3}(v)$ are normalized B-spline basis functions of order 3 in the u and v directions, respectively. For each slice surface of a uniform cubic B-spline, the basis function can be expressed as

$$N_3(u) = \frac{1}{3}\begin{bmatrix} -1 & 3 & -2 & 1 \\ 3 & -6 & 0 & 4 \\ -3 & 2 & 3 & 1 \\ 1 & 0 & 0 & 0 \end{bmatrix}\begin{bmatrix} u^3 \\ u^2 \\ u \\ 1 \end{bmatrix} \tag{3.3}$$

$N_3(v)$ can be expressed similarly.

Surface data matching is realized through Rigid-Body-Transformation (RBT) using a homogenous transformation matrix (HTM). For the HTM using transition and rotation in coordinate systems, t_x, t_y and t_z denote the transition distances while α, β and γ denote the rotation angles along X, Y and Z axes, respectively. Hence, the transformation matrix can be expressed in Equation (3.4):

$$Tr(\alpha,\beta,\gamma,t_x,t_y,t_z) = \begin{bmatrix} \cos\beta\cos\gamma & \sin\alpha\sin\beta\cos\gamma - \cos\alpha\sin\gamma & \cos\alpha\sin\beta\cos\gamma + \sin\alpha\sin\gamma & t_x \\ \cos\beta\sin\gamma & \sin\alpha\sin\beta\sin\gamma + \cos\alpha\cos\gamma & \cos\alpha\sin\beta\sin\gamma - \sin\alpha\cos\gamma & t_y \\ -\sin\beta & \sin\alpha\cos\beta & \cos\alpha\cos\beta & t_z \\ 0 & 0 & 0 & 1 \end{bmatrix} \tag{3.4}$$

To minimize the residual error within the matching process, the method of the least mean squares was employed which is run iteratively to search for the best fit value or the minimum value of interpolation distance as a reference to the whole profile. The optimization criteria and major processes in precise matching are shown in Figure 3.24. Having completed the matching process, the design data or ideal profile is subtracted from the measured data. Finally, the form error of the MLA can be determined by the MLA characterizer system. The parameters for assessing three dimensional surface qualities such as S_a and S_q would be the output, as well as the surface topography after subtraction is shown in Figure 3.25.

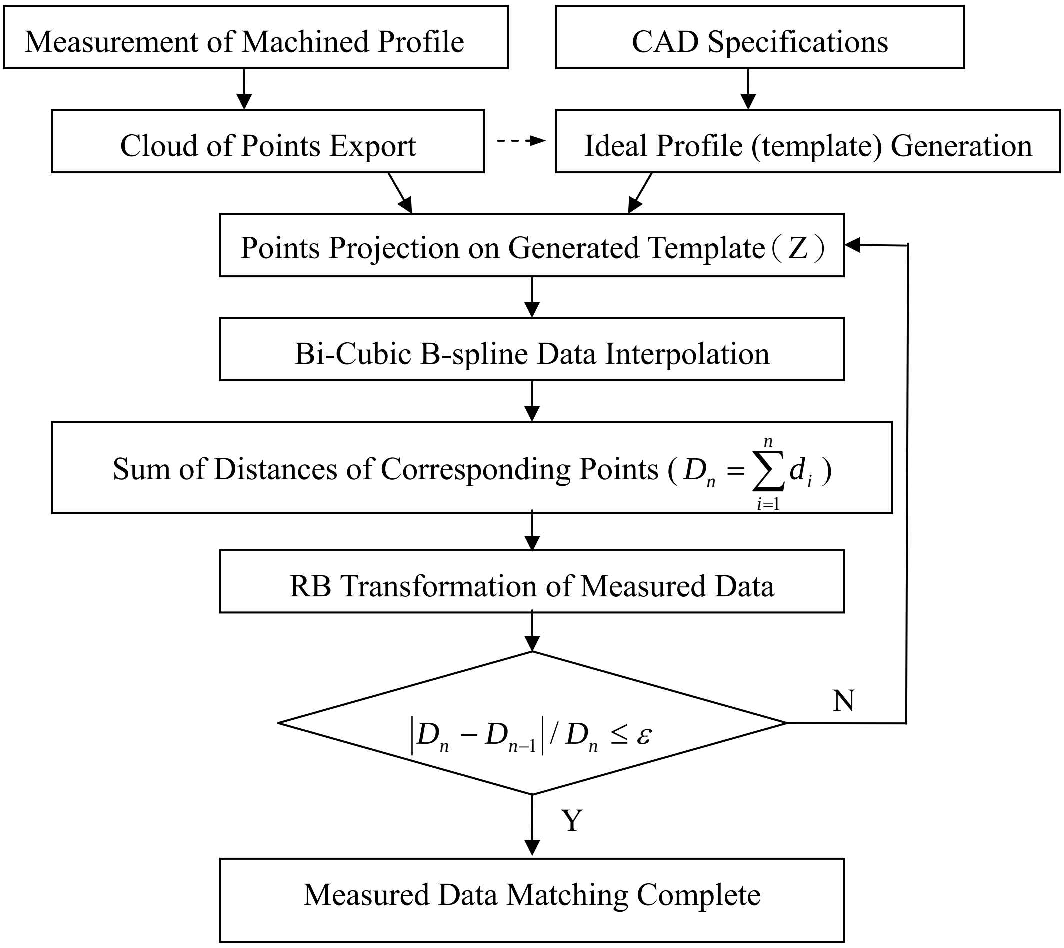

Figure 3.24 Precise matching between measured MLA and generated ideal profile

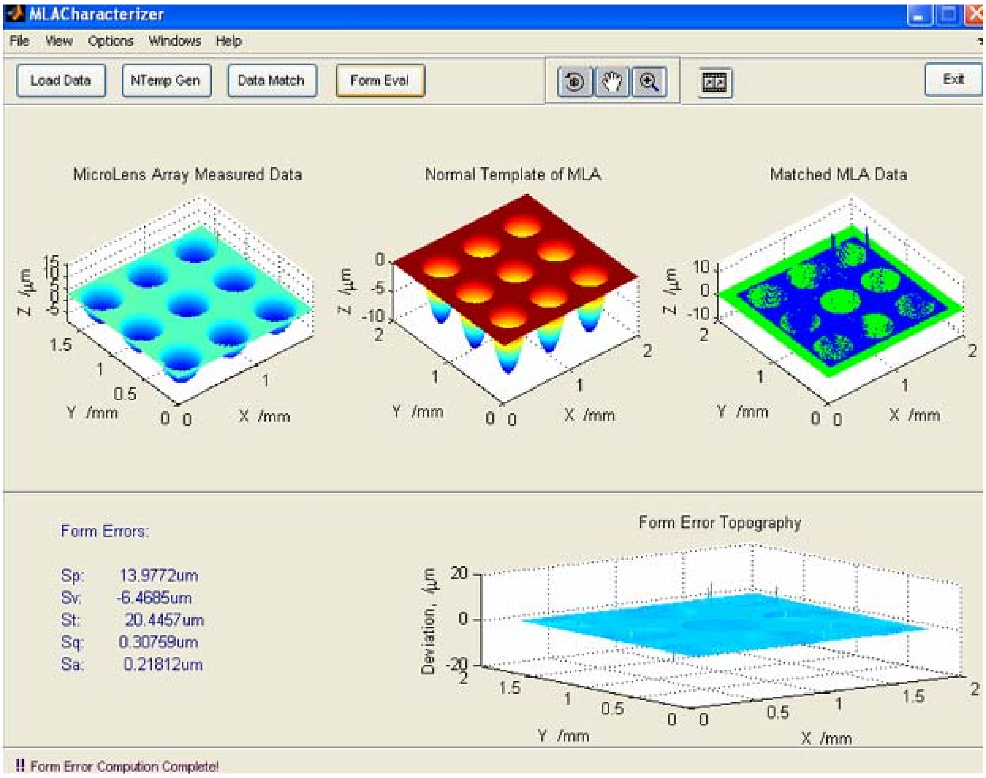

Figure 3.25 Output of form error parameters and topography after template subtraction

3.5 Summary

In this chapter, the research methodology and theoretical background involved in this study has been mentioned. First of all, the overall research framework is introduced, divided into three phases, which are:

(i) a series of experimental investigations on factors affecting surface generation,

(ii) a study of the characterization of tool wear in FTS machining

(iii) a theoretical analysis is conducted for the study of the characteristics of error motion and the stroke error of actuation involved in FTS machining.

The cutting mechanics of FTS machining is introduced, which is a superior technology developed on the basis of single point diamond turning technology. The ultra-precision machining equipment for cutting tests and measurement instruments for data collection and analysis has also been mentioned. In addition, the theoretical background of characterization methods employed in the study have been outlined. They are separately employed for characterizing individual and patterns of surfaces such as those found in microlens arrays.

CHAPTER 4 EXPERIMENTAL INVESTIGATION OF PROCESS FACTORS AFFECTING SURFACE GENERATION IN FTS MACHINING

With the increasing use of display systems in photonic products nowadays, more attention has been paid on the research and development of fabrication technology for high precision optical components such as optical microstructures. Ultra-precision machining with a fast tool servo (FTS) is one of the technologies for the fabrication of high-quality optical surfaces. The diamond tool fixed on the FTS is activated back and forth by a stacked type piezoelectric actuator. Complex profiles such as optical microstructures with sub-micrometer form accuracy and nanometric surface finish can be fabricated without the need for any subsequent post processing.

However, the current understanding of the cutting mechanics and the relationship to surface generation in the FTS machining is still far from complete. Although there has been extensive research work conducted in filling the research gaps of FTS machining, most of the studies were focused on the design of FTS with better performance and modeling characteristic of FTS actuators. The study of the process factors affecting surface generation in FTS machining has received relatively little attention. In this chapter, the aim is to study the effect of process parameters on surface generation involved in FTS machining, such as spindle speed, feed rate and depth of cut. Moreover, a series of cutting experiments were carried out for studying any defects in FTS machining. Tool compensation was also carried out for enhancing the surface quality of machined surfaces. Finally, pattern array analysis was undertaken out to further explore surface generation in FTS machining micro-structural surfaces.

4.1 Factors Affecting Surface Generation in FTS Machining

To study the characteristics of the FTS machining process, the first step is to identify the factors affecting surface generation. Figure 4.1 shows the factors affecting surface generation in SPDT technology which also forms the basis of the factors affecting surface generation in FTS machining. The material removal process of SPDT is mainly governed by three major categories of factors, which are machine tools and control, process factors and diamond tools, respectively.

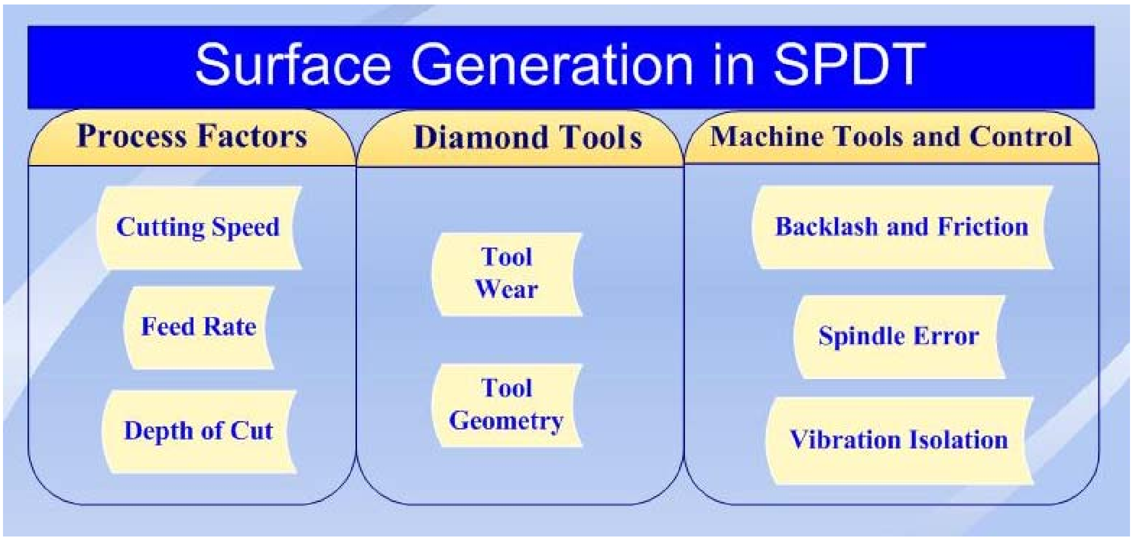

Figure 4.1 Factors affecting surface generation in SPDT technology

In ultra-precision machining, any minute change in machine tools and control or the machining environment affects the surface generation. The vibration control of the cutting system is of prime importance. Although the ultra-precision machine (Nanoform 200 from Precitech in US) is equipped with 'air-mounts' to support the machine base in preventing vibration from the foundation, small amplitude and low frequency vibration (less than 10Hz) is still inevitable, even if the machine is housed on a specially constructed vibration attenuation foundation. For minimizing the error from machine tools and control, such as backlash and friction of slideways and axial error of the rotational spindle, both X and Z axes of Nanoform 200 utilize high stiffness, hydrostatic oil bearing slide-ways with an aerostatic, slot-type thrust bearing spindle to achieve ultra-precision contouring performance. (See Figure 4.2) The feedback resolution of the ultra fine pitch linear glass scales for positioning feedback used in the slideways is only 8.6 nm and optional finer resolution scales are also available.

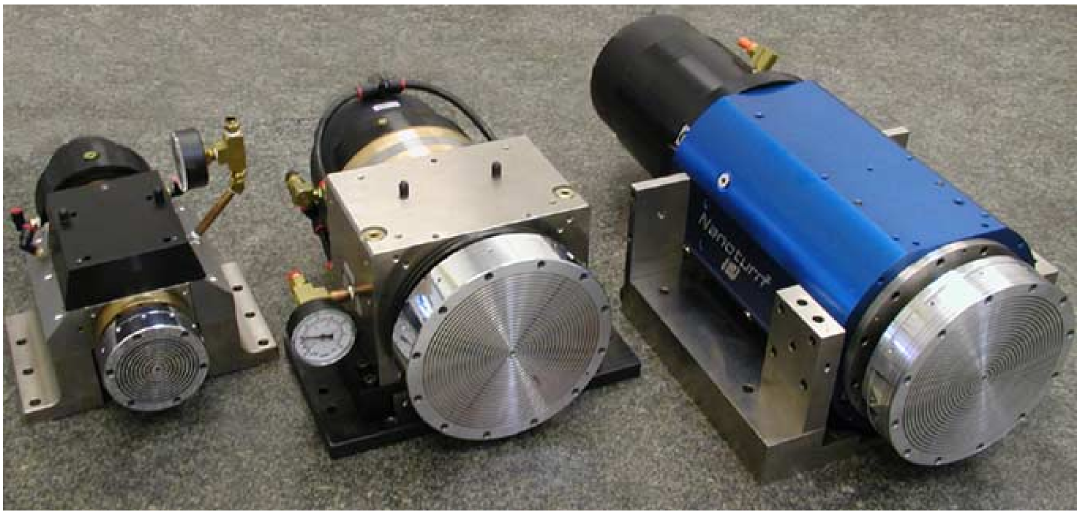

Figure 4.2 Hydrostatic oil bearing spindle with air chuck of Nanoform 200 (from Precitech Inc. USA)

Moreover, diamond tools employed in ultra-precision machining technology are also critical in surface generation. Since the profile of a machined surface is basically composed of the repetition of the tool profile transferred in the plane normal to the cutting direction, the geometrical accuracy of the cutting edges and the stability or tool wear have a great influence on the surface roughness of the machined profile. Cutting parameters involved in SPDT include spindle speed, feed rate, and depth of cut, which are categorized as process factors.

Based on the literature published in the last two decades (Whitehouse, 1994), process factors affect the machined surface in almost all machining technologies. These process factors include the cutting parameters employed in the machining processes. For example, increasing the spindle speed and decreasing the feed rate can improve the surface finish of the machined profile in SPDT.

The main difference between FTS and SPDT is that a FTS is mounted on the Z axis of the ultra-precision machine. As a result, the factors affecting surface generation in SPDT technology also apply in the FTS machining process. The exclusive error involved in FTS machining is the error motion of FTS actuation. To investigate the factors affecting surface generation in FTS machining, the factors as shown in Figure 4.3 have been studied and a series of cutting tests have been carried out and the results are discussed in the following chapters.

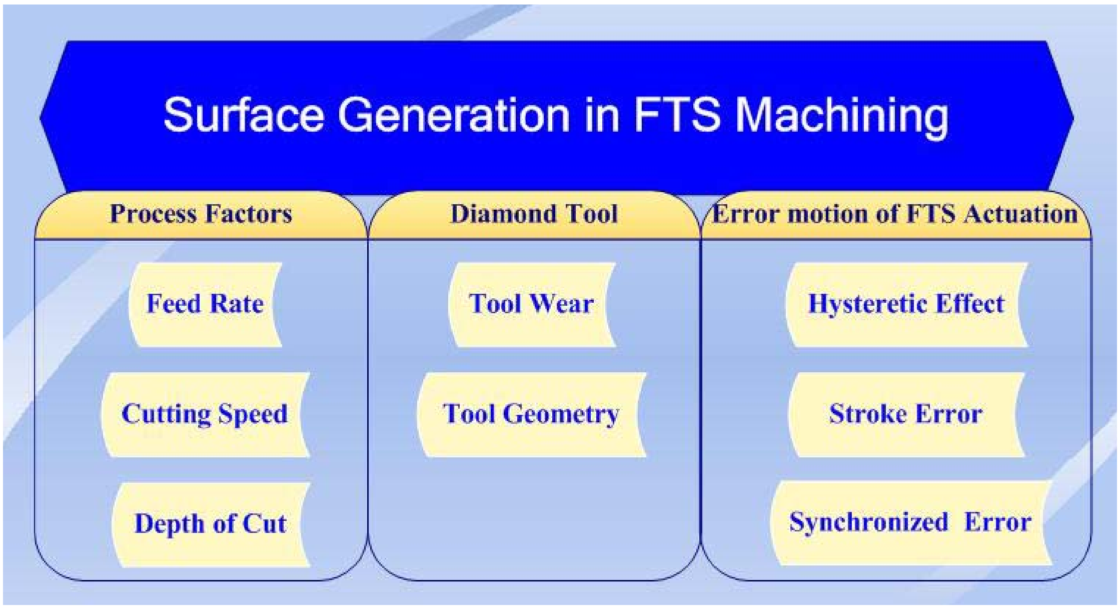

Figure 4.3 Critical factors affecting surface generation in FTS machining

The error motion of FTS actuation is composed of three sources of errors which are hysteric effect, stroke errors and synchronized errors. It is well known that a piezoelectric actuator is often used for the purpose of micro-positioning and active control. However, one of the drawbacks of piezoelectric actuators is the presence of hysteresis which leads to oscillation and vibration (Yu, 2002). Moreover, the non-linear behavior of the piezoelectric material affects the mechanical outputs in the cutting process, as discussed in Chapter 2.

As mentioned previously, a piezo-electric actuator is mounted on Z axis of an ultra-precision lathe to activate a diamond tool moving back and forth to enable FTS machining. This leads to another error source of the actuation motion which is defined as stroke error or positioning error, in the present study. This actuation motion is also the main difference between SPDT and FTS machining. The stroke of FTS machining is defined as the fully actuated distance or movement of diamond tool. Stroke error affects the surface quality of the fabricated profile and even leads to an over cut phenomenon. To further explore the effect of stroke error on the surface generation in FTS machining, an analytical study focusing on actuation error motion in FTS machining is discussed in Chapter 6.

Besides, the synchronized error, which can be described as the tracking error between the actuation motion of the diamond tool and spindle rotation or rotation of the workpiece, also affects the surface quality of machined surfaces. It is mainly due to the failure of the FTS in actuating the diamond tool to cut the pre-set position in the program. In FTS machining, the kernel of the digital signal processor (DSP) is capable of determining the real-time position of the spindle and the diamond tool in accordance with the feedback signals from the rotational and linear sensors. Moreover, the feedback signal can be employed to calculate the location being cut in the next moment. This calculation is according to the program of the geometry of the desired profile preset in the SOP control system. Too high rotational frequency of the spindle could lead to errors in the trajectory generation. This error could also be described as improper computing of the cutting position in real-time which causes a geometrical shift of the machined profile and large form errors.

In SPDT technology, it is well known that the surface roughness of the fabricated profile can be improved by increasing the spindle speed. When selecting the machining conditions in FTS machining, it is not possible to achieve a better surface finish merely by increasing the spindle speed. This is due to the fact that a maximum value of bandwidth for FTS limits the range of process factors (e.g. spindle speed) employed. An actuated diamond tool would fail to cut the pre-determined position when the rotational frequency of the workpiece is higher than the bandwidth of the FTS actuator. This is another reason why further study is needed to explore the effect of the factors, including spindle speed on surface generation in FTS machining.

Figure 4.4 summarizes the main factors affecting SPDT technology and FTS machining. Since ultra-precision machining with FTS is conducted by an ultra-precision lathe under a precisely controlled environment, the main focus of the present study is the process factors and diamond tools which are the critical factors affecting surface generation in both in SPDT and FTS machining. Compared with SPDT, the exclusive error of FTS machining is the error motion of FTS actuation, which would also be one of the major focuses of the study.

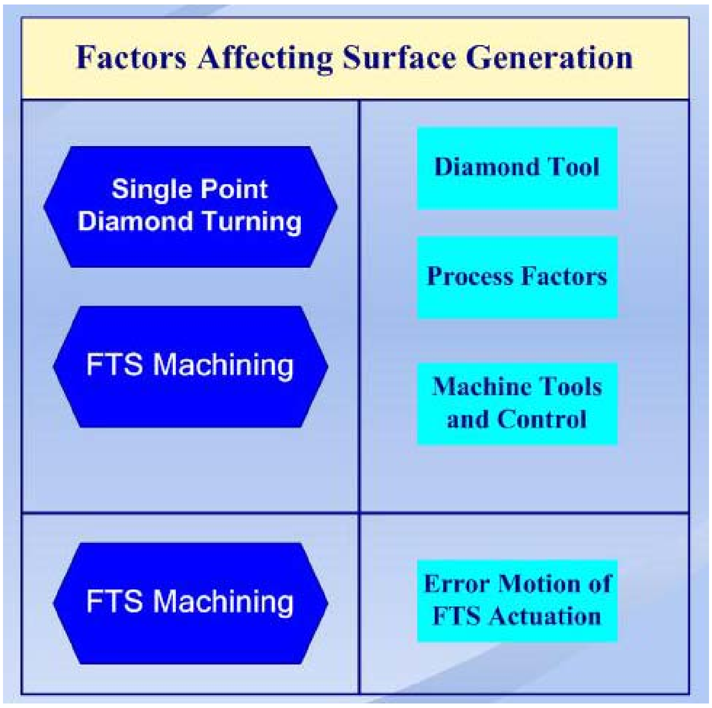

Figure 4.4 Comparison of factors affecting surface generation in SPDT and FTS machining

4.2 Experimental Set-up

To achieve high form accuracy and a super mirror surface finish, the process factors play critical roles in affecting the surface quality of the fabricated profiles. In the present study, a series of experiments were conducted for investigating the effect of cutting conditions such as spindle speed, feed rate and depth of cut in FTS machining of optical microstructures. As shown in Figure 4.5, the cutting experiments were conducted on a Nanoform 200 ultra-precision machine equipped with a FTS, from Precitech Inc in USA. Mounted on each of these slides is a laser holographic glass scale and read head assembly. This state of the art device provides cost effective, stable position feedback to the control system, with a resolution of 8.6 nanometers.

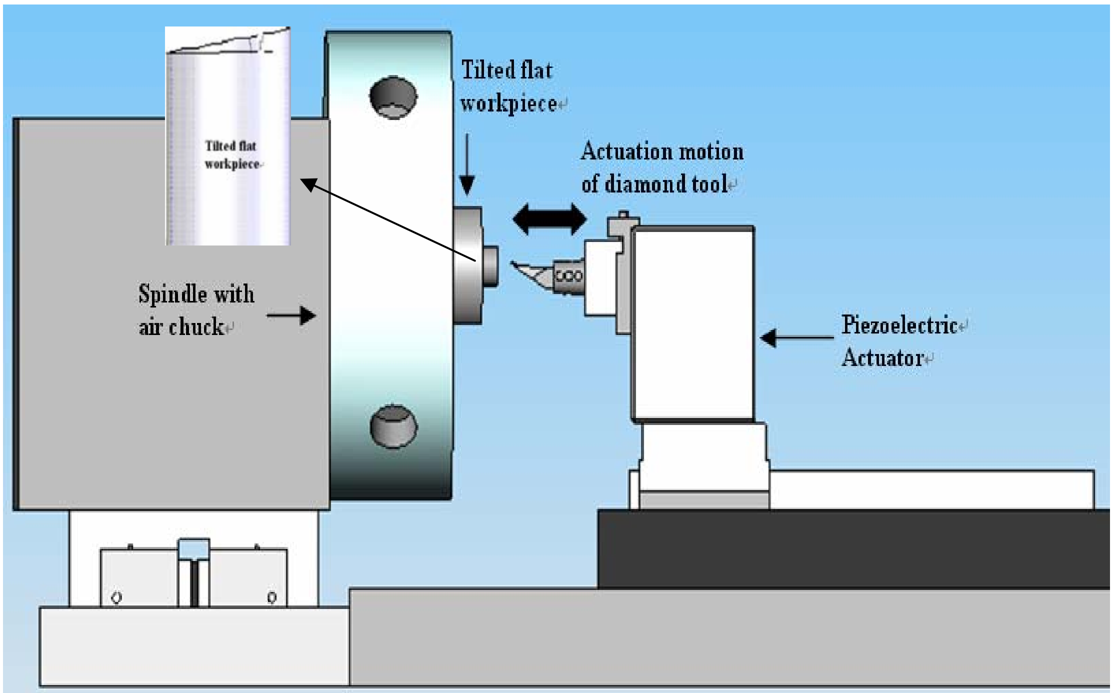

Figure 4.5 Nanoform 200 Ultra-precision machining system

Generally, a desired profile needs to be converted into a C-program for communication with the turning lathe. A program simulation was performed by SOP which is a control system to assist the FTS for locating the position being cut in real time, and provides a user friendly software interface. Details are given in Chapter 3.

The surface quality of the machined surfaces were measured by a Wyko NT8000 non-contact 3D profiler system and analysed by the software – Vision. The pattern of the optical microstructures can also be measured by Wyko and analysed by a purpose built surface characterization system which is described in Chapter 3. The results of cutting the tests are summarized and further discussed in this chapter.

To investigate the effect of the process factors on surface generation in fabricating the micro-structural profile by FTS machining, a microlens array pattern was machined in the cutting experiments. In conventional production of optical microstructures, the designed profile would be fabricated on the mold insert and then the mass production would be carried out by injection molding. In the present study, the workpiece material is nickel copper since it is a commonly used raw material for optical mold inserts. The design of the microlens array pattern is shown in Figure 4.6 and the detailed specifications of designed microstructure are summarized in Table 4.1. All samples are rough cut by a conventional CNC machine to a cylindrical shape and a standard height according to the dimensions of the design sample which is shown in Figure 4.7.

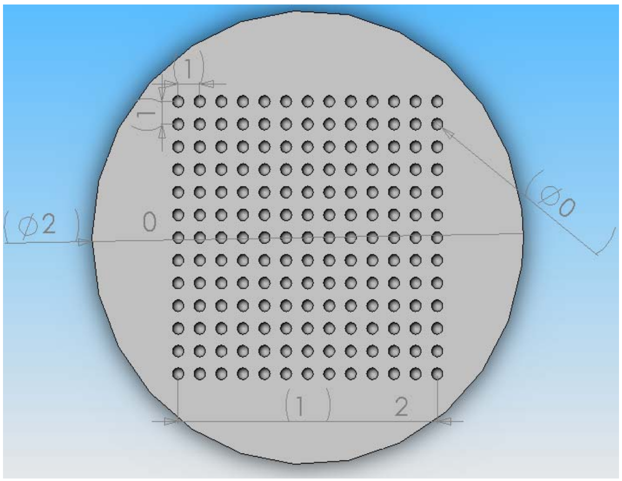

Figure 4.6 Design of micro-lens array on the workpiece

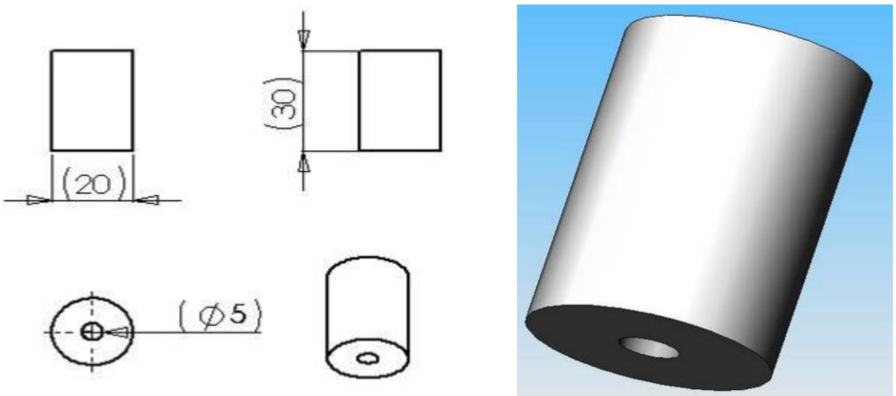

Figure 4.7 Dimensions of workpiece

Table 4.1 Specifications of the design of optical microstructures

Surface topography	Micro-lens array
Diameter of array (mm)	20
Diameter of micro-lens (μm)	526.6
Radius of curvature of micro-lens (mm)	1.1705
Sag height (μm)	30
Number of micro-lens	13x13
Spacing of adjacent micro-lens (mm)	1.0

Table 4.2 shows the specification of diamond tool employed in the present cutting tests. It is known that distortions may occur in the machined topography while

operating the FTS at high frequency if the clearance angle of diamond tool employed is not steep enough.

Table 4.2 Diamond tool specification

Clearance angle	15^{o}
Tool rake angle	0^{o}
Tool nose radius	0.025 mm
Work materials	Ni-Cu
Lubricant	Clairsol 330

To further confirm this situation won't happen in the cutting tests, Figure 4.8 illustrates the derivation of critical clearance angle α. R and R_x are separately defined as the radius of the microlens and cutting profile perpendicular to the surface speed. d is the distance between the microlens curvature center and the base plane. ϕ is the diameter of machined microlens and x is the variable distance between microlens machining center and the mentioned cutting profile surface.

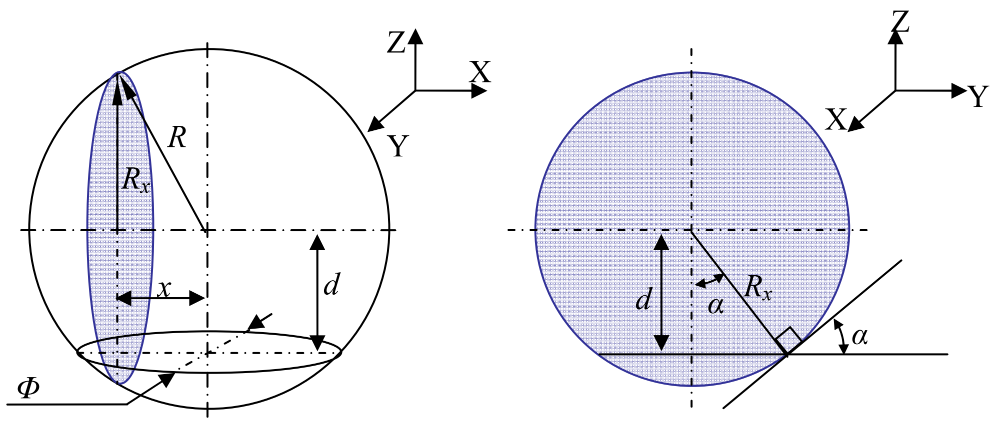

Figure 4.8 Illustration for the derivation of critical clearance angle

Based on the illustration in Figure 4.8, the following equations are obtained:

$$R_x = \sqrt{R^2 - x^2}, \quad 0 \le x \le \phi/2 \tag{4.1}$$

$$d = \sqrt{R^2 - (\phi/2)^2} \tag{4.2}$$

$$\cos\alpha = \frac{d}{R_x} \tag{4.3}$$

Substitution Eq.(4.3) with Eqs (4.1) and (4.2) generates

$$\cos\alpha = \frac{\sqrt{R^2 - (\phi/2)^2}}{\sqrt{R^2 - x^2}}, \quad 0 \le x \le \phi/2 \tag{4.4}$$

Therefore,

$$\alpha = \cos^{-1}\left(\frac{\sqrt{R^2 - (\phi/2)^2}}{\sqrt{R^2 - x^2}}\right), \quad 0 \le x \le \phi/2 \tag{4.5}$$

Based on the specification of the microlens to be machined, the critical clearance angle is determined according to different values of x. The detailed relationship between the variable x and the critical clearance angle α is depicted in Figure 4.9. It can be observed that the largest value of clearance angle α is at the center of machined microlens ($x = 0$), which is 4.9974°. As a result, the diamond tool employed in the cutting tests with 15° clearance angle would not be a source of distortion.

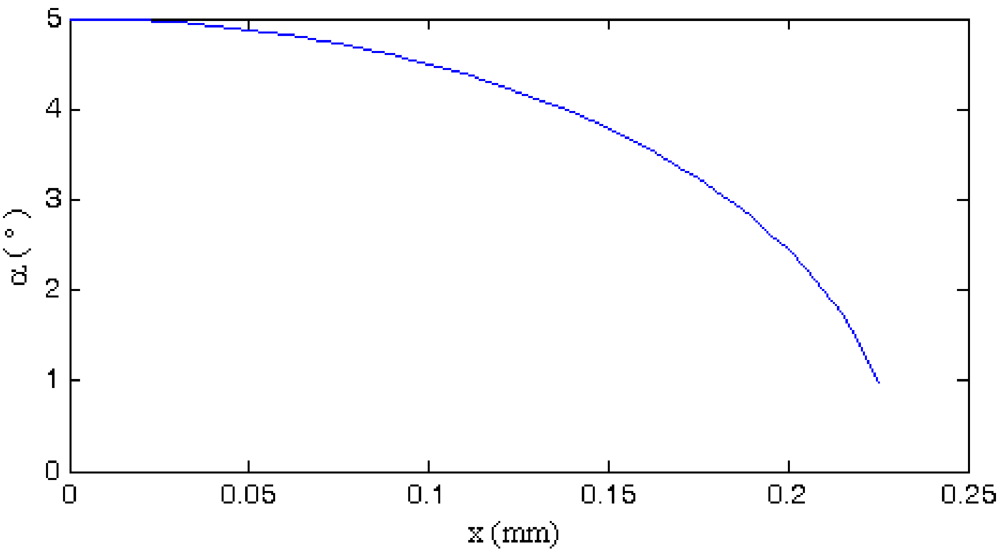

Figure 4.9 Critical clearance angles vs. different cutting profile in the microlens

In measuring the machined profile, it is interesting to note that there is a variation of surface quality of the microlens array with respect to the distance from the centre of the workpiece. It can be explained by the existence of different surface speeds. From Equation (4.6), it is well known that even if the surface profile is machined at a constant spindle speed; the surface speed is varied with respect to the distance to the centre of the workspiece.

$$SpindleSpeed(r.p.m.) = \frac{SurfaceSpeed}{2\pi R} \tag{4.6}$$

As a result, it is proposed to measure the surface quality of the microlenses at specific locations (i.e. L2, L4 and L6) on different samples. Figure 4.10 shows the geometrical patterns and the location of measured microlens array. By using this method, the sample measured should be at the same surface speed. The effect of other cutting conditions, especially spindle speed, can be more significantly observed.

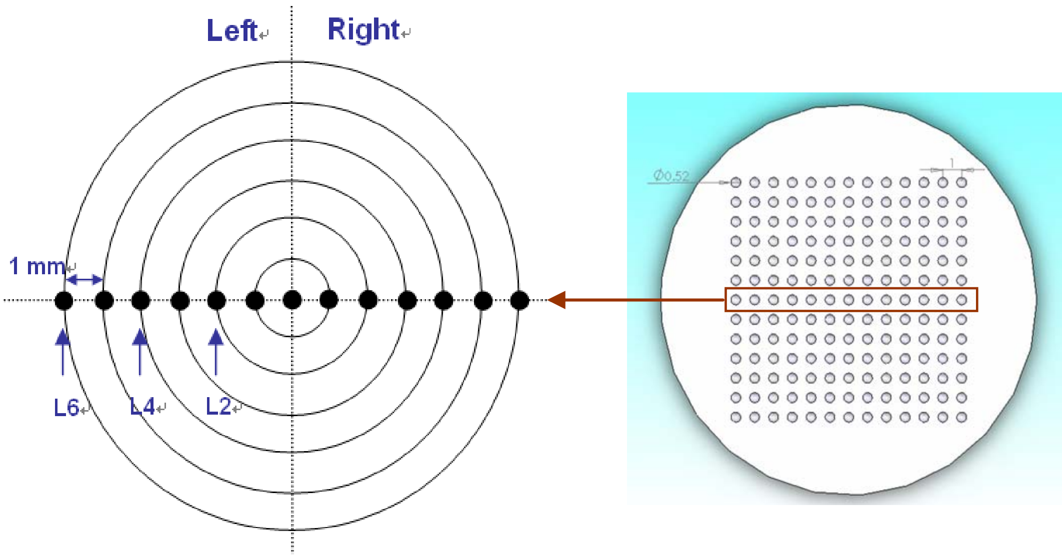

Figure 4.10 Geometrical pattern of the micro-lens array being measured

In the present study, a series of experiments have been conducted under various spindle speeds, feed rates, depth of cut, etc. To study the effect of spindle speed on surface generation when fabricating the optical microstructures, different spindle speeds were employed while other cutting conditions were kept constant. The cutting conditions are shown in Table 4.3. In the experiment for the study of the effect of feed rates, various feed rates are used while the other cutting conditions are kept constant. The feed rate ranged from 0.125 mm/min to 5 mm/min. Table 4.4 shows the cutting conditions for investigating the effect of feed rate. Table 4.5 shows the cutting conditions for the investigation of the effect of depth of cut on surface generation in FTS machining.

Table 4.3 Cutting conditions for investigating the effect of spindle speed

Spindle speed (rpm)	50, 75, 100, 150,200
Feed rate (mm/min)	1
Depth of cut (μm)	5

Table 4.4 Cutting conditions for investigating effect of feed rate

Feed rate (mm/min)	0.125, 0.25, 0.5, 1, 5
Depth of cut (μm)	1
Surface speed (m/s)	1.25

Table 4.5 Cutting conditions for investigating effect of depth of cut

Feed rate (mm/min)	1
Depth of cut (μm)	0.4, 1, 2.4, 5, 10
Surface speed (m/s)	1.25

4.3 Results and Discussion

4.3.1 Effect of spindle speed

In the study of the effect of spindle speed on form error of machined microstructures, surface data are separately collected in the region with constant surface speed (V_s). This is accomplished by measuring the lenses of those microstructures which are located at the same distance from the center of workpiece. The result was obtained was based on the root-mean-square value (R_q) as shown in Figure 4.11. It appears that better form accuracy in terms of smaller form error can be achieved by increasing the spindle speed.

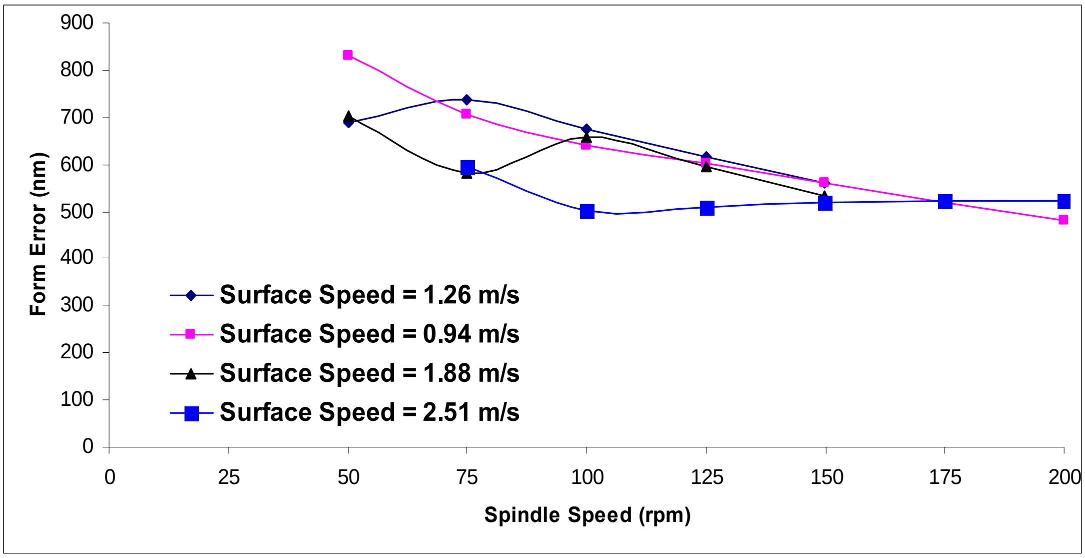

Figure 4.11 Effect of Spindle Speed on form error (R_q)

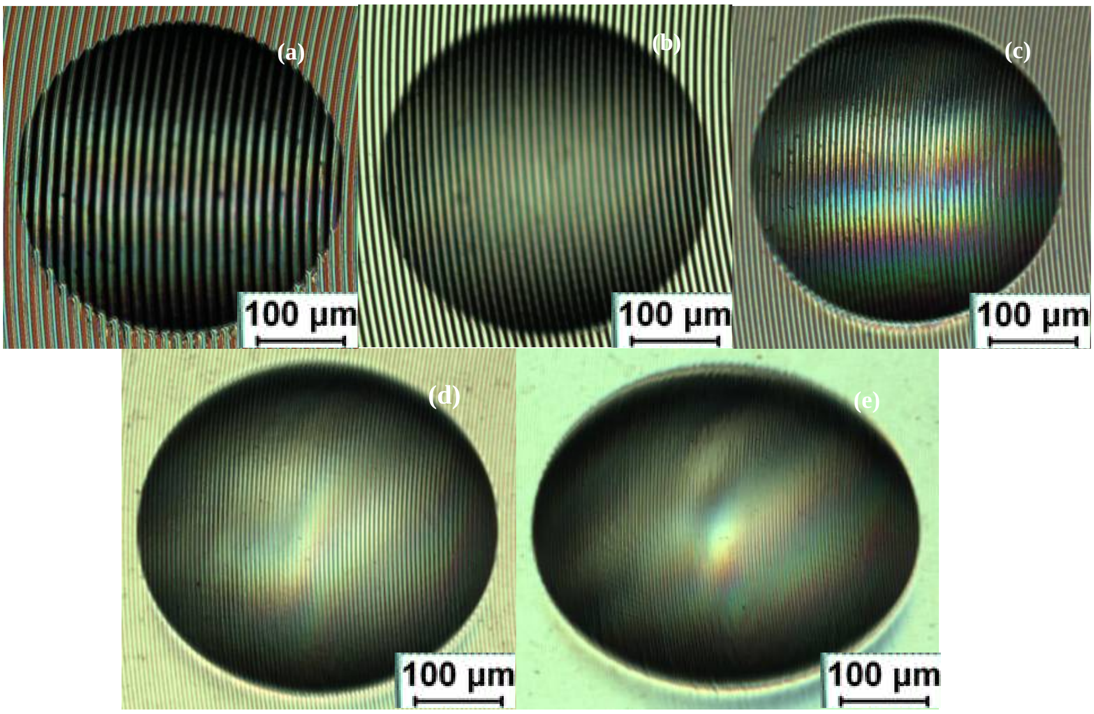

Figure 4.12 Monograms of microlens (L4) machined under various spindle speeds: (a) 50 rpm, (b) 75 rpm, (c) 100 rpm, (d)150 rpm and (e) 200 rpm

Figure 4.12 shows the monograms captured by an optical microscope. It is interesting to note that tool marks are more obviously seen when the workpiece is machined with a lower spindle speed. On the other hand, it appears that the surface quality of the microlens may not be improved with increasing spindle speed, in some cases. When the spindle speed is over 100 rpm, prominent distortion of the microlens is found at the edges of the machined lens. At a spindle speed of 50 rpm, 75 rpm and 100 rpm, no distortion is observed. This is due to the fact that the diamond tool could be actuated to cut the predetermined position when the spindle speed is higher than 100 rpm. Although a higher spindle speed is preferable for achieving better surface quality, the operating range of the spindle speed is constrained in FTS machining because of the limited bandwidth of the FTS actuator.

4.3.2 Effect of feed rate

To determine the effect of feed rate on the form error in FTS machining, the surface data are separately obtained at different spindle speeds of 50 rpm, 100 rpm and 200 rpm, and are assessed on the basis of root-mean-square value R_q. As shown in Figure 4.13, better surface quality can be achieved by employing a lower feed rate. Moreover, it is interesting to note that the form error increases rapidly when feed rate employed is higher than 0.5 mm/min.

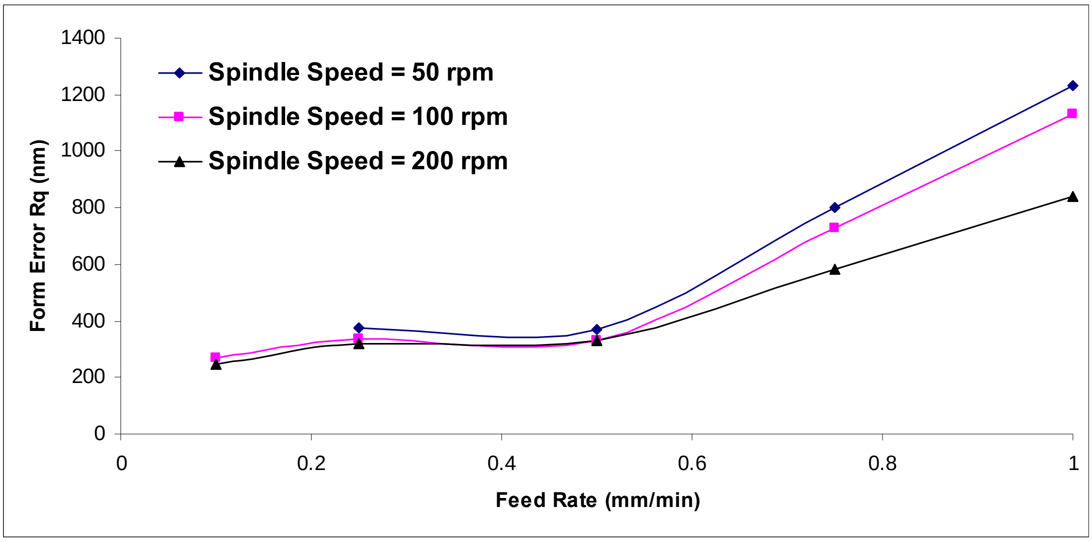

Figure 4.13 Effect of feed rate on form error (R_q)

4.3.3 Effect of depth of cut on surface generation

The effect of depth of cut on form error is shown in Figure 4.14. The range of variation of the form error is within 0.1 μm, even when the depth of cut changes from 0.4 μm to 10 μm. It is found that there is little effect brought by the depth of cut on the surface generation in FTS machining. On the other hand, it is not recommended to use a large depth of cut in single point diamond turning with FTS since the diamond tool may be seriously damaged. The result of this experiment shows that the best depth of cut to use is 5 μm, as this minimizes the form error of the workpiece.

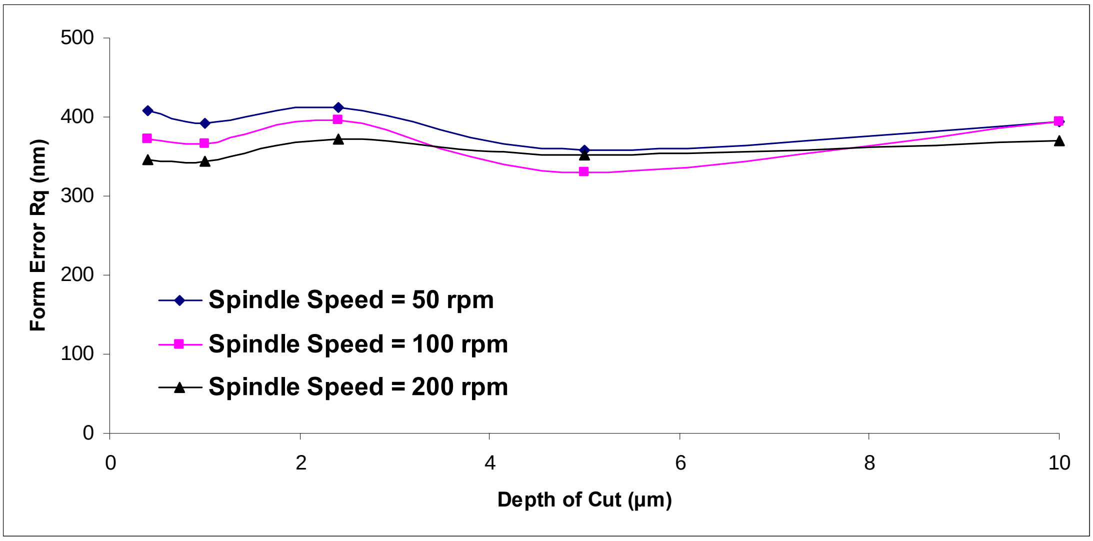

Figure 4.14 Effect of depth of cut on form error (R_q)

4.3.4 Defect analysis

To further investigate the effect of spindle speed and feed rate, a defect analysis was carried out to determine the effect of inappropriate process parameters on the surface quality in FTS machining. In the previous sections, it is found that a higher spindle speed can help to achieve better surface quality. To determine the preferable range, another series of cutting experiments were undertaken. The spindle speed employed in the experiments varied from 25 rpm to 600 rpm, and the machined profile was captured by an optical microscope, and the surface quality in terms of form error was measured by a Wyko NT8000 optical profiler system, separately. The results are shown in Figures 4.15 to 4.17. It is found that the form of microlens is significantly deteriorated when a high spindle speed (e.g. 200 – 600 rpm) is employed in the cutting tests.

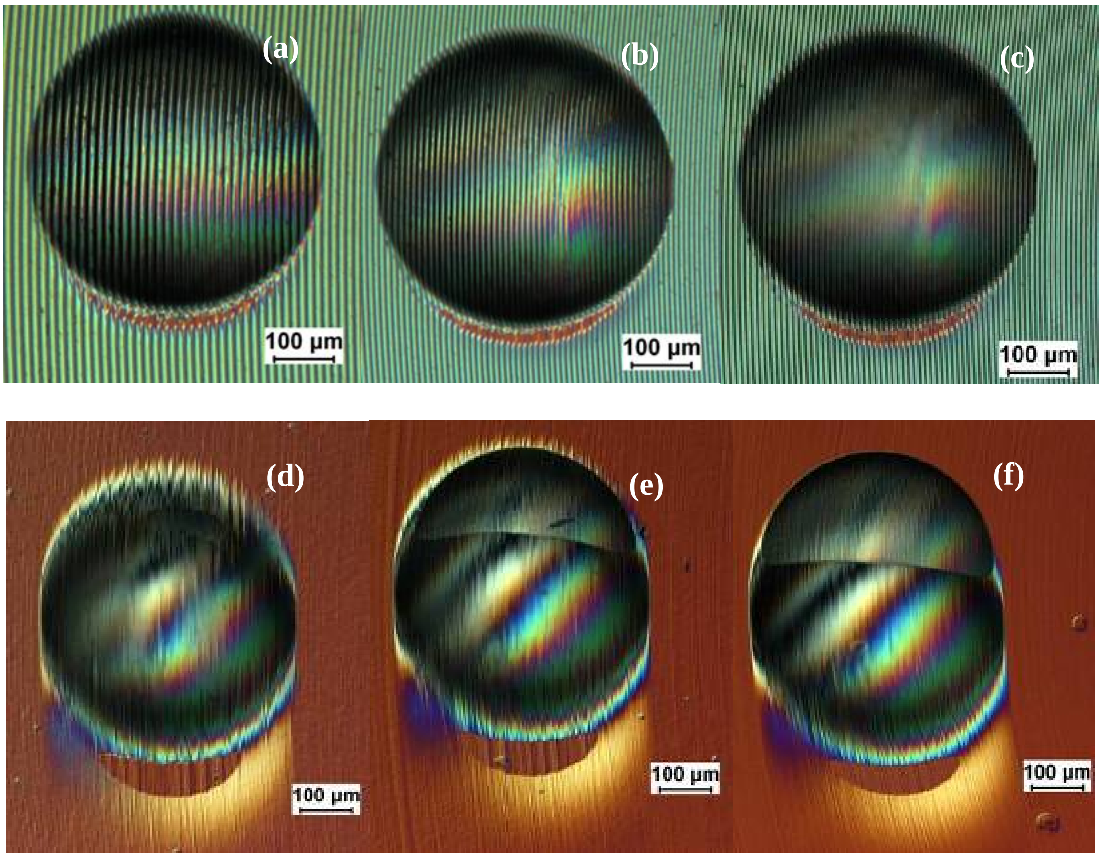

Figure 4.15 Monograms of microlens (L4) machined under various spindle speeds: 25 rpm, (b) 50 rpm, (c) 100 rpm, (d) 200 rpm, (e) 300 rpm and (f) 600 rpm

As shown in Figure 4.18, it is found that there is an optimum spindle speed at which the form error is the minimum. The form error decreases with increasing spindle speed within the range from 25 rpm to 200 rpm, while the form error increases greatly when the spindle speed is over 200 rpm. Nevertheless, it is interesting to note that there is significant form distortion of the machined spherical profile when the spindle speed is higher than 200 rpm. The existence of this distortion may be due to the fact that the cutting tool fails to return to the correct cutting path. The time between two successive cutting points is too short to enable the stacked type piezoelectric actuator in the fast tool servo to move the diamond tool back when the spindle speed is too high. As a result, the diamond tool cannot perform the cutting process accurately. The results infer that there is a limited operating range of spindle speeds and there is an optimum spindle speed for minimizing form error in FTS machining. This finding provides an important means to optimize the surface quality in FTS machining.

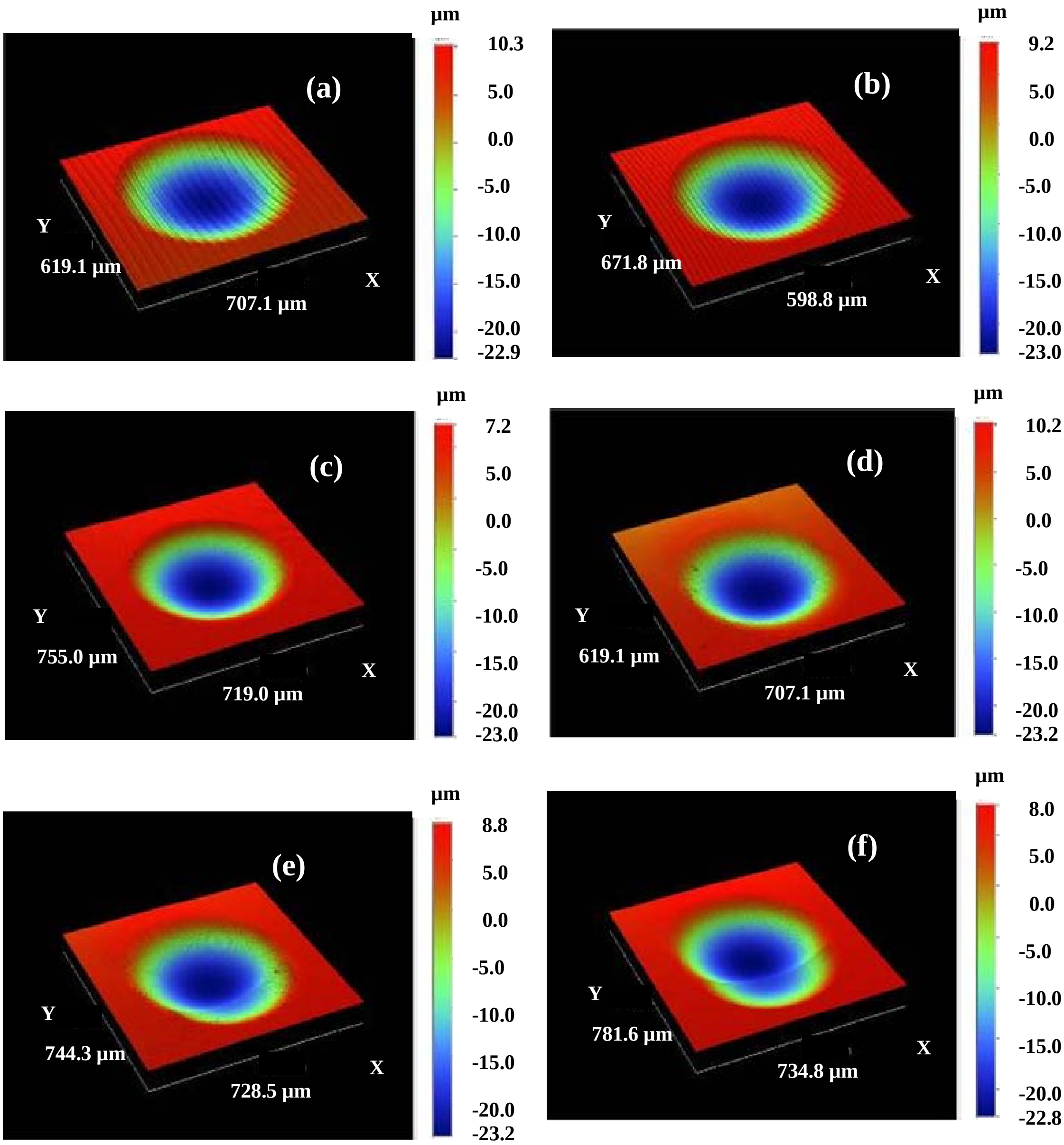

Figure 4.16 3D original shape of monograms of microlens (L4) machined under various spindle speeds: (a) 25 rpm, (b) 50 rpm, (c) 100 rpm, (d) 200 rpm, (e) 300 rpm and (f) 600 rpm

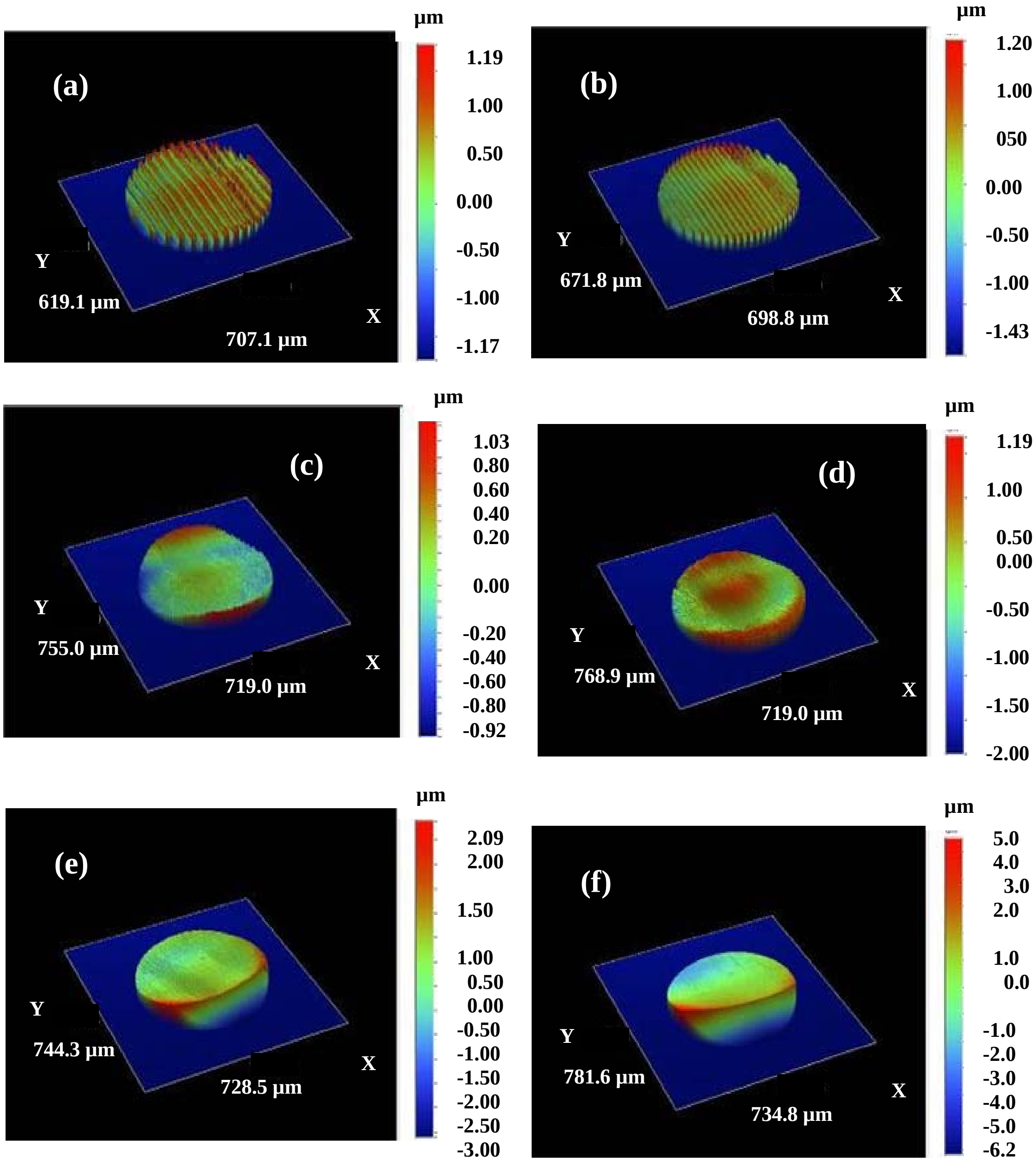

Figure 4.17 3D Form error plot monograms of microlens (L4) machined under various spindle speeds: (a) 25 rpm, (b) 50 rpm, (c) 100 rpm, (d) 200 rpm, (e)300 rpm and (f) 600 rpm

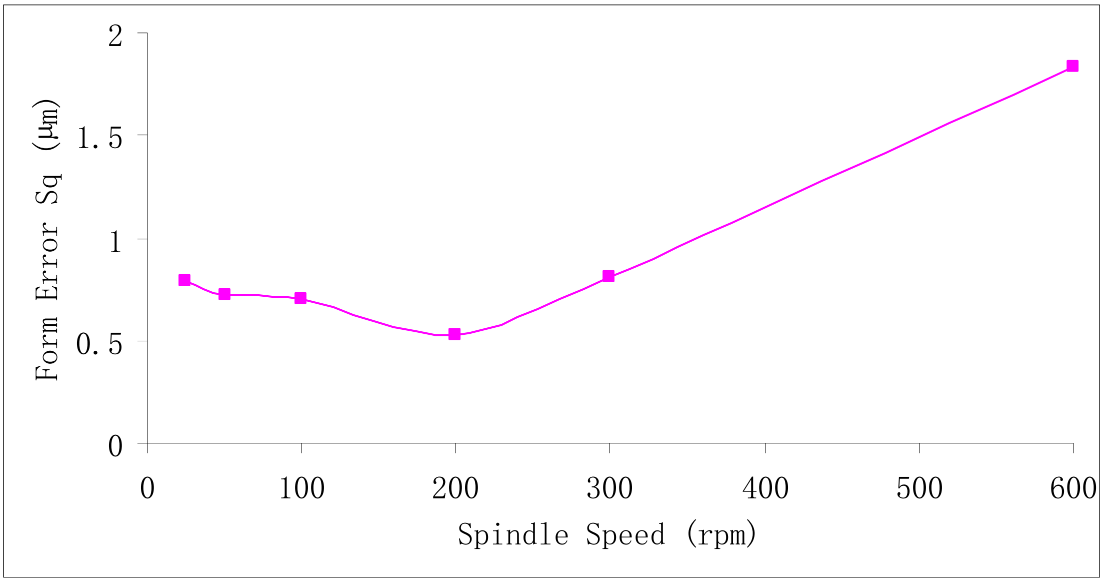

Figure 4.18 Defect analysis of spindle speed

On the other hand, another set of cutting experiments was conducted to determine the most appropriate range of feed rates for FTS machining at different spindle speeds. The experiments were conducted using various feed rates ranging from 0.25 mm/min to 5 mm/min. The results are shown in Figures 4.19 to Figure 4.27, respectively. It is found that the tool marks formed on the workpiece become finer as the feed rate decreases. This shows that the feed rate plays a significant role in affecting surface generation in the FTS machining of optical microstructures. As the feed rate employed is too high (i.e. 5 mm per minute), it can be observed that an incomplete surface profile is generated. This phenomenon adversely affects the form accuracy of the microlens array and is not acceptable in FTS machining. In order to ensure a high quality of surface generation in FTS machining of optical microstructures, there is an operating range in which the complete lens can be produced. This provides an important means for ensuring surface quality in FTS machining. For example, a feed rate of less than 1 mm/min is preferable in FTS machining, as found in the present study.

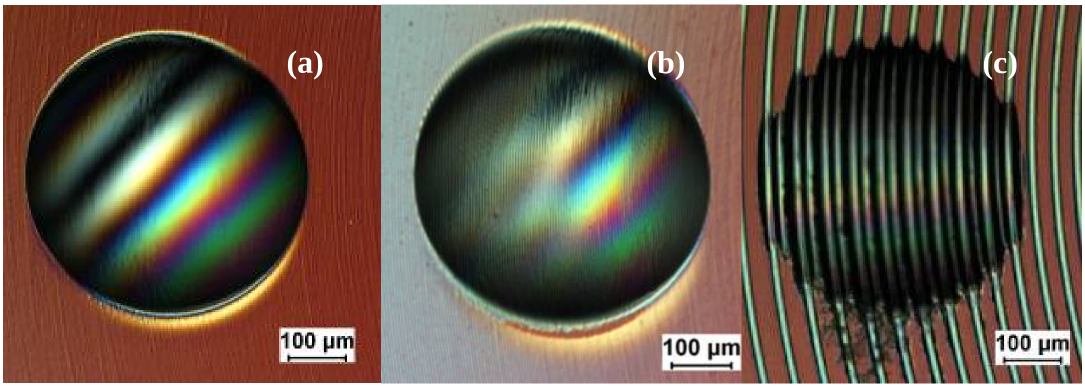

Figure 4.19 Monograms of microlens machined under spindle speed of 100 rpm: (a) f = 0.25 mm/min, (b) f = 1 mm/min 50 mm/min, (c) f = 5 mm/min

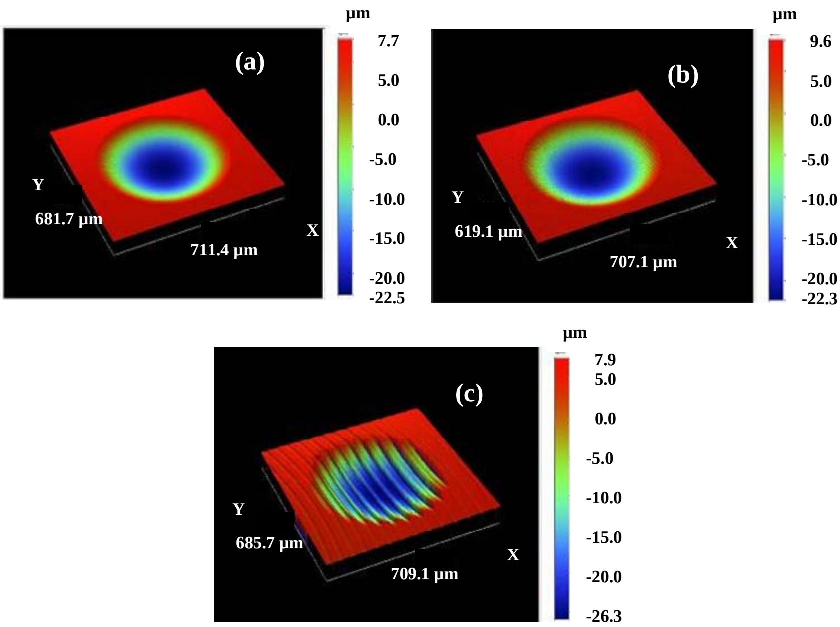

Figure 4.20 3D original shapes of monograms of microlens machined under spindle speed of 100 rpm: (a) f = 0.25 mm/min, (b) f = 1 mm/min 50 mm/min, (c) f = 5 mm/min

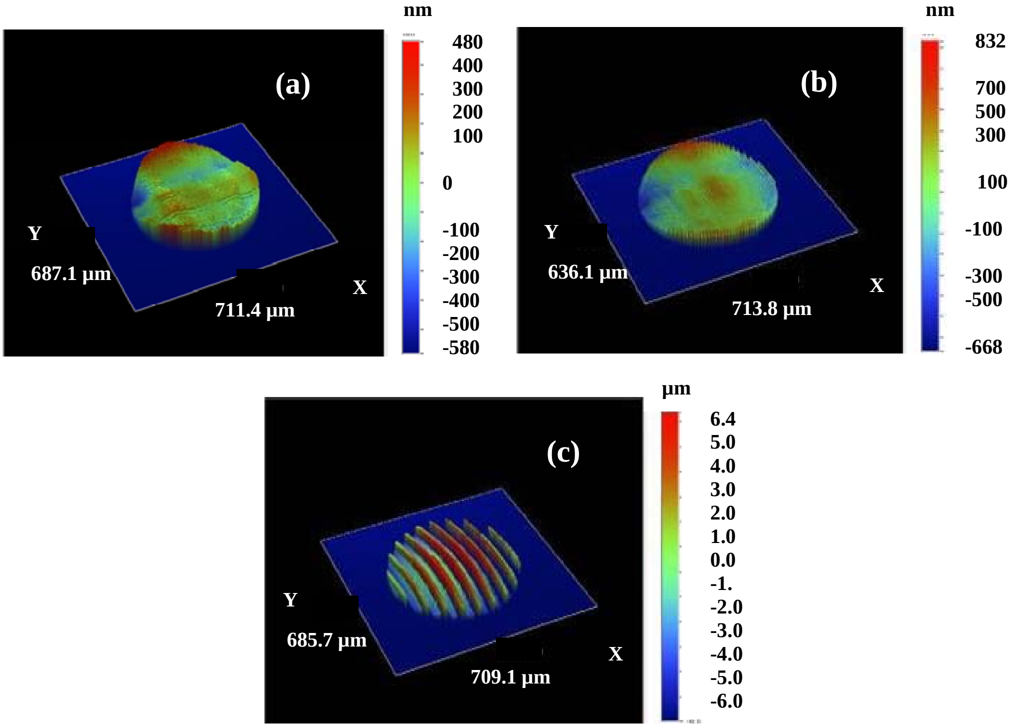

Figure 4.21 Form error plot of monograms of microlens machined under spindle speed of 100 rpm: (a) f = 0.25 mm/min, (b) f = 1 mm/min 50 mm/min, (c) f = 5 mm/min

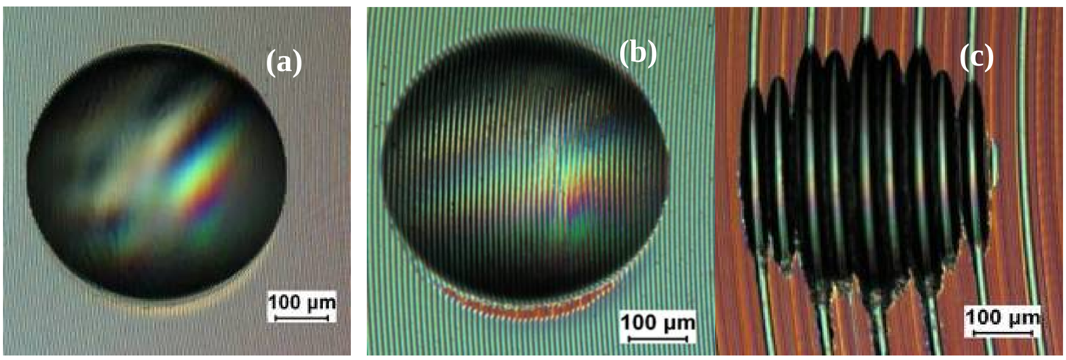

Figure 4.22 Monograms of microlens machined under spindle speed of 50 rpm: (a) f = 0.25 mm/min, (b) f = 1 mm/min 50 mm/min, (c) f = 5 mm/min

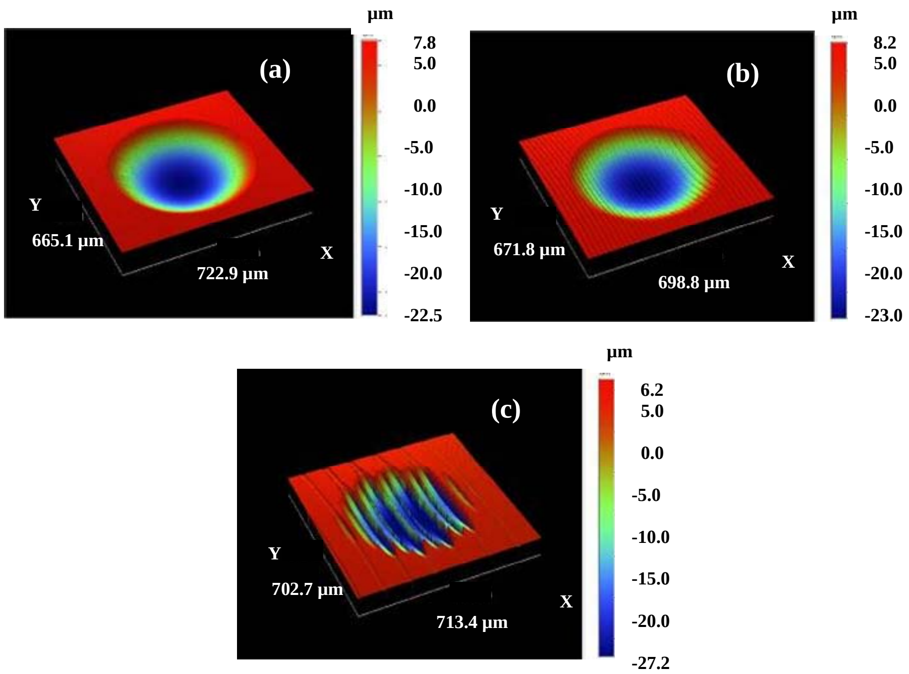

Figure 4.23 3D original shape of monograms of microlens machined under spindle speed of 50 rpm: (a) f = 0.25 mm/min, (b) f = 1 mm/min 50 mm/min, (c) f = 5 mm/min

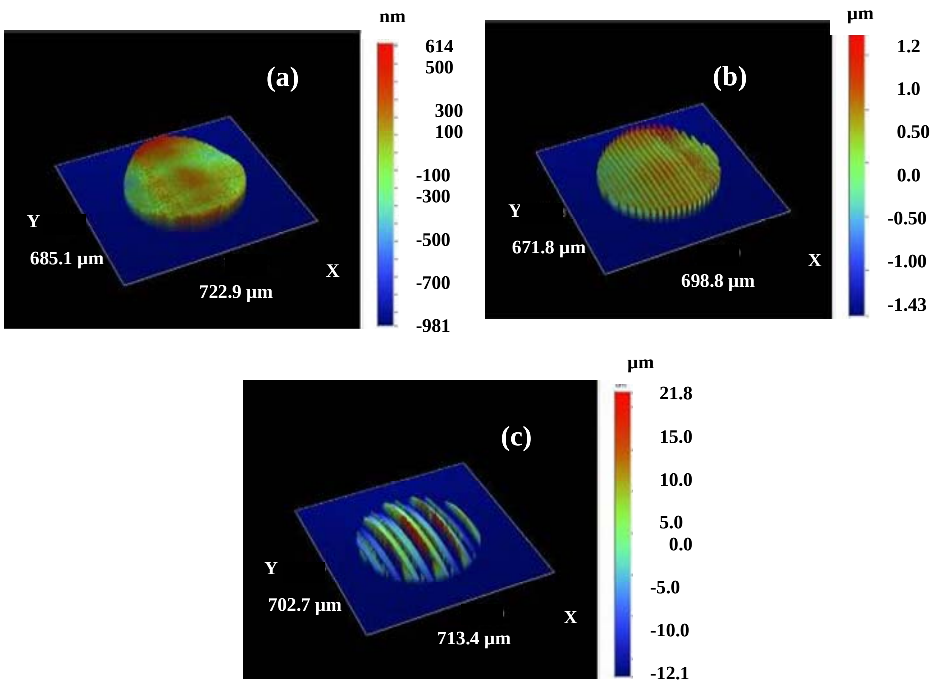

Figure 4.24 Form error plot of monograms of microlens machined under spindle speed of 50 rpm: (a) f = 0.25 mm/min, (b) f = 1 mm/min 50 mm/min, (c) f = 5 mm/min

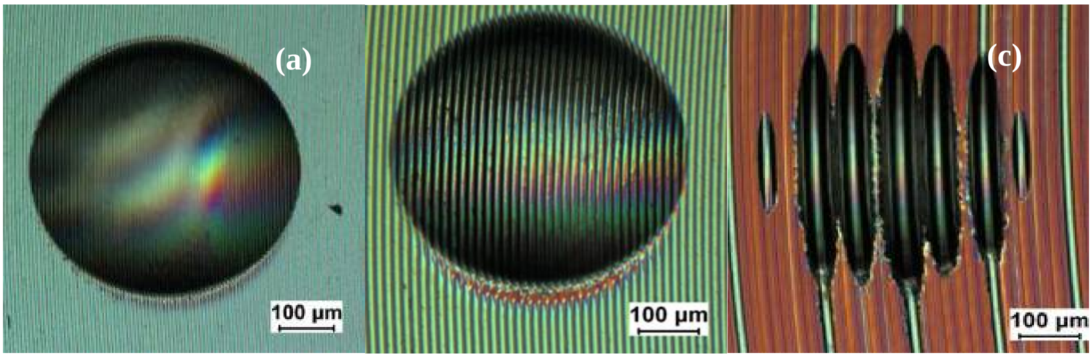

Figure 4.25 Monograms of microlens machined under spindle speed of 25 rpm:

(a) f = 0.25 mm/min, (b) f = 1 mm/min 50 mm/min, (c) f = 5 mm/min

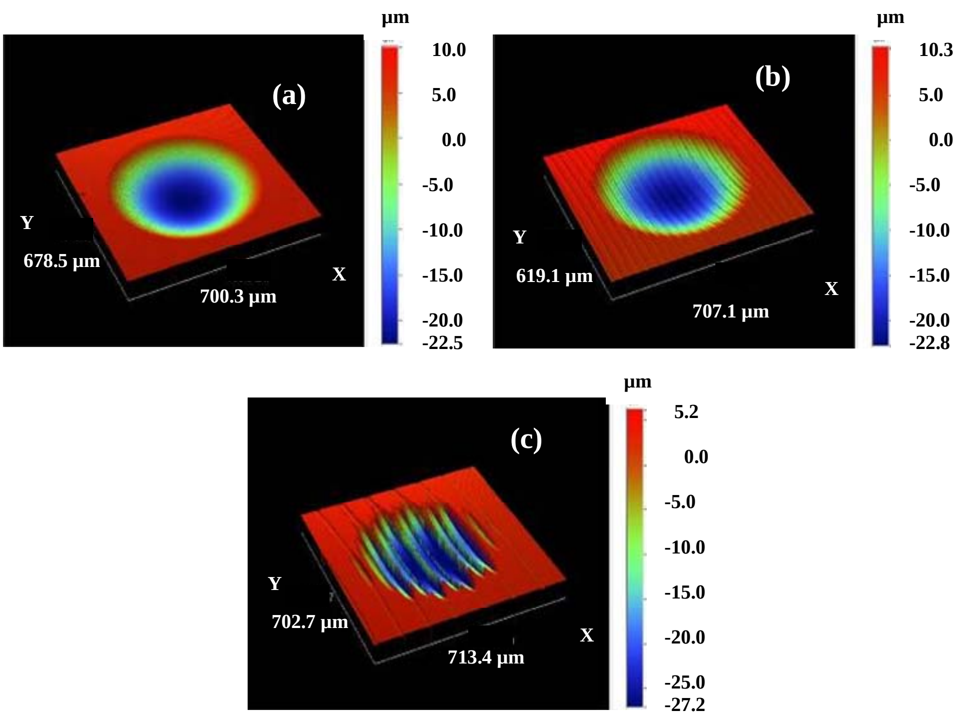

Figure 4.26 3D original shape of monograms of microlens machined under spindle speed of 25 rpm: (a) f = 0.25 mm/min, (b) f = 1 mm/min 50 mm/min, (c) f = 5 mm/min

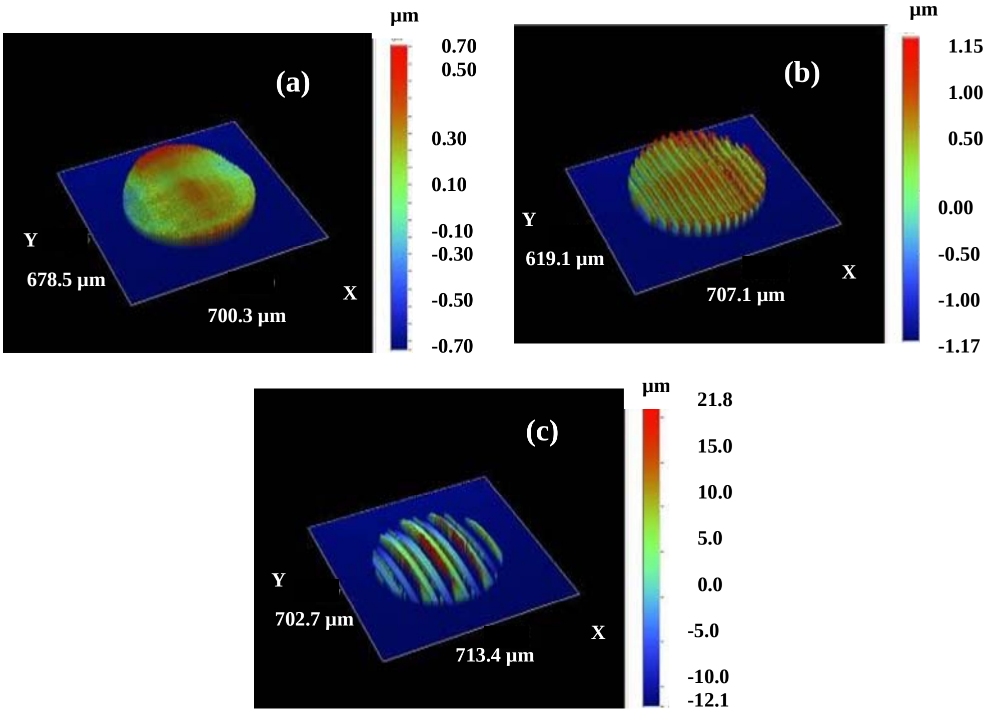

Figure 4.27 Form error plot of monograms of microlens machined under spindle speed of 25 rpm: (a) f = 0.25 mm/min, (b) f = 1 mm/min 50 mm/min, (c) f = 5 mm/min

4.3.5 Effect of tool compensation

After the study of the effect of cutting parameters on the surface generation in FTS machining, tool compensation is developed to further improve the surface quality of the machined profile. During the fabrication of the microlens array with FTS machining, the radius of the diamond tool tip is assumed to be perfectly zero, theoretically. However, the diamond tool possesses a small radius and this should be considered. The conceptual idea of the compensation methodology is to focus on compensation for the radius of the diamond tool. It can be described as a means to provide a shift of the desired radius of curvature in the C-program to modify the tool path of the SOP control system. After the tool compensation, the tool path is shifted a distance, which is equivalent to the value of the tool radius, in the normal direction of the surface of the microlens profile.

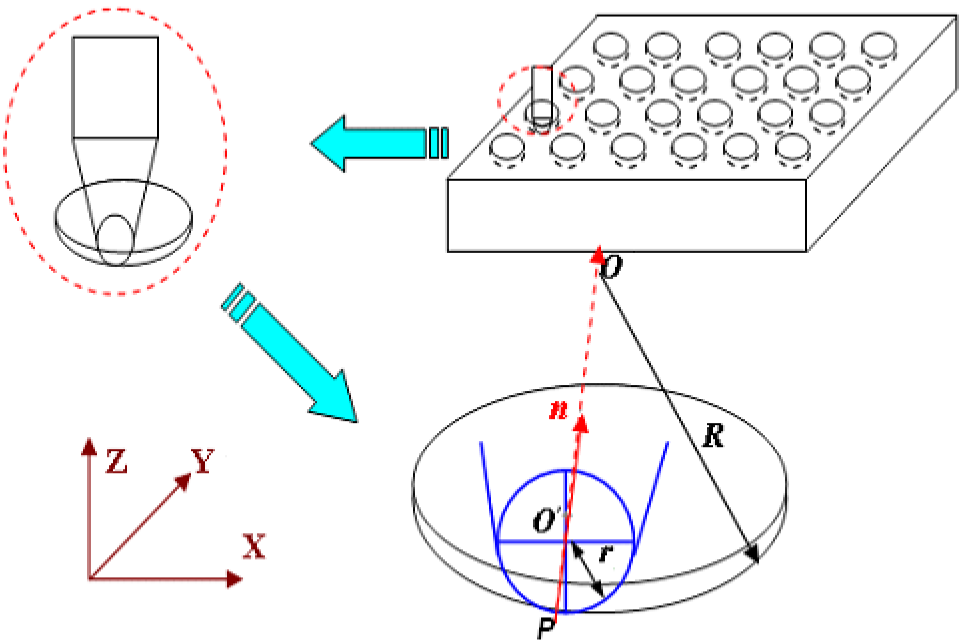

Figure 4.28 Conceptual idea of tool radius compensation

Figure 4.28 shows the conceptual idea of the tool compensation. Without tool compensation, the tool path is generated according to the position of the contact point $P_i(x_i, y_i, z_i)$ of the diamond tool tip. After the tool compensation, the center of diamond tool is set as the reference of the cutter location point $O_i^{'}(x_i^{'}, y_i^{'}, z_i^{'})$ and the error can be eliminated from the over-cut. The simultaneous value of the cutter location $O_i^{'}(x_i^{'}, y_i^{'}, z_i^{'})$ can be determined by Equation (4.7):

$$O_i' = P_i + \mathbf{n}_i \times r \tag{4.7}$$

where $\mathbf{n}_i$ is the unit normal vector of $P_i(x_i, y_i, z_i)$ on the surface of the microlens profile.

The location of the cutter is expressed as Equation (4.8):

$$\begin{cases} x_i' = x_i + rn_{i,x} \\ y_i' = y_i + rn_{i,y} \\ z_i' = z_i + rn_{i,z} \end{cases} \tag{4.8}$$

where $n_{i,x}$, $n_{i,y}$ or $n_{i,z}$ is the projection of $\mathbf{n}_i$ in the X ,Y and Z axis, respectively.

Assume the surface being cut is defined as $\mathbf{r} = \mathbf{r}(u, w) = \mathbf{r}(x(u, w), y(u, w), z(u, w))$, the unit normal vector can be expressed as follows:

$$\mathbf{n} = \frac{r_u \times r_w}{|r_u \times r_w|} \tag{4.9}$$

Before the implementation of tool compensation, the least square radius or the best fit radius of the machined surface profile needs to be determined by analyzing the measurement data in the cutting test, without tool compensation. The calculated least square radius is 1.20251 mm which is around 0.03 mm or 30 μm larger than the radius of curvature (1.1705 mm) of the desired profile, the result of which is shown in Figure

4.29. This value is approximately the same magnitude as the radius of the diamond tool used in the cutting experiments. Hence, this value is entered into the SOP control system for modifying the C-program and the new program is used for another set of cutting experiments which aims at evaluating the effectiveness of the tool compensation method.

The results of the cutting experiments with tool radius compensation indicate that the absolutely radius is 1.17 mm, which is closer to the desired radius of curvature as shown in Figure 4.30. Furthermore, the form error is found to be reduced from 0.8269 μm to 0.5255 μm. Table 4.6 tabulates the resulting residual form error. This demonstrates the efficiency of tool radius compensation. The tool compensation used in the present study is effective in correcting the residual form error in FTS machining of microlens arrays.

Table 4.6 Residual form error and efficiency of tool compensation

	Before Tool Compensation	Tool Radius Compensation
Residual form error [μm]	0.8269	0.5255
Efficiency [%]	Not applicable	57.4

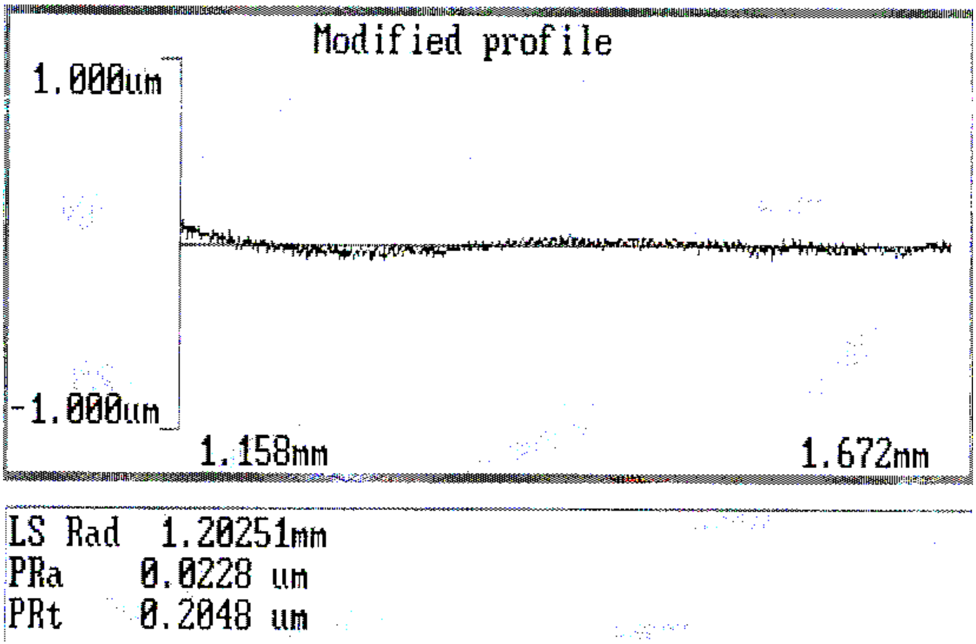

Figure 4.29 The least square radius before tool compensation

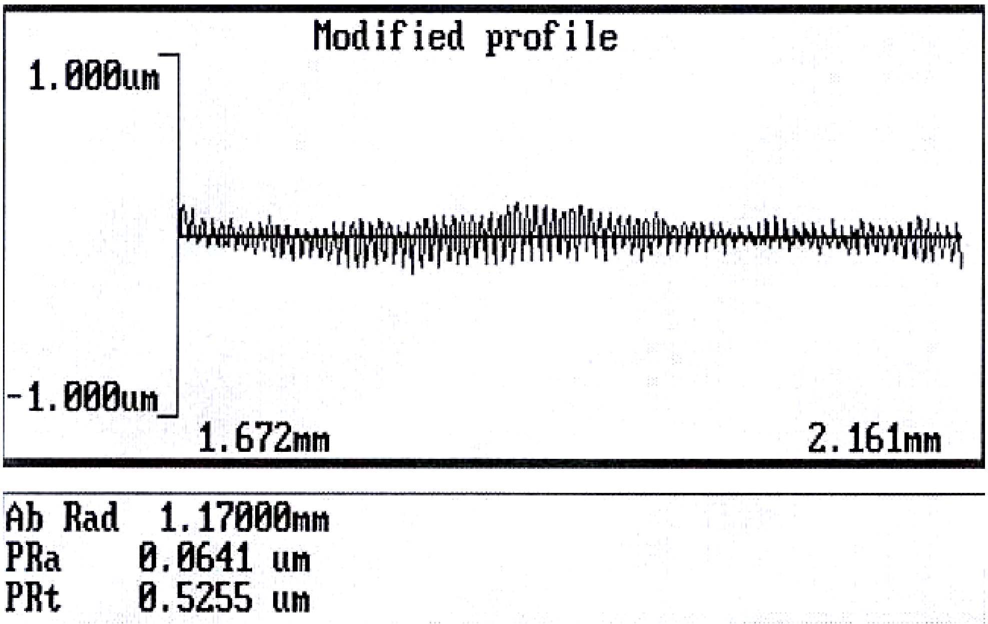

Figure 4.30 Form error of the absolute radius after tool compensation

4.4 Result of Pattern Analysis

Optical microstructures are small surface topologies which are organized with a spatial relationship in terms of a pattern, such as pyramids, microlens arrays, lenticulations and echells. Characterization of surface generation based on single surface topology on the optical microstructure may not be sufficient to reflect the surface quality as a whole. Further analysis of the surface generation of the pattern of surfaces and their spatial relationships in FTS machining is useful for better understanding the surface generation of the optical microstructure as a whole.

In the present study, a surface characterization method is purposely built, based on pattern analysis. It is used to characterize the surface generation of microlens arrays, focusing on an investigation of the process factors involved. The pattern analysis was conducted in order to investigate the effect of spindle speed and feed rate on form error, which is critical in the surface generation of micro-structural patterns by FTS machining. The results are shown in Tables 4.7 and 4.8.

As shown in Figure 4.31, the form error in term of the root-mean-square value in the pattern analysis is relative larger than for single lens measurements, since a larger area of three dimensional profiles is assessed. It is interesting to note that the trend of form error variation with spindle speed agrees well with that for single lens analysis. The form error of machined patterns of microlens arrays is found to decrease with increasing spindle speed at various surface speeds.

Table 4.7 Result of effect of spindle speed in pattern analysis (feed rate = 1 mm/min, depth of cut = 5 μm)

Surface Speed	0.5652 m/s	0.7536 m/s	1.1304 m/s
Spindle Speed (rpm)	Form Error in root-mean-square value S_q (μm)		
25	0.66493	0.69528	N/A
50	0.27127	0.28495	0.27157
75	0.18337	0.18337	0.17704
100	0.36688	0.3702	0.38968
125	0.24006	0.23759	0.23734

Table 4.8 Result of effect of feed rate in pattern analysis (depth of cut = 5 μm)

Spindle Speed	165rpm	110rpm	82rpm	55rpm
Feed Rate (mm/min)	Form Error in root-mean-square value S_q (μm)			
0.25	0.760	0.773	0.779	0.803
0.5	0.287	0.249	0.257	0.232
0.75	0.685	0.712	0.761	0.872
1	0.330	0.341	0.267	0.310
1.25	0.286	0.269	0.340	0.523

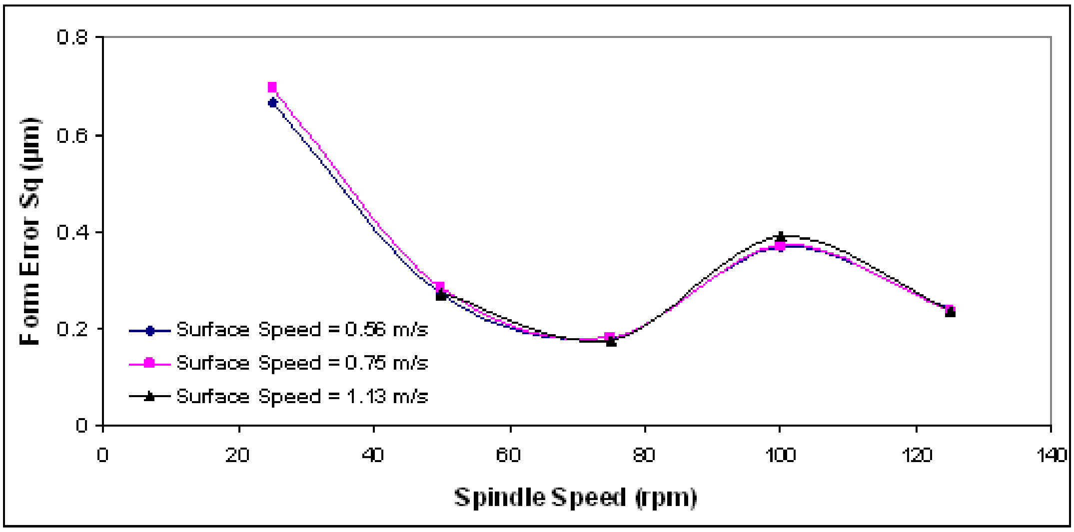

Figure 4.31 Effect of spindle speed in form generation (S_q)

The effect of feed rate on surface generation in form generation of MLA patterns is shown in Figure 4.32. In the pattern analysis, the effect of feed rate is found to be inconsistent as compared with the result in single lens analysis. The form error fluctuates instead of decreasing with increasing feed rate. This may be due to the fact that the effect of feed rate on form error is small when an appropriate range of cutting parameters is employed. However, poor surface finish would result when the feed rate is much larger than the approximate range. Figure 4.33 shows the 3D surface topography of machined patterns. Significantly larger tool marks can be observed when a higher feed rate is employed. It can be concluded that better surface generation can be obtained by selecting an appropriate range of cutting parameters instead of solely increasing the feed rate.

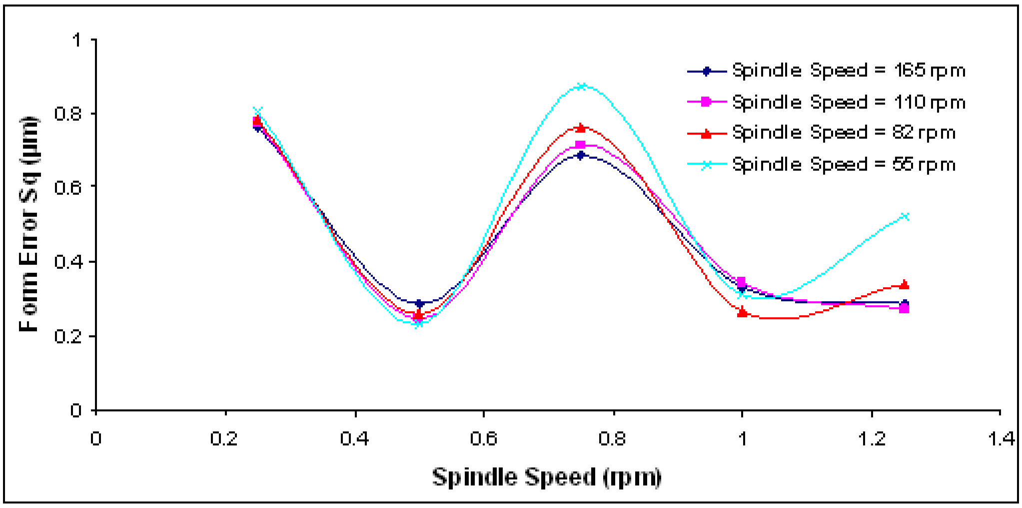

Figure 4.32 Effect of feed rate in form generation (S_q)

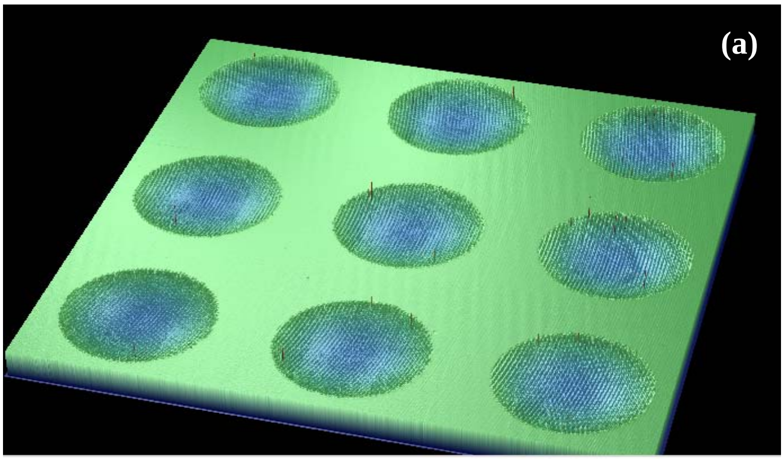

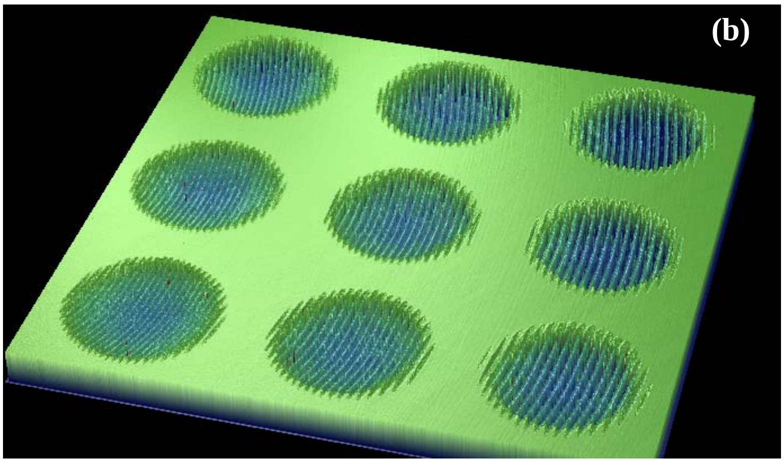

Figure 4.33 3D topography in investigating effect of feed rate in pattern analysis:

(a) Feed rate = 0.25 mm/min (b) Feed rate = 1.25 mm/min

4.5 Summary

A better understanding of the factors affecting surface generation of the machined profile is of prime importance for the further development of ultra-precision machining technology, and for the better design of machines to meet the need for ultra-high precision. As described in this Chapter, the surface quality of the workpiece in FTS machining is found to depend largely on the selection of cutting conditions and on the tool path. Process factors affecting surface quality in ultra-precision machining with FTS, consist of feed rate, spindle speed and depth of cut. Moreover, a theoretical analysis has been undertaken to study the effect of the critical clearance angle which may affect the form of the machined surface and cause the microlens distortion. Hence, a criterion for the determination of the critical clearance angle has been derived which provides an important means for selecting an appropriate front clearance angle of the tool so as to avoid the distortion of the lens. In the present study, a series of cutting experiments were conducted under various cutting conditions. To analyse the surface generation in FTS machining of micro-structural surface, single lens analysis and pattern array analysis of the micro-lens array are carried out and the results of the analyses show a consistent trend.

Experimental results indicate that the influence due to process factors can be minimized by appropriate selection of cutting conditions. Moreover, a defect analysis of these process factors was conducted as well as further exploring the appropriate range of cutting parameters in FTS machining. Within the predetermined range, the surface quality in FTS machining can be improved by increasing the spindle speed and by reducing the feed rate. The depth of cut appears to have comparatively little effect on the surface quality in FTS machining. The results in the present study provide an important means for the optimization of the surface quality in FTS machining and this has previously received relatively little attention.

CHAPTER 5 CHARACTERIZATION OF TOOL WEAR IN FTS MACHINING

5.1 Introduction

As discussed in Chapter 3, the diamond tool plays a crucial role in surface generation in ultra-precision machining with a fast tool servo. The profile of a machined surface is basically generated by the repetition of the tool profile in the plane of the normal cutting direction. The geometrical accuracy of the cutting edge and its stability has a great influence on the surface quality of the machined profile. Since diamonds have little affinity with many materials, a diamond cutting edge is considered to have high fidelity, which is the ability to transfer the profile of a cutting edge to the workpiece. The wear on the cutting edge grows substantially as the cutting length increases (Taminiau, 1991; Keen, 1971).

Tool wear not only degrades the product quality but also raises the machining cost. This is particularly true of the single crystal diamond tool employed in FTS machining, because it is expensive and is easily susceptible to wear due to the fact that the tool is sharp with a very small tool nose radius. In this chapter, a study of the tool wear is presented which provides a better understanding of the performance of diamond tools in FTS machining. This contributes significantly to the enhancement of the fabrication process and helps to better control of the surface quality of the machined profile.

To minimize the wear of the diamond tool, many studies have been carried out which explore its characteristics (Jiwang 2003, M. Sharif Uddin, 2004 and 2006 and Durazo-Cardenas 2007). However, most of the studies focus on investigation of the wear phenomena in ultra-precision machining. The study of tool wear for FTS machining has received relatively little attention. To investigate the effect of the tool wear in FTS machining, a series of cutting experiments have been conducted by cutting tilted flat surfaces. Several methodologies have been employed to study the wear characteristics. Two direct methods have been proposed for quantitative analysis of the tool wear in FTS machining. The first direct method compares the maximum dimension of wear height (VB_{max}) and the width of flank wear captured by SEM monograms with respect to the cutting distance. It is a methodology commonly employed in quantifying the tool wear. To characterize the tool wear in a more quantitative way, a digital image processing method has been developed based on the research work undertaken by the research team in the AOMC. Finally, the investigation was focused on the establishment of the relationship between surface generation in FTS machining and tool wear.

5.2 Design of Experiments

In the present study, the cutting experiment is a continuous process by machining samples with the same specifications. As shown in Figure 5.1, the dimensions of the sample are 10 mm in diameter and an inclination of the surface is dependent on the specific study. Each sample of cut is equal to a predetermined distance. By accumulating a number of machined samples, the cumulative cutting distance can be calculated. Moreover, surface quality of the machined samples after a certain distance can be measured as well. To minimize the error due to the geometry of the microstructure and to test the performance of the FTS, a workpiece is machined to a tilted flat surface which can allow the FTS to actuate the tool to move in a sinusoidal trajectory, at full amplitude. In addition, a tilted flat surface is also widely used in the optical industry such as in the fabrication of complex optical microsystem (Stoebenau and Sinzinger, 2009) and micro-lithography applications (Wagner et al., 2006). In order to ensure that the tool wear experiment is undertaken under consistent conditions, the whole life of the individual diamond tool was studied under the same cutting conditions.

In the present study, the cutting experiments were performed in three stages. After each stage, the diamond tips were observed by scanning electron microscopy (SEM). The wear characteristics of single crystal point diamond tools in terms of wear pattern are further investigated by analyzing the image of the cutting edges, captured by SEM.

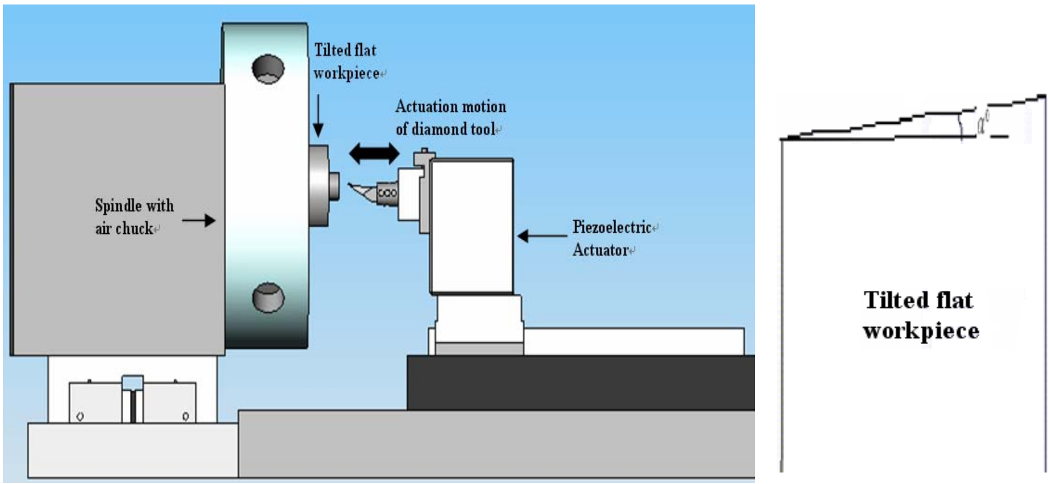

Figure 5.1 Fabrication of tilted flat surface by ultra-precision machining with FTS

The material of the workpiece is NiCu which is a material commonly used in mold inserts of ultra-precision optical molds. Conical non-controlled waviness tools are used, with specifications shown in Table 5.1. To minimize the factors affecting the accuracy of the final result, only one diamond tool and consistent cutting conditions are used, as shown in Table 5.2.

Table 5.1 Specifications of Diamond Tool (N0.025mLEC)

Radius	0.025 mm
Rake angle	0 ^{o}
Front clearance	15 ^{o}
Primary Depth	0.05mm
Arc	120^{o}
Secondary clearance	60 ^{o}
Included angle	30 ^{o}
Shank	6.35 x 6.36 x 51 mm

Table 5.2 Cutting conditions for tool wear experiments

Spindle Speed	100 rpm
Feed Rate	0.1 mm per min
Depth of Cut	5 μm
Depth of machined workpiece	10 μm
Tool rake angle	0 ^{o}
Tool nose radius	0.032 mm
Front clearance angle	15 ^{o}

As mentioned previously, each sample cut represents a certain predetermined distance. By accumulating a number of machined samples, the cutting distance can be calculated. The following describes the calculation procedure. Figure 5.2 shows a specimen 10 mm diameter with an α degree tilted surface. The cutting path can be described as a spiral locus, as shown in Figure 5.3.

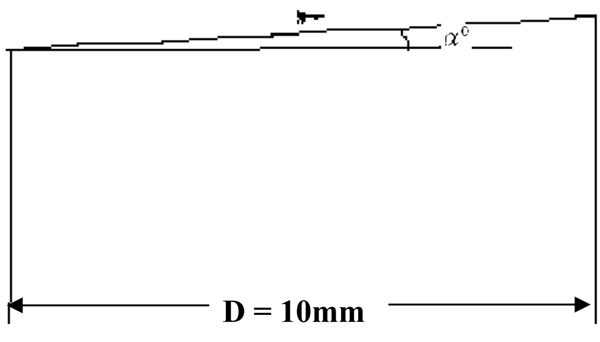

Figure 5.2 Tilted flat surface of workpiece

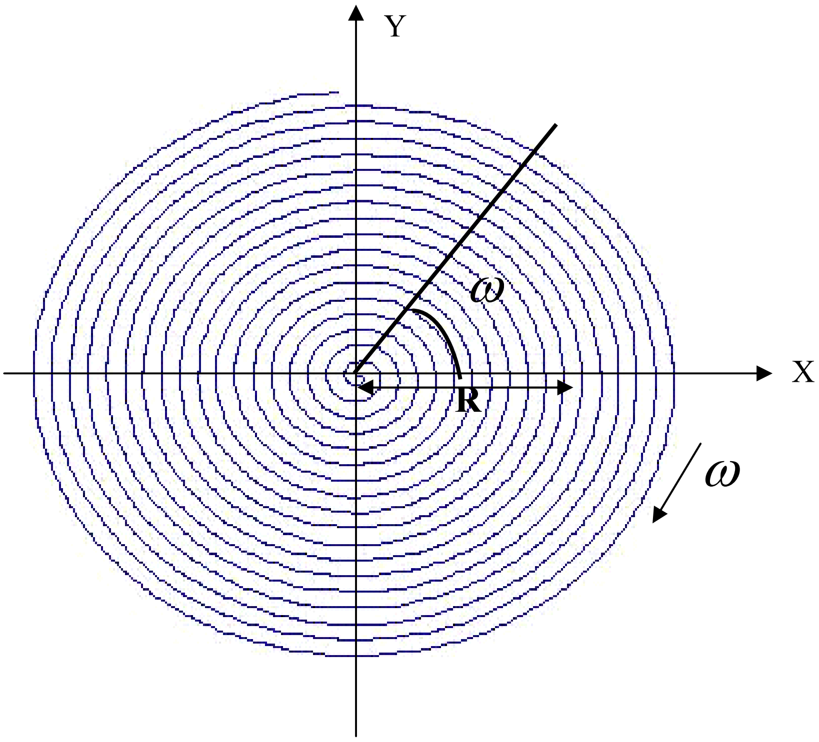

Figure 5.3 Spiral cutting path in the cutting tests

For convenience, Table 5.3 lists nomenclature used in this chapter.

Table 5.3 Nomenclature

L	Tilted cutting distance
L_0	Horizontal spiral cutting path
D	Diameter of workpiece
R_0	Radius of workpiece (mm)
R	Radial location of diamond tool (mm)
α	tilted angle
r	radius of the diamond tool
f	feed rate (mm/min)
T	real time in second
S	rotational spindle speed in rpm
$\theta(t)$	Radial location of spindle (degree)

In order to estimate this titled spiral cutting path, the parameters of the cutting path are derived as follows:

$$L = \frac{L_0}{\cos\alpha} \tag{5.1}$$

$$R_0 = \frac{D}{2}$$

$$R(t) = R_0 - f \bullet t/60 \tag{5.2}$$

$$\begin{cases} \theta(t) = \frac{S}{60} \bullet 2\pi \bullet t \\ X(t) = \left(D/2 - f(t)\right) \bullet \cos\theta(t) \\ Y(t) = \left(D/2 - f(t)\right) \bullet \sin\theta(t) \\ Z(t) = \left(D/2 - f(t)\right) \bullet \sin\theta(t) \tan\alpha \end{cases} \tag{5.3}$$

$$\begin{aligned} L_0 &= \int_0^{D/2f} \sqrt{\left(\frac{dx}{dt}\right)^2 + \left(\frac{dy}{dt}\right)^2 + \left(\frac{dz}{dt}\right)^2}\, dt \\ &\approx \sum_{t=0}^{D/2f} \sqrt{\left(\frac{dx}{dt}\right)^2 + \left(\frac{dy}{dt}\right)^2 + \left(\frac{dz}{dt}\right)^2}\, \Delta t \end{aligned} \tag{5.4}$$

The derived functions are entered into a MatLab program as well as the conditions employed in the cutting experiments. The program source codes are given as follows:

```
function dist=funCutDist
% D: diameter of the cylinder(mm);S: spindle speed(rpm);f: feed
% rate(mm/s);a: angle of slope(rad);
D=10;S=100;f=0.1/60;a=0.002*pi; % for test!
syms t;
R0=D/2;
Rt=R0-f*t;
tht=S/60*2*pi*t;
xt=Rt*cos(tht);
yt=Rt*sin(tht);
zt=Rt*sin(tht)*tan(a);
Ff=sqrt(diff(xt,t)^2+diff(yt,t)^2+diff(zt,t)^2);
```

```
t1=R0/f;
dt=1e-3;
t=0:dt:t1;
Ff0=eval(vectorize(Ff));
figure;
subplot(1,2,1);plot3(eval(vectorize(xt)),eval(vectorize(yt)),eval(vec
torize(zt)));title('Cutting trace');
subplot(1,2,2);plot(t,Ff0);title('Cutting integration');
L=sum(dt*Ff0); % cutting length;
dist=L
```

The calculated distance of one cutting path (L) is 78 m. With a depth of cut of 5 μm, two complete feeds are required to cut a tilted flat surface 10 μm and the cutting distance is calculated as 156 m. Consistent cutting conditions were employed to ensure a constant accumulative distance.

After finishing the cutting of each sample, the surface quality is measured. After each stage of cutting, an image of the diamond tool tip is captured by SEM. The cutting experiment was carried out in three stages, as shown in Table 5.4. Figure 5.4 shows a SEM photograph of the diamond tool, captured before cutting. A sharp cutting edge and contour of the diamond tool are observed. One of the methods for the characterization of the tool wear makes use of direct observation and measurement of flank wear by SEM, after each stage of cut. While another makes use of digital image processing for a quantitative characterization of the tool wear.

Table 5.4 Cutting schedule for the experiments for the study of diamond tool wear

Stage	Samples machined	Cutting Distance(m)	Accumulative Cutting Distance(m)
1st	5	780	780
2nd	5	780	1560
3rd	7	1092	2652

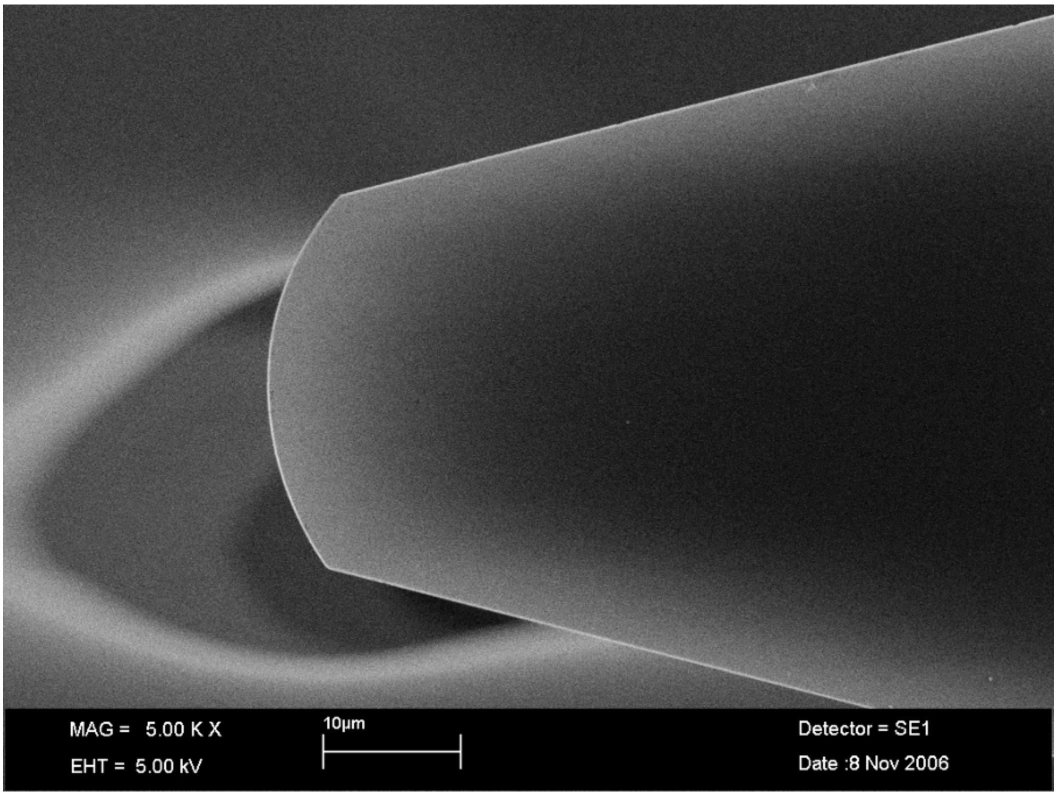

Figure 5.4 SEM monogram of diamond tool before tool wear cutting test

5.3 Flank Wear in FTS Machining

After cutting the predetermined lengths, the wear characteristics of single crystal diamond tools in terms of wear pattern are investigated by direct measurement, which is performed by using microscopy techniques, such as scanning electron microscopy (SEM) (Asai et al., 1990; Uddin et al., 2004). The wear of the diamond tool is characterized by measuring the tool's flank wear land (VB) and/or the tool-tip profile recession. The method of comparing VB_{max} and the width of flank wear with respect to the cutting distance has commonly been used in quantifying the tool wear.

Ultra-precision machining with FTS is a technology developed based on the single point diamond turning process, which cuts at an undeformed chip thickness in the nanometer range. In FTS machining, the basic tool wear is likely to be a gradual process. This is due to a combination of mechanical abrasive wear and adhesive wear. Since the tool is initially very sharp, the stresses on the cutting edge of the tool are very high, and this results in a micro-ruggedness on the cutting edge. Besides, the surface of the workpiece may not be perfectly flat. Shear deformation occurs at various depths of cut during the machining even if a constant depth of cut was preset. This may lead to some micro-grooves being generated on the flank region, along with gradually increasing flank wear. These micro-grooves along the cutting edge of a diamond tool were proposed as critical damage phenomena by Keen (1971). Figure 5.5 shows a captured image of the tool tip of a wear tool by SEM, with grooves on the flank face.

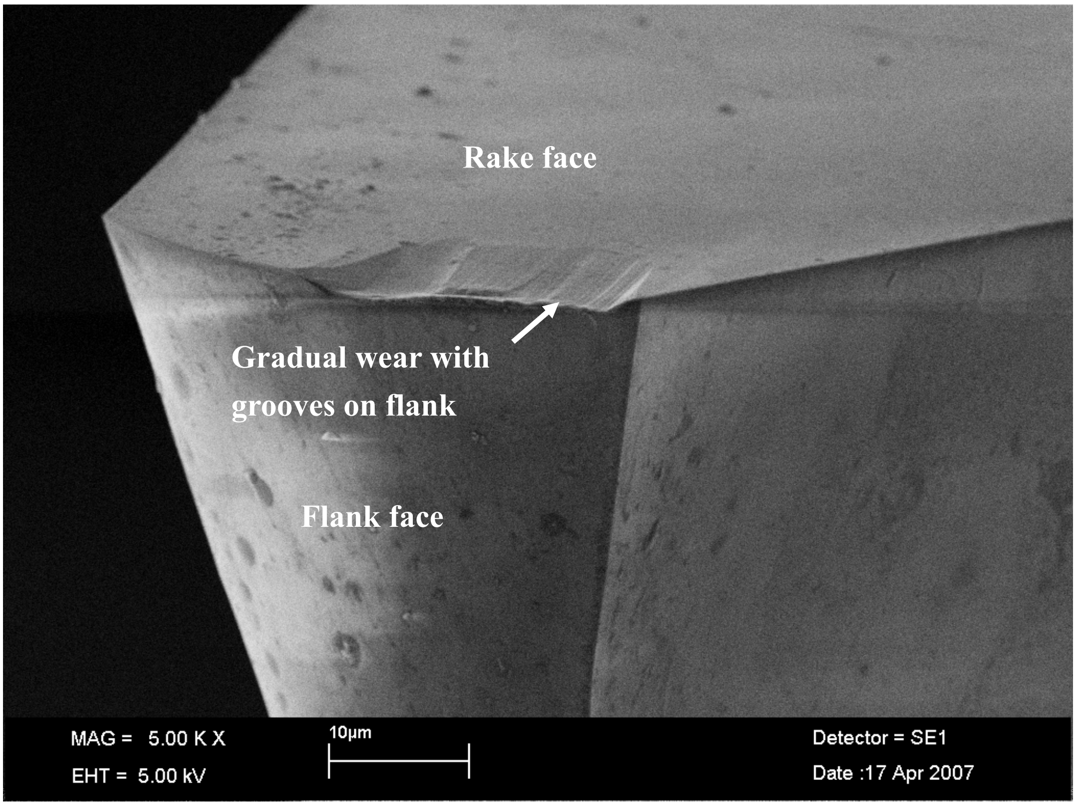

Figure 5.5 Captured image of tool tip by SEM with gradual wear with grooves on flank

In the present study, the tool wear characterization is based on the assessment of the material loss that typically occurs on the tool rake and flank face. To assess the tool wear, VB_{max} and the width of the flank wear have been used as two parameters for quantitatively determining the diamond tool wear (M. Sharif Uddin, 2004 and 2006). Figure 5.6 shows typical flank wear and its measurement for a diamond tool. The value of VB_{max} and width were measured on the captured image taken by SEM after each cutting stage, as shown in Table 5.4.

Table 5.5 shows the relationship between flank wear of the diamond tool and the cutting distance. After cutting for about 0.78 km, the flank wear land of the diamond tool indicates that the height and width of the flank wear increase gradually with the cutting distance. The height and width of the flank wear are measured as 2.16 μm and 21.86 μm. With the increase of cutting distance, the cutting edge of the tool wears more severely and the flank wear region should become predominant. After cutting for 1.56 km, the end of stage 2 cutting, more and more grooves are found on the flank, which are larger in length and depth. The height and width of the flank wear are measured as 2.7 μm and 22.16 μm, which signifies progressive wear of the tool. After finishing stage 3 of the cutting i.e. 2.65 km, it can be observed that there is significant material loss on the diamond tool tip and indicating progressive wear of the tool. The height and width of the flank wear are measured as 3.24 μm and 25.95 μm.

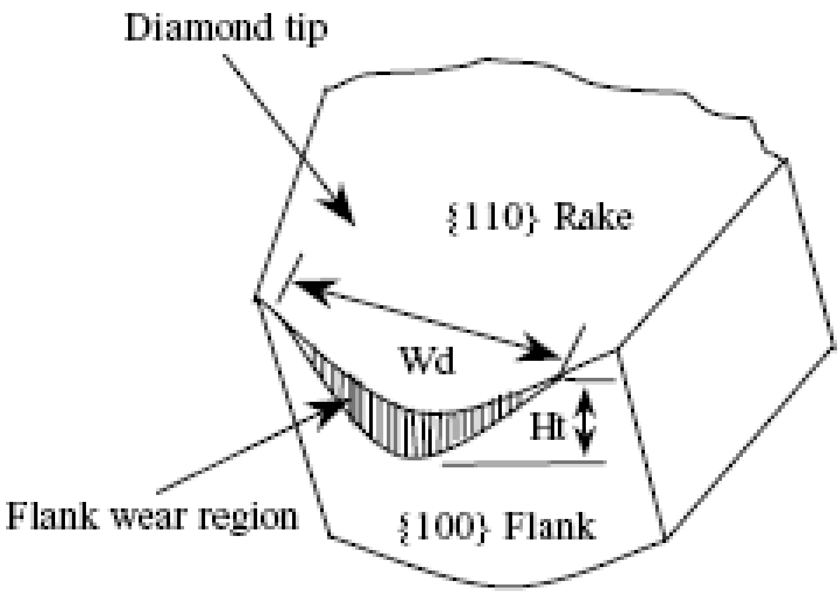

Figure 5.6 Typical wear and its measurement on a diamond tool (from Uddin et al., 2004)

Table 5.5 Captured image of diamond tool wear in FTS machining by SEM

<table>
<tr><th>Cumulative Cutting Distance</th><th>Wear VB_{max}</th><th>Wear Width</th></tr>
<tr><td>0.78 km</td><td>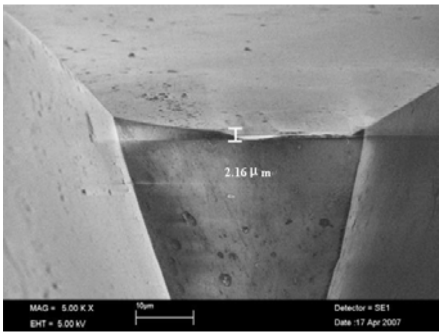
</td><td>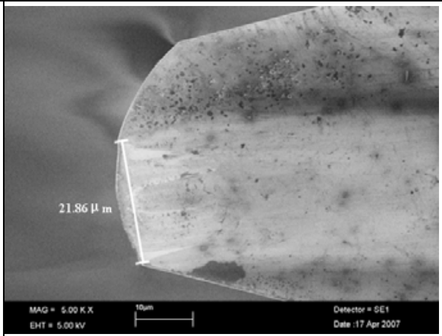
</td></tr>
<tr><td>1.56 km</td><td>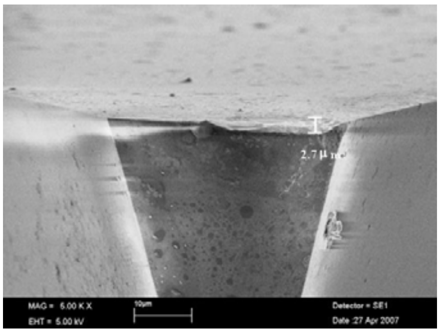
</td><td>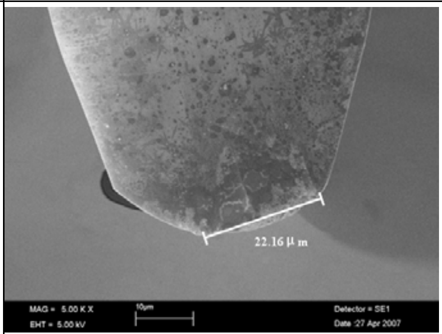
</td></tr>
<tr><td>2.65 km</td><td>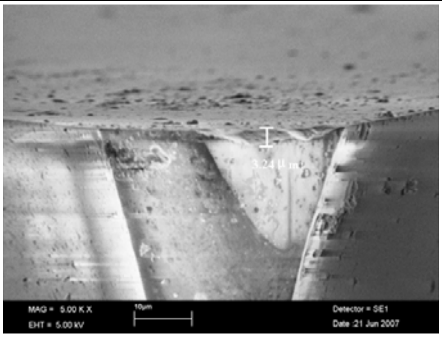
</td><td>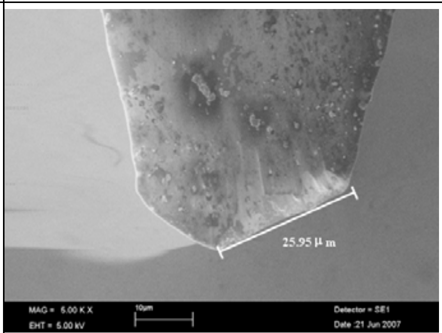
</td></tr>
</table>

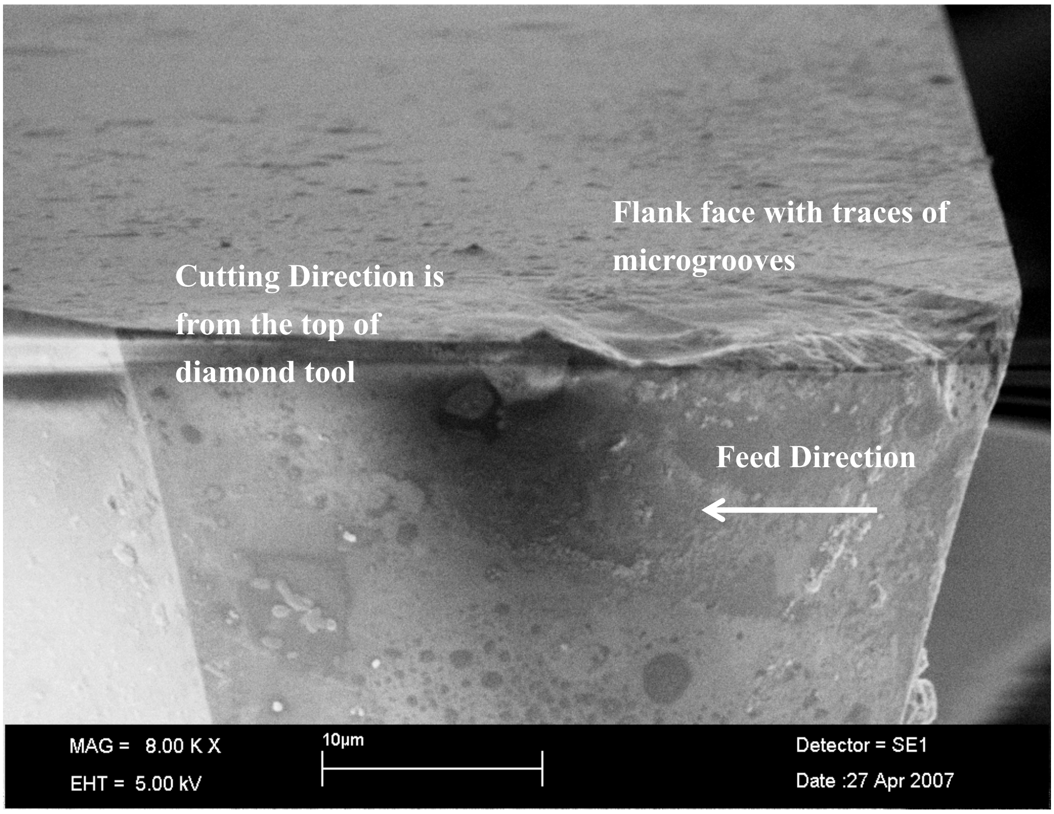

Figure 5.7 Image of a worn diamond tool captured by SEM

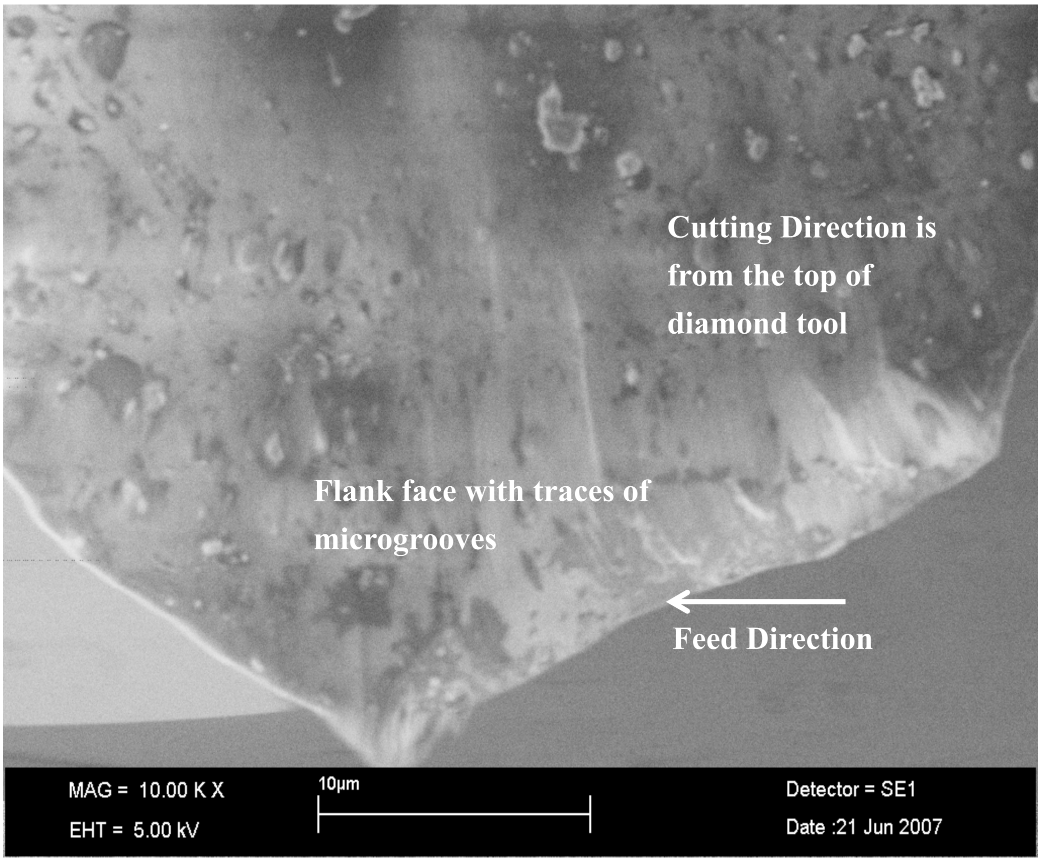

Figure 5.8 Image of a worn diamond tool captured by SEM

Figure 5.7 shows the flank face with traces of microgrooves which induces severe material loss on the diamond tool tip. Figure 5.8 shows another SEM image of the diamond tool tip from the top view. When compared with Figure 5.4, it's easily observed that the original shape or radius of the diamond tool is no longer preserved. Based on the measured value of flank wear, it seems not to be easy to accurately reflect the exact damage on the diamond tool tip. Comparing the SEM captured images after 1.56 and 2.65 km, the value of flank wear fluctuate slightly, but the shape of the diamond tool tip changes a lot. To further support the finding, a more quantitative method, the digital image processing method, is proposed and discussed for the characterization of tool wear in the following section.

5.4 Characterization of Tool Wear

Although the method of measurement of wear VB_{max} and width has been widely applied in assessing the tool wear, it cannot fully quantify the material loss and reflect exactly the damage on a diamond tool tip. For characterizing tool wear quantitatively, the captured image of the cutting edges of diamond tools is examined by a digital image processing method purposely built for the study. The method computes the area and the volume of material loss on the diamond tool tip by the image processing algorithm.

Figure 5.9 graphically illustrates the digital image processing technology employed in the present research. The major framework is outlined by totally three lines, which are the A-line of the new tool outer contour, the B-line of the outer contour of the tool wear and the C-line of the inner contour of the tool wear. Moreover, the BC-line which is the VB_{max} of the tool wear, can be derived. One of the assumptions in the present study is that the BC-line is a straight line (I. Durazo-Cardenas, 2007). The front clearance angle β is referred to the specifications of the diamond tool.

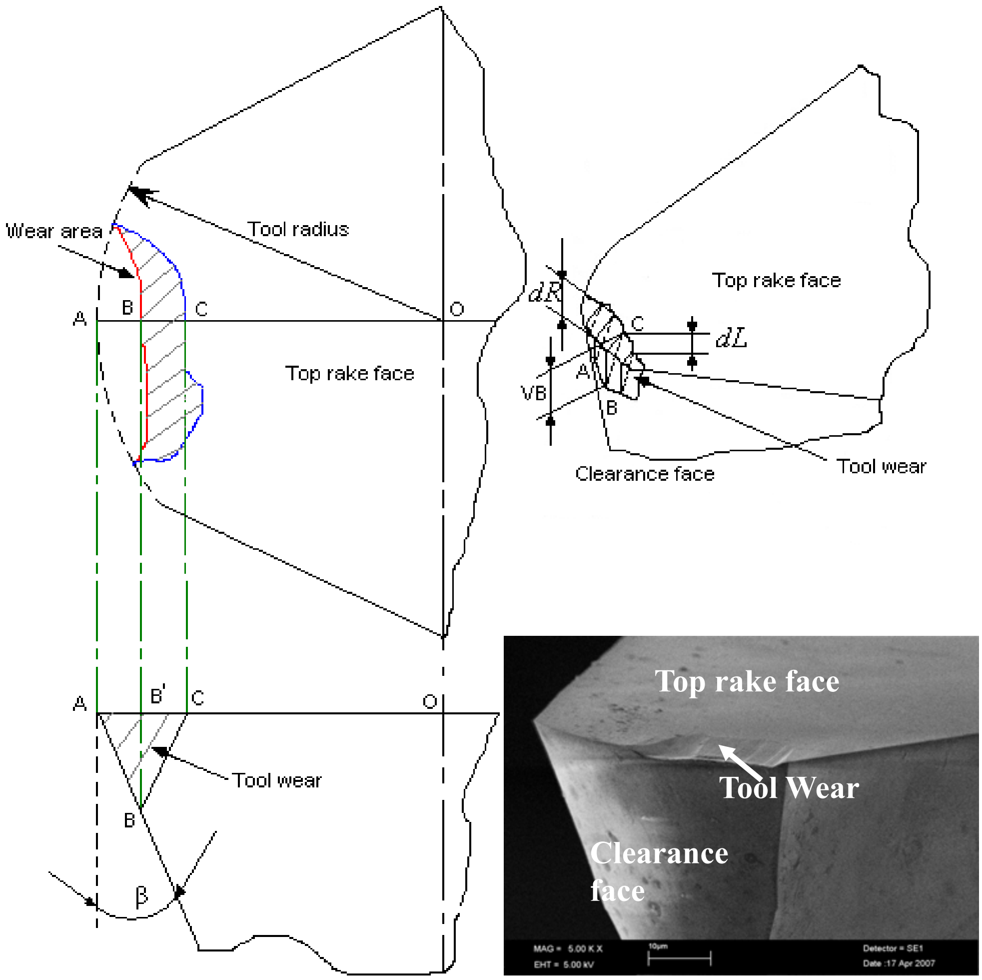

Figure 5.9 Graphical illustration of the characterization of tool wear

Eventually, the area and volume of material loss can be computed by Equation (5.5) and (5.6), respectively.

The area of tool wear can be calculated by Equation (5.5) as follows:

$$W_a = dR * dL \tag{5.5}$$

Where, dR is the distance between line A and line C calculated in pixels; dL is the width of each pixel in the digital image, which is 0.075 μm by calibration.

The volume of tool wear can be determined by Equation (5.6)

$$W_V \approx \int \frac{1}{2} * AC * \frac{AB^{'}}{\tan\beta} dL \approx \frac{1}{2} * \sum AC * \frac{AB^{'}}{\tan\beta} \tag{5.6}$$

After discussing the fundamental algorithm for the determination of the area and the volume of tool wear, the detail method of processing the digital image captured by SEM is described. Table 5.6 shows the progress of the digital image processing for the characterization of diamond tool wear. The first step of digital image processing is using a median filter to extract the worn area and unworn area from the background, into different gray levels. After processing the original image by the neighborhood averaging filter, the gray-level histogram of the image is generated. The processed image consists of three layers of pixels which are black, grey and white, corresponding to the background, unworn, and worn areas, respectively. By the threshold value of different segments, critical areas such as worn areas can be identified. For detecting the contour of diamond tool or the B' line, the edge detection method is employed. The image processing operators used are the 3×3 Sobel operators for determining the diamond tool contour in the present study.

Afterwards, the Hough transform is used to compute the arc radii and arc center coordinates of the original diamond tool in the image plane. This method is commonly employed on extracting the locations of regular curves such as lines or circles when a number of points that fall on the perimeter are known. Moreover, Hough transform is able to detect circular arcs by considering circular arc as partial shape of a circle. The coordinates of a peak in the parameter space indicate center and radius of the detected arc. The equation for a circle is given by

$$(x-a)^2+(y-b)^2=r^2 \tag{5.7}$$

where r is radius which is unknown, (a, b) is circle center or arc (one part of a circle) which is unknown and (x, y) is each point of a circle which is known.

Table 5.6 Progress of digital image processing for investigation of diamond tool wear

Median filtered rake face	Two threshold value segments	Fitting contour of worn diamond tool	Fitting contour of original diamond tool
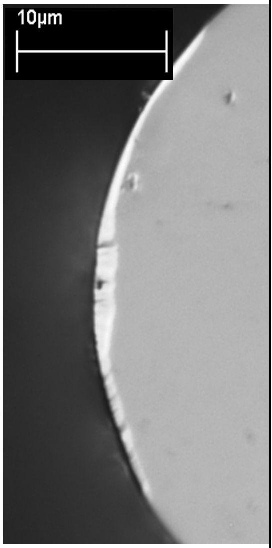	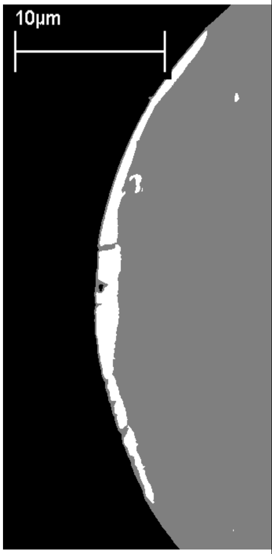	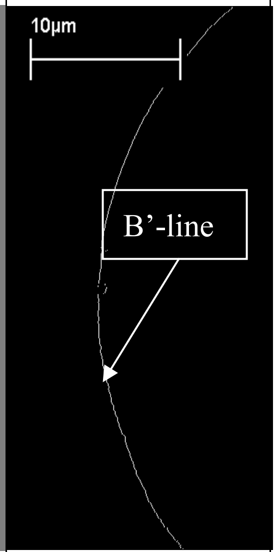	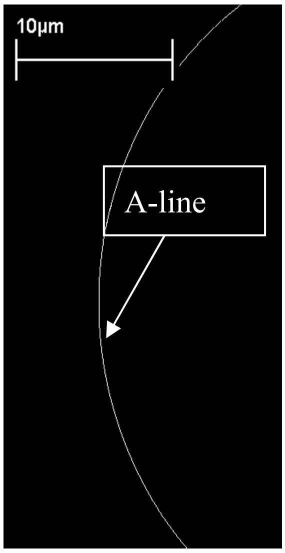
Worn regions	Combining worn regions with outer contour of original diamond tool	Combined image of worn region and contour of original diamond tool	Fitting contour of worn regions
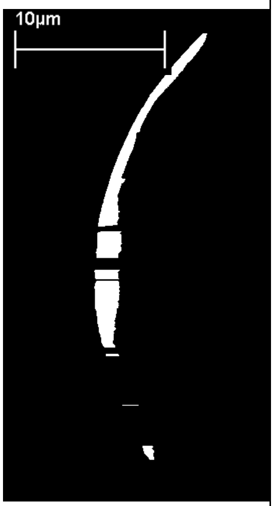	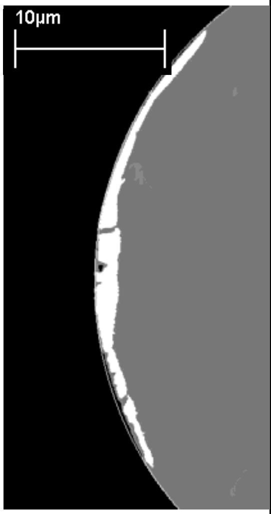		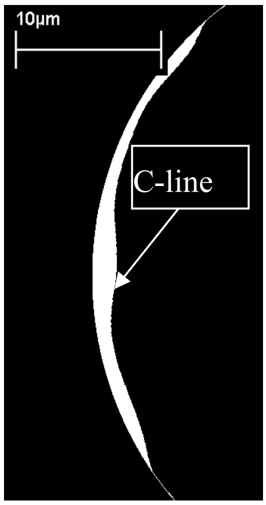

Choosing center and radius as the parameters of Hough transform, e.g. if an image contains many points, some of which fall on perimeters of circles. Firstly, the searching program is to find out parameter triplets (a, b, r) for charactering each circle. The locus of parameters composed with one point on the edge inside image space will be a right circular cone. Therefore, as long as there is one circle in image space, all right circular cones composed with points lie on it will intersect with a common point in parametric space. Coordinates of this common point are parameters of the equation for the circle in image space. A circle detected by Hough transform is calculated on basis of all the detected edge points and representing all possible circles through these points. Considering one point as (a, b), then the set of all circles through this point is represented as the set of all possible values of (a, b, r).

By filtering out the noise, the worn region can be identified by counting the number of white pixels. In order to find the C-line or the contour of the worn diamond tool, the processed image is combined with the identified original contour of the diamond tool. Least squares polynomial curve fitting is employed to determine the best fitting curve. With the use of the previous procedures, the A line, B’ line and C line can be determined for calculating the area and volume of the tool wear.

Figure 5.10 shows the distribution of white pixels after digital image processing. The curve of the worn contour of the diamond tool tip is determined by the least square polynomial fitting method. Hence, the contour of the diamond tool tip after cutting a certain distance can be computed, and is shown in Figure 5.11. Eventually, the number of pixels inside the A-line and C-line is used to compute the area of material loss from the diamond tool, and the volume is calculated based on the known value of the A-line, B'-line and C-line.

After analyzing the SEM captured diamond tool tip contour, the tool wear can be characterized by the digital image processing method, as shown in Figure 5.11. It is interesting to note that the area within line A and line B', or the worn area, is getting larger especially after cutting a distance of 1.56 km. After cutting for 780m, the worn area is using tens of pixels or the maximum length between line A and line B' is approximate 20 pixels. After cutting for 1.56 km, the worn area quantity is increased to hundreds of pixels or the maximum length between line A and line B' is approximate 100 pixels. The detailed results of analyzing the worn area and volume by digital image processing are summarized in Table 5.7.

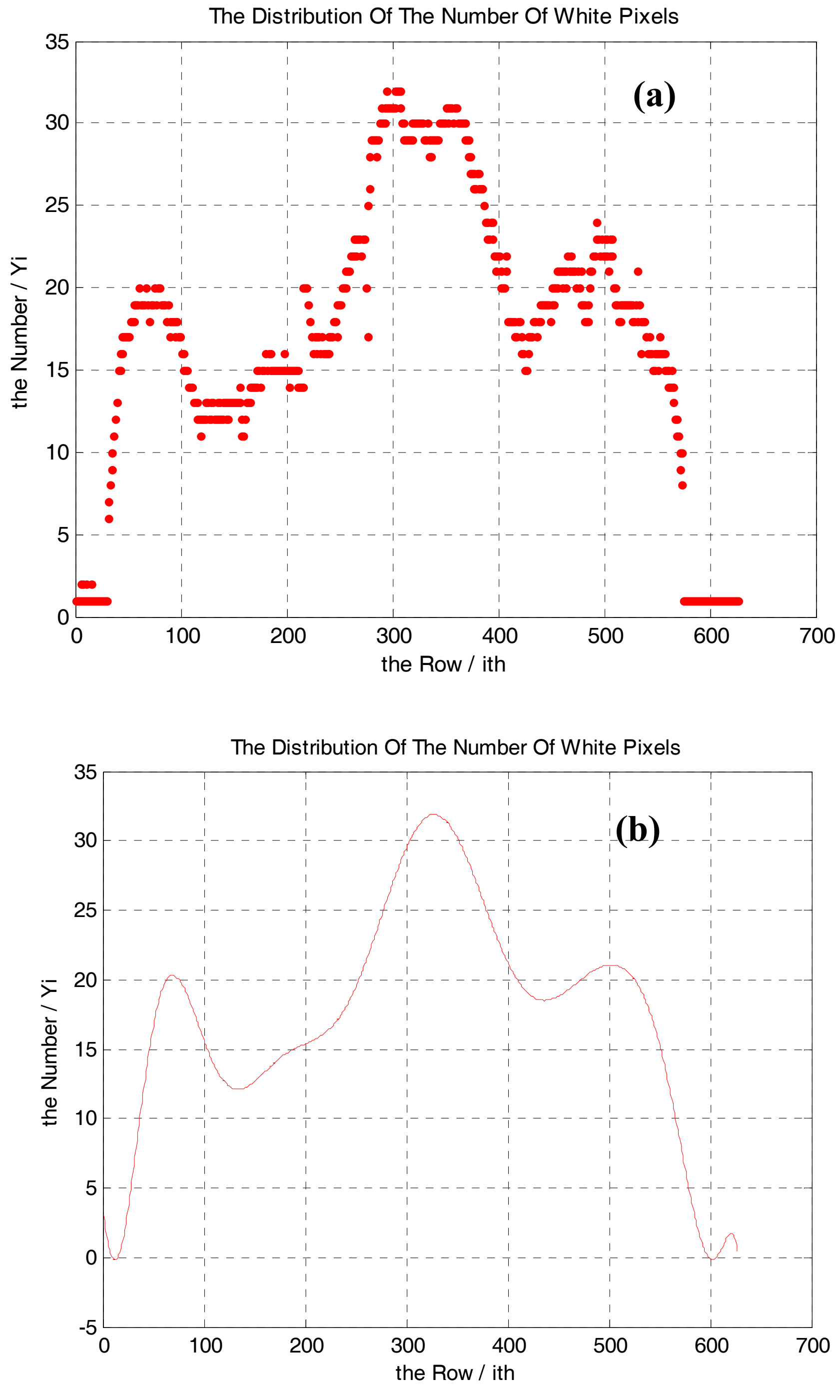

Figure 5.10 (a) Distribution of white pixels (b) Least square polynomial curve fitting

<table>
<tr><th>SEM Image</th><th>Result of image processing</th></tr>
<tr><td>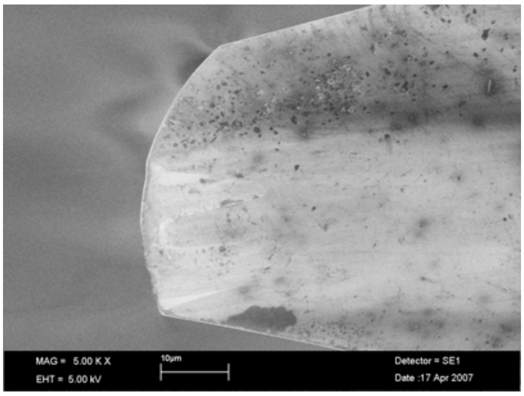
</td><td>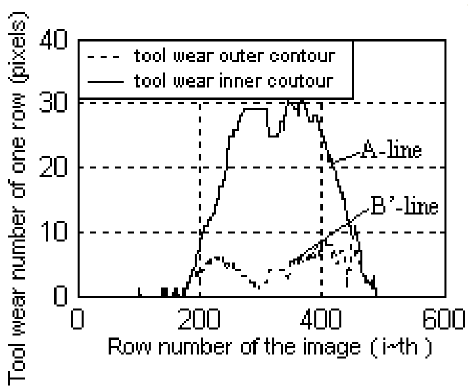
</td></tr>
<tr><td colspan="2">Cumulative Cutting Distance = 0.78 km</td></tr>
<tr><td>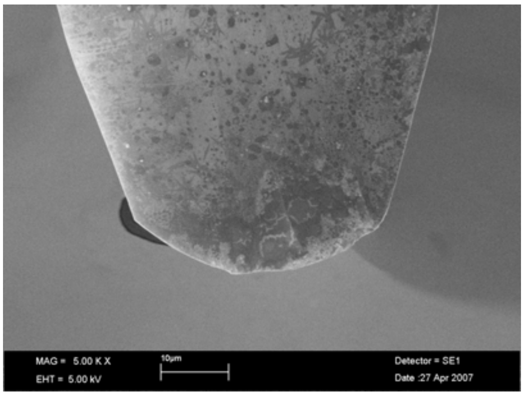
</td><td>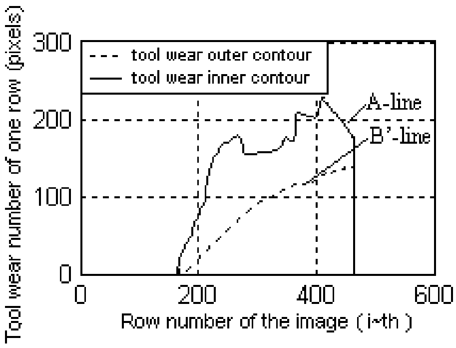
</td></tr>
<tr><td colspan="2">Cumulative Cutting Distance = 1.56km</td></tr>
<tr><td>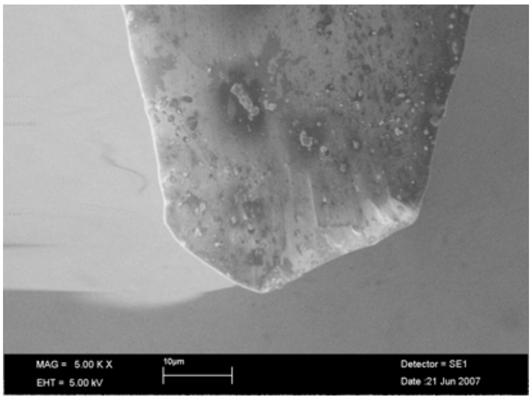
</td><td>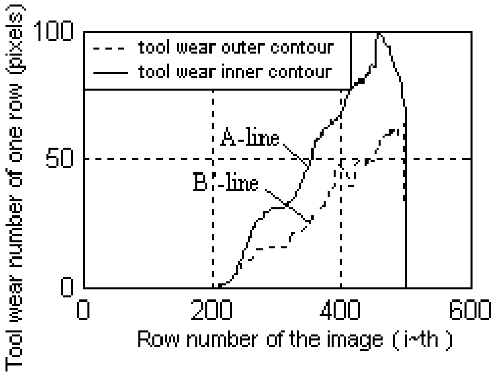
</td></tr>
<tr><td colspan="2">Cumulative Cutting Distance = 2.65km</td></tr>
</table>

Figure 5.11 Result of characterization of tool wear by digital image processing method

Table 5.7 Calculated result of tool wear by digital image processing

Cutting Stage	1	2	3
Accumulative Cutting Distance (km)	0.78	1.56	2.65
Number of pixel of Worn Area	6090	14657	47363
Worn Area (μm^2)	34.26	82.45	266.42
% Increase (Worn Area)	N/A	140	778
Number of pixel of Worn Volume	52842	1146400	8479900
Worn Volume (μm^3)	22.29	483.64	3577.46
% Increase (Worn Volume)	N/A	2169	16050

Similar to the previous result, the cutting tool material loss increases with the cutting distance. It's interesting to note that the phenomenon is not solely directly proportional to the cutting distance. The worn area increased 140% after the accumulative cutting distance was doubled or after stage 1 of cutting. After stage 3 of cutting, the area of material loss increases more rapidly. The case is more significant in the worn volume of the diamond tool tip. The diamond tool volume loss increased 2169% or around 21 times the original one. After stage 3 of cutting, the worn volume is 16050% or around 161 times as compared with the worn volume after stage 1 of cutting. This infers that the diamond tool tip is worn more rapidly within stage 3 of cutting, or the wear rate of the diamond tool appears to be significantly increased after cutting for a distance of 1.56 km. This agrees well with the result discussed in the previous experiment which was obtained by the method of measuring VB_{max} and the width of flank wear. The result infers that the material loss of a diamond tool tip increases significantly when the cutting distance accumulates from 1.56 km to 2.65 km. Although this situation is not easily projected by measuring wear VB_{max} and width, the finding could be determined by quantitative characterization of the tool wear by the digital image processing method.

Even the quantitative result shows the significant material loss found on the diamond tool after a cutting distance of 2.65 km or after stage 3 of the cutting, and it is not easy to determine if the diamond tool is worn at this stage. Based on the literature, rapid material loss of a diamond tool occurs at the first stage of tool wear which corresponds to the run in wear and the final stage of tool wear, which is corresponding to the accelerated tool wear. In the accelerated wear of the tool, the diamond tool tip contour should deteriorate. From both SEM captured figures and the results of the image processing method, it can be easily deduced that the diamond tool has lost its original contour already.

5.5 Effect of Tool Wear on Surface Quality

For the fabrication of complex surfaces, the surface quality of the workpiece would be adversely affected by the wear of the diamond tool, and as a result, it is vital for the study of the effect of tool wear on the surface quality in FTS machining. To further understand the phenomena of tool wear in FTS machining, the surface quality of machined samples were investigated. Since the fabricated profile is formed by a repetition of the tool marks as shown in Figure 5.12, the quality of a machined surface can be used as an indirect indicator for tool wear (Jiwang Yan, 2003; C.H. Che-Haron, 2001; A. Pramanik, 2003). Moreover, it is interesting to explore the surface generation when FTS machining a tilted flat surface by a diamond tool without the original shape.

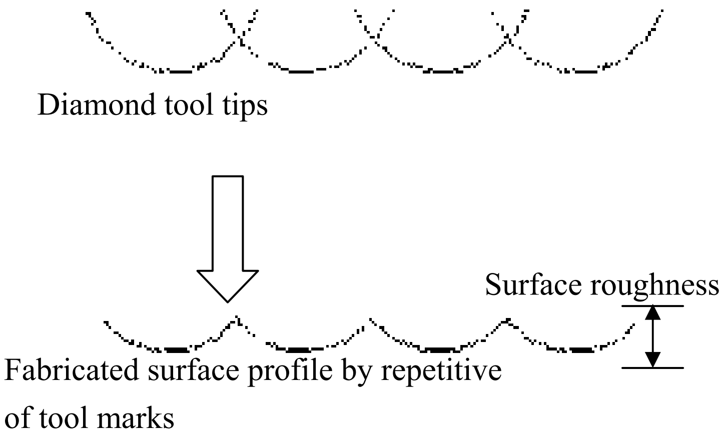

Figure 5.12 Illustration of formation of fabricated profile

In this section, the aim is to establish the relationship between tool wear and surface quality of machined tilted flat surfaces by FTS machining. After each predetermined cutting distance of 156 meter length, a tilted flat surface profile, with 10 μm depth, is fabricated. The surface profiles of the machined samples were measured by a Wyko optical profiler system. The measured data is used to compare with the image of the diamond tool tip captured by SEM after each stage of cut. The comparison is shown in Table 5.7. The scale of surface quality is between +1 μm to -1 μm.

As shown in Table 5.8, the SEM captured image of the diamond tool tip after each cutting stage can be observed. The surface height ranges from +0.25 μm to -0.20 μm, from +0.20 μm to -0.10 μm and from +0.10 μm to -0.15 μm. Figure 5.13 shows the surface roughness measured on the first machined sample. After 156 meter cutting distance, the tool wear should be at the first stage. The diamond tool should have a sharp radius and the original shape. However, the surface roughness fluctuates within a relatively large range from +0.9 μm to -0.6 μm. The finding shows the effect of tool wear on surface quality is not very significant when machining a tilted flat surface. Even the original contour of diamond tool cannot be observed any more, and the surface roughness is not significantly affected. This is why the surface roughness fluctuates within a relative small range when compared with the surface quality after cutting for 156 m.

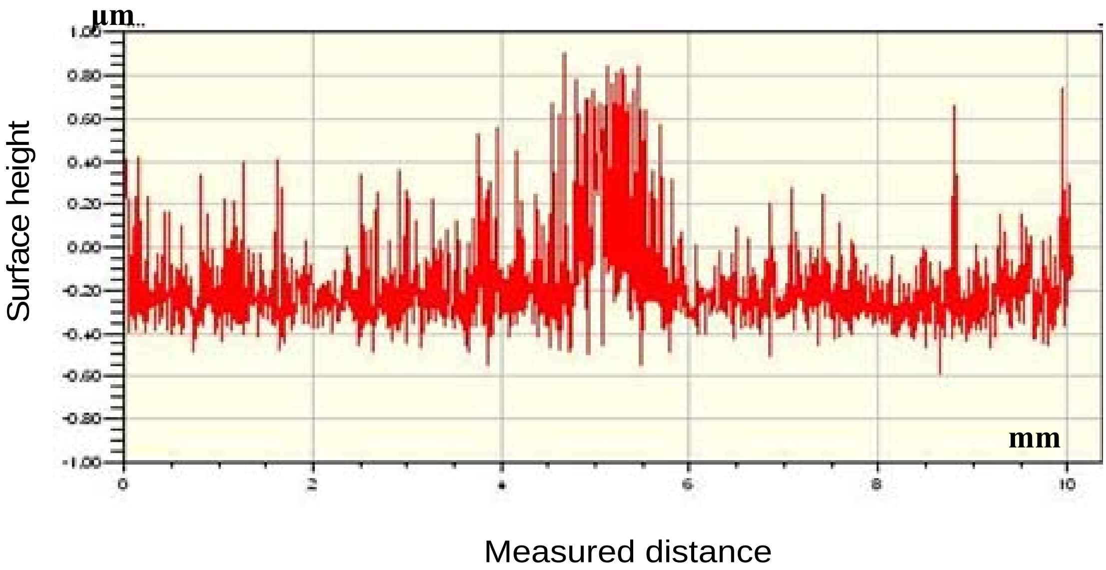

Figure 5.13 Surface roughness of first machined tilted flat surface

Actually, this phenomenon is quite reasonable. When the diamond tool wears gradually, the radius of the tool tip increases at the same time. This results in the cutting of the tilted flat surface with a larger radius diamond tool and thus a better surface roughness is achieved. As a result, the effect of the tool wear is not significant for surface generation in FTS machining of a tilted flat surface. To explore the significant effect of tool wear on surface generation, the study was extended to the cutting of an optical surface with a complex profile, such as microstructure.

Table 5.8 SEM captured image of diamond tool wear and FTS machined surface profile

SEM Image	X-Profile of Wyko result
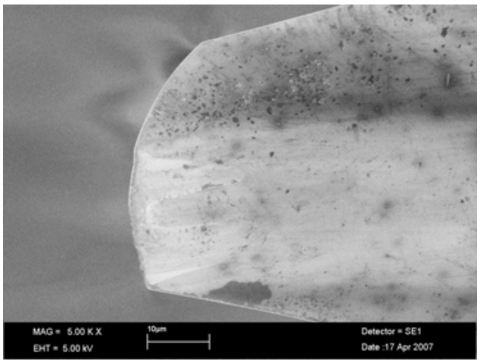	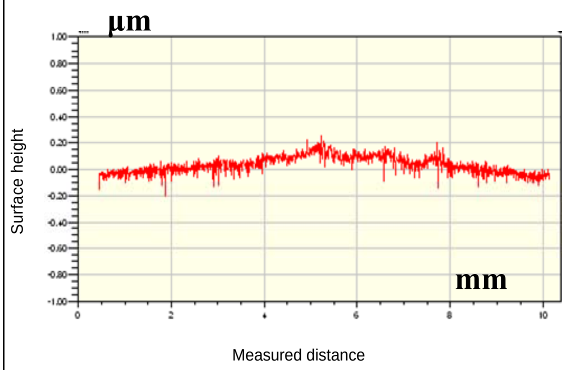
Cumulative Cutting Distance = 0.78 km	
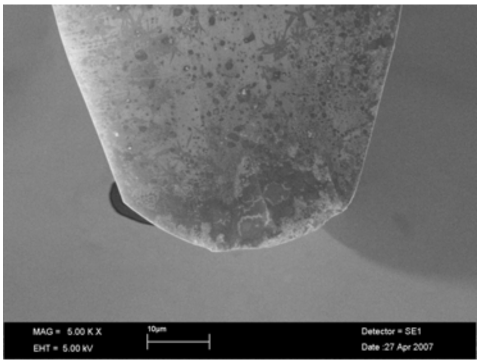	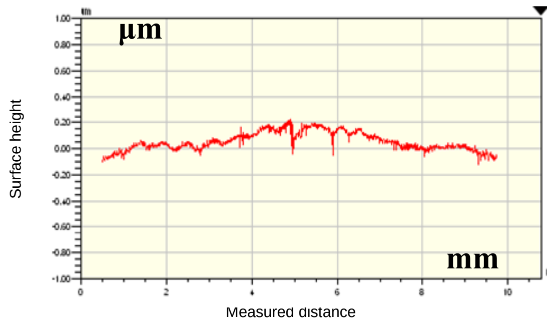
Cumulative Cutting Distance = 1.56km	
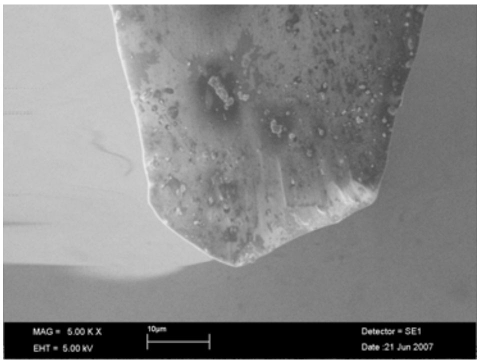	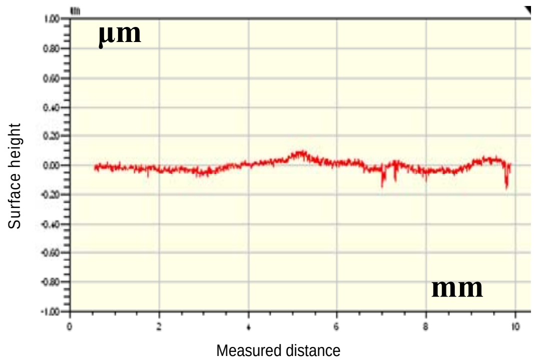
Cumulative Cutting Distance = 2.65km	

FTS machining is well recognized as one of the superior ultra-precision machining technologies for the fabrication of optical microstructures. In the machining process, one of the fundamental requirements is that the radius of the diamond tool must be smaller than the radius of curvature of the desired profile. This is why a diamond tool with a small radius is always employed for cutting complex optical surfaces such as microlens arrays. Better form accuracy helps to enhance the performance of the optical components they are applied to. In FTS machining, it can be deduced that the effect of using a worn diamond tool should be even worse than using one with improper radius, and leads to failure in achieving the required standard.

To verify this speculation, cutting tests were done to find out the effect of tool wear on form generation when FTS machining a microstructural surface. The cutting conditions were kept constant at 100 rpm spindle speed, 0.5 mm/min feed rate and 5 μm depth of cut and a diamond tool with the same radius is employed. The fabricated profiles by using sharp and worn diamond tools were measured separately. Figure 5.14 shows the worn diamond tool employed in the cutting tests. As shown in Figure 5.15, material loss on the diamond tool and micro-grooves are observed at the cutting edge of diamond tool.

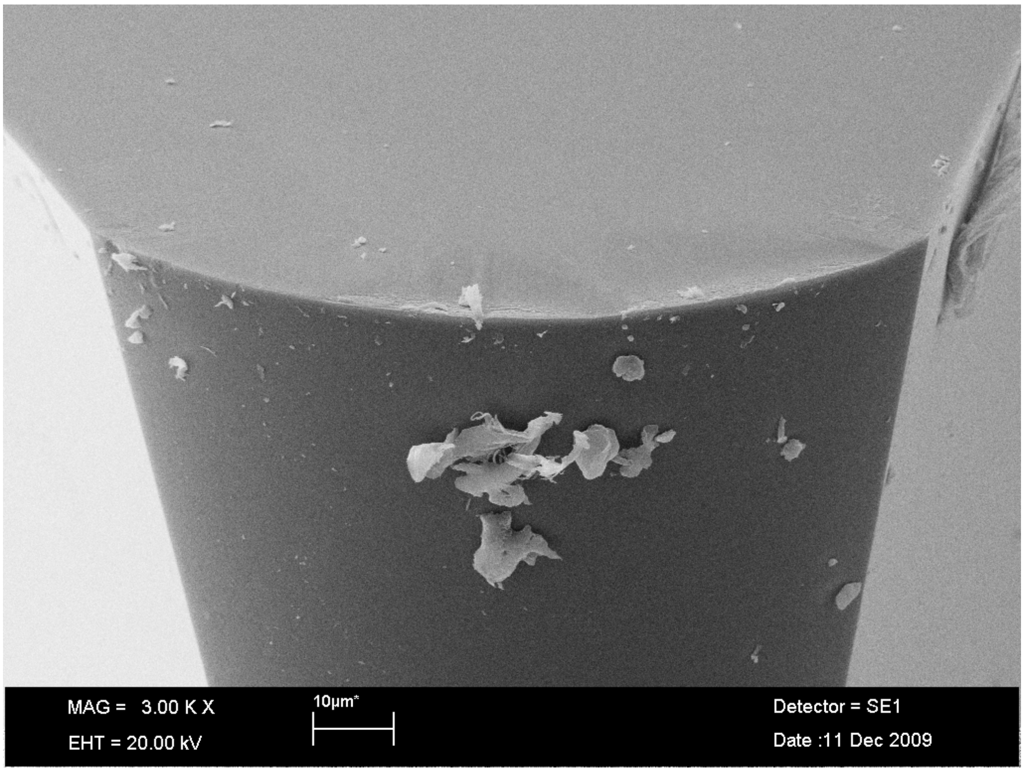

Figure 5.14 SEM captured figure of worn diamond tool employed in cutting test

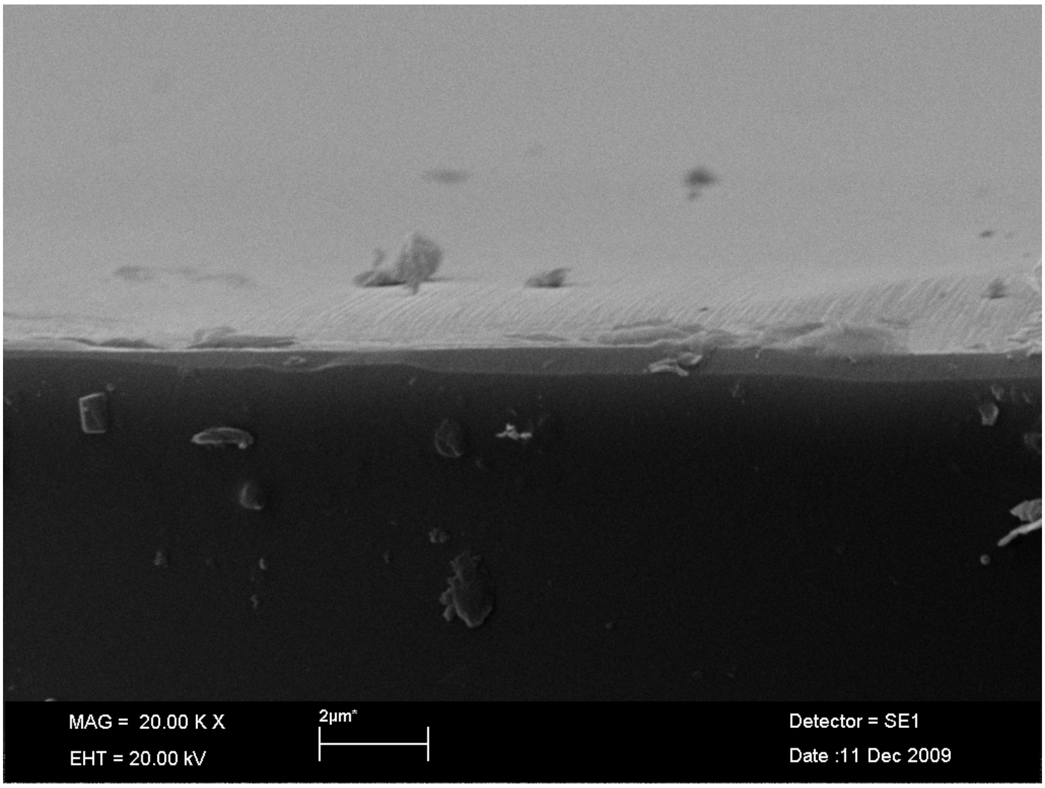

Figure 5.15 SEM captured figure of worn diamond tool employed in cutting test

In the present study, the cutting tests were carried out separately by sharp and worn diamond tools. The measurement of machined surfaces has been carried out at relative positions of the microlens array pattern. This helps to minimize the effect of other cutting conditions, and the detailed methodology has been mentioned previously. Figure 5.16 illustrates the locations of measured profiles.

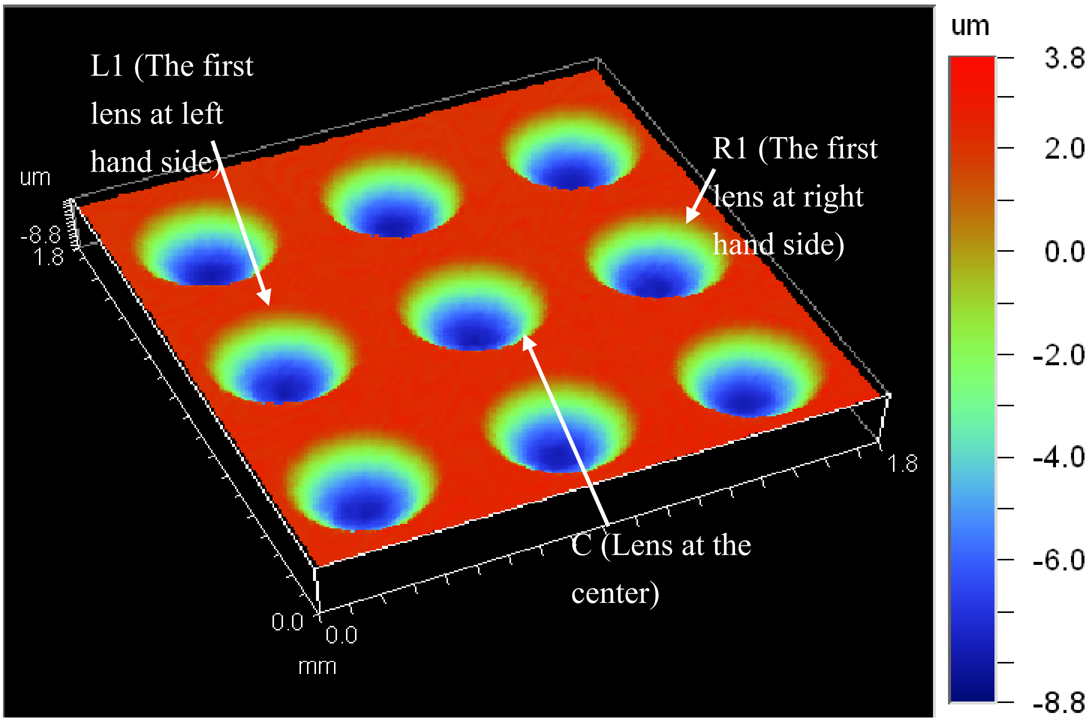

Figure 5.16 Illustration of measuring microlens array

It's well known that the microstructural surface with large form error can hardly achieve its expected optical performance. However, the highest impact of a worn tool in FTS machining should be the form accuracy of the machined profile. As a result, the form error of a machined lens is thus used to project the effect of surface generation. Figure 5.17 shows the results by comparing the surface generation by worn and sharp diamond tools at different lens positions where the lens position is referred to Figure 4.10. Before the diamond tool is worn, the form error of the machined surface varies within the range of 100 nm to 150 nm. Using a worn diamond tool, the form error varies between 200 nm and 360 nm. There is notable increase in form error by the worn diamond tool. The average percentage increase is 90.63% which deduces tool wear should be considered as a critical factor affecting surface generation in FTS machining. Moreover, the captured single machined lens profile shown in figure 5.17 appears to be oblique instead of circular. This further proved the significant effect of tool wear in FTS machining of optical surfaces with complex profiles such as microlens arrays.

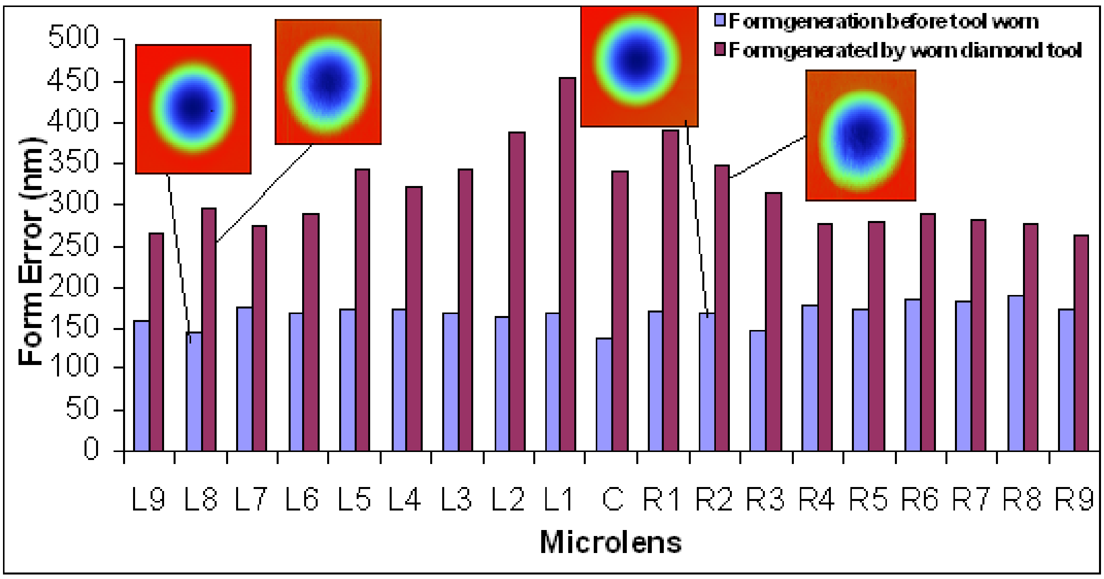

Figure 5.17 Result of surface generation by worn and unworn diamond tool

5.6 Summary

In FTS machining, a small diamond tool radius is always employed for the fabrication of high value added optical profiles. Tool wear adversely affects the surface quality in FTS machining. The impact of diamond tool wear becomes more significant. In order to investigate diamond tool wear in FTS machining, a series of cutting experiments have been conducted under consistent cutting conditions. The cutting experiments consist of 3 preset cutting distances. The wear characteristics of the diamond tool are captured by SEM after each preset cutting distance. Within a 2.65 km cutting distance, 17 titled flat surface samples are fabricated and their surface profiles are measured.

The first analysis employed is the determination of VB_{max} and the width of flank wear by direct measurement on the captured SEM image of the diamond tool tip after each stage of the wear study. The results show both flank wear parameters increase with cutting distance. It is interesting to note that the material loss of the diamond tool tip in stage 3 cutting increases more severely compared with that for the previous stages. After cutting distance of 2.65 km, the original shape of the tool radius was no longer observed. Although VB_{max} and width of flank wear are common parameters employed in the determination of tool wear, the result cannot significantly project the phenomena.

In order to investigate the diamond tool wear quantitatively and accurately, a digital image processing method has been purposely built for the characterization of the tool wear in terms of area and volume of material loss from the diamond tool. The method has been successfully implemented to quantitatively determine the tool wear. The results agree with the findings in the previous section. There is a substantial amount of material loss on the diamond tool tip when the cutting distance increases from 1.56 km to 2.65 km.

To explore the effect of tool wear on surface generation, an experiment has been carried out in correlating the tool wear with the quality of the machined surfaces. The results shows that there is little effect from tool wear on the surface roughness of FTS machining of tilted flat surfaces. However, its effect on form generation in FTS machining of complex surfaces is significant.

On the whole, the study of tool wear in FTS machining provides an important means to better understand the tool wear phenomena which are found to adversely affect the surface quality of the workpiece. The digital image processing method developed in the present study helps to quantitatively determine the wear of the diamond tool which is proven to be more effective than the traditional wear analysis based on VBmax and flank wear analysis.

CHAPTER 6 ANALYSIS OF EFFECT OF ERROR MOTION ON SURFACE GENERATION IN FTS MACHINING

6.1 Introduction

Although high-quality optical surfaces can be fabricated directly by FTS machining with submicrometer form accuracy and nanometric surface finish without the need for any subsequent post processing, the achievement of a superior mirror finish and form accuracy still depends largely on the experience and skills of the machine operators. This skill is acquired through an expensive trial-and-error approach when using new materials, new surface designs, or new machine tools. According to the literature review discussed in Chapter 2, the material removal process and surface generation in FTS machining is not only governed by the geometry of fabricated profile, tool geometry, tool wear, material properties, and cutting parameters such as feed rate, spindle speed and depth of cut, but also affected by the errors that occur during the actuation motion of FTS. It is associated with the bandwidth and the stroke of the FTS, and the synchronized motion between the cutting tool and the workpiece. These movements play an important role in the material removal process and surface generation in FTS machining. However, these issues have received relatively little attention.

In this chapter, a model-based simulation system has been presented which is composed of a surface generation model, tool path generator and an error model. The major components of the error model include the stroke error or the characteristics of the FTS and the error motion of the machine slide in the feed direction of the ultra-precision machine. The form error due to the stroke errors can be extracted empirically by the proposed regional analysis. After incorporating the error model in the surface generation model, the model-based simulation system is capable of predicting the surface generation in FTS machining. To verify the performance of the model-based simulation system, a series of cutting tests have been conducted and the predicted results have been compared with the measured results.

6.2 Model-based Simulation System

Figure 6.1 shows a framework of the model-based simulation system. It is composed of an input module, a surface generation module, an error module and an output module, respectively. In the input module, the cutting parameters employed in FTS are imported. These include feed rate, spindle speed, depth of cut, specifications of the workpiece, etc. According to the specifications of the workpiece, the range of travel per stroke is determined. The surface generation model is composed of three parts, which are the ideal spiral turning path, the actuation of the FTS, and tool compensation, respectively. To enhance the accuracy of the theoretical analysis, an error module is incorporated. This error module consists of the motion error of the machine slide and the motion error in FTS actuation. After combining the surface generation model and the error module, the fabricated surface can be generated by FTS machining. By using this model-based simulation system, three-dimensional surface topography and the predicted surface parameters in terms of form error can be determined in the output module. In the coming sections, some important models and algorithms in the surface generation are presented respectively.

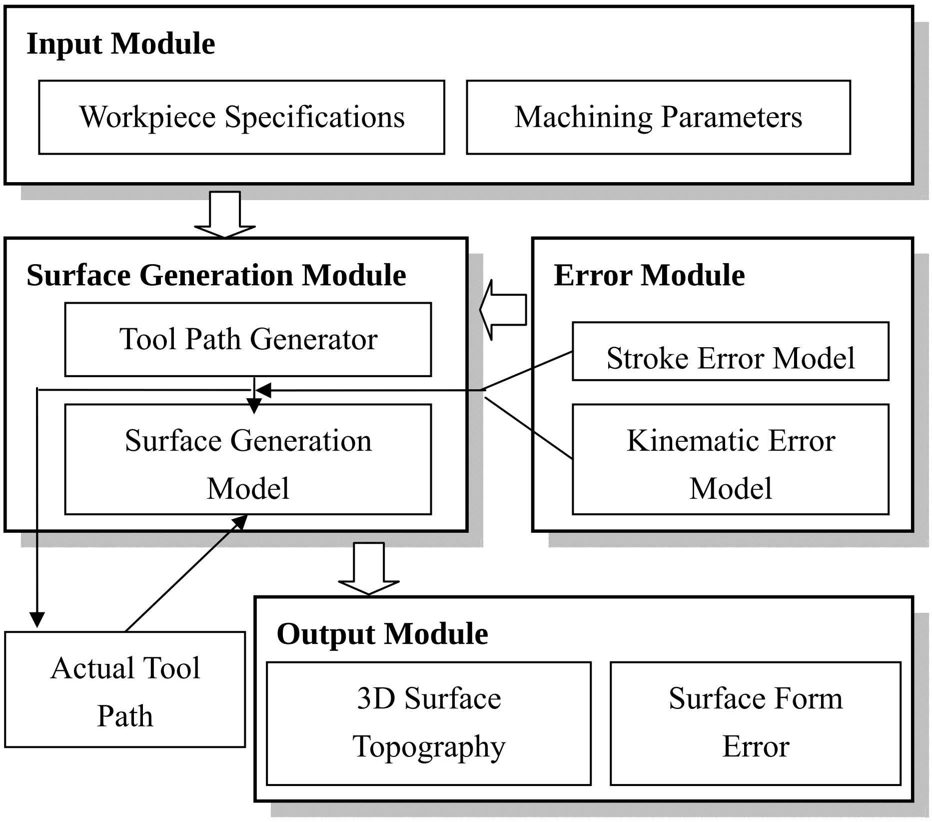

Figure 6.1 Framework of model based simulation system in FTS machining

6.2.1 Tool Path Generator

After defining the components involved in the error model, the study is continued by building the surface generation model for FTS machining. To study the performance of FTS machining system, the first step is to define the fundamental elements involved. In this research, two major parts of the critical machining parameters involved in the fabrication and general characteristic of FTS35 are employed. The general characteristics are listed in Table 6.1, which are used to characterize the cutting parameters in FTS machining. Apart from these, there are some machining parameters affecting surface generation in FTS machining such as feed rate, spindle speed, surface speed, depth of cut, etc. These critical cutting parameters have been reported in earlier chapters.

Table 6.1 General Characteristics of FTS35

Drive	**Bearing Technology**	**Full range of Travel**	**Characteristic Bandwidth**	**Position Sensor**	**Control System**
Voice Coil	Air bearing & counter mass	35 um	1000 Hz	Analog	SOP

All these factors are subsequently involved in the definition of the theoretical model for determining the form error of the machined profile. They are then formulated as mathematical equations and are used to derive for the empirical prediction of the surface generation in FTS machining.

First of all, the maximum spindle speed ($V_{\max}$, rpm) or suggested limit of rotational spindle speed in the model is determined by Equation (6.1).

$$V_{\max} = 60\frac{f_{\max}}{N_r} \tag{6.1}$$

Where, $f_{\max}$ is the maximum frequency or bandwidth of FTS;

N_r is the number of elements per revolution;

Maximum dimension (L) of the workpiece in the model is illustrated in Equation (6.2).

$$L = V_{sm} \cdot \Delta t \tag{6.2}$$

Where, V_{sm} is the maximum surface speed, which is defined by Equation (6.3)

$$V_{sm} = \frac{V}{60} \cdot 2\pi \cdot \frac{D}{2} \tag{6.3}$$

Where, V is the spindle speed in rpm;

D is the workpiece diameter.

Δt is the minimum time needed per stroke or travel of FTS, which is determined by Equation (6.4)

$$\Delta t = \frac{1}{2}\frac{1}{f_{\max}} \tag{6.4}$$

Where, $f_{\max}$ is the bandwidth of FTS which is 1000Hz in the present study.

Equations (6.3) and (6.4) are substituted in Equation (6.2) which is rewritten as Equation (6.5)

$$L = \frac{V\pi D}{120 f_{\max}} \tag{6.5}$$

The frequency of FTS drive can be found by Equation (6.6).

$$F_d = \frac{2\pi V}{60D} \tag{6.6}$$

Cycle time per cut per minute can be determined by Equation (6.7).

$$CT = \frac{D}{2S_f V} \tag{6.7}$$

Where, S_f is the feed distance per revolution;

Since the feed rate f_d (in X direction, mm per min) is fixed in entire machining process, then

$$S_f = \frac{f_d}{V} \tag{6.8}$$

Equation (6.7) can be rewritten so as to determine cycle time as:

$$CT = \frac{D}{2 f_d} \tag{6.9}$$

Surface generation (S) in FTS machining is mainly contributed by two components which are S_T, contributed by the ultra-precision turning machine, and S_F, contributed by the actuation motion of FTS, and S can be expressed as

$$S = S_T + S_F \tag{6.10}$$

Where, S_T is the contribution of ultra-precision turning process;

S_F is the contribution of Fast Tool Servo. As mentioned previously in the cutting mechanism of FTS machining, it is well known that two specific parameters are defined for locating the position of a diamond tool in a rotational coordinate system. They are radius (r) and theta (θ) which indicate the distance between the cutting tool and the center of the spindle and the angular location of the rotational spindle, respectively. By using radius (r) and theta (θ), both conventional and non-rotationally symmetric optical elements can be described in the FTS machining system mathematically. The surface generated by the turning process in three dimensions can be described as follows:

$$S_T : \begin{cases} X_T = r\cos(\theta) \\ Y_T = r\sin(\theta) \\ Z_T = f_1(X_T) \end{cases} \tag{6.11}$$

Where r and θ can be written as

$$\begin{cases} r = f \cdot t \\ \theta = \omega \cdot t = \dfrac{V}{60} 2\pi \cdot t \end{cases} \tag{6.12}$$

Where, f is the feed rate in mm/min;

V is the spindle speed in rpm.

The function $f_1(X_r)$ defines the surface profile in Z plane. For example, $f_1(X_r) = C$ (constant) can be used to define a plane. The surface generation in the Z plane, is solely contributed by the actuation motion of FTS.

$$S_F : \begin{cases} X_F = 0 \\ Y_F = 0 \\ Z_F = f_2(r, \bar{\theta}) \end{cases} \tag{6.13}$$

Where, $\bar{\theta} = \mathrm{mod}(\theta, 2\pi)$, $\mathrm{mod}(a,b)$ means the modular after division of a/b.

By commanding the motion of the diamond tool actuated in the Z direction, non-rotationally symmetric (nrs) profiles can be fabricated and derived as

$$Z_{nrs}(r,\varphi) = Z_{rot}(r) + Z^{*}(r,\varphi) \tag{6.14}$$

Where, $Z_{rot}(r)$ represents the conventional rotational symmetrical surface, which can be defined by

$$Z_{rot}(r) = \frac{cr^2}{1+\sqrt{(1-(k+1))c^2r^2}} + \sum_{i=1}^{n} a_i r^i \tag{6.15}$$

For cutting non-rotationally symmetric profiles, $Z^{*}(r,\varphi)$ is employed in commanding the actuation motion of FTS. Figure 6.2 shows the simulation algorithm for the prediction of surface generation in FTS machining. The major variable is time *t*, and is used to determine the change of regional variables, radius (r) and theta (θ), which indicate the distance between the cutting tool and the center of the spindle and the angular location of the rotational spindle, respectively. The surface generation in FTS machining mainly consists of two components. The first part is contributed by the traditional rotational spindle and feeding system in SPDT while the other component is the actuation of FTS, which determines the characteristic profile of a fabricated spherical or an aspherical surface.

Having defined the algorithm involved in the surface generation, it is used to generate the ideal tool path. For the first step in programming the CN machining code, the cutting tool path is described as the real-time position to be cut in the machining process. To fabricate the desired profile accurately, it is critical to compensate the error of tool nose radius involved in the tool path generation. The effect of tool compensation in FTS machining has been investigated in the previous chapter.

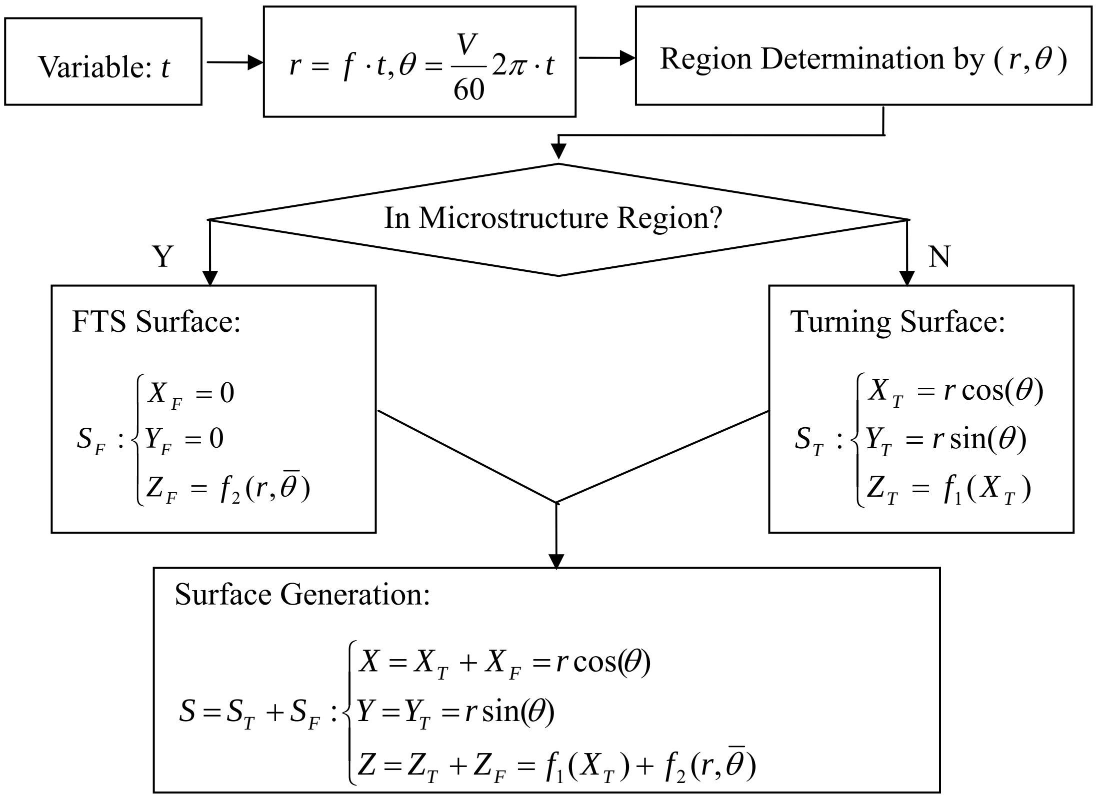

Figure 6.2 Simulation algorithm of surface generation in FTS machining

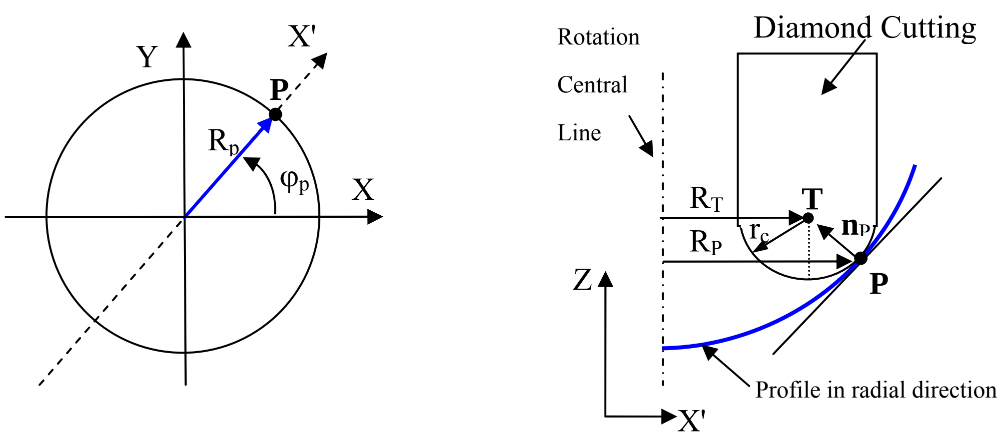

Figure 6.3 Compensation of tool nose radius for tool path generation

The motion axes involved in diamond turning with FTS are the X-axis (feed direction) and the Z-axis (cutting direction). The compensation for the tool nose radius is only necessary in the feed profile, which can be illustrated as a two dimensional (2D) curve as shown in Figure 6.3. The cutting locus or ideal surface profile of the workpiece has been derived previously. It means that the trace of the cutting point $\mathbf{P}:(P_x, P_y, P_z)$ or (R_p, φ_y, P_z) has been preset and the tool path is generated by compensating for the tool nose radius, which was calculated based on the center location of the diamond tool nose. Supposing the tool nose center is $\mathbf{T}$: (T_x, T_y, T_z) or (R_T, φ_T, T_z) and the radius is r_c, the normal vector of the workpiece profile at the point $\mathbf{P}(R_p, \varphi_p)$ is $\mathbf{N}_p(n_x, n_Z)$. It is interesting to note that $\mathbf{N}_p$ is not the normal vector of the surface at point $\mathbf{P}$. The following relation can be derived:

$$\begin{cases} T_x = R_T \cdot \cos(\varphi_T) \\ T_y = R_T \cdot \sin(\varphi_T) \\ T_z = P_z + \dfrac{n_{x'}}{\sqrt{n_{x'}^2 + n_z^2}} \cdot r_c \end{cases} \tag{6.16}$$

Where

$$\begin{cases} R_T = R_P + \dfrac{n_z}{\sqrt{n_{x'}^2 + n_z^2}} \cdot r_c \\ \varphi_T = \varphi_P \end{cases} \tag{6.17}$$

To compute the normal vector at a point in a 2D curved line, suppose the 2D curve line is presented as

$$F(x,z)=0 \tag{6.18}$$

Then the normal vector at point $P_0(x_0, y_0)$ is

$$N_{p0} = (F_x(P_0), F_z(P_0)) = (F_x, F_z)\big|_{x=x0,z=z0} \tag{6.19}$$

Where,

$$F_x = \frac{\partial F}{\partial x}, F_z = \frac{\partial F}{\partial z} \tag{6.20}$$

6.2.2 Error Model

FTS machining is enabled by two sources of motions, which are the feed motion of the slides of the ultra-precision machine and the actuated motion of the FTS. The feed motion of an ultra-precision machine is mainly composed of two slides which are the X-axis slide and the Z-axis slide, respectively. As shown in Figure 6.4, the rotational spindle feed is the feed of the X-axis slide and the diamond tool is actuated back and forth within the cutting process. The actuated motion of FTS employed in the present study has a 35 μm of the maximum traveling distance. The cutting process with feed motion of the X-axis slide won't commence until the Z-axis has been adjusted to the pre-set depth of cut. This infers that the main error motion contributed by the machine slides to the surface generation in FTS machining is the feed motion of the X-slide. This motion is taken into consideration in the error model which is built based on the kinematics error model defined by Kong et al (2008). Another major source of error motion in FTS is defined as the stroke error in the present study, and is contributed by the actuated motion in FTS machining. As a result, the proposed model of the error motion in FTS machining is composed of the kinematics error of the ultra-precision machine and the stroke error of FTS actuation.

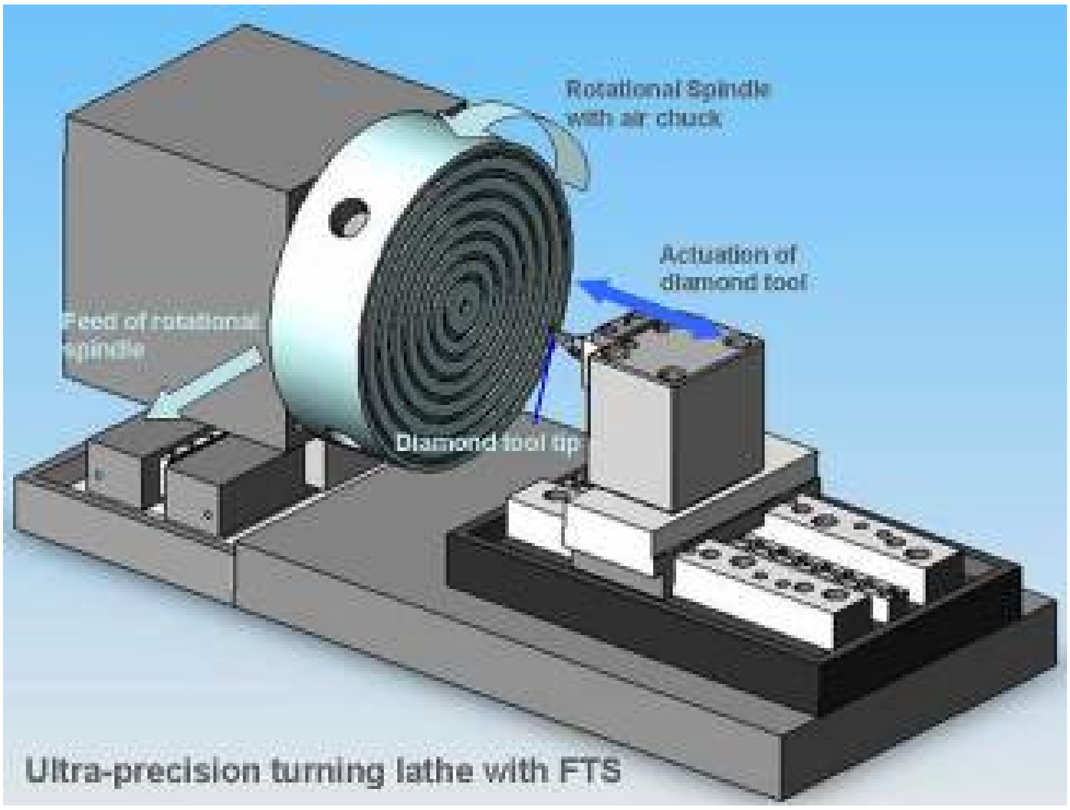

Figure 6.4 Illustration of ultra-precision machining with FTS

On the whole, the theoretical model of error motion in FTS machining consists of the feed motion of an ultra-precision machine and the stroke motion of FTS. By combining the surface form error of the machined workpiece by FTS process (Err_w), the form error caused by stroke error (Err_s), and the error caused by kinematic errors is (Err_k), the surface form error model can be derived as

$$Err\_w = Err\_s + Err\_k \tag{6.21}$$

The kinematic error motion of the machine slides is an intrinsic systematic error when the machine tool is manufactured, and consists of a total of six error components. Three of them are distance errors, which are straightness in X axis, Y axis and Z axis, respectively. Moreover, there are three angular errors which are roll, yaw and pitch. Figure 6.5 shows the error components schematically.

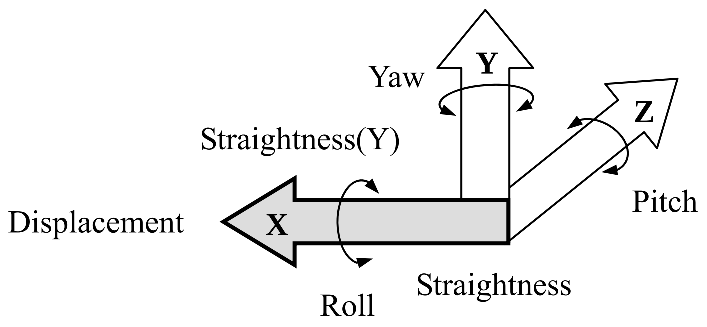

Figure 6.5 Error components for X slide motion

In FTS machining, the dominant error component is the straightness in the Z direction; therefore the X slide motion error in the Z axis direction is employed in the model to predict the kinematic errors. The proposed kinematic error model involves the slides motion errors of the machine tool. During machining process, different segments of the slides are employed and it is also interesting to note that the slide motion errors vary with different segments of the slides that are used. By selecting different slide starting positions (SSP), different form errors caused by the systematic slide motion errors are determined.

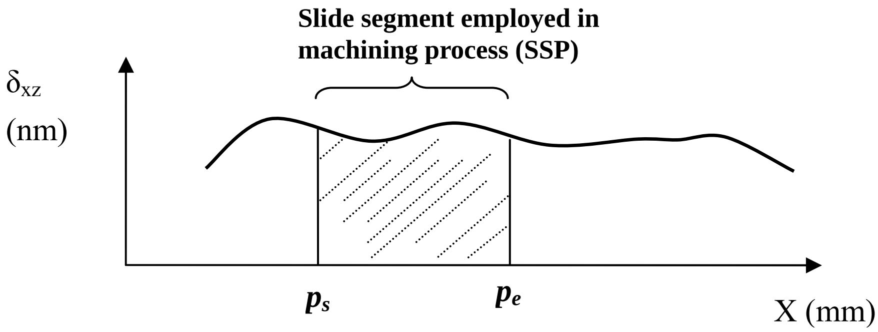

Figure 6.6 Graphical illustrations for X slide motion error

Assume the slide motion error of X-axis in horizontal direction is Xe_h, the starting position of X-axis is SSP_x, and then the kinematic error model is expressed as

$$Err\_k = Xe\_h(R_x) - Xe\_h(SSP\_x) \tag{6.22}$$

Where, R_x is the distance from the cutting position to the swing center of the workpiece as shown in figure 6.6.

Another major component of error defined in the present study is the stroke error which is the error encountered when the diamond tool is actuated by the FTS in the cutting process. The stroke of FTS is defined as the full travel range of the FTS actuator to enable the cutting process. This can also be referred as the tracking error, which is the error in the position of the diamond tool as compared to the reference signal of the control system. The stroke motion is always constrained by the limitations of the FTS employed and the details are discussed in Chapter 2.

In the present study, an empirical stroke error model is developed to predict the systematic error caused by different stroke ranges of the FTS. It is determined by a purposely designed cutting experiment to fabricate a tilted flat surface with the assistance of FTS. A tilted flat surface is selected as the machined profile in the cutting experiments since the FTS is required to move the tool in a sinusoidal path with full amplitude of the FTS during the cutting of a tilted flat surface. The detailed experimental set up is similar to that for the cutting experiments in the study of the tool wear in Chapter 5. The experimental data are extracted by the method of regional analysis. As shown in Figure 6.7, the machined surface profile is divided into six equally spaced regions for measurement. The measured result of each region represents the stroke error occurring in different ranges of stroke, which vary from 0μm to 30 μm.

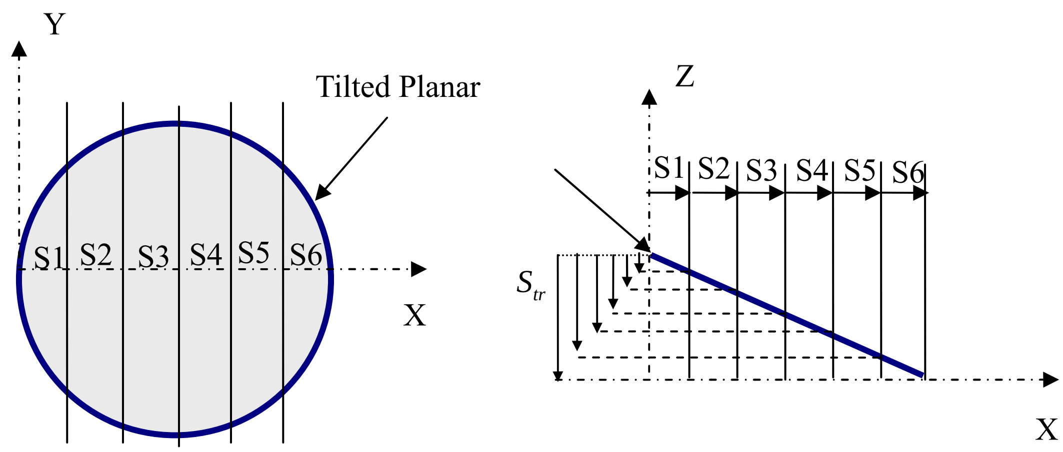

Figure 6.7 Tilted flat surface for studying errors induced by different stroke range

In practical cutting, a large depth of cut is not recommended since too large depth of cut may cause a larger cutting force to act on the diamond tool, which results in tool wear. A commonly used depth of cut is about 5μm. Therefore, it takes a total of 6 cut feeds to finish the fabrication of a profile with 30 μm depth. Moreover, the stroke error varies by using different ranges of stroke (e.g. 5 - 30 μm). As shown in figure 6.7, the fabrication regions S1 and S6 need to employ 5 μm and 30 μm separately. It means that the empirical stroke error for whole stroke range could be extracted by measuring the entire machined tilted flat surface. The measured result for S1 induces stroke error by using 5μm stroke motion and so on. Regarding the real cutting mechanism, the model helps to predict the form error of the surface by employing different stroke ranges.

There are stroke errors or deficient stroke errors when the workpiece is machined at a high rotational frequency. The proposed Stroke Error Model is an experiment-based model which is built by machining a series of tilted flat surfaces.

Assume the form error of the flat surface is Err_f , the form error of the tilted flat machined under the same cutting conditions is Err_t, then the stroke error is obtained by

$$Err\_s = Err\_t - Err\_f \tag{6.23}$$

The measured surface data of the workpiece is interpolated and fitted to construct a continuous data surface so as to obtain any point data in the measured surface. The interpolation or extrapolation of the measured surface data to obtain the continuous error surface is based on cubic spline algorithm, which is expressed as

$$P(u,v) = \sum_{i=0}^{m}\sum_{j=0}^{n} P_{ij} N_{i,3}(u) N_{j,3}(v) \tag{6.24}$$

Where, P_{ij} are the control points, $N_{i,3}(u)$ and $N_{i,3}(v)$ are the cubic B-spline functions in parametric u and v, respectively.

6.2.3 Surface Generation Model

Based on the tool path generator mentioned previously, the ideal or theoretical tool path F_I with tool compensation can be determined based on the design of the surface profile and cutting parameters. To obtain the actual three dimensional (3D) surface topography F_R, the error model is needed to be incorporated in the surface generation model. In the error model, the major sources of errors encountered Err_w by workpiece are stroke error and kinematic error of feed motion separately. As a result, the mathematical description of the surface topography can be expressed as follows.

$$F_R = F_I + Err\_w \tag{6.26}$$

Rather than 3D surface topography, the model-based simulation system can be used to determine the predicted parameters of surface quality in terms of form error at the output module. The surface form error parameter S_q is defined as

$$S_q = \sqrt{\frac{1}{N}\sum_{i=1}^{N} Err_i^2} \tag{6.27}$$

Where, Err_i is the form deviation of each data point, N is the total number of data point.

6.3 Experimental Evaluation of Theoretical Analysis

A prototype of the model-based simulation system has been built using Matlab software. A few sets of experiments were conducted for extracting the form error of the machined profile with different ranges of stroke. In the cutting test, a flat surface with no tilting was machined by SPDT. The cutting conditions included a spindle speed of 100 rpm, a feed rate of 1 mm per min and a depth of cut of 5 μm. To exclude the influence of the other systematic errors on the form error of the machined surface, FTS is not employed in the cutting experiment. The result of the machined profile serves as a reference for the sole contribution of the slide error of the ultra-precision machine. By subtracting this reference from the FTS machined result, the real stroke error can be determined.

In the second cutting test, the machined samples are tilted flat surfaces with the angle of inclination kept constant at 0.057 degree. The samples are machined under the same cutting conditions as the first experiment. The difference is that the FTS has been employed in the cutting. Table 6.2 shows the dimensions and travel range of the machined workpiece in the cutting experiment.

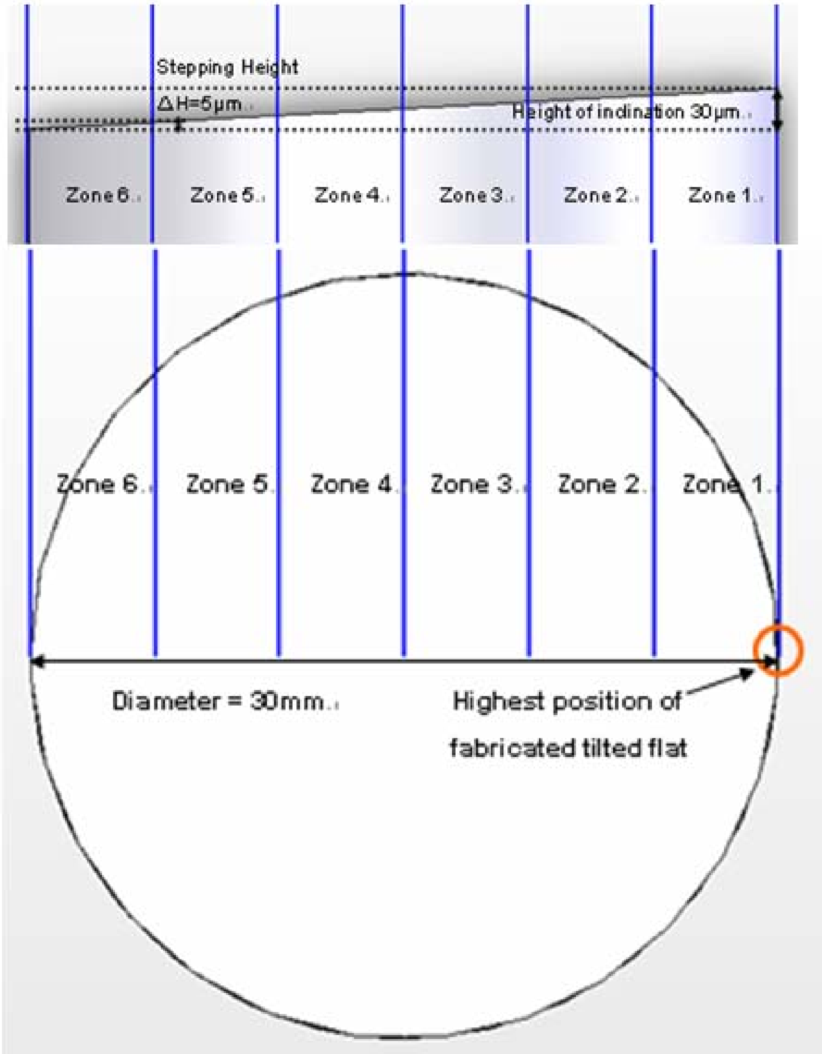

Figure 6.8 Schematic illustration of regional analysis of stroke error

To study the performance of the FTS in specific range of actuation, regional analysis is proposed in the data collection stage. Figure 6.8 shows the regional analysis of the stroke error schematically. This methodology was proposed for analyzing the stroke error of the machined profile regionally. The machined profile was measured across the diameter of the fabricated tilted flat surface from the highest position to the lowest position. The most oblique position of the measured surface should be 30 μm. In addition, the measured data of the tilted flat surface could be equally divided into six zones. The depth of cut in machining is 5 μm for each feed of cut. There are a total of 6 cuts required to finish the cutting of a tilted flat surface of 30 μm depth. As a result, the stroke error of specific travel ranges of the FTS can be determined by an analysis of the form error of equally distributed zones. Afterwards, the measured data are analyzed zone by zone by removing the tilted form in the determination of the form error of the specific zone.

In order to determine the real stroke error which is defined as without any contribution from the systematic error of the ultra-precision machine, the measured form errors of the tilted flat surfaces fabricated by FTS machining is subtracted from that fabricated by the pure diamond turning process. The real stroke error can be determined. Figure 6.8 shows the measured 3D surface topography (a) and the form error interpolation (b) for the flat surface without tilt, respectively. Figure 6.10 shows (a) the measured surface form error 3D topography and (b) form error interpolation for the tilt flat workpiece), respectively.

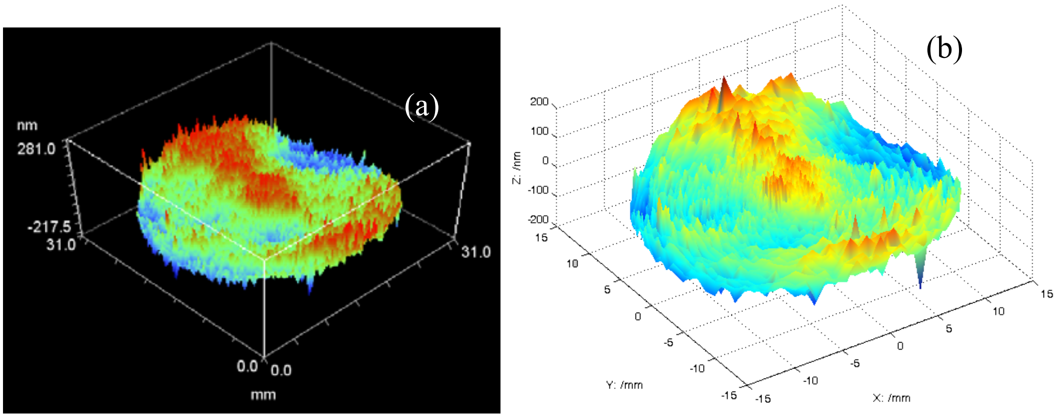

Figure 6.9 (a) measured 3D surface topography and (b) form error interpolation for the flat surface without tilt (diameter: 30 mm)

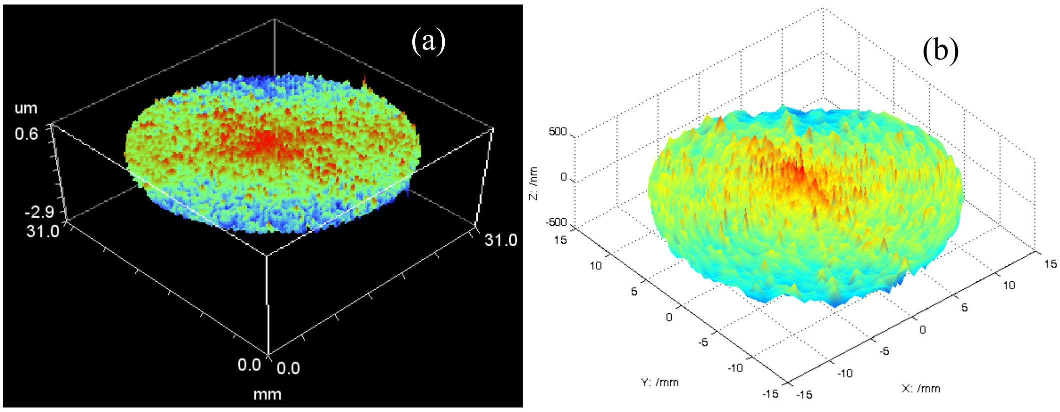

Figure 6.10 (a) measured surface form error 3D topography and (b) form error interpolation for the tilt flat workpiece (tilt: 30 μm / 30 mm)

To verify the proposed model, another tilt flat (tilt: 25μm/25mm) workpiece was machined. Figure 6.11 shows the theoretical workpiece surface generation and the tool path locus for the tilt flat surface. Figure 6.12 shows (a) the predicted 3D surface topography and (b) the measured 3D surface topography for the tilt flat workpiece, respectively; while Figure 6.13 provides a comparison of (a) the measured form error

3D topography and (b) the predicted form error of the 3D topography for the tilted flat workpiece, respectively. It is interesting to note that the predicted surface form generation as well the form error agrees well with the measured ones. This verified the validity of the proposed surface generation model.

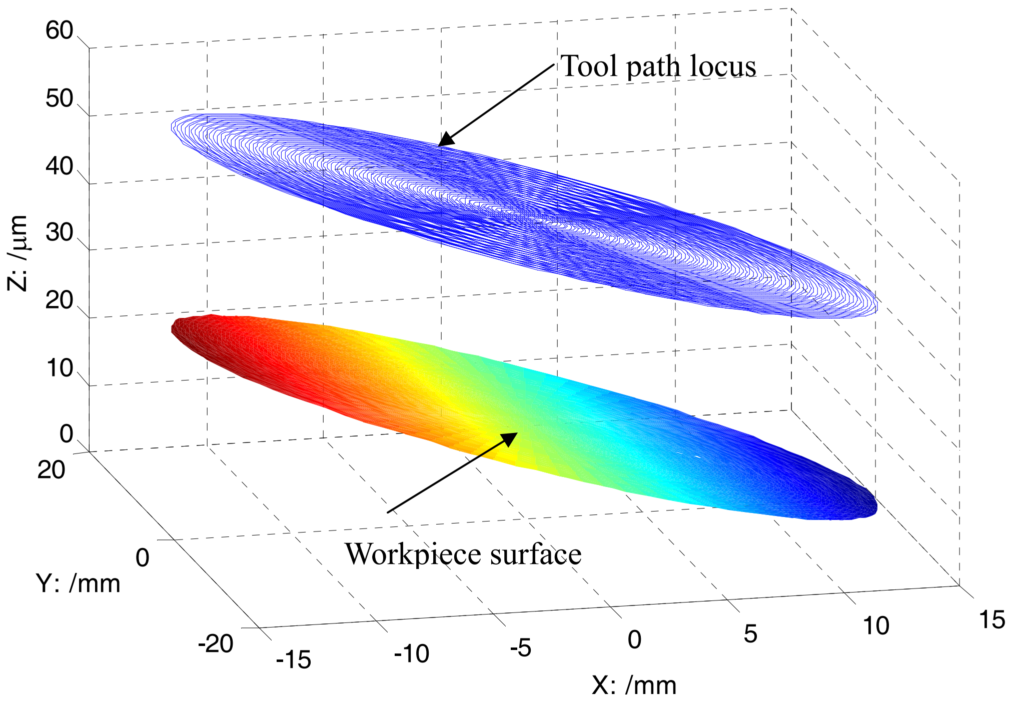

Figure 6.11 Theoretical workpiece surface generation and the tool path locus for the tilt flat surface (tilt: 25µm/25mm)

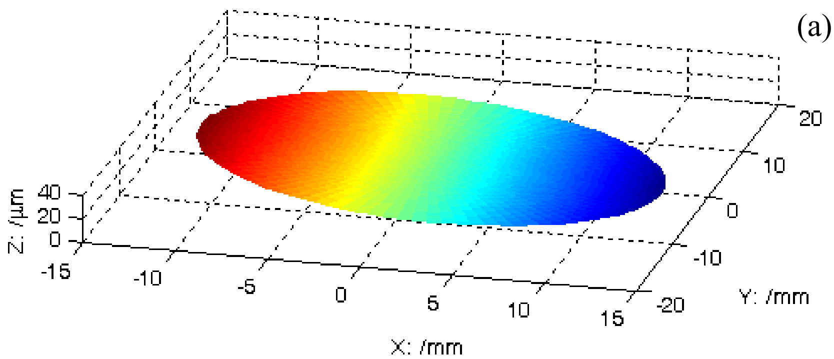

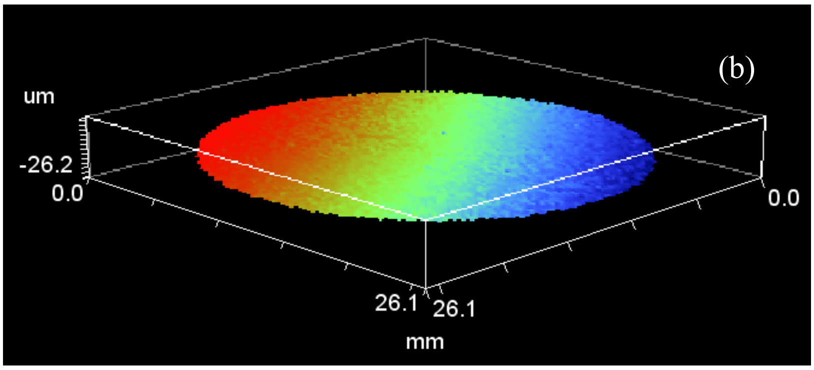

Figure 6.12 (a) Predicted surface 3D topography and (b) measured surface 3D topography for the tilt flat workpiece (tilt: 25µm/25mm)

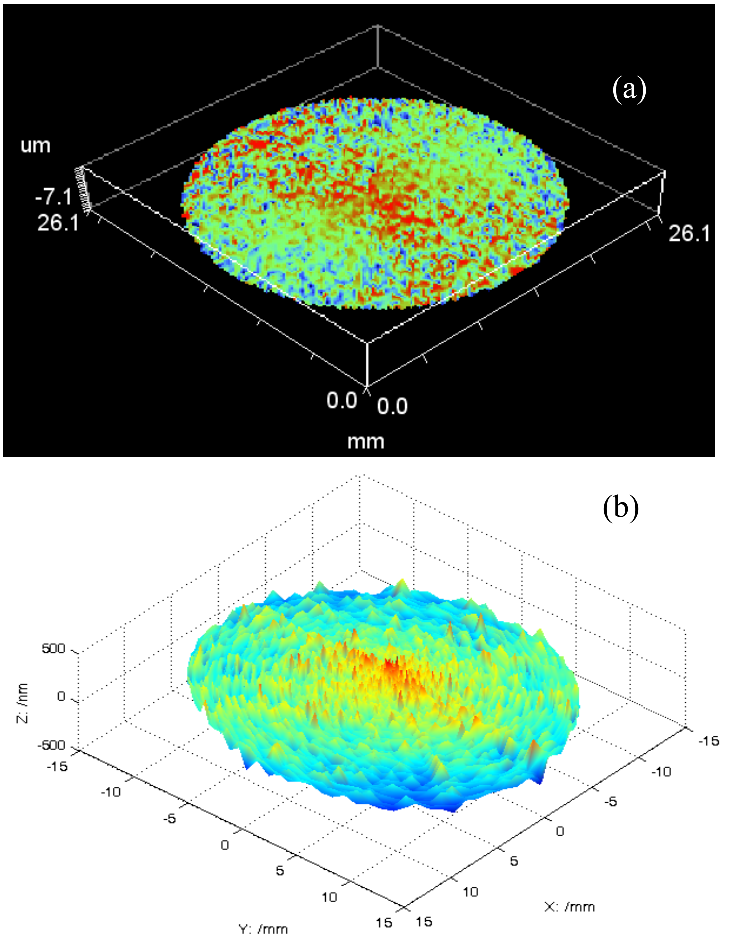

Figure 6.13 (a) measured form error 3D topography and (b) predicted form error 3D topography for the tilted flat workpiece (tilt: 25µm/25mm)

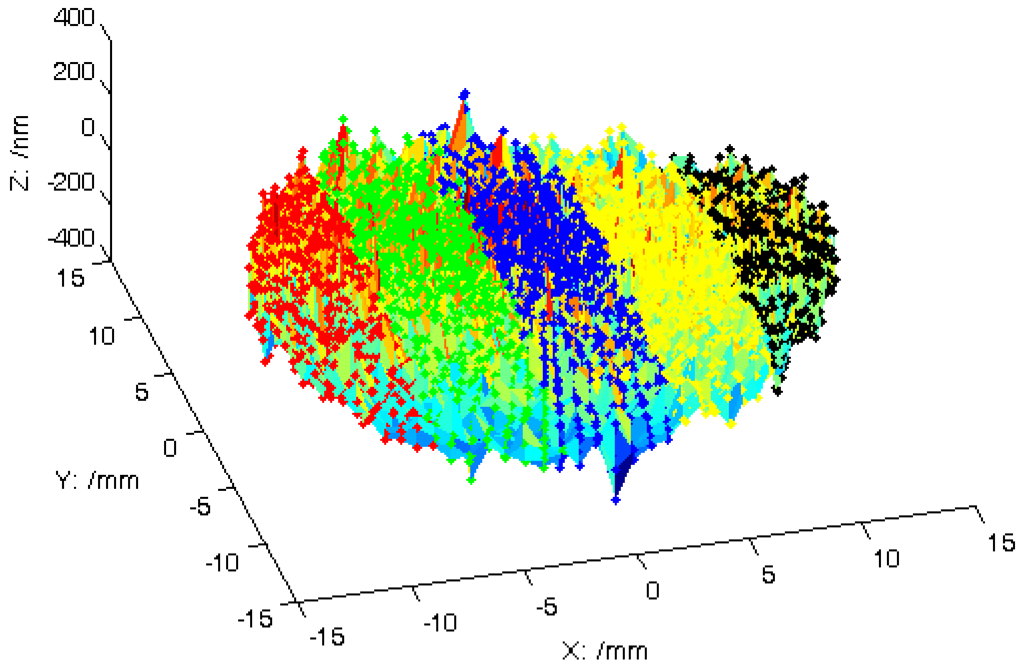

Figure 6.14 Predicted surface form errors in the divided five zones

Table 6.2 Comparison of predicted and measured form errors (Sample: 25μm/25mm)

Zone No.		1	2	3	4	5
Sq (nm)	Predicted	67.91	70.49	80.97	70.79	68.11
	Measured	61.10	65.45	94.78	58.63	65.50
% of Deviation		11.15	7.70	14.57	20.74	3.98
			Averaged % of Deviation			11.63

To provide a more precise comparison in terms of form error parameters between the predicted value and the measured result in the FTS process, the form error topography was divided into five equally spaced zones with the space intervals of 5 mm. This methodology is based on the regional analysis as proposed previously and the regional results indicates surface generation by using different strokes which is changed from 5 μm to 25 μm with an increment of 5 μm. Figure 6.14 shows the predicted surface form errors in the divided five zones. Table 6.2 provides a comparison of predicted and measured form errors and the averaged percentage of deviation is 11.63%.

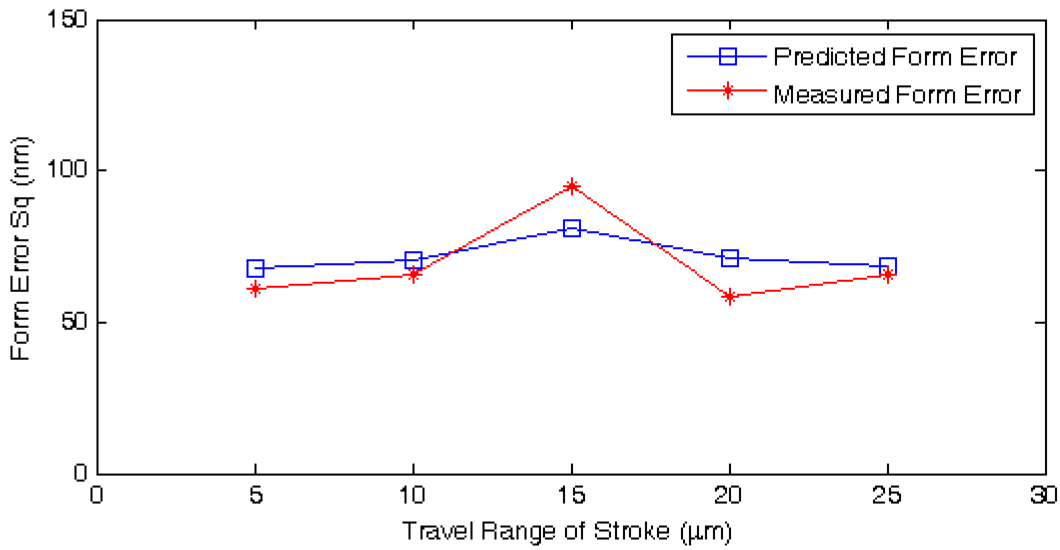

Figure 6.15 Plot of predicted and measured form errors of the tilt flat workpiece

(tilt: 25 μm / 25 mm)

Figure 6.15 shows the plot of the predicted and the measured form errors of the tilt flat workpiece. The predicted trend is found to agree well with the measured results. It is considered to be reasonably acceptable. Since one critical part of the theoretical analysis is derived empirically, there exists set up error in the cutting experiments and measurement. At data collection, result would also be influenced by limited sampling. For example, when extracting stroke error empirically, more control point can further enhancing the accuracy of the prediction. Moreover, the variation of the prediction error may be due to other factors such as materials; environmental factors and nonlinear behavior of piezoelectric materials (see Figure 2.10). Modeling of all these factors is not within the scope of the present study. The result infers that the proposed theoretical model can be used for predicting the trend of the effect of error motion on the surface generation in FTS machining.

6.4 Summary

In this chapter, a model-based simulation system was presented. The model is composed of five major modules which include the input module, surface generation module, error module and the output module, respectively. By importing surface profile parameter and cutting conditions, ideal cutting path can be generated. To further improve the accuracy of the theoretical analysis, an error module is incorporated. This error module consists of two major errors, which are due to the systematic characteristics of the ultra-precision machine and the actuation motion of

FTS. The error motion of the machine slides of the ultra-precision machine is a systematic error inherent in the machine since it was manufactured. Another component is the stroke error which is the exclusive error in FTS machining. Stroke error is due to the imperfect synchronization motion between the rotational spindle and the actuation of the FTS.

After combining the surface generation module and the error module, three-dimensional surface topography and the predicted parameters of surface quality in terms of form error can be determined and generated at the output module. Hence, a prototype model-based simulation system has been established to simulate various machined profiles and output surface quality parameters. Finally, a series of experiments were performed to verify the theoretical study. A reasonably acceptable agreement was found between the theoretical predicted results and experimental results.

The theoretical analysis provides an important means for better understanding the effect of error motions on the surface generation in FTS machining. This contributes significantly to the knowledge of ultra-precision machining with a fast tool servo, as well as to the further development of the performance of the FTS ultra-precision machining system.

Chapter 7 CONCLUSIONS

Ultra-precision machining with a fast tool servo (FTS) or FTS machining is an emerging technology which allows the fabrication of super mirror finished optical microstructure surfaces, with sub-micrometre form accuracy and surface finish in the nanometer range. FTS machining is based on single-point diamond turning (SPDT) technology and an independently operated fast tool servo, which serves as a positioning device and is mounted on the X-Y stage of an ultra-precision machine. The FTS enables the diamond tool to be actuated back and forth, and the rapid actuation facilitates the fabrication of complex optical profiles, such as non-symmetric surfaces and micro-optical structures, such as micro-lens arrays.

Although there is extensive research information available on the design and control of tool actuators for FTS machining, relatively little research work has been reported in the investigation of surface generation in FTS machining. Consequently, a better understanding of surface generation in ultra-precision machining with FTS is of prime importance for the further development of ultra-precision machining technology.

In the present study，an investigation of the factors affecting surface generation in FTS machining has been conducted. The cutting mechanisms of FTS machining was studied first and then an experimental investigation into the process factors affecting the surface generation in FTS machining was undertaken. The surface quality of a machined micro-structural surface by FTS machining was found to be affected by the cutting conditions such as spindle speed, feed rate and depth of cut. To analyse the surface generation in FTS machining of micro-structural surfaces, a series of cutting experiments were conducted and a defect analysis of the process factors was carried out to study the critical ranges of the process parameters for optimizing the surface quality. A tool compensation method was also built for further improving the surface quality. The surface quality of the machined surface is characterized by a single lens analysis and a pattern array analysis.

The experimental results indicated that the influence of the process factors can be minimized when the appropriate cutting conditions are selected. Within the predetermined range, the surface quality in FTS machining can be improved by increasing the spindle speed and by reducing the feed rate. It is interesting to note that there is a limit for the operating range of the spindle speed and there is an optimum spindle speed for minimizing the form errors. The proposed tool compensation method was also found to be effective in reducing the residual errors in FTS machining of optical microstructures such as microlens arrays. These findings provide an important means for the optimization of the surface quality in FTS machining.

Diamond tools with a small radius are usually used for increasing the flexibility of fabricating complex optical profiles. They are easily susceptible to tool wear which adversely affects the surface quality in FTS machining. In order to have a better understanding of the effect of tool wear on surface generation, a series of experiments were carried out by machining tilted flat surfaces with individual diamond tools. To investigate the tool wear characteristics, the traditional method for the determination of tool wear – VBmax and the width of flank wear – was firstly employed. Afterwards, a new digital image processing method was used to characterize the tool wear quantitatively. The material loss in the cutting stages was successfully quantified by the new method. This also helps to explore the phenomena in which there is a gradual loss of tool material during cutting, with the diamond tool being completely worn out, with a drastic loss of tool material, after cutting over a long distance (i.e. 2.65 km). By comparing the analytical results with the surface quality of the machined tilted flat surface and microlens array, it was found that the tool wear of the diamond tool adversely affected the form error in FTS machining of complex optical surfaces, such as micro-lens array.

Finally, a theoretical and experimental analysis was conducted to establish a surface generation model for predicting form error in ultra-precision machining with FTS. The error motions were found to be composed of two major sources of errors;

the motion errors of the machine slides of the ultra-precision machine and the stroke error of the FTS. The stroke error of the FTS is defined as an exclusive error in FTS machining due to the imperfect synchronization of the motion between the rotational spindle and the actuation of the FTS. An empirical based theoretical analysis was undertaken for the motion errors. The results were incorporated in the simulation system which was purposely built for generating the simulated surface profile and surface quality parameters. The system was experimentally verified by a series of cutting experiments and a good agreement was found between the trends of the experimental and the theoretical results.

On the whole, the present study not only provides an important means for a better understanding of the surface generation in FTS machining, but also contributes significantly to knowledge of ultra-precision machining with fast tool servo, as well as further development of the performance of the FTS ultra-precision machining system.

CHAPTER 8 SUGGESTIONS FOR FURTHER WORK

Fast tool servo (FTS) machining is a supreme technology for fabricating micro-structural surfaces and non-rotational symmetric surfaces which require higher bandwidth than those fabricated using the rotational spindle of an ultra-precision machine. The machined profile can achieve a superior mirror surface finish with sub-micrometric form accuracy and nanometric surface roughness without the need for any post-processing. Since the cutting mechanics, kinematics and dynamics characteristics of the FTS machining process are complex, our understanding of surface generation in FTS machining is still far from complete. Therefore, the following topics are suggested for further study:

8.1 Study the Effect of Materials Factors in FTS Machining

In the present study, the cutting experiments have been conducted on one of the most popular materials named nickel copper under various cutting conditions by FTS machining. Based on the literature presented in the last two decades, the material removal process is not only governed by the cutting conditions but also by the work materials. Work materials must be chosen to give an acceptable machinability on which a nanometric surface finish can be achieved.

Up to present, the typical work material used in ultra-precision machining can be classified into four main types which include ductile materials (i.e. copper and aluminum); brittle materials (i.e. silicon and germanium); single crystal materials (i.e. KDP) and amorphous materials (i.e. electroless nickel and PMMA). Ultra-precision machining with FTS is also frequently employed for machining brittle materials such as silicon which have not been investigated in this research. Material factors also play an essential role in the surface generation. It is proposed that further work includes an investigation into surface generation for FTS machining for more types of different materials.

8.2 Study of the Geometrical Effect of Optical Microstructures

In the present study, the process factors have been studied for exploring the characteristics of surface generation in FTS machining. Experimental cutting tests have been conducted on microlens array patterns as well as on tilted flat surfaces. From the results of the cutting test, it has been found that the geometry of the machined workpiece would also significantly affect the surface generation in FTS machining. The form errors involved in complicated freeform surfaces such as optical microstrutures are greater extend as compared with the form errors found on tilted flat surfaces even when the same cutting conditions are employed. This phenomenon is understandable since cutting complex profiles is more demanding on the actuation motion of the FTS actuator. There is a need to further study the effect of the geometry of the machined surface in FTS machining.

8.3 Effect of Hysteresis Effect of FTS actuation on Surface Generation

In FTS machining, a piezo-electric actuator is always employed to activate the diamond tool in order to fabricate the desired profile. The actuation motion is mainly controlled by the magnitude of the applied voltage. A piezo-electric actuator is commonly employed as the actuator in FTS machining system because of its strengths (e.g. there is neither backlash nor friction in the actuators, it can produce large forces and it is small and easy to control). However, there are still disadvantages of using a piezo-electric type actuator which affect its performance such as the hysteresis effect. This effect largely depends on the magnitude of the input voltage magnitude, which will increase with a larger input of voltage. The characteristic of the hysteresis effect is suggested for further study for improving the surface generation of FTS machining.

8.4 Modeling of Tool Wear in FTS Machining Complex Profile

In present study, a series of cutting experiments were carried out for exploring the effect of tool wear in FTS machining. It is found that the tool wear of diamond tool adversely affect the surface generation in FTS machining. This is particularly true for machining complex optical surfaces. It is suggested to further study of the development of theoretical model for the prediction of tool wear in FTS machining.

8.5 Modeling and Simulation of Surface Topography

A theoretical study is proposed in the present study and a simulation system has been built which is composed of an input module, surface generation model, error module and output module. The error involved is solely from the error module which consists of the error motion of the feeding slide and the error motion in FTS actuation. In addition, the simulation system developed in the present research can only predict the form error of surface generation in FTS machining.

As a result, further work is suggested for the development of an optimization model and system for optimizing the cutting performance in FTS machining. It is suggested to further study the modeling and simulation of 3D surface topography in FTS machining. The simulation of the surface topography is useful for better understanding the effect of different factors on the surface generation in FTS machining. The prediction of surface topography is much more complex and requires more theoretical work on the study of the effect of cutting mechanics on surface generation in FTS machining. The successful establishment of a theoretical model for modelling of the surface topography and hence the optimization model and system would contribute significantly to the development of ultra-precision machining technology with FTS. This helps to avoid expensive and time consuming trial and error approach for establishing the optimum cutting conditions for achieving the best surface quality in FTS machining. Moreover, the model would be more comprehensive and could be used to predict the surface roughness as well.

8.6 Surface Characterization of Optical Microstructures

The successful study of surface generation of the FTS machining relies heavily on the associated surface metrology which helps to characterize the generated quality of the machined surface. Nowadays, there is still a lack of universal standard for assessing the form error of optical microstructures. This also increases the difficulty of the present study. To characterize the form error of the optical microstructure, its continuous surface needs to be reconstructed from discrete data. Further research work should focus more on the development of a general function for characterizing the surface features in the optical microstructure. Another issue is to derive functional parameters for correlating the surface quality and functional features of the surfaces fabricated by FTS machining.

References

Alter DM, Tsao TC (1993), Implementation of a direct drive linear motor actuator for dynamic control of the turning process. *In: Proceedings of the 1993 American Control Conference Part 6:1971–1975.*

Anderson, RH: Close up imaging of documents and displays with lens arrays. *Appl. Opt. 18, P477– 484, 1979.*

Artzner, G: Microlens arrays for Shack-Hartmann wavefront sensors. *Opt. Eng. 31, P1311–1321, 1992.*

Asai, S. and Kobayashi, A., Observations of Chip Producing Behavior in Ultra-Precision Diamond Machining and Study on Mirror-Like Surface Generating Mechanism, *Precision Engineering, Vol. 12, No. 3, pp.137-143, 1990.*

Biddut, A.Q.; Rahman, M.; Neo, K.S.; Rezaur Rahman, K.M.; Sawa, M.; Maeda, Y., Performance of single crystal diamond tools with different rake angles during micro-grooving on electroless nickel plated die materials. *International Journal of Advanced Manufacturing Technology, vol.33, no.9-10 , p.891-9, 2007.*

Brinksmeier, E., PreuR, W., Schmutz, J., Manufacture of microstructures by ultrasonic lapping. *Proceedings of the 13th Annual Meeting of the ASPE, S. 169-172, 1998.*

Brinksmeier, E., Malz, R., PreuR, W., Investigation of a novel tool concept for ductile grinding of optical glass. *Proceedings ASPE, Annual Meeting, S. 74-77, 2000.*

Brinksmeier, E., Schmutz, J., Dynamic forces and energy dissipation in vibration diamond cutting of copper. *Proceedings of the 15th ASPE Annual Meeting, Vol. 22, S. 592 - 595, 2000.*

Brinksmeier, E., Preuβ, W., Gessenharter, A., Trumpold, H., Frenzel, C., Ultraprazise Fertigung von Kalibriernormalen fur Oberflachenmesssys-teme, *Harterei-Technische Mitteilungen 56, 134, 2001.*

Brinksmeier, E., Riemer, O., Stern, R., Machining of precision parts and microstructures. *Proceedings of the 10th International Conference on Precision Engineering (ICPE), Initiatives of Precision Engineering at the Beginning of a Millennium, Japan, 3 – 11, 2001.*

Brinksmeier, E., PreuR, W., Autschbach, L., Diamond Contour Boring and Ball-end Milling of Microstructures. *Proceedings of the 3rd euspen Int. Conf. - Eindhoven, The Netherlands, 2, 423-426, 2002.*

Bryan J, Clouser R, Holland E. Spindle accuracy. *Am Mach; 612 P149-164, 1967.*

Casstevens, J.M. “Diamond Turning of Steel in Carbon-Saturated Atmosphere,” *Precision Engineering, Vol. 5, No. 1, p.9, 1983.*

Cetinkunt S, Yu WL, Filliben J, Donmez A., Friction characterization experiments for precision machine tool control at very low speeds. *Proceedings of The American Control Conference, Chicago, IL, pp. 404-8, 1992.*

Che-Haron C.H., Tool life and surface intergrity in turning titanium alloy, *Journal of Material Processing Technology, P231-237, 2001.*

Cheung, C.F., Lee, W.B. Chiu, W.M. and Leung, T.P. “The Manufacturing of High Quality Aspheric Surfaces for Optical Products,” *CIRP International Symposium-Advanced Design and Manufacture in Global Manufacturing Era, August 21-22, Hong Kong, p.37 , 1997.*

Cheung, C.F. and To, S., Aspheric CCD Camera Lenses-A Profitable Product for CCTV and Multimedia Application, *Plastic Newsletter Special Issue: Optical Products, p.7, 1998.*

Cheung C. F., Lee W. B., A theoretical and experimental investigation of surface roughness formation in ultra-precision diamond turning; *International Journal of Machine Tool and Manufacture 40, P979-1002, 2000.*

Cheung C. F. and Lee W. B., Characterisation of nanosurface generation in single-point diamond turning, *International Journal of Machine Tools and Manufacture, Volume 41, Issue 6, Pages 851-875, May 2001.*

Craft, NC, Feldblum, AY, Optical interconnects based on arrays of surface-emitting lasers and lenslets. *Appl. Opt. 31, P1735–1739, 1992.*

Cross KJ, McBride JW. 3-D laser metrology for the assessment of curved surfaces. *In Proceedings of the Lamdamap Conference ’97, pp. 537–47, 1996.*

Dagnall H. Exploring Surface Texture. *Thurmaston, Leicester, UK: Taylor Hobson Ltd., 1998.*

De Chiffre L., Lonardo P., Trumpold H, Lucca D.A., Goch G., Brown C.A., Hansen H.N., Quantitative characterisation of surface texture, Keynote paper, Annals of the CIRP, 49/2:635-651, 2000.

De Chiffre L., Kunzmann H., Peggs G.N., Lucca D. A., Surfaces in Precision Engineering, Microengineering and Nanotechnology, *CIRP Annals - Manufacturing Technology, Volume 52, Issue 2, Pages 561-577, 2003.*

Donaldson RR, Thompson DC., Design and performance of a small precision CNC turning machine. *Ann CIRP 35(1):373–6, 1986.*

Douglas S. S. and Green W., Machine tool control system for turning nonaxisymmetric surfaces, *in Proc. Joint Automatic Control Conf., 1979.*

Douglas C.M., Design and Analysis of Experiments, *fourth ed., Wiley, New York, pp. 243–245, 1997.*

Dow T. A., Miller MH, Falter PJ., Application of a fast tool servo for diamond turning of nonrotationally symmetric surfaces. *Precision Eng. 13(4):233–50, 1991.*

Dresel Th. and Schwider J., Fabrication of optical components by laser lithography, *Applied Surface Science, Volume 106, P.379-382, 1996.*

Durazo-Cardenas I., Shore P., Luo X., Jacklin T., Impey S.A., Coxc A., *3D* *characterisation of tool wear whilst diamond turning silicon, Wear 262, P340–349, 2007.*

Engdahl, R.E., Chemical vapour deposited (CVD) silicon carbide mirror technology, *Reflecting Optics for Synchrotron Radiation, Proc. SPIE, 315, 1981.*

Evan, C. “Cryogenic Diamond Turning of Stainless Steel,” *Annals of the CIRP, Vol. 40, No. 1, p. 571, 1991.*

Evans CJ, Hocken RJ, Estler WT. Self-calibration: reversal, redundancy, error separation and ‘absolute testing’. *Ann CRIP 45 (2), P617-634, 1996.*

Falter P. J. and Dow T. A., “A diamond turning apparatus for fabrication of nonrotationally symmetric surfaces,” *in Proc. Int. Congr. Ultraprecision Technology, Aachen, Germany, pp. 187–201, 1988.*

Fawcett SC., Small amplitude vibration compensation for precision diamond turning. *Precision Eng vol 12, no. 2:91–6, 1990.*

Fawcett SC, Engelhaupt D., Development of Wolter I X-ray optics by diamond turning and electrochemical replication. *Precision Eng 17(4):290–7, 1995.*

Forbes A. Least-squares best-fit geometric elements. *NPL Report DITC 140/89; 1991.*

Franse, J., "Manufacturing Techniques for Complex Shapes with Submicron Accuracy". *Rep. Prog. Phys. Vol.53, p.1049-1094, 1990.*

Gao W, Kiyono S, Sugawara T. High accuracy roundness measurement by a new error separation method. *Precision Engineering 21 (2/3), P123-133, 1997.*

Gao W, Hocken RJ, Patten JA, Lovingood J, Lucca DA., Construction and testing of a nanomachining instruments. *Precision Eng. 24(4):320–8, 2000.*

Hanson RD, Tsao T-C., Development of a fast tool servo for variable-depth-of-cut machining. *ASME Dyn Syst Control 2: 863–71, 1994.*

Hara Y, Motonishi S, Yoshida K, Ikawa N., A new micro-cutting device with high stiffness and resolution. *Ann CIRP 39(1):375–8, 1990.*

Huixing Z, Linna Z, Xiankui W, Jinling L, Repetitive control and application to linear servo unit for CNC machining of elliptical pistons. *In: Proceedings of the IEEE International Conference on Industrial Technology 12:630–633, 1994.*

Hutley, MC, Savander, P, Schrader, M, The use of microlenses for making spatially variant optical interconnections. *Pure Appl. Opt. 1 P337–346, 1992.*

Ikawa N., Shimada S., Tanaka H., Minimum thickness of cut in micromachining, *Nanotechnology 3 P6 – 9, 1992.*

Ishii, Y, Koike, S, Arai, Y, Ando, Y, Ink-jet fabrication of polymer microlens for optical-I/O chip packaging. *Jpn. J. Appl. Phys. 39, Part 1 P1490–1493, 2000.*

Jiwang Yan, Katsuo Syoji, Jun’ichi Tamaki, Some observations on the wear of diamond tools in ultra-precision cutting of single-crystal silicon, *Wear 255, P1380–1387, 2003.*

Johnson, W. and Meller, P.B., Engineering Plasticity, D. van Nostrand Co, London, UK (1973)

Jung Seung-Bae, Lee Young-Ho and Kim Scung-Woo, Profile measurement of micro-machined surface by scanning tunneling microscopy, *Korean Soc. Mech. Engng 17(7), 1731-1739, 1993.*

Kasa I. A circle-fitting procedure and its error analysis. *IEEE Trans Instrum Meas; 25:8 –14, 1976.*

Jung Seung-Bae, Nonlinear modeling for positioning uncertainty of piezoelectric actuators driven by voltage input. Ph.D Thesis, *Korean Advanced Institute of Science and Technolog , 1993.*

Jung Seung-Bae and Kim Seung-Woo, Improvement of scanning accuracy of PZT piezo-electric actuator by feed-forward model-reference control, *Precision Engng 16(1), 49-55, 1994.*

Kazuhiko S, Yoichi Y, Norio S, Development of a noncircular high speed generating mechanism by hybrid system with VCM and PZT. *J Japan Soc Precis Eng 58(9):1503–1508, 1992.*

Keauskopf B. Diamond-turning: reflecting demands for precision. *Manufacturing Engineering. pp. 90-100, 1984.*

Keen, D.: Some observation on the wear of diamond tools used in piston machining, *Wear, Vol. 17, P195-202, 1971.*

Keyworth, BP, Corazza, DJ, McMullin, JN, Mabbott, L: Single-step fabrication of refractive microlens arrays. *Appl. Opt. 36, P.2198–2202, 1998.*

Kim Jeong-Du and Kim Dong-Sik, Waviness compensation of precision machining by peizo-electric micro cutting device, *International Journal of Machine Tools & Manufacture 38, P.1305-1322, 1998.*

Kim J-D, Kim D-S., Waviness compensation of precision machining by piezo-electric micro cutting device. *Int J Machine Tools Manufact 38 P1305–22, 1998.*

Kim J-D, Nam S-R., Development of a micro-depth control system for an ultra-precision lathe using a piezoelectric actuator. *Int J Machine Tools Manufacture 37(4):495–509, 1997.*

Kim BS, Control of multiple degree of freedom fast tool stages for noncircular turning progress. *Dissertation, University of Illinois, 2001.*

King TG. Piezo-electric ceramic actuators : a review of machinery application. *Precision Engineering 12(3):131-6, 1990.*

Kirk Rogers, Jeff Roblee, Freeform Machining with Precitech Servo Tool Options, *Precitech Inc: http://www.precitech.com, May 2005.*

Kong L.B., Cheung C.F., Lee W.B., To S. and Zhang Z.J., A Kinematics and Experimental Analysis of Form Error Compensation in Ultra-precision Machining, *Int.*

J. Mach. Tool & Manuf. Vol.48, P1408-1419, 2008.

Kong M.C., Lee W.B., Cheung C.F. and To S., A study of materials swelling and recovery in single-point diamond turning of ductile materials, *Journal of Materials Processing Technology, Volume 180, Issues 1-3, 1, Pages 210-215, December 2006.*

Kouno K. A fast response piezoelectric actuator for servo correction of systematic errors in precision machining. *Ann CIRP 33(1):369– 72, 1984.*

Ku Sang-soon, Gary Larsen, Sabri Cetinkunt, Fast tool servo control for ultra-precision machining at extremely low feed rates, *Mechatronics 8 P.381-393, 1998.*

Larsen G, Cetinkunt S, Donmez A., CMAC neural network control for high precision motion control in presence of large friction. *ASME Journal of Dyn. Syst. Meas. and Control 117(3):415-20, 1995.*

Lee W.B., Cheung C.F., To S., Materials induced vibration in ultra-precision machining, *Journal of Materials Processing Technology 89–90, P.318–325, 1999.*

Lee W.B., Gao D., Cheung C.F., etc, A NC Tool Path Translator for Virtual Machining of Precision Optical Products, *Journal of Materials Processing Technology, 140(1-3): 211-216, 2003.*

Lee Yung-Chun, Chen Chun-Ming and Wu Chun-Ying, A new excimer laser micromachining method for axially symmetric 3D microstructures with continuous surface profiles, *Sensors and Actuators A: Physical, Volume 117, Issue 2, P.349-355, 2005.*

Lindlein, N, Pfund, J, Schwider, J: Algorithm for expanding the dynamic range of a Shack-Hartmann sensor by using a spatial light modulator array. *Opt. Eng. 40, 837–840, 2001.*

Lonardo, P.M., Lucca, D.A., De Chiffre, L., Emerging trends in surface metrology, *Annals of the CIRP, 51/2 701-723, 2002.*

Lucca, D.A., Brinksmeier, E., Goch, G., Progress in assessing surface and subsurface integrity, *Annals of the CIRP, 47/2:669-693, 1998.*

Ludwick SJ, Chargin DA, Calzaretta JA, Trumper DL. Design of a rotary fast tool servo for ophthalmic lens fabrication. *Precision Eng 23(4):253–9, 1999.*

Marc Crudele, Thomas R. Kurfess, Implementation of a fast tool servo with repetitive control for diamond turning, *Mechatronics 13, P.243–257, 2003.*

Mater. J.; Taguchi method, Process. *Technol. 84, P 122-129, 1998.*

McBride JW, Cross KJ. The measurement and analysis of three dimensional form of curved surfaces. *Int J Machine Tools Manufact 36(5):597– 610, 1996.*

McBride JW, Cross KJ, Shark SM. The evaluation of arc erosion on electrical contacts using three-dimensional surfaces profiles. *IEEE Trans—Part A 19(1):87–97, 1996.*

Miller MH, Garrard KP, Dow TA, Taylor LW., A controller architecture for integrating a fast tool servo into a diamond turning machine. *Precision Eng 16(1):42–8, 1994.*

Moorefield G.. M., Generation of rotationally asymmetric optical surfaces using a fast tool servo, *in Proc. ASPE Annu. Conf., vol. 10, pp. 45–48, 1994.*

Moriwaki T., *Int. J. Jpn. Soc. Prec. Eng. 29 P287, 1995.*

Moriwaki, T., Horiuchi, A. and Okuda, K., Effect of cutting heat on machining accuracy in ultra-precision diamond turning, *Annals of the CIRP, Vol. 39(1), pp.81-84 ,1990.*

Nakasuji, T., Kodera, S., Hara, S., and Matsunaga, H., Diamond turning of Brittle materials for optical components, *Annals of the CIRP, Vol. 39. No.1, p.89, 1990.*

O’ Neill F. T., Owen G. and Sheridan J. T., Alteration of the profile of ink-jet-deposited UV-cured lenses using applied electric fields, *Optik – International Journal for Light and Electron Optics*, *Volume 116, Issue 4, P.158-164, 2005.*

Okazaki Y., A micro-positioning tool post using a piezoelectric actuator for diamond turning machines. *Precision Eng; 12(3):151–6, 1990.*

Ong S., Koh Y. H. and Fu,Y. Q. Microlens array produced using hot embossing method, *Microelectronic Engineering 60 P.365-379, 2002.*

Pahk HJ, Lee DS, Park JH, Ultra precision positioning system for servo motor-piezo actuator using the dual servo loop and digital filter implementation. *Int J Mach Tools Manuf 41(1):51–6, 2001.*

Patterson S. R. and Magreb E. B., Design and testing of a fast tool servo for diamond turning, *Precision Eng., vol. 7, no. 3, pp. 123–128, 1985.*

Pekka Savander, Microlens Arrays Etched into Glass and Silicon, *Optics and Lasers in Engineering 20 P.97-107, 1994.*

Pramanik, A.; Neo, K.S.; Rahman, M.; Li, X.P.; Sawa, M.; Maeda, Y. (2009), Ultra-precision turning of electroless-nickel: effect of phosphorus contents, depth-of-cut and rake angle. *Journal of Materials Processing Technology, vol.208, no.1-3 , p.400-8.*

Pramanik A. , Neoa K.S., Rahmana M., Li X.P. a, Sawab M., Maedab Y., Cutting performance of diamond tools during ultra-precision turning of electroless-nickel plated die materials, *Journal of materials processing technology 140, P308-313, 2003.*

Quan, C. et al., Integrated Optical Inspection on Surface Geometry and Refractive Index Distribution of a Microlens Array, *Optics Communications, 225, 223–231, 2003.*

Quan C., Wang S.H., Tay C.J., etc, Integrated optical inspection on surface geometry and refractive index distribution of a microlens array, *Optics Communications, (225): 223–231, 2003.*

Rai-Choudhury (ed.), 1997, Handbook of microlithography, micromachining and microfabrication, Volume 1: Microlithography, *SPIE Optical Engineering Press, Washington, USA. ISBN 0852969066.*

Rasmussen JD, Tsao T-C, Hanson RD, Kapoor SG., Dynamic variable depth of cut machining using piezoelectric actuators. *Int J Machine Tools Manufact; 34(3):379–92, 1994.*

Reddy RG, DeVor RE, Kapoor SG, Sun Z, A mechanistic model based force-feedback scheme for voice-coil actuated radial contour turning. *Int J Mach Tools Manuf 41(8):1131–1147, 2001.*

Rice JR. Numerical methods, software, and analysis. *New York: McGraw-Hill, Inc., 1983.*

Ross P., Taguchi Techniques for quality engineering – Loss Function, Orthogonal experiments, parameter and tolerance design, *McGraw-Hill, New York, P 10-50, 1988.*

Ross P.J., Taguchi Techniques for Quality Engineering, *second ed., McGraw-Hill, New York, 1996.*

Sechenz, R. R., Patterson, S.R. Saito, T. T.; Direct machining of a non-axisymmetric phase corrector. *Proc. SPIE, 966, P43-59, 1988.*

Schilling, A, Merz, R, Ossmann, C, Herzig, HP: Surface profiles of reflow microlenses under the influence of surface tension and gravity. *Opt. Eng. 39, 2171 – 2176, 2000.*

Shamoto E, Moriwaki T. Development of a "walking drive" ultraprecision positioner. *Precision Eng;20(2):85–92, 1997.*

Shamoto E, Moriwaki T. Ultraprecision diamond cutting of hardened steel by applying elliptical vibration cutting. *Ann CIRP 48(1):441–4, 1999.*

Sharif Uddin M., Seah K.H.W. ∗,Li X.P., Rahman M., Liu K., Effect of crystallographic orientation on wear of diamond tools for nano-scale ductile cutting of silicon, *Wear 257, P751–759, 2004.*

Sharif Uddin M., Seah K.H.W., Rahman M., Li X.P., Liu K., Performance of single crystal diamond tools in ductile mode cutting of silicon, *Journal of Materials Processing Technology, 2006.*

Shaw, M.C., Historical aspects concerning removal operations on metals, *Metal Transformations, Gordon and Breach, N.Y., pp211, 1968.*

Shen, X-J, Pan, L-W, Lin, L: Microplastic embossing process: experimental and theoretical characterizations. *Sensors and Actuators A 332, 1–6N, 2002.*

Shinno H, Mitsui K, Tanaka N, Omino T, Tabata T. A new method for evaluating error motion of ultra precision spindle. *Ann CIRP 36(1): 381–4, 1987.*

Stoebenau, S. and Sinzinger, S., Ultraprecision machining techniques for the fabrication of freeform surfaces in highly integrated optical microsystems. *Proc. SPIE - Int. Soc. Opt. Eng. Vol. 7426, P08, 2009.*

Sweeney DW, Sommargren GE. Harmonic diffractive lenses. *Appl Opt 34(14):2469–75, 1995.*

Stevens, RF, Davies, N: Lens arrays and photography. *Jour. Photographic Science 39, 199–208 1991.*

Taguchi G., S. Konishi, Taguchi Methods, Orthogonal Arrays and Linear Graphs, Tools for Quality Engineering, *American Supplier Institute, 1987.*

Taguchi G., Introduction to quality engineering, *Asian Productivity Organization, 1990, Japan.*

Taguchi G., Taguchi on Robust technology development methods, *ASME, New York, P 1-40, 1993.*

Taminiau, D.A. and Dautzenberg, J.H.: Bluntness of tool and process forces in high precision cutting, *Annals of the CIRP, Vol. 40, P65-71, 1991.*

Toshiro H, Yamaguchi T, Development of a high speed noncircular machining NC lathe for cutting a piston head of a reciprocating engine by use of a new servomechanism actuated by electromagnetic attractive force. *J Japan Soc Precis Eng 62(3):453–457, 1996.*

Tsao TC, Masayoshi T Robust adaptive and repetitive digital tracking control and application to a hydraulic servo for noncircular machining. *J Dyn Systems Measure Cont Trans ASME 116(3): 24–32, 1994.*

Tzou H.S., Design of a piezoelectric exciter/actuator for micro-displacement control: theory and experiment, *Precision Eng 13(2), 104-110, 1991.*

Volkel, R, Herzig, HP, Nussbaum, P, Da¨ ndliker, R: Microlens array imaging system for photolithography. *Opt. Eng. 35, P. 3323–3330, 1996.*

W.H. Wang, Y.S. Wong, G.S. Hong, 3D measurement of crater wear by phase shifting method, *Wear 261, P164–171, 2006.*

Wagner, M.; Kunzelmann, U.; Schenk, H. ; Lakner, H., Global flatness of spatial light modulators. *Proc. SPIE - Int. Soc. Opt. Eng. Vol. 6114, P04-12, 2006.*

Wei Gao, Takeshi Araki, Satoshi Kiyono, Yuichi Okazaki and Masashi Yamanaka, Precision nano-fabrication and evaluation of a large area sinusoidal grid surface for a surface encoder, *Precision Engineering, Volume 27, Issue 3, Pages 289-298, 2003* .

Whitehouse D.J., Handbook of Surface Metrology, *Institute of Physics, Bristol, Philadelphia, 1994.*

Whitehouse D J, Handbook of surface and nanometrology, *P16-18, 2003.*

Wolter, H. Mirror systems with grazing incidence as image-forming optics for x-rays. *Ann. Phys.* 6^{th} *Series, 10, 94-114.*

Yan, J., Yoshino, M., Kuriagawa, T., Shirakashi, T., Syoji, K. and Komanduri, R., "On the Ductile Machining of Silicon for Micro Electro-Mechanical Systems (MEMS), *Opto-Electronic and Optical Applications", Materials Science and Engineering A, Vol.*

297, Issues 1-2 , pp.230-234, 15 January, 2001.

Yang Min-yang and Kwon Oh-dal, Crater wear measurement using computer vision and automatic focusing, *Journal of material processing technology 58, P362-367, 1996.*

Yang W., Tang Y., Design optimization of cutting parameters for turning techniques based on the orthogonal arrays. *Journal of Material Processing Technology 132 P340-344, 2003.*

Yong jin Kwon, Gary W. Fischer, A novel approach to quantifying tool wear and tool life measurements for optimal tool management, *International Journal of Machine Tools & Manufacture 43, P359–368, 2003.*

Yu Y., Nagi N., Rao D., Preisach modeling of hysteresis for piezoceramic actuator system, *Mechanism Machine Theory 37, P.49–59, 2002.*

YUAI Hong-Tzong and MENQ Chia-Hsiang, A unified least-squares approach to the evaluation of geometric, Errors using discrete measurement data, *Int. J. Math. Tools Manufact. Vol. 36, No. 11, pp. 1269-1290, 1996.*

Yuan Z.J., Yao Y.X., Zhou M., Bai Q.S., Lapping of single crystal diamond tools, *Ann. CIRP, 52 (1) P.285 – 288, 2003.*

Zhang Yuan-liang; Zhou Zhi-min; Xiu Wei; Xia Zhi-hui (2007), Influence of cutting parameters on diamond turning titanium alloy. *Proceedings of the SPIE - The*

International Society for Optical Engineering, vol.6722 , p.67221J-1-6.

Zhong Z. and Nakagawa T., Development of a micro-displacement table for ultra-precision machining and grinding for curved surfaces by the use of it, *Japan Soc. Precision Engng 26(2), 102-107, 1992.*

Zhou M., Ngoi B.K.A., Factors affecting form accuracy in diamond turning of optical components, *Journal of Materials Processing Technology 138, P.586–589, 2003.*

Zhu W-H, Jun MB, Altintas Y. A fast tool servo design for precision turning of shafts on conventional CNC lathes. *Int J Machine Tools Manufact41:953–65, 2001*.

Appendix I

Specification of Fast Tool Servo System (Precitech)

FTS® Fast Tool Servo System

Features & Benefits

Introducing the **New** Fast Tool Servo (*FTS*™) system adaptable to our Nanoform® machines. These *FTS*™ systems enable the diamond turning of surface structures such as micro-prisms, torics, off-axis aspheres, and various lens array formations at either *70* or *500* microns of stroke.

The tool path software uses a C-program or bitmap image to describe the desired part topography. An external PC with DSP (digital signal processor) uses high resolution angular feedback on the work spindle and the linear position feedback of the machine translational slide to "real-time" calculate the axial position of the tool.

The Precitech *FTS*™ systems are designed to produce very high dynamic movement during the turning process with low mechanical noise.

Specifications

Sinusoidal Acceleration

FTS™ 70 - 70µm (0.0028") travel - 700 Hz bandwidth*

FTS™ 500 - 500µm (0.02") travel - 1000 Hz bandwidth*

*For small excursions only.

Power limitations restrict the operational frequency for large excursions.

Drive Mechanism

FTS™ 70 - Piezo actuation.

FTS™ 500 - Linear motor (voice-coil) actuation with active counterbalance to eliminate reaction forces.

- The FTS™ 70 includes a high stiffness flexure type tool holder.
- The FTS™ 500 utilizes air bearing guides

Both systems include:

- Capacitance gage position feedback
- C program or grayscale bitmap imaging for tool path generation of desired surface.

Precitech ultra precision technology

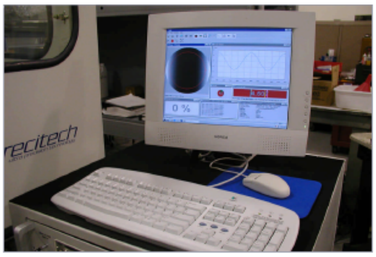

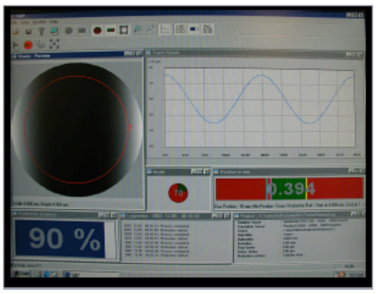

Appendix II

Freeform Machining with Precitech Servo Tool Options

Freeform Machining with Precitech Servo Tool Options

Kirk Rogers, Jeff Roblee

A growing number of optics manufactures are investigating servo tool machining technologies. The goal of this document is to provide:

- A practical understanding of the operating characteristics of the various Precitech servo tool options.
- Information to determine which servo tool best fits an application.
- A method to calculate servo tool machining cycle times.

Benefits of servo tool machining
Using Precitech servo tool options, non-rotationally-symmetric surfaces (including freeform surfaces) can be produced economically on Precitech's two-axis diamond turning lathes, the Precitech Nanoform 200, 350, and 700 systems.

With servo tool machining customers can produce non-rotationally-symmetric surfaces via a turning operation at significantly lower costs over traditional manufacturing methods (e.g. raster fly cutting).

Components that can be turned off-axis (i.e. off-axis-rotationally-symmetric parts: high order aspheres, parabolas, torics etc.) can now be turned on-axis with servo tool machining. Advantages of this approach include:

- Increasing the range of components that can be made on your existing Nanoform lathes. Off-axis parts that can't be produced because the off-axis setup exceeds the swing capacity of the diamond turning machine can now be produced on-axis with servo tool machining.
- Reducing cost and lead times for work piece holding fixtures. On-axis fixtures are typically less expensive and less technically challenging than off-axis fixtures (aka "surrounds"). This is particularly useful when producing a low quantity part or when a short lead time to a first-piece prototype is critical.

Servo Tool Machining – typical system configuration
A typical machine configuration for servo tool machining is shown below.
The work piece is mounted on the C axis (a work holding air bearing spindle with precision velocity and position encoders). The C axis is mounted to the X axis carriage. The servo tool option is mounted on the Z axis carriage. Machining with this machine configuration is also known by the shorthand term "**XZC machining**".

Precitech ultra precision technology

Freeform Machining with Precitech Servo Tool Options

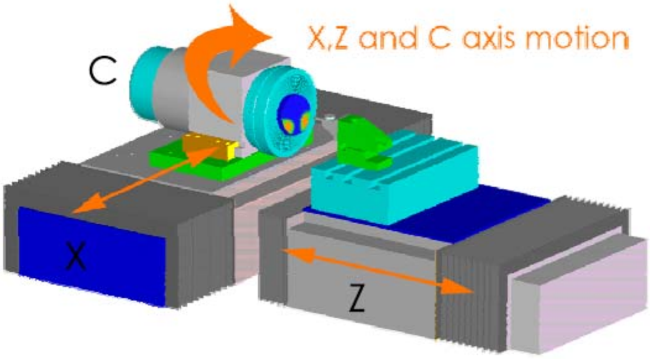

Three servo tool options

Precitech offers three servo tool options to cover the widest range of application requirements. Table 1 shows the general characteristics of the **Slow Tool Servo (STS)** and two fast tool servo (FTS) options: the **FTS500** and **FTS70**.

Table 1 General Characteristics Precitech STS, FTS500 and FTS70 servo tools

	STS	**FTS 500**	**FTS 70**
Drive & "bearing" technology	Linear motor / Hydrostatic Oil bearing	Voice coil / Air bearing and counter mass	Piezoelectric stack / Flexure element
Characteristic Travel*	10 mm (@ 2 Hz)	500 um	70 um
Characteristic Bandwidth**	70 Hz	1000 Hz	700 Hz
Characteristic Surface finish^	5 nm Ra	8 nm Ra	5 nm Ra
Characteristic form accuracy^	250 nm PV	300 nm PV	600 nm PV
Position sensor	Scale	Analog	Analog
Programming Software	Diffsys	SOP	SOP

* See Figure 1 for a more complete description
** Related to servo control design and performance
^ Typical performance for test specimens (also typical real world results for many applications)

The **STS** option (lower acceleration, long excursion) is typically used to produce high amplitude non-rotationally-symmetric continuous surfaces. A continuous surface does not feature any inflection points (instantaneous changes) in the surface slope or step changes in surface height that require radical changes in tool velocity.

2

The **FTS70 and FTS500** options (high acceleration, short excursion) are typically used to produce higher frequency (higher spatial density), lower amplitude, surface structures that may also have discontinuities in the surface.

Discontinuous surfaces can be found on optical components like micro-mirror arrays, lenslet arrays and components where two or more optical elements are integrated into one surface (e.g. bifocals). The FTS servo tools feature very fast reaction times so that the tool can accurately follow the surface of a component across surface discontinuities.

Which servo tool option best fits an application?

In many cases an application can be produced by more than one of the servo tool options. Choosing the correct servo tool is a function of:

- Surface finish requirements
- Form accuracy requirements
- Transition area specifications (i.e. the area between clear apertures on discontinuous surfaces)
- Cycle time (productivity) goals

Each of the servo tool options also has unique operating characteristics related to their physical design, drive technology and servo control algorithms. These subtle differences can be exploited to provide ultra-high performance in relation to a specific application.

Each of the servo tool options also has unique operating characteristics related to their physical design, drive technology and servo control algorithms. These subtle differences can be exploited to provide ultra-high performance in relation to a specific application.

The **STS** and **FTS500** (linear motor and voice coil drives) both excel in the area of form accuracy. Both of these drive systems feature very linear response curves which contribute to their achieving high form accuracy.

The **FTS70** (piezo stack) excels in the area of surface finish. The low mass, high characteristic bandwidth and extremely high positioning resolution of **FTS70** is an ideal combination for generating high quality surface finishes.

The first step in choosing the most suitable servo tool option is to determine if the tool path amplitude and the drive frequency required by the application falls within the operational limits of the servo tool.

Figure 1 (below) shows the maximum amplitude of tool motion vs. drive frequency curves for each Precitech servo tool. The tool path amplitude and tool excitation frequency required to generate a surface can be plotted as an operation point (Hz, mm) in relation to these curves. In general, as the operation point approaches the amplitude/frequency limits of the servo tool, form accuracy and/or surface finish degrade. This may be acceptable depending on the cost / performance requirements of the application.

Figure 1. Operational Limits for STS and FTS (XZC) Machining

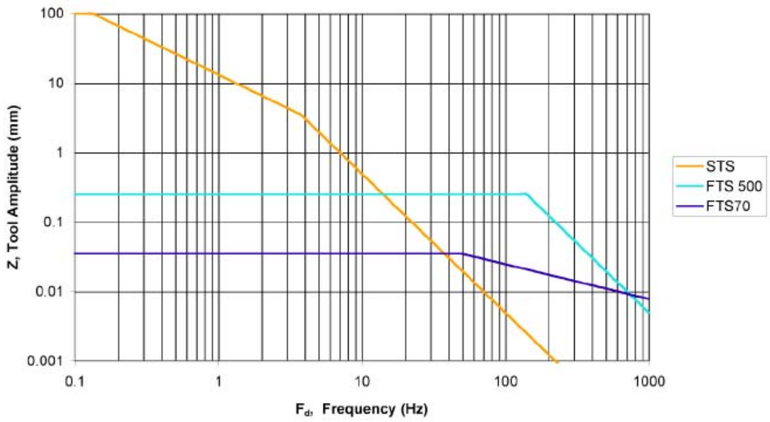

Drive amplitude
Amplitude represents one half of the total Z axis motion (worst case) for a given revolution of the work piece. This motion is the non-rotationally symmetric component of the desired surface. Example: A 2mm tilted flat requires a 1mm excursion in +Z and a 1mm excursion in the –Z direction, so the drive amplitude is 1 mm.

Tool drive (excitation) frequency
Drive frequency is the number of tool motion cycles per second. It is directly related to the rotational speed of the work piece. Continuous surfaces typically feature simple arithmetic relationships between excitation frequency and rotational velocity (RPM). A tilted flat surface completes one cycle of the tool motion per revolution of the part. A tilted flat being cut at 400 RPM will require a tool excitation frequency F_d of 400/60 or 6.66 Hz. A toric surface features two tool motion cycles per revolution. A toric surface being cut at 400 RPM will require a tool driving frequency of 2*400/60 or 13.33 Hz.

In general, any off-axis-rotationally-symmetric continuous surface can be reduced to predominantly two tool motion cycles per revolution. While higher order motions (4 cycle/rev, 8 cycle/rev) may be generated by the surface path, the amplitude of these higher order motions are typically < $1/10^{th}$ that of the fundamental 2 cycle/rev path. At such small amplitudes, the higher harmonic components have little effect on the operational limits.

Determining the drive frequency for discontinuous surfaces like lenslet arrays needs to be treated in a different fashion.

For discontinuous surfaces, maximum tool excitation frequency can be approximated by the following formula:

$\mathbf{F_d}$ (Hz) $= (2\,\pi\,R_{max})N(\text{rpm})/60P$

Where:
- P = the pitch (spacing in mm) of the optical elements' center lines (or chord distance across an element).
- R_{max} = the maximum turning radius in mm from the center of rotation to the most outlying optical element.
- N = spindle speed

A lenslet array with 1 mm lenses on a 10 mm diameter mold insert being cut at 200 RPM (assumed for the moment) would require a tool drive frequency of: (2xπx5x200)/(60x1) or 105 Hz.

As noted, tool drive frequency is a function of spindle speed. In theory, if you slow down the spindle enough the STS option, even with its lower bandwidth, could cut any size feature. The down side to this is obviously productivity. Secondly, very long cycle times (e.g. many hours) allow the machine to respond to thermal disturbances from the environment. Finally, some materials are not easily machined at very low speeds.

For discontinuous surfaces, maximum spindle speed is often limited by the following error created when the tool bit is instructed to make a radical change in its path as it crosses a discontinuity in the surface. The recovery time of the servo tool should be considered whenever there are abrupt changes in the slope of the surface or steps in the height of the surface.

Transition areas in discontinuous surfaces

Components that feature discontinuities in their surfaces or repetitive shapes nested together across the surface (lenslet arrays for example) typically specify the clear aperture area of each optical element. Between the clear apertures is a transition area or edge zone. Form errors in the edge zone are allowed to exceed those in the clear aperture. A reasonably sized edge zone enables the part to be manufactured at reasonable cost.

The following items are typically known from the component specifications and the characteristics of the servo tool:

- The allowable form error in the clear aperture area,
- The physical dimensions of the clear aperture and transition areas,
- The characteristic bandwidth of the servo tool

With this information and using Figure 3, the maximum surface velocity of the part relative to the tool bit can be calculated. From this the spindle speed and the part cutting cycle time can then be determined. This will be demonstrated later.

Background

Figure 2 shows a classic control loop response to a tool path command that changes the direction of motion. In this example, the circumferential speed (V_s) of the work piece as it passes by the tool is 150 mm/sec.

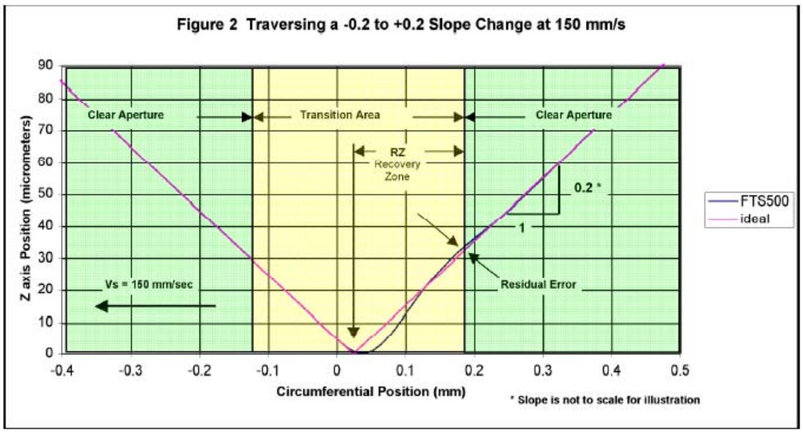

The difference between the ideal motion and the actual motion results in form error in the surface of the part. How "quickly" the tool path can correct for radical changes in slope or surface height is related to the characteristic bandwidth of servo tool's control loop. The period of the sinusoidal error motion shown in Figure 2 is the inverse of the natural frequency of the servo tool control loop. The characteristic bandwidth of the servo tools shown in Table 1 is the drive frequency where resulting (output) tool motion amplitude is 3 dB (30%) down from the commanded (input) amplitude. The natural frequency of the servo tool control loop is typically 30% lower in frequency than the characteristic bandwidth.

Within a small number of cycles the error motion (form error) decays to a very low value. The term "Residual Error" (RE) is equal to the allowable form error in the clear aperture region. Typically the cutting speed is tuned so that the residual error on exiting the transition area (at the end of the recovery zone) is less than (just under) the allowable form error.

Bringing it all together

Figure 3 is a dimensionless presentation of the relationships between:

- Error motion amplitude and tool path slope (S) , error = f(S)
- Recovery zone width (RZ) and Servo tool bandwidth (BW), RZ = f(1/BW)
- Tool surface velocity (Vs) and Recovery Zone width RZ, Vs = RZ x BW / RZ_{bar}

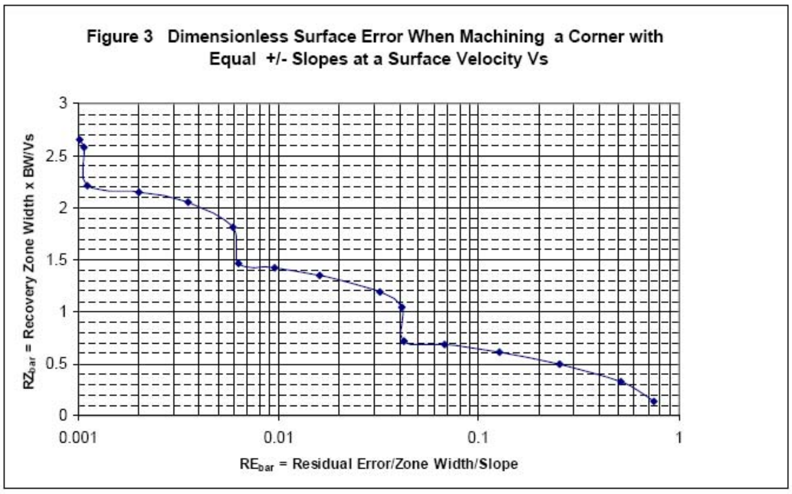

Figure 3 is used to determine the maximum surface velocity at which the servo tool's cutting path can meet the clear aperture form error specifications of the component.

Here is an example showing how to apply this information to determine the correct servo tool to use for an application and then estimate the cycle time for a finish cut.

Application: Lenslet Array

- Component size: 50mm diameter
- Lens diameter (pitch) (P) 5 mm
- Lens form spherical R = 12.5mm (PV sag = 0.25 mm)
- Allowable form error within the clear aperture (also equal to the residual error(RE)) RE = 0.00031 mm = 0.31 μm
- Clear aperture diameter 4.61mm (clear aperture area is 85% of the overall lens area)
- Recovery Zone width (Transition area span / 2 ^^): RZ = 0.195 mm
- Tool path slope (rise/run) within transition area (S) S = 0.2

^^ Note: In this example the part is designed with the transition area placed symmetrically about the boundary between the lens features. Tool path error is not symmetric in relation to these boundaries. Following error predominates. This can be exploited to further reduce part manufacturing costs if the optical design allows for non-symmetric transition areas.

Servo Tool Amplitude

Based on the tool amplitude needed (125μm = 0.25mm / 2) and referring to Figure 1 this component could be cut using either the **FTS 500** or the **STS** servo tool but cannot be cut with **FTS 70** servo tool.

Maximum Spindle Speed:
The maximum spindle speed is calculated next using Figure 3.

RE_{bar} = RE(μm) / RZ(μm) / S = 0.31 / 195 / 0.2 = 0.00795

Using the RE_{bar} value and the curve in Figure 3 the RZ_{bar} value can be found: ~ **1.3**

Assuming for the moment the **FTS 500** servo tool option (BW= 1000 Hz) the maximum surface velocity Vs is:

Vs = BW (Hz) * RZ(mm) / RZ_{bar} = 1000 * 0.195 mm / 1.3 = **150 mm/sec = 9,000 mm/min**

Spindle speed, RPM = Vs / (circumference $_{max}$) = 9000 / (Π * 50) = **57 RPM**

Servo Tool Drive Frequency
The tool drive frequency can be calculated next:

$\mathbf{F_d}$ = (2 * Π * N(RPM) / (60 * P)) = (2 * Π * 57 / (60 * 5) = **30Hz**

Referring back to Figure 1 this drive frequency and amplitude combination exceeds the capabilities of the **STS** servo tool. More to the point, because of the lower bandwidth of the **STS** option the spindle speed would have to be lowered to 4 RPM in order to meet the clear aperture form error requirements of the part.

Finish Cut Cycle Time
Assuming a constant spindle speed (not required, see below) and 3 μm feed / rev, the cycle time for the finish cut is:

Cycle time (min) = Part dia. / (2 * feed/rev * RPM) = 50/(2*0.003*57) = **146 min.**

(For comparison, using the STS servo tool to cut this part, the spindle speed would need to be reduced to 4 RPM. The finish cut cycle time would be 2080 min or 34 hours.)

If spindle speed is kept constant, the part surface velocity will fall as the tool approaches the center of rotation. Within practical limits, spindle RPM over the course of a part cut can be increased to shorten part cutting cycle time.

Other application examples:
Table 2 (attached) lists relevant operational parameters for a variety of applications. All of these examples are based on actual cutting experiments performed at Precitech. The results in Table 2 are consistent with practical production results reported by our customers.

Summary:
Precitech offers the widest range of servo tool options in the ultra-precise machining industry. Selecting the best servo tool for your applications requires consideration of many factors. The Precitech application engineering team frequently works with new and existing customers to help find the best solutions to demanding applications. Precitech's XZC machining solutions are also robust and production ready.

Beyond the scope of this paper, but key to the successful use of XZC machining, is the Precitech UPX controller. The UPX features the fastest code execution rate in the ultra-precision industry: The UPX controller can execute 1800 blocks of tool path instructions per sec. A block or line of instructions can control up to six axes of motion. This computational power allows users to produce excellent surface finishes at much higher cutting rates (lower part cutting cycle times) than could be realized with older technologies. The UPX does not use motion control cards. Customers do not have to down-grade surface definitions (increase point to point spacing) to accommodate motion control card rotary buffer limitations. A simple example of the robustness and stability of UPX is the use of manual panel controls (like spindle override and cycle hold) while XZC programs are running without affecting overall system stability. Finally part cutting programs can be set up to cut multiple roughing and/or finish passes without operator intervention between each pass.

The Precitech SOP programming environment for fast tool servo XZC machining greatly simplifies the task of programming tool paths for complex freeform surfaces. For example, the entire cutting path for the lenslet array application above is defined within SOP with only ten lines of C-code.

Research and development is ongoing to both improve form/finish results of the current STS and FTS servo tools and develop new servo tool configurations.

In March 2005 Precitech was awarded a sizeable Phase II STTR contract from NASA to develop a new "Fast Linear Axis" (aka "Live-Axis") servo tool configuration. This work will build on the Phase I contract received in 2003. A description of the goals of the NASA project can be found at:

http://sbir.gsfc.nasa.gov/SBIR/abstracts/03/sttr/phase2/STTR-03-2-T4.01-9768.html

Table 2 Cutting results using various servo tool options

Application Description	Servo Tool	Part Dia. (mm)	Spindle (rpm)	Feed/ Rev (μm)	Cycle Time (min.)	Z amplitude (mm)	Drive Freq. (Hz)	Tool Radius (mm)	Measured Form Error PV (μm)	Ideal Surface Finish Ra (nm)	Measured Surface Finish Ra (nm)
2mm Tilted flat – Cu	STS	50	50	10	50.0	1	0.83	1.5	0.35	2.1	2.7- 4.7
2mm Tilted flat – Cu	STS	50	150	5	33.3	1	2.50	1.5	<0.25	0.53	2.9 - 4.5
2mm Tilted flat – Cu	STS	50	150	8	21	1	2.50	2.5	0.2	0.82	3.0-4.0
2mm Tilted flat – Cu	STS	50	225	10	11.1	1	3.75	1.5	<0.25	2.1	5.0 - 8.1
A12TF 200um Tilted flat - Cu	FTS500	12	500	2	6.0	0.1	8.30	0.77	0.25	0.16	3.1 - 4.5
A13TF 200um Tilted Flat - Cu	FTS500	12	1000	2	3.0	0.1	16.70	0.77	0.25	0.16	3.2 - 5.4
500um Tilted Flat - Cu	FTS500	12	500	2	6.0	0.24	8.3	0.5	0.3	0.26	3.2 – 6.4
500um Tilted Flat - Cu	FTS500	12	1000	2	3.0	0.24	16.7	0.5	0.3	0.26	3.2 –11.0
Toric surface in 303 SST (Aps Note 0303) (CBN tool)	FTS70	9	2000	2.5	0.9	0.031	66.67	0.5	<.35, .42	0.40	N/A
Toric – Cu (Aps Note 0301)	FTS70	9	2000	2.5	0.9	0.032	66.67	0.5	< .25, .37	0.40	3.5 – 8.5
70um Tilted flat - Cu	FTS70	12	500	4	3.0	0.035	8.30	2.16	0.35	0.24	2.8 - 3.7
2mm Lenslet Array -- Nickel (Aps Note 03.11-1DT)	FTS70	12	250	4	6.0	0.031	75.00	0.5	1.5	1.02	3.7 - 10
35um Tilted flat– Cu (Aps note 0306)	FTS70	20	1000	1	10.0	0.017	16.67	0.5	0.206	0.70	1.3
35um Tilted Flat – OFHC Cu (Aps Note A-0316)	FTS70	50	1000	2.5	10.0	0.017	16.67	0.5	0.017	0.70	1.54
Corner Cube Lens Array -- OFHC Cu (Aps Note A-0214)	FTS35	50	150	5.3	31.4	0.015	87.27	1.0	0.097	0.92	3.4

Appendix III

Standard procedure of asphere subtraction by Vision

Step 1: Data import for Asphere Generation

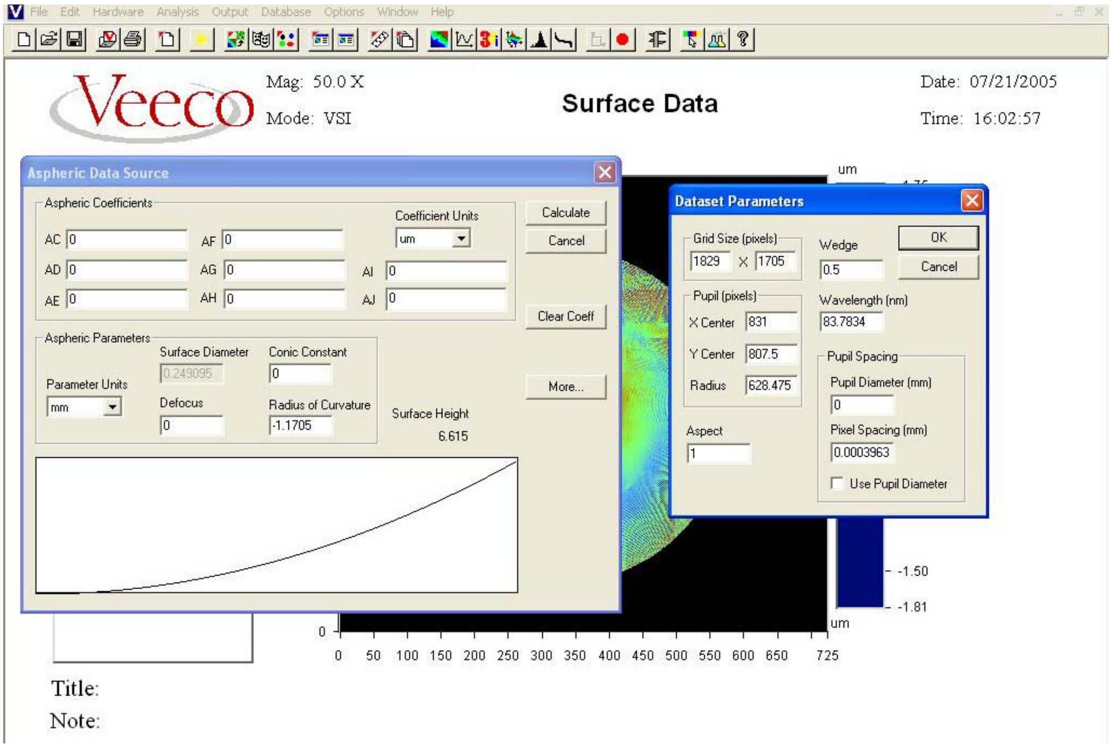

Step 2: Enable masking function

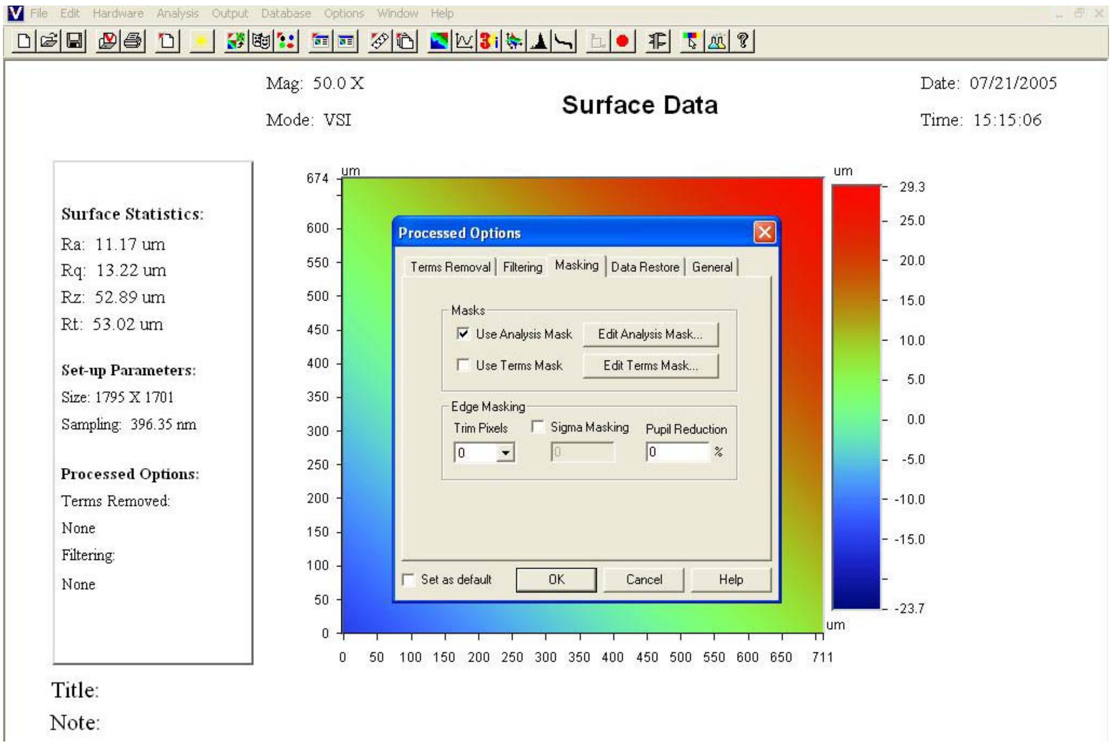

Step 3: Choosing masking area

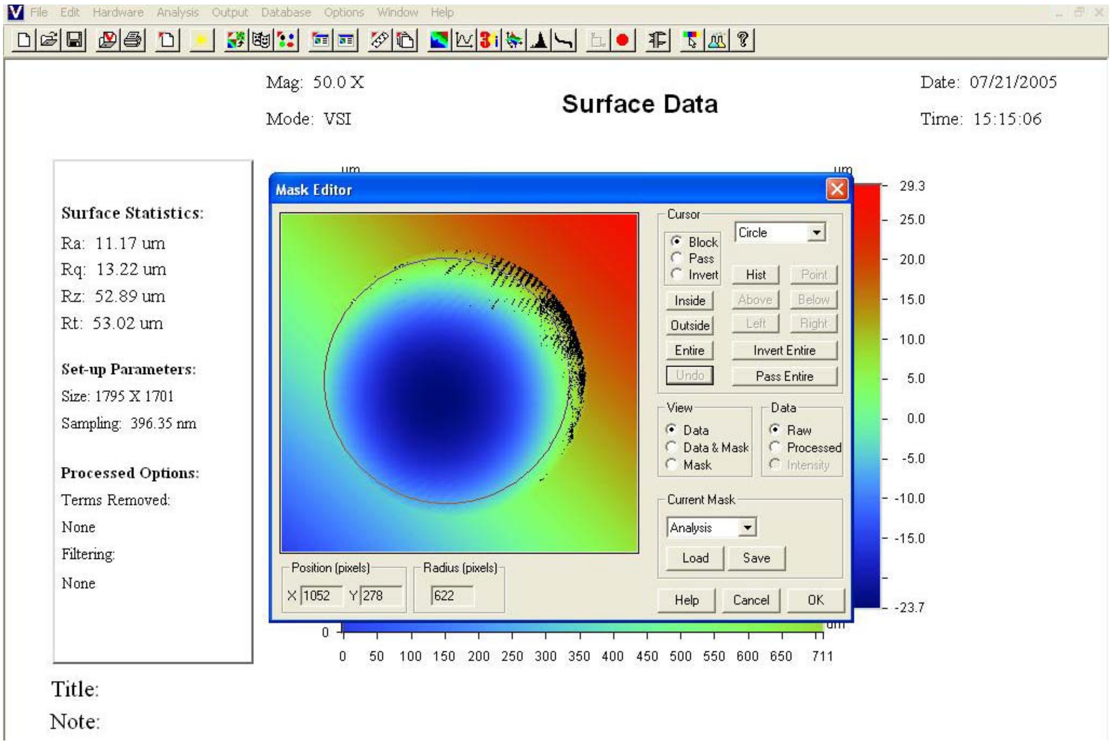

Step 4: Block the area outside the masking region

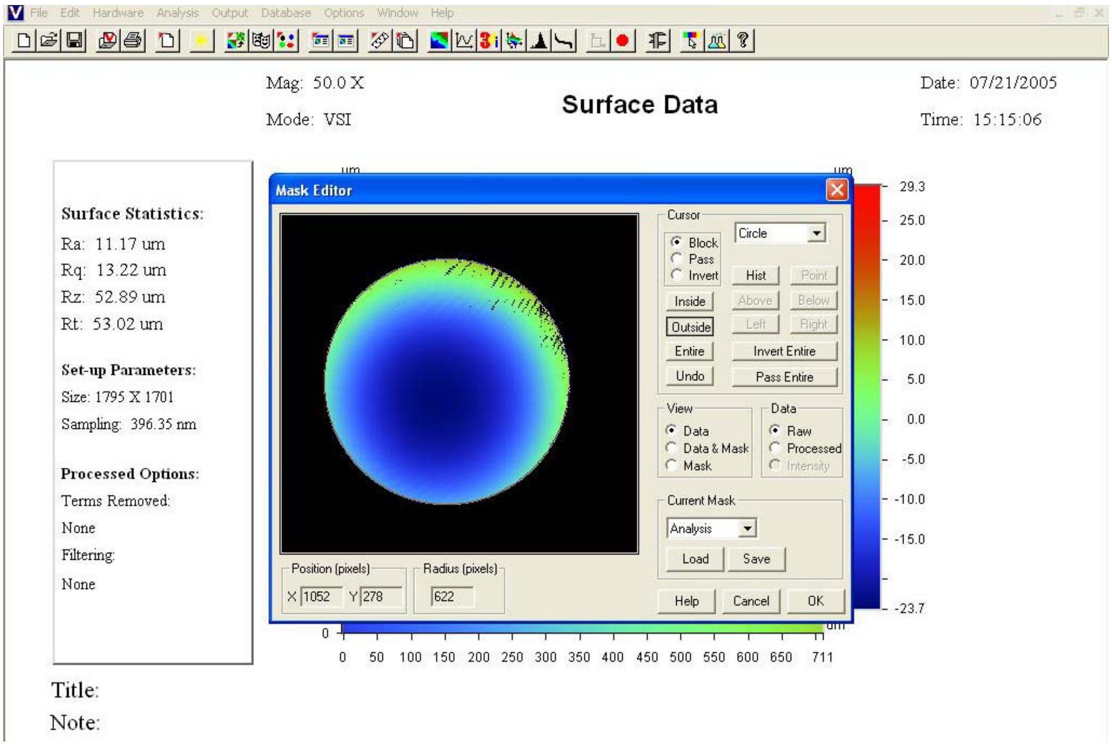

Step 5: Choosing analysis option as Asphere Subtraction

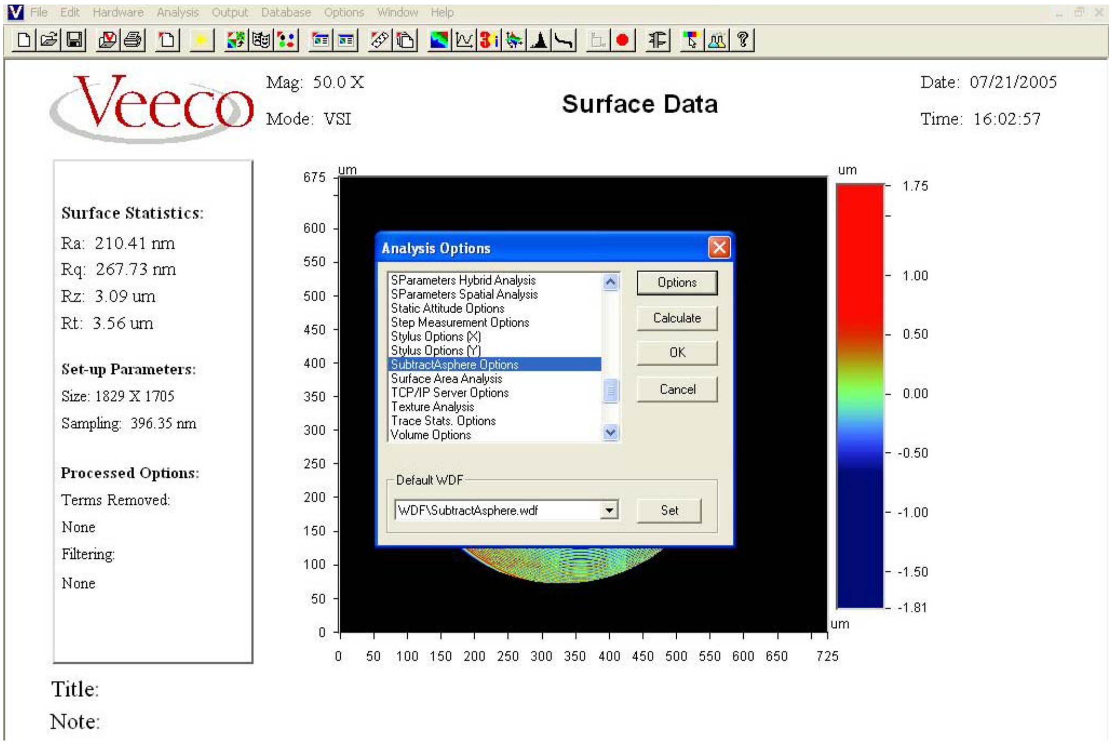

Step 6: Advanced setting of search window

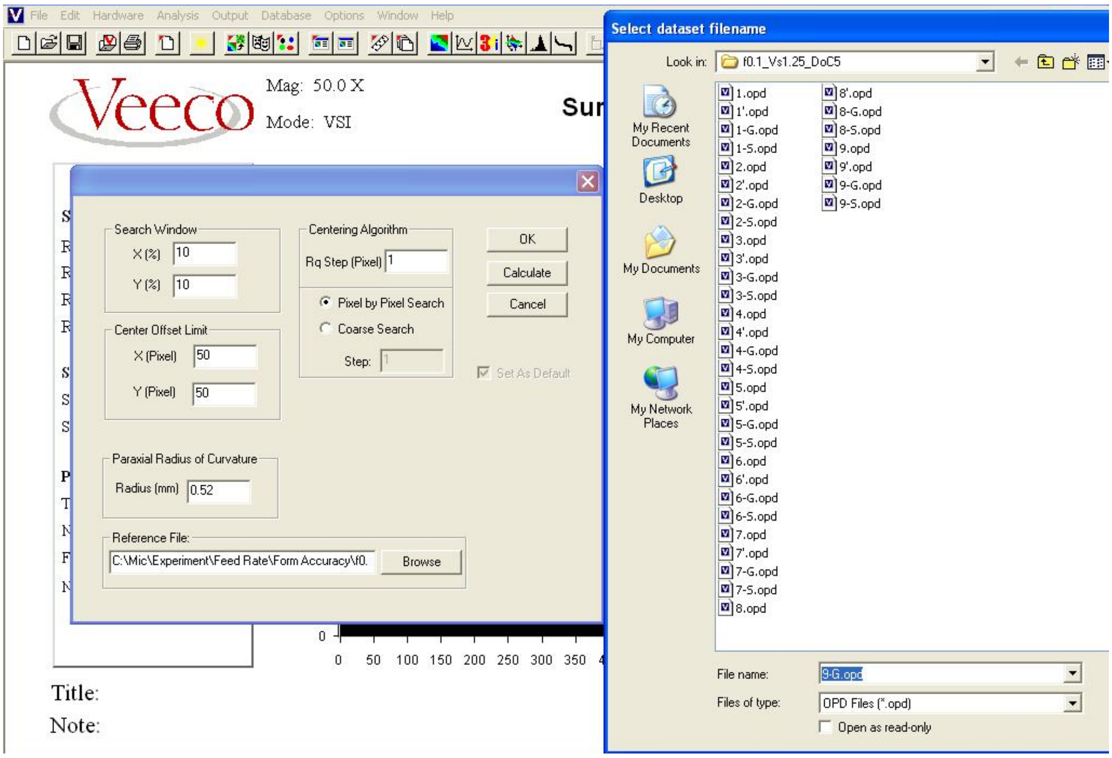

Step 7: Selection of output resolution

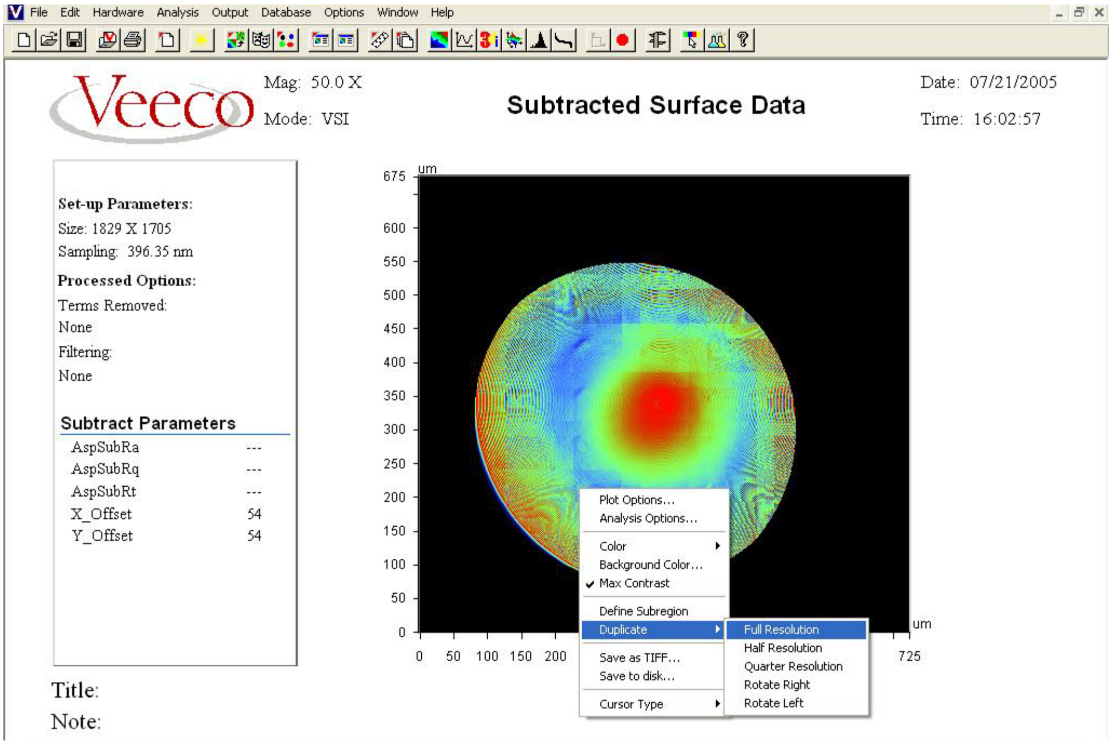

Step 8: Analyzed result by removal of tilt surface